



**HAL**  
open science

# Characterization and improvement of a surface aerator for water treatment

Hayder Mohammed Issa

► **To cite this version:**

Hayder Mohammed Issa. Characterization and improvement of a surface aerator for water treatment. Chemical and Process Engineering. Institut National Polytechnique de Toulouse - INPT, 2013. English. NNT : 2013INPT0111 . tel-04301416

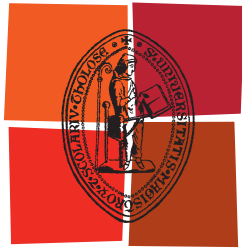
**HAL Id: tel-04301416**

**<https://theses.hal.science/tel-04301416v1>**

Submitted on 23 Nov 2023

**HAL** is a multi-disciplinary open access archive for the deposit and dissemination of scientific research documents, whether they are published or not. The documents may come from teaching and research institutions in France or abroad, or from public or private research centers.

L'archive ouverte pluridisciplinaire **HAL**, est destinée au dépôt et à la diffusion de documents scientifiques de niveau recherche, publiés ou non, émanant des établissements d'enseignement et de recherche français ou étrangers, des laboratoires publics ou privés.



Université  
de Toulouse

# THÈSE

En vue de l'obtention du

## DOCTORAT DE L'UNIVERSITÉ DE TOULOUSE

Délivré par :

Institut National Polytechnique de Toulouse (INP Toulouse)

---

**Présentée et soutenue par :**

**Hayder Mohammed ISSA**

le 24 Octobre 2013

**Titre :**

CHARACTERIZATION AND IMPROVEMENT OF A SURFACE AERATOR  
FOR WATER TREATMENT

---

**École doctorale et discipline ou spécialité :**

ED MEGEP : Génie des procédés et de l'Environnement

**Unité de recherche :**

Laboratoire de Génie Chimique (LGC), Toulouse

**Directeur(s) de Thèse :**

Martine POUX, Ingénieur de Recherches (HDR), INP-ENSIACET, Toulouse

Catherine XUEREB, Directrice de Recherches CNRS-LGC/INPT, Toulouse

**Jury :**

Cathy CASTELAIN, Directrice de Recherches CNRS-LTN/INP, Nantes, Examineur

Michel SARDIN, Professeur, ENSIC/INPL, Nancy, Rapporteur et Examineur

Denis BOUYER, Professeur, Université de Montpellier II, Rapporteur et Examineur

Jean-Pierre GRASA, Président-Directeur Général, Biotrade, Toulouse, Examineur



## ***Remerciements et Dédicace***

Je voudrais tout d'abord remercier mes directrices de thèse **Catherine Xuereb** et **Martine Poux**, pour la confiance, le temps et la patience qu'elles m'ont accordé au long de ces trois années, ainsi que pour leurs conseils avisés qu'elles ont porté au projet.

J'adresse ma reconnaissance à M. **Michel Sardin**, Professeur à INPL Nancy et M. **Denis Bouyer**, Professeur à l'Université de Montpellier II, qui ont accepté de juger ce travail et d'en être les rapporteurs.

Je remercie également Mme. **Cathy Castelain**, professeur à l'Université de Nantes d'avoir accepté de présider le jury de thèse.

Je remercie M. **Jean-Pierre Grasa**, PDG Biotrade pour son intérêt à ce travail, pour son aide et ses conseils avisés et pour accepter de juger ce travail.

Mes remerciements s'adressent à **Joëlle Aubin** et **Karine Loubiere** pour leur soutien qu'elles m'ont fourni tout au long de ce travail.

Je souhaite remercier l'équipe technique du LGC pour leur aide, tout particulièrement, **Jacques Labadie**, **Lahcen Farhi** et **Alain Muller**, pour leur disponibilité, et pour leur aide dans la mise au point expérimentale. Mes remerciements s'adressent également aussi au service administratif du LGC particulièrement **Danièle Bouscary** pour sa disponibilité. Je remercie tous mes collègues du laboratoire LGC.

Je dédie ce travail à la mémoire de ma chère mère. Je dédie ce travail aussi à ma chère épouse **Aseel**, merci pour ton soutien et à mes enfants **Abdullah**, **Danya** et **Mohammed**, qui m'attendent avec impatience.

Enfin, je tiens à remercier tous ceux qui, de près ou de loin, ont contribué à la réalisation de ce projet.

## Abstract:

A new surface aeration system for water and wastewater treatment has been studied. Its uniqueness lies in its ability to operate in two modes: aeration or simply blending (mixing) by just reversing the direction of rotation. An experimental plant has enabled to focus on mass transfer performance and hydrodynamics. The flow pattern and the velocity field measurements inside the agitated tank were performed by both the Laser Doppler Velocimetry (LDV) and the Particle Image Velocimetry (PIV) techniques for the single phase (Mixing) mode and for the two phases (Aeration) mode. The oxygen mass transfer occurs both in the water bulk and in the spray above water surface and has been independently investigated. Different configurations and operational conditions were tested during the experimental part in order to interpret phenomenon effect of the draft tube and RTP propeller, rotational speed, turbine blades submergence and else on the flow field and the oxygen mass transfer in the agitated system that produced mainly by a cone shape turbine. The experimental part dealing with hydrodynamics and flow field shows that the down-pumping operation mode with the draft tube has the most convenient results in the mixing mode with respect to turbulent flow field and mixing time. Whilst for the up-pumping aeration mode the hydrodynamics experimental results show the whole system configuration is the most convenient with regarded to mean velocities, turbulent flow intensity and mixing time. For the oxygen mass transfer experimental part, it is found that the highest standard liquid bulk aeration efficiency is achieved ( $SAE_b = 2.65 \text{ kgO}_2 \text{ kw}^{-1}\text{h}^{-1}$ ) when the whole system configuration is used. The highest standard aeration efficiency at 20 °C for the water spray zone is accomplished ( $(E_{sp})_{20} = 51.3 \%$ ) with the whole system configuration. Several correlations models have been derived for the oxygen mass transfer in water bulk and spray zones, power consumption and mixing time, on the basis of experimental results. They can be used as tools to estimate these parameters for geometrical and dynamical similar systems at industrial scales.

**Keywords:** Surface aeration, Agitated tank, Mass Transfer, Oxygen mass transfer, Hydrodynamics, Multiphase Flow, LDV, PIV, Dimensional analysis, Modelling

## Résumé :

Un nouveau système d'aération de surface pour le traitement des eaux usées a été étudié. Sa spécificité réside dans sa capacité à fonctionner selon deux modes : aération ou simple brassage, en modifiant uniquement le sens de rotation du système. Un pilote a permis de cibler le travail sur l'étude expérimentale du transfert de matière et de l'hydrodynamique.

Les champs d'écoulement et les mesures de vitesse à l'intérieur de la cuve agitée ont été réalisés par vélocimétrie laser à effet Doppler (LDV) et par vélocimétrie par images des particules (PIV) pour le mode monophasique (brassage) et pour le mode diphasique (aération). Le transfert d'oxygène se produit à la fois dans la cuve et dans le spray au-dessus de la surface de l'eau. Il a été étudié dans les deux zones. Différentes configurations et conditions opératoires ont été testées afin de comprendre les phénomènes d'interaction : tube de guidage, hélice complémentaire RTP, vitesse de rotation, niveau de submersion des pales de la turbine. La partie expérimentale sur l'hydrodynamique et les champs d'écoulement montre que le mode de fonctionnement en pompage vers le bas (brassage) avec tube de guidage procure les meilleurs résultats en termes de mélange si on se réfère aux champs d'écoulement et à la mesure du temps de mélange. Pour le mode de fonctionnement en pompage vers le haut (aération), les résultats expérimentaux montrent que la configuration du système complet est la plus efficace si on considère le transfert d'oxygène, les vitesses moyennes, l'intensité de l'écoulement turbulent et le temps de mélange. Il est constaté que la meilleure efficacité d'aération standard est atteinte ( $SAE_b = 2.65 \text{ kgO}_2\text{kw}^{-1}\text{h}^{-1}$ ) lorsque le système complet est utilisé. L'efficacité d'aération standard à 20°C la plus élevée au niveau du spray d'eau est obtenue ( $(E_{SP})_{20} = 51,3\%$ ) avec la configuration du système complet.

Plusieurs modèles sont proposés pour calculer le transfert d'oxygène dans la cuve et dans le spray, la consommation énergétique et le temps de mélange. Ces relations permettent d'évaluer l'influence des différents paramètres géométriques et de fonctionnement dans des systèmes similaires à une échelle industrielle.

**Mots-clés:** Aération de surface, Cuve agitée, Transfert de matière, Transfert d'oxygène, Hydrodynamique, Ecoulement multiphasique, LDV, PIV, Analyse dimensionnelle, Modélisation

## **Table of Contents**

<b>Introduction and Outlines</b> .....	<b>1</b>
<b>Chapter 1: Surface Aeration Process for Water Treatment</b> .....	<b>7</b>
<b>1.1. Presentation of Different Aeration Technologies in Water Treatment</b> .....	<b>9</b>
1.1.1. Diffused Aeration.....	10
I. Porous Diffusers.....	10
I.1. Plate Diffusers.....	10
I.2. Panel Diffuser.....	11
I.3. Tube Diffuser.....	11
I.4. Dome Diffusers.....	11
I.5. Disc Diffuser.....	11
II. Non Porous Diffusers.....	11
II.1. Fixed Orifice Diffusers.....	11
II.2. Valved Orifice Diffusers.....	11
II.3. Static Tube Diffusers.....	11
1.1.2. Submerged Aeration.....	12
I. Submerged Turbine Aerators.....	13
II. Jets Aerators.....	14
1.1.3. Aeration with High-Purity Oxygen.....	14
1.1.4. Aspirating Aeration.....	15
1.1.5. Surface Aeration.....	16
<b>1.2. Surface Aeration for Water Treatment Processes</b> .....	<b>16</b>
1.2.1. Types of Surface Aerators.....	16
I. Low Speed Surface Aerators.....	16
I.1. Low Speed Vertical Flow Aerators.....	16
I.2. Low Speed Horizontal Flow Aerators.....	18

II. High Speed Surface Aerators .....	18
1.2.2. Principals and Characterization .....	19
I. Principals .....	19
II. Surface Aerator Characterizations .....	23
II. Dissolved Oxygen Concentration Gradient Calculation Methodology .....	24
IV. Surface Aeration Oxygen Mass Transfer .....	27
IV.1. Operational Condition Effects .....	28
A. Rotational Speed Effect .....	28
B. Number of Impellers Effect .....	29
C. Liquid Level Effect .....	29
D. Clearance and Submergence Effect .....	30
IV.2. Geometry Effect .....	31
A. Tank Geometry .....	31
B. Baffles Effect .....	32
C. Draft Tube Effect .....	33
D. Surface Aerators Geometry .....	34
D.1. Surface Aerator Diameter .....	36
V. Impeller Position in the Treatment Tank .....	36
IV. Temperature Effect .....	37
V. Hydrodynamics .....	38
V.1. Flow Patterns .....	38
A. Flow Patterns Characterization .....	38
B. Vortex Formation .....	40
V.2. Air Bubble Size Distribution and Hold-up .....	40
V.3. Mixing Time .....	41
A. Mixing Time Characterization .....	41
B. Mixing Time Modeling .....	42

V.4. Air Bubbles Entrainment .....	43
V.5. Surface Aeration Power Consumption .....	43
A. Operational Condition Effect .....	44
B. Power Consumption Relation with Oxygen Mass Transfer .....	44
VI. Contact Time between Water Droplets and Atmospheric Air .....	45
VII. Environmental Effects .....	46
<b>1.3. Conclusions .....</b>	<b>46</b>
<b>Chapter 2: Experimental Setup and Calculation Methods .....</b>	<b>51</b>
<b>2.1. Introduction .....</b>	<b>51</b>
<b>2.2. Experimental Installation and System Description .....</b>	<b>51</b>
<b>2.3. The Measurement of Power Consumption .....</b>	<b>54</b>
<b>2.4. Hydrodynamics and Mean Velocity Measurements Techniques .....</b>	<b>54</b>
2.4.1. Laser Doppler Velocimetry (LDV) .....	54
I. LDV Apparatus Description .....	54
II. Tracer Particles Seeding .....	55
III. Measurement Principals .....	55
IV. Signal Post-Processing .....	58
2.3.2. Particle Image Velocimetry (PIV) .....	58
I. Theory .....	58
II. Tracer Particles Seeding .....	59
III. PIV Principles .....	59
IV. Scattered Light .....	60
V. Laser Source .....	61
VI. Recording Techniques .....	61
VII. Image Analysis Method .....	62
VIII. The Cross-Correlation Calculation .....	62

2.4.3. Other Flow Related Measurements Parameters .....	63
I. Mixing Time ( $t_m$ ) .....	63
II. The Pumping Number ( $N_{Qp}$ ) .....	64
III. Circulation Number ( $N_{Qc}$ ) and Flowrate .....	65
IV. Agitation Index ( $I_g$ ) and Flow Quantification .....	66
<b>2.5. Mass Transfer Experimental Setup and Calculation Methods .....</b>	<b>67</b>
2.5.1. Oxygen Probe Description .....	67
2.5.2. Mass Transfer Coefficient .....	69
I. Liquid Bulk Oxygen Mass Transfer Zone .....	69
I.1. Introduction .....	69
I.2. Bulk Zone Oxygen Mass Transfer Calculation Methodology .....	71
I.3. Testing Different Probe Positions in the Vessel .....	71
I.4. Repeatability of Experimental Results .....	72
I.5. De-oxygenation and Re-oxygenation Processes .....	73
I.6. Oxygen Probe Response Time Measurement Verification .....	73
I.7. Determination Model of the Bulk Zone Oxygen Mass Transfer Coefficient .....	75
I.8. Measurement Procedure for the Bulk Zone Oxygen Mass Transfer Coefficient .....	76
I.9. Temperature Correction for the Oxygen Mass Transfer Coefficient .....	77
I.10. Oxygen Transfer Rate for the Bulk Mass Transfer Zone ( $OTR_b$ ) .....	77
I.11. Standard Oxygen Transfer Rate for the Bulk Mass Transfer Zone ( $SOTR_b$ ) .....	77
I.12. Standard Aeration Efficiency for the Bulk Mass Transfer Zone ( $SAE_b$ ) .....	78
II. Spray Oxygen Mass transfer Zone .....	78
II.1. Introduction .....	78
II.2. Spray Zone Oxygen Mass transfer Coefficient Calculation Methodology .....	79
II.3. Determination Model for the Spray Zone Oxygen Mass Transfer Coefficient .....	79
II.4. Temperature Correction for the Spray Mass Transfer Zone .....	81
II.5. Oxygen Transfer Rate in the Spray Mass Transfer Zone ( $OTR_{sp}$ ) .....	82

II.6. Spray Zone Mass Transfer Coefficient ( $k_{ad}$ ) Measurement Procedure .....	82
<b>2.6. Water Droplets Flight Time (<math>t_f</math>) .....</b>	<b>83</b>
<b>2.7. Water Droplets Velocity and Volumetric Flow Rate .....</b>	<b>84</b>
<b>2.7. Conclusions .....</b>	<b>87</b>
<b>Chapter 3: Oxygen Mass Transfer in the Surface Mode .....</b>	<b>91</b>
<b>3.1. Water Bulk Mass Transfer Zone .....</b>	<b>91</b>
3.1.1. Introduction .....	91
3.1.2. The Experimental Results .....	92
I. Effect of Geometrical Configuration .....	92
II. Effect of Impellers Rotational Speed .....	93
III. Turbine Blades Submergence Effect .....	95
IV. Effect of the Spacing between the Impellers .....	97
V. Power Consumption Measurements .....	98
VI. Standard Aeration Efficiency ( $SAE_b$ ) and Standard Oxygen Transfer Rate ( $SOTR_b$ ) for the Water Bulk Zone .....	101
3.1.3. The Modeling .....	106
I. Mass Transfer .....	106
II. Power Consumption .....	108
<b>3.2. Spray Mass Transfer Zone .....</b>	<b>110</b>
3.2.1. Introduction .....	110
3.2.2. The Experimental Results .....	110
I. Impellers Rotation Speed Effect .....	110
I.1. Aeration Efficiency for the Water Spray Zone ( $E_{sp}$ ) .....	111
I.2. Spray Zone Mass Transfer Coefficient ( $k_{ad}$ ) .....	115
I.3. Surface Aeration Water Spray Discharge Velocity and Volumetric Flow Rate .....	117
I.4. Spray Zone Oxygen Transfer Rate ( $OTR_{sp}$ ) .....	118

I.5. Contribution Percentage of the Spray and Bulk Zones in the Overall Mass Transfer Operation .....	119
II. The Effect of Turbine Blades Submergence .....	121
II.1. Water Spray Velocity and Volumetric Flow Rate .....	121
II.2. Spray Zone Aeration Efficiency ( $E_{sp}$ ) .....	122
II.3. Spray Zone Mass Transfer Coefficient ( $k_{ia_d}$ ) .....	126
II.4. Spray Zone Oxygen Transfer Rate ( $OTR_{sp}$ ) .....	127
II.5. Contribution Percentage of the Spray and Bulk Zones in the Overall Mass Transfer Operation .....	129
III. Effect of Propeller and the Draft Tube .....	130
III.1. Spray Zone Aeration Efficiency ( $E_{sp}$ ) .....	130
III.2. Spray Zone Mass Transfer Coefficient ( $k_{ia_d}$ ) .....	133
III.3. Water Spray Velocity and Volumetric Flow Rate .....	134
III.4. Spray Zone Oxygen Transfer Rate ( $OTR_{sp}$ ) .....	135
IV. Comparing the $OTR_{sp}$ for the Whole System and Turbine Alone Configurations .....	136
3.2.3. The Modeling .....	137
3.2.4. Conclusions .....	142

**Chapter 4: Hydrodynamics in the Single Phase Non-Aerated Agitated Tank for Up and Down Pumping Directions Modes ..... 147**

**4.1. Experimental Aspects ..... 147**

**4.2. Mean Velocity Field and Flow Pattern ..... 150**

4.2.1. Down-Pumping Condition ..... 150

I. Propeller and Draft Tube Configuration ..... 150

II. Propeller Alone Configuration ..... 158

4.2.2. Up-Pumping Mode ..... 162

I. Propeller and Draft Tube Configuration ..... 162

II. Propeller Alone Configuration ..... 165

<b>4.3. Power Consumption</b> .....	<b>168</b>
<b>4.4. Pumping Capacity</b> .....	<b>170</b>
<b>4.5. Agitation Index and Liquid Volume Quantification for the Down-Pumping Mode with Draft Tube Configuration</b> .....	<b>171</b>
<b>4.6. Mixing Time</b> .....	<b>172</b>
4.6.1. The Effect of RTP Propeller Rotational Speed.....	166
<b>4.7. Conclusions</b> .....	<b>178</b>
<b>Chapter 5: Hydrodynamics and Flow Pattern in Aerated Agitated Tank</b> .....	<b>183</b>
<b>5.1. Introduction</b> .....	<b>183</b>
<b>5.2. Flow Pattern and Mean Velocity Field in the Aerated Tank</b> .....	<b>183</b>
<b>5.3. The Effect of the Propeller and Draft Tube</b> .....	<b>185</b>
5.3.1. Flow Pattern and Mean Velocity Field in the Aeration Tank.....	185
<b>5.4. The Effect of the Draft Tube</b> .....	<b>186</b>
5.4.1. Flow Pattern and Mean Velocity Field in the Aeration Tank.....	186
<b>5.5. Turbine Pumping Number and System Circulation Number</b> .....	<b>199</b>
<b>5.6. Agitation Index and Liquid Quantification for the Whole System Configuration</b> .....	<b>199</b>
<b>5.7. The Mixing Time</b> .....	<b>200</b>
5.7.1. Impellers Rotational Speed Effect.....	203
5.7.2. Effect of Propeller and Draft tube Presence.....	204
5.7.3. Effect of the Spacing between Two Agitators.....	205
5.7.4. The Effect of the Turbine Blades Submergence.....	206
5.7.5. Mixing Time Modelling.....	207
<b>5.8. The Power Consumption in the Aerated Mode</b> .....	<b>209</b>
<b>5.9. Conclusions</b> .....	<b>211</b>

<b>General Conclusions and Prospective</b> .....	<b>215</b>
--	------------

<b>Appendix I: A Review for Biological Wastewater Treatment with Activated Sludge</b> .....	<b>223</b>
---	------------

<b>I.1. Industrial and Domestic Wastewater Treatment</b> .....	<b>223</b>
--	------------

I.1.1. Preliminary Treatment Process.....	225
---	-----

I.1.2. Primary Treatment Process.....	225
---------------------------------------	-----

I.1.3. Secondary Waste Water Treatment.....	226
---	-----

I.1.4. Tertiary Wastewater Treatment.....	226
---	-----

<b>I.2. Activated Sludge Process</b> .....	<b>226</b>
--	------------

I.2.1. Nutrient Removal.....	228
------------------------------	-----

A. Nitrogen Removal.....	228
--------------------------	-----

B. Phosphorus Removal.....	229
----------------------------	-----

<b>I.3. Aeration Process in the Activated Sludge Treatment</b> .....	<b>231</b>
--	------------

<b>I.4. Additional Treatments</b> .....	<b>232</b>
---	------------

I.4.1. Sludge Treatments.....	232
-------------------------------	-----

I.4.2. Odor treatment.....	233
----------------------------	-----

<b>Appendix II: The Derivation of Spray Flowrate for the Surface Aeration System</b> .....	<b>237</b>
--	------------

<b>List of Symbols</b> .....	<b>241</b>
------------------------------	------------

<b>List of Figures</b> .....	<b>247</b>
------------------------------	------------

<b>List of Tables</b> .....	<b>257</b>
-----------------------------	------------

<b>References</b> .....	<b>259</b>
-------------------------	------------

# **INTRODUCTION AND OUTLINES**



### **Introduction**

Clean water is growingly demanded in the different fields of human activities, for example water is more and more being used in the industry (Roubaty and Boeglin, 2007). On the other hand the continuous diminution of existing water resources made water and wastewater treatment to become a truly developing and problematic question. One of the ways used to maintain clean water resources for the diverse industrial or urban demands, is wastewater treatment.

The implementation of the surface aeration process in the water and wastewater treatment is established as an effective treatment for various wastewater types especially in activated sludge biological and aerobic water treatment processes. This technology has an important capacity of delivering the needed oxygen to the aerobic micro-organisms for respiration and ensures efficient mixed condition for the entire treatment tank through maintaining the microbial flocs in continuous state of agitated suspension by accompanied mixing in order to achieve maximum contact surface area between the flocs and wastewater (Gary, 2004). Surface aeration has various desirable characteristics such minimum sludge residual is produced for the used activated sludge process as a continuous operation of recycling the used sludge is implemented for wastewater treatment plant (Nair et al., 2008; Ramalho, 1977).

Taking in to consideration the capacity of now used surface aerators in the water treatment field with respect to the accomplished aeration efficiency, energy consumption and the complicated maintenance as described in the related works.

It is expected from this work to provide the necessary investigations to prove the flexibility and capability of the purposed innovative surface aerator to work in two ways, aeration and mixing by simply reversing the sense of the rotation and acting on a clutching system. The novel investigated surface aerator (FR Patent Demand, 2012) is found useful and promising after the new method for combination between the delivering the necessary oxygen into the water treatment tank by the up-pumping aeration mode and to achieve an efficient mixing for the treatment tank constituents by the down-pumping mixing mode.

Implementing the new surface aeration technology enables easy maintenance and more energy saving. In addition the operation may be performed with minimum cost. This research can be regarded as an approach that may open new opportunities to enhance the aeration efficiency with optimized operation condition.

During the last decades, the surface aeration is considered as an effective oxidation mean among the existed wastewater treatments tools. It consists in the dispersion of the waste water into droplets and there projection through the atmospheric air, where

a large contacting area is accomplished between the two phases the continuous atmospheric air and the dispersed water droplets allowing much higher quantity of oxygen transferred towards the droplets. Then these enriched oxygen droplets are remixed and well distributed inside the tank. The large interfacial area generated between the water droplets and the atmospheric air by the surface aeration leads to high oxygen transfer. The oxygen mass transfer from the gas phase (atmospheric air) to dispersed water droplets is only limited by the ability of the aerator to provide the highest water volumetric rate that is exposed to air, (Mueller et al., 2002). Generally the high speed surface aerators work with the rotational speed range of (1800 to 3600 rpm) depending of the specific conditions applied, while the low speed surface aerator rotates between 40 to around 100 rpm; these speeds are varied depending upon the power level of motors utilized. Normally the low speed aerators are fabricated for life expectancy of 11.4 years before major maintenance or replacement (Stukenberg, 1984).

Mixing and agitation operations are considered as essential factors during the surface aeration process, where the wastewater treatment process regarded as an effective treatment according to the mixing condition occurred (Albal et al., 1983).

Both of the concerned mixing and aeration processes are governed by many constrains that limit their performance, among of them is the mixing time beside the power consumption, as its always desirable to achieve homogenization condition in shorter time and lowest consumed energy to optimize power consumption and reaching the sought contact condition between air bubbles and treated water in the liquid bulk and its included microbial flocs. Usually the mixing time is considered as a criterion of flow pattern in aerated and non-aerated conditions (Hadjiev et al., 2006).

There are two main aspects to evaluate a surface aeration system for water treatment process, the oxygen mass transfer and the hydrodynamics investigations. Oxygen mass transfer investigation is crucial to figure out the ability of the surface aeration system and to attain a successful transfer of the oxygen from the atmospheric air to the water inside the treatment tank or lagoon. Usually the oxygen mass transfer capability of a surface aeration system is identified by determination two main characteristic parameters; the standard aeration efficiency SAE, and the standard oxygen transfer rate STOR. These parameters depend mainly on the achieved volumetric oxygen mass transfer coefficient in the liquid phase  $k_{1a}$  during the operation at standard condition (Sardeing et al., 2005).

For the surface aeration, most of the oxygen transfer is occurred in the generated spray. The same characteristic parameters that the ones obtained for the liquid bulk are determined in the spray zone such as the spray standard aeration efficiency  $(SAE)_{sp}$  and the spray standard oxygen transfer rate  $(SOTR)_{sp}$ . These parameters are calculated by determination the spray zone volumetric oxygen mass transfer coefficient  $k_{1a_d}$  (Huang et al., 2009; McWhirter et al., 1995).

The other aspect of the surface aeration investigation is the hydrodynamic, where basically for each agitated tank the hydrodynamic is studied to figure out the flow pattern, the velocity field, turbulence intensity and the pumping capacity of the implemented impellers. During the past three decades the main measurement means that applied in this field are the Laser Doppler Velocimetry, LDV and Picture Image Velocimetry, PIV, because these techniques are non-intrusive and don't interfere the flow during the measurement (Adrian, 1991). Both the LDV and PIV allow us to study the flow inside the agitated tank. The essential requirement for these flow measurement techniques is that the measurement have to be carried out in a transparent vessel and -if cylindrical- placed in a larger one filled with the same liquid of the investigation to avoid laser beam diffraction (Aubin et al., 2001).

### **Outlines**

The main objective of this work is to characterize the performance of the surface aeration system in aeration mode and its blending capacity in the mixing mode. This will be fulfilled by identifying the affecting parameters on the oxygen mass transfer process that developed within the liquid bulk inside the tank and in the spray at the water surface. These parameters are the operation conditions and the geometrical configurations such as; the rotational speed, mixing time, impellers configurations and the power consumption.

The other main objective of this work is to acquire the flow behavior for the two phase (gas-liquid) condition (Aerated mode) and for the single phase condition (Mixing mode) with related power consumption and impellers configurations.

This thesis consists in five chapters,

Chapter one presents a brief description for aeration types in the water treatment process. In this chapter the literature review on the surface aeration according to the most important characteristic parameters, such as the oxygen mass transfer, the power consumption, the geometrical configuration, flow patterns and aerator types is presented.

Chapter two includes the description for the pilot and the experimental techniques and implemented apparatus in the hydrodynamic and the oxygen mass transfer investigations, such as the LDV, PIV and dissolved oxygen concentration probes. In this chapter the calculation methods and models applied for the oxygen mass transfer, power consumption and fluid flow measurements are explained in details.

In chapter three the analysis is focused on the oxygen mass transfer operation accomplished in the tested surface aeration system by means of dissolved oxygen concentration measurement both in water bulk and water spray. The effect of the

impellers rotation speed and turbine blades submergence and presence of the RTP propeller and the draft tube are investigated. Models for the oxygen mass transfer dimensionless parameters in the water bulk and spray with effecting parameters will be built.

Chapter four is dedicated to the hydrodynamics of the single phase stirred tank (Mixing mode). In this case the aim of operation is to achieve an efficient mixing condition of the water bulk without further aeration. The experimental runs of the generated flow by the RTP propeller are carried out using the LDV and PIV for both up-pumping and down-pumping modes. The effect of the presence of a draft tube will be tested for these modes. The flow characterization is made through mixing time, circulation number power number, and agitation index. A model is derived for the mixing time for the down-pumping mixing mode correlating the influencing factors with the dimensionless mixing time.

Chapter five involves the hydrodynamics investigations of the up-pumping flow in the air-water system (Aerated mode). The flow patterns and velocity fields generated by the turbine in the aerated tank will be characterized by the agitation index, mixing time, pumping number and circulation number. The effect of different impellers configuration and the draft tube effect have been tested. A model is derived for the mixing time for the up-pumping aerated mode correlating the influencing factors with the dimensionless mixing time.

# **CHAPTER ONE**

## **SURFACE AERATION PROCESS FOR WATER TREATMENT**



## **Chapter One**

### **Surface Aeration Processes for Water Treatment**

#### **1.1. Presentation of Different Aeration Technologies in Water Treatment**

In the actual field of the water treatment, the oxygen mass transfer to the biologically active microorganism masses is considered as an essential part of water treatment. This transfer is improved with implementing the activated sludge in the treatment tank. Different types of aeration systems have been employed in the water and wastewater treatment field, the choice is made depending on the location and specific treatment requirements.

The aeration process for water treatment is a way to achieve higher mass transfer rate between the oxygen and the water by increasing the interfacial area between them. Usually the agitation plays an important role in this process by keeping the homogeneity of the liquid phase (water) with its included biomasses and creating an acceptable dispersion of the oxygen gas phase. In this process, the size of oxygen bubbles and the interfacial area are highly dependent on the condition and degree of mixing (Ju and Sundarajan, 1992). The agitation has also another important role that is to keep the bubbles as long time as possible inside the tank in order to prolong the bubbles residence time.

Water and wastewater treatment by the aeration can be basically classified into four main systems; (i) Diffused Aeration: the aeration is accomplished by various types of aerators to diffuse the air into the treatment tanks and without implementing agitation tools or pure oxygen gas sources. (ii) Mechanical and Submerged Agitators Aeration: the aeration is achieved with the presence of one or more different types of the agitators in the treatment tank beside the injected air sources. (iii) Surface Aeration: the aeration is achieved by entraining the atmospheric air into the water bulk by one or multiple impellers located in the treatment tank without injection of air or oxygen gas. (iv) Pure Oxygen Aeration: this system is similar to the submerged aeration except that the pure oxygen is injected through the water instead of air.

In order to improve these aeration processes many studies were made with various operation variables such as: the gas hold-up, bubble size distribution, the flow pattern for gas and water, the circulation time (mixing and aeration time), the properties of operating mediums (air and water), the transition between dispersion and flooding states, rotational speed of the aerators, power consumption, geometrical

configurations (i.e. number of impellers, types of impellers, geometric ratios) and oxygen mass transfer rate and coefficient in the water.

### 1.1.1. Diffused Aeration

The diffused aeration is defined as the injection of air or oxygen enriched air under pressure below the water surface. Beside the gas injection, additional operations are used like mechanical pumping or mixing and various devices are implied in these additional operations such as jet aerators or sparged turbine aerators.

The diffused aeration was the first effort in the wastewater treatment with activated sludge (Stukenberg et al., 1977). The mass transfer occurred for this type of aeration is in fact consisting of two zones: the gas bubbling dispersion transfer inside the treatment tank and the turbulent liquid surface transfer at the water surface. The diffused aeration contains many configurations and operational variations such as the bubble size formed, diffuser placement, tank circulation, gas flow rate and oxygen transfer efficiency. The bubbles formed by the diffuser aerator vary from large bubbles of diameter  $d_B > 6$  mm, to medium size bubble of diameter  $d_B$ , range of 4 – 6 mm, or fine bubbles diameter less than 4mm.

Many types of diffusers are used in the diffused aeration but generally they are classified into two major types, depending on the size and distribution of the gas bubbles preferred (Mueller et al., 2002):

#### I. Porous Diffusers

They also in turn have many types as follows:

I.1. Plate Diffusers: These are usually having a form of (30 cm) square surface and (25-38 mm) thick; most are constructed of ceramic media or made of porous plastic media of (30 cm x 61 cm) surface area. Air is introduced below the plates through a plenum (See Fig. 1.2).



Figure (1.1): Plate diffuser aerator,  
(Permax H ceramic plate diffuser, (Supratec Co. Ltd.)

I.2. Panel Diffuser: These usually employ a plastic membrane which is stretched over (122 cm) wide placed on base material of reinforced cement compound or fiber reinforced plastic.

I.3. Tube Diffuser: These are constructed from stainless steel or a durable plastics, they have generally (51-61 cm) long with (6.4 – 7.7 cm) diameter (Figure 1.2,a).

I.4. Dome Diffusers: They are usually used with the dimensions (18 cm) in diameter and (38mm) high, the used medium is usually is ceramic materials.

I.5. Disc Diffuser: they are relatively flat but they differ in size, shape, method of attachment and kinds of diffuser materials. Generally they have configuration of (18-51 cm) diameter (Figure 2.13, b).



(a)



(b)

Figure (1. 2) : (a) Tube diffuser aerator, (b) Disc diffuser aerator, (Gemgate GmbH)

## II. Non Porous Diffusers

These types are classified into:

II.1. Fixed Orifice Diffusers: They vary from a very simple form as an opening in pipes to especially configured opening in a number of housing shapes. They employ holes that usually range from (4.76 - 9.5mm).

II.2. Valved Orifice Diffusers: Their opening is designed in a way that provides adjustment of the number or the size of air discharge openings. The air flow ranges from (9.4 to 18.8 m<sup>3</sup>/h) and diameter hole is about (7.6 cm).

II.3. Static Tube Diffusers: They consist of stationary vertical tube placed over air header that delivers bubbles of air through drilled holes, the tube diameters are normally about (0.3 – 0.45 m), the average flow ranges are between (15.7 – 70.7 m<sup>3</sup>/h) (See Figure 1.3).



Figure (1.3): Static tube diffusers (Process Engineering s.r.l)

For the diffused aeration system with deep tanks between (4-6m), a combination of aeration systems is used to the water treatment plants in order to improve the transfer of oxygen. Usually one of applied means is using turbo-compressors to increase the flowrate of injected air.

### 1.1.2. Submerged Aeration

The aeration takes place with the presence of an aerator inside the water treatment tank or basin near the bottom. There are many types of submerged aerators such as jet aerators or jet turbines. Mostly the turbines are joined with a sparger placed beneath. Generally for these systems the compressed air is injected at lowest point in the treatment tank below the aerators by using blowers. Then the aerators disperse the air bubbles, which are in turn distributed in the water during their rising upward to the surface. Low volatile organic compounds (VOC) are released to the atmosphere by submerged aeration (Schultz, 2005). To achieve a satisfactory mass transfer between the oxygen and the water for the submerged aeration systems, the interested characters of the hydrodynamic of flow regimes occurring inside the tank and the interfacial area between the gas and the liquid and the mass transfer coefficient,  $k_L a$  are always taken in account (Tatterson, 1991).

There are many probabilities of operation conditions, when more than one impeller is used the lower impeller always has very important effect over the operation. In the agitated aerated systems, gas cavities can be developed behind the impeller blades (Lu and Ju, 1989), which it may reduce the power consumption by the impellers or it also

may affect the flow characteristics in the tank. The cavity might be formed due to many reasons; the most important one is the insufficient gas flow rate when it is injected separately. There are three kinds of cavities the swirl cavity, adherent cavity and grand cavities (Xuereb et al., 2006).

### **I. Submerged Turbine Aerators**

These turbines are submerged deeply inside the water tank or basin and consist of an open-bladed turbine mounted on a vertical shaft driven by a gear motor assembly with air sparger located under the turbine (As shown in Figure 1.4).

The submerged turbine develops both radial and axial flow. The oxygen transfer is achieved within the turbulent flow created by the impeller crossed by the bubbles discharged from the sparger holes. These aerators are generally implemented in deep tanks aeration.

In the aeration with submerged turbines are mostly equipped with air injection supply at the bottom of the tank, the most usual type is the disc turbines because they may act as a second distributor. They collect an important proportion the rising bubbles from its source before they reach the surface of the liquid and then they redirect them toward the medium of the dispersion. Nowadays there are other types used to achieve same objectives such as inclined blade-disc type turbine which admits for higher gas flow rates at the system. The usual forms for the air distributors or spargers are as punched ring type or cross-type. They have very effective influence on the dispersion because they control the process and the flow pattern of the air. The air bubbles are delivered from the holes on the upper part of the distributors. The best performances are obtained when the number of holes is limited and has a small diameter. There are two modes of operation for the air outlet from distributors; first is direct mode, where all the air will go toward the distributor and then it is swept toward dispersion medium in the tank; second, the indirect mode where a part of the outlet gas will stay around the distributor; if the circulation of water is sufficient and the size of bubbles is small, a part of it is withdrawn by the water flow from upper part of the impeller. The indirect mode is occurred when larger size and the diameter of the distributor is used, when ratio sparger to the impeller diameters ( $D_s/D_{tur}$ ) is equal to 1.2 (Tatterson, 1991; Xuereb et al., 2006).



Figure (1.4): Submerged turbine aerator, (ARS-ARS/S Radial submersible aerator, (Caprari S. p. A.)

## II. Jets Aerators

These aerators combine a liquid pumping with gas pumping to result in a plume of liquid and entrained air bubbles. They are always positioned at the base near the wall of the basins; the waste water is re-circulated and introduced with gas (that pumped through separate header) within mixing chamber (Figure 1.5) (Engineers and Federation, 1988).



Figure (1.5): Hydro Jet Aerator, Plaquette Aerodyn, (Biotrade Co.)

### 1.1.3. Aeration with High-Purity Oxygen

High purity oxygen aeration is implemented when an increase oxygen mass transfer rate is highly needed. A 100% pure source of oxygen gas phase is used instead of air supply. It could be carried out in covered and non-covered aeration. The pure oxygen is supplied into the water by distributors positioned inside the tank (See Figure 1.6). Usually mixing impellers are employed to enhance aeration potentials.

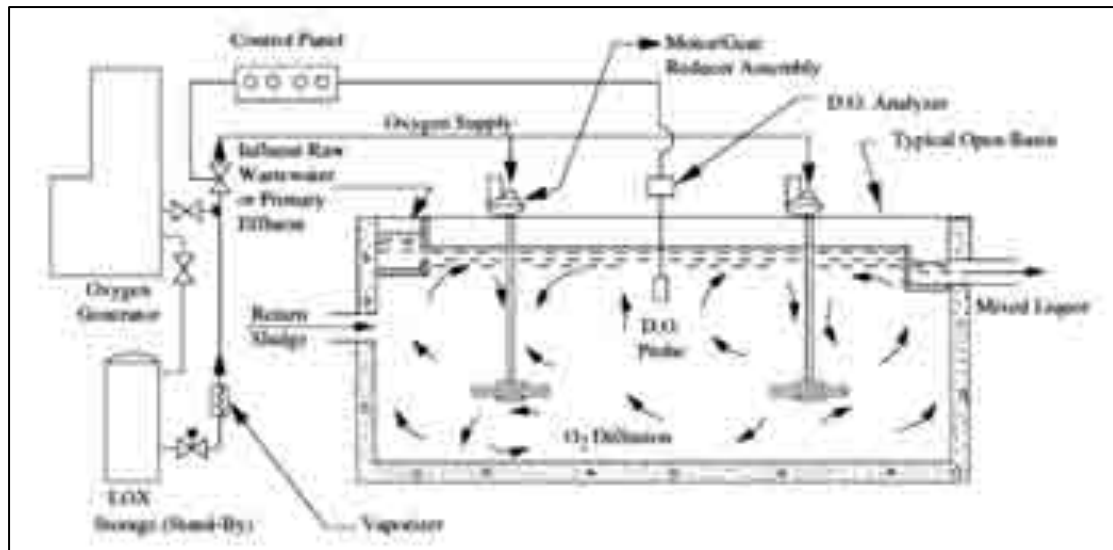


Figure (1.6): Flow diagram for uncovered pure oxygen aeration (Mueller et al., 2002).

#### 1.1.4. Aspirating Aerators

They primarily consist of rotating hollow shaft attached to the motor shaft. These aerators draw the atmospheric air into mixing chamber, where the wastewater will contact the air and then the air-water mixture is discharged into the treatment tank (See Figure 1.17). The submerged end of the rotating shaft is consist of propeller fixed under the water mounted on a shaft, the rotation speed of the propeller is high about (1800-3600 rpm) to ensure a drop in the pressure over the diffusing surface, where the pressure is lowered around it and the air was entrained and mixed with water and then enter the tank as fine bubbles then thoroughly dispersed though the tank. The advantages for these aerators are; they create less noise than others, easy to handle and portable, the projection of water drops not needed that is preferable with limited size of basins but these types are lower efficiency of oxygen rate and more complicated with mechanical point of view. There are two configuration of this aerator, the first uses a tube mounted at an angle in the water with a motor and intake the air above the water surface and the propeller is located below the surface, the second type has submersible pump supplemented with a vertical air intake tube open to the atmosphere. These types of aerators are manufactured in a variety of sizes from 0.37 to over 11 kwatt, the angle of the shaft with water surface made by supported float can be adjusted the control depth of the shaft operation (Boyd and Martinson, 1984; Kumar et al., 2010a).

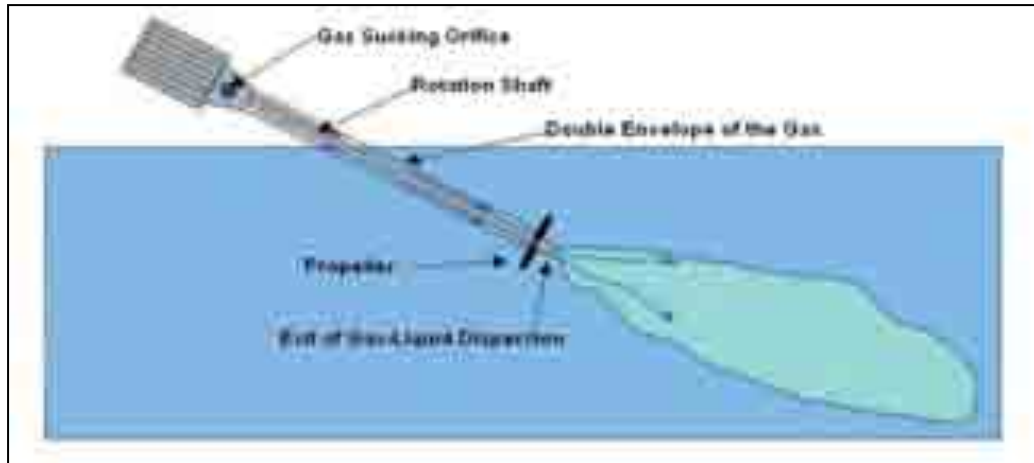


Figure (1.7): horizontal flow aspirating aerator, Aspirator, (AIRE-O2 Aeration Industries International).

### 1.1.5. Surface Aeration

This system will be discussed in detail in next section.

## 1.2. Surface Aeration for Water Treatment Processes

### 1.2.1. Types of Surface Aerators

There are many types of surface aerators that are implemented in water and wastewater treatment. They are primarily classified into several major groups (Cumby, 1987a; Sardeing et al., 2005; Stenstorm and Rosso, 2008)

#### I. Low Speed Surface Aerators

Low speed surface aerators are divided into two major categories:-

##### I.1. Low Speed Vertical Flow Aerators

The aerators in this category are the older types that generate an upward axial flow inside the tank and then the water is projected laterally in the air. They essentially consist in blades fixed under a tray or directly to the shaft of agitation. These blades are usually immersed in the water (See Figure 1.8).

This category contains some disadvantages that occur during the operation such as the emission of aerosols or unwanted smells or it is source of noise but all these can be overcome by installing a cover on the system unit. Usually the peripheral speed or the blades tips speed is about (4-5 m/s) but this may change depending on the types of motors used, like using powerful motors (75 KW) or using smaller motors. The volumetric power consumption may vary between (30-80 W/m<sup>3</sup>). The surface aerators

of down-ward axial flow are developed recently, where in this type floated agitators used, where the gas arrive point is fixed on the jacket of the aerator, the non-dissolved gas was captured by this jacket and then recycled toward the water.

There is low speed aerator with downward flow, where instead of propelling water droplets throw the air, the air is pumped into the tank near the impeller position and then dispersed downward (See Figure 1.9). The up-ward flow category contains some disadvantages that occur during the operation such as the emission of aerosols or unwanted smells or it is source of noise same us upward type.

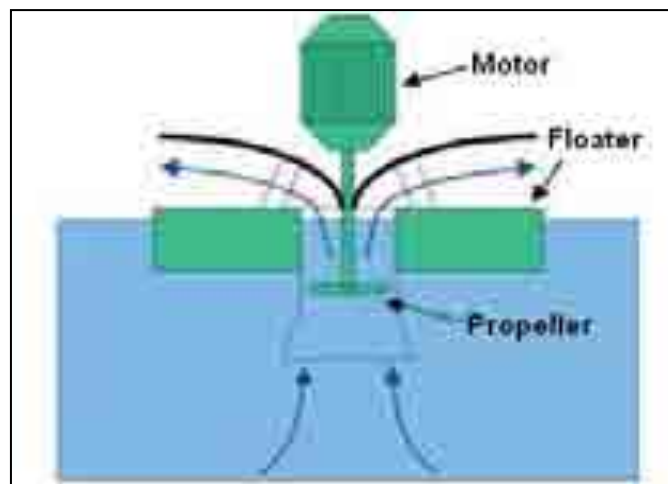
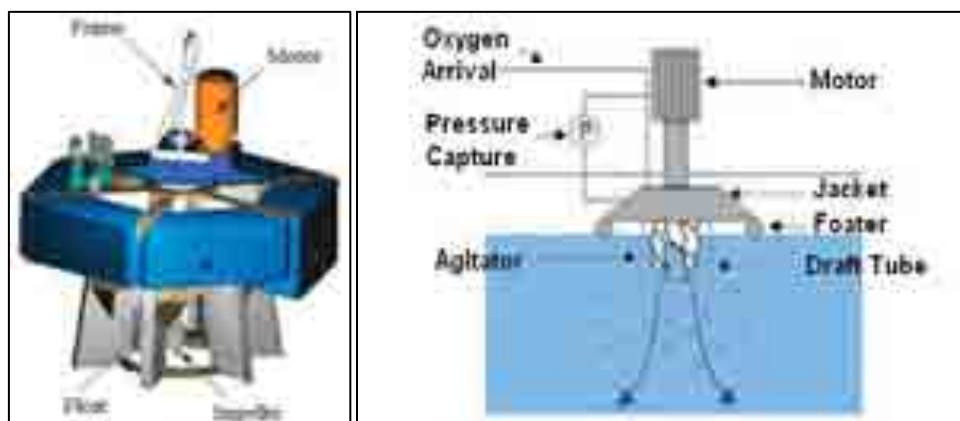


Figure (1.8): Low speed vertical flow aerator (Up-ward flow) (Praxair Technology).



(a)

(b)

Figure (1.9): Low speed vertical flow aerator (Down-ward flow), (a) Turboxal (Aire Liquide), (b) Praxair (Praxair Technology).

### I.2. Low Speed Horizontal Flow Aerators

These surface aerators are similar in action with vertical axis type. They are also called horizontal rotors. Their shapes are like horizontal cylinder with blades, steel angles, curvilinear or flat steel blades, plastic bars, or plastic discs. They are submerged in the wastewater at one-half diameter fixed on its surface. These aerators are usually used in oxidation ditches or in large rectangular treatment tanks. Their aeration work is occurred while they span the channel or the tank. These rotors spray the water up and down streams, with imparting a velocity to the water as the blades rise out of the water. The oxygen is transferred when the droplets contact the atmospheric air (See Fig. 1.10). The volumetric dissipated power is about ( $30\text{W/m}^3$ ). For the rotating diameters of ( $0.7\text{m}$ ), the peripheral speed at blade tips is about ( $4\text{m/s}$ ).



Figure (1.10): Low speed horizontal flow aerator (Twin mini rotor aeration, (Botjheng Water Ltd.).

### II. High Speed Surface Aerator

These aerators are usually used with electrical motors of rotational speed ranged ( $750\text{-}1500\text{ rpm}$ ) without reducer; generally they contain a propeller or other types of impellers with small diameter placed inside. The two advantages of this type are their moderate price and high flexibility to apply; on the other side they consume excessive energy and weak ability of agitation (See Figure 1.11). The oxygen transfer capability and power consumption of this type are close to the aspirating horizontal flow aerator.

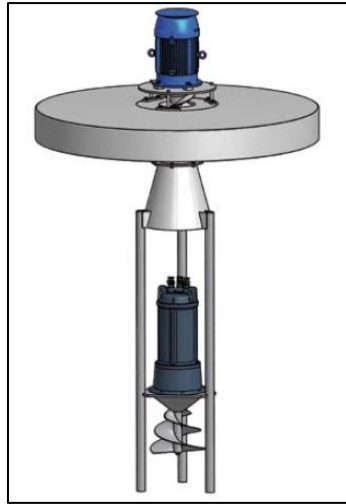


Figure (1.11): High speed surface aerator, Aqua turbo (AER-AS), (AQUATURBO SYTEMS inc.) .

### 1.2.2. Principals and Characterization

#### I. Principles

Surface aeration is a mechanical tool that used to entrain the atmospheric oxygen into the water bulk by surface agitation. The use of surface aeration becomes very important to overcome several difficulties in the aeration processes. Because of their simplicity and reliability and competitive oxygen transfer rate, surface aeration is a popular choice for biological water and wastewater treatment systems (Huang et al., 2009). It is applied to lessen the economic cost by decreasing the power consumption requirements compared to other types of aeration. The surface aeration is applied to improve the mass transfer rate between air and water by achieving larger interfacial contact between water and atmospheric air. The surface aerators are designed to promote growth of the aerobic micro-organisms, which in turn they reduce the biologically demanded oxygen (BOD) of the wastewater by increasing dissolving the oxygen in the water by creating largest possible contact area. This area is represented by several calculation parameters such as the standard oxygen transfer efficiency and the overall transfer efficiency.

The surface aeration process achieved either due to the projection and propelling the water into the atmospheric air then re-falling of these liquid droplets into the water again or/and the entrainment of the atmospheric air into the water by the rotation function of impellers placed inside the liquid phase. Mixing is essential with the surface aeration to insure the dissolution and the distribution of the oxygen of the air bubbles into the water for the falling droplets or the directly entrained air bubbles in inside the tank. The surface aeration includes the refreshment of water surface. In the water and wastewater treatment the rotation speed of surface aerator should be higher than specific speed which differs from one case to another on depending its operation

and configuration to prevent sedimentation of the deposits (Roustan, 2003). Surface aeration is applied to treat waters of needed rates of oxygen up to 80 mg/l h (Stukenberg et al., 1977).

The principle performances of the surface aerators and other types of aerators are delivering the oxygen to the aerobic micro-organisms at appropriate conditions (i.e. the temperature, impeller rotation speed .... etc.) and accomplishing a homogenous distribution of oxygen by the accompanied mixing process of the treatment tank. The characteristic parameters of surface aerators performance can be represented by various parameters that are related with the operation condition and the applied system configurations such as; the mass transfer coefficient of oxygen in clean water at standard condition  $kla_{20}$ . For example the values of  $kla_{20}$  between ( $3.5 - 10 \text{ h}^{-1}$ ) correspond to the standard capacity of oxygenation of ( $30 - 90 \text{ g/m}^3 \cdot \text{h}$ ) respectively and for a power consumption between ( $20-60 \text{ W/m}^3$ ) (Roustan, 2003; Roustan, 2005).

The optimum immersion of the surface aerator turbine is very important and varies from 2-3 cm to 15 cm depends on the type of turbine used. The treated standard specific wastewater properties may change due to the variation of several centimeters of the immersion of aerator. Also the power draw and the oxygenation capacity also change and each aerator turbine has its optimum rotational speed (Roustan, 2003).

When another impeller is employed with the main surface aeration turbine, this additional impeller is usually positioned below the main surface aerator turbine inside the water bulk. The lower impeller helps to disperse more of the air bubbles so the flow will be modified in order to draw the air bubbles or to delay their rising toward the surface.

The basic concept of the surface aeration is entraining the atmospheric air into the water bulk. This objective is accomplished either by:

- (i) Propelling the water from the surface by a turbine through the atmospheric air to create direct contact with the air and then entraining the air bubbles into the water with droplets impingement at the water surface.
- (ii) The second way of surface aeration is air entraining from the atmospheric air into the water bulk by the surface vortices that generated due to the impeller (usually axial) rotation; these impellers are positioned near the water surface, the entrained air bubbles are dispersed by the impeller blades (See Figure 1.12).

In the surface aeration process, there are numerous types of turbines that applied to entrain the air as bubbles into the water bulk, where during the last decades many types of impellers are invented to achieve the process successfully. Some of these impellers has equipped with auxiliary propeller to enhance the gas bubbles dispersion inside the water treatment tank.

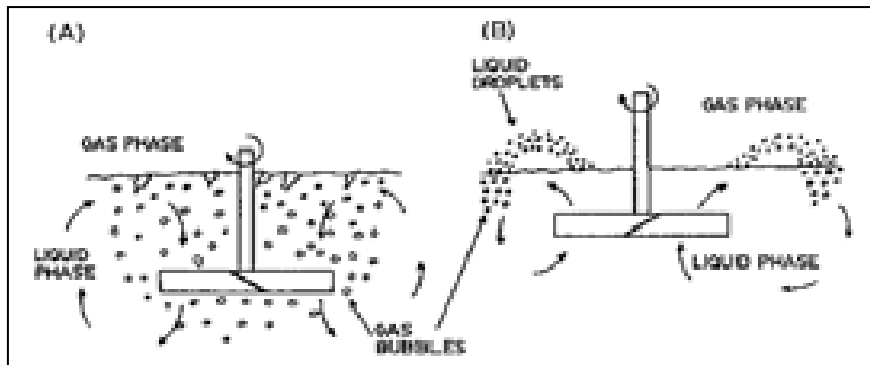


Figure (1.12): The surface aeration regimes applying air entrainment from free liquid surface (A) Direct entraining of the atmospheric air, (B) Spray formation and entraining the air with droplets impingement at the surface,(Patwardhan and Joshi, 1998).

Various geometries are developed for surface aeration turbines, where the design is emphasized to project highest quantity of water droplets into the atmospheric air by achieving the largest contact area between the two phases. The limiting factor for the surface aeration turbines is always taking in account reducing the radial discharge flow of the droplets toward water surface level. The circulation of the water and comprised air bubbles in the treatment tanks is generally consist of a main loop in entire the tank, many secondary loops can be generated depending on many system specifications like the number and type of impellers, tank geometry and impeller position in addition to many system characterizations such as air bubbles hold-up and retention time and else. For instance when the impeller is placed in the water bulk, the secondary loops may appear around the impellers, or they can be developed in the upper or lower part of the tank. When surface aeration turbine is positioned at the water surface, the water bulk is usually engaged with one main circulation loop. Deeper treatment tanks are generally preferred to ensure the needed residence time of the air bubbles but on the other hand these tanks need sophisticated tools to let air bubble reach the bottom of the tanks (Jakobson, 2008; McCabe et al., 1985; Nagata, 1975; Roustan, 2003; Tatterson, 1994; Xuereb et al., 2006) .

The circulation or mixing time is considered as a measurement indicator of the average water bulk motion that generated by the impeller in tank. Measurements of circulation and mixing times are considered as an indicator to understand the scalar transport in the tank (Edwards and Baker, 2001 ). The circulation time in the surface aeration is generally associated with; tank overall flow rate, air entrainment flow and impeller pumping capacity. For more complicated configurations with multiple impellers, the mixing or circulation time behavior depends on the created circulation resultant of these impellers, where it's not evident always when the number of impellers increased that leads to shorten the mixing time (Wang et al., 2010).

For continuous flow surface aeration systems that is the case with open channels, the circulation time is related with; the impeller speed, bulk motion and convective

transport (impeller water pumping capacity). Only one circulation is known during this process that is the overall circulation related with that actually is of two types of circulation times that the jet and mechanical agitation mixing times (Tatterson, 1991).

It is important to mention that surface aeration efficiency is highly affected by the ambient temperature, since the major part the aeration is achieved at water surface it is normal to have different efficiencies in winter and summer seasons. Each of surface aeration systems has its characteristics of operation condition, where the selection is generally made according to the view of the cost consideration and aeration efficiency (McWhirter and Hutter, 1989).

Table 1.1 illustrates the comparison of the standard aeration efficiencies for different aeration systems (SAE is defined as the transferred oxygen mass rate to the liquid per the power consumed at standard condition). This efficiency is dependent on the input power, air injection flow rate, the aerator submergence operation condition and tank or basin volume and geometry as it can be noticed in Table 1.2, the performance of fine bubble diffused aeration is varied according to the type of treatment. The pure oxygen aeration has higher standard aeration efficiency but this aeration system has limited application because it required pure oxygen source which is expensive.

Table (1.1): The standard aeration efficiency (SAE) for various aerators types

Aerator Type	SAE (KgO <sub>2</sub> /kWh)
High Oxygen Purity Aerator	(3.5-5.5) <sup>b</sup>
Submerged Jet Aerator	(2.1-2.55) <sup>h</sup>
Diffuser Aerator (Fine Bubble)	2.50 <sup>a</sup>
Horizontal Flow Surface Aerator	1.55 <sup>a</sup> , (1.5-2.1) <sup>b</sup> , 1.66 <sup>d</sup> , 2.2 <sup>f</sup> , 2.27 <sup>g</sup>
Slow Speed Surface Aerator	1.50 <sup>a</sup> , (1.9-2.2) <sup>b</sup>
Submerged Turbines (with Draft Tube)	(1.6-2.4) <sup>b</sup>
High Speed Surface Aerator	1.05 <sup>a</sup> , (1.1-1.4) <sup>b</sup> , 1.81 <sup>e</sup>
Submerged Turbines(Axial)	(1.0-1.6) <sup>b</sup>
Submerged Turbines(Radial)	(1.1-1.5) <sup>b</sup>
Diffuser Aerator (Medium Bubble)	1.00 <sup>a</sup> , 0.9 <sup>e</sup>
Aspirating Aerator	(0.4-0.9) <sup>b</sup> , 0.42 <sup>c</sup> , 1.6 <sup>e</sup>
Orifice Diffuser Aerator	0.60 <sup>a</sup>

<sup>a</sup> (Duchene and Cotteux, 2002); <sup>b</sup> (Mueller et al., 2002); <sup>c</sup> (Kumar et al., 2010a); <sup>d</sup> (Moulick and Mal, 2009);  
<sup>e</sup> (Cancino, 2004a); <sup>f</sup> (Boyd, 1998); <sup>g</sup> (Thakre et al., 2009); <sup>h</sup> (Taricska et al., 2009).

Table (1.2): The standard aeration efficiency of the fine bubble diffused aeration in different water treatment basins (Duchene and Cotteux, 2002)

Basin Type	SAE (KgO <sub>2</sub> /kWh)
Large Open Channels	3.41
Small Open Channels	1.95
Cylindrical Tank (Flat floor)	3.11
Cylindrical Tank (Grid Arraignment)	2.12

## II. Surface Aeration Systems Characterizations

The attempt to reach the desirable oxygen mass transfer in the different surface aeration systems depends on both the capacity of the oxygen dispersion in the water bulk and the achieved interfacial contact area between water droplets and air at the surface for the each method. The employed mixing impeller has very important effect on the flow of the water in the tank. Mostly the geometry of the tank and the surface aerator determine the limits between the surface aeration systems, moreover the performance of the surface aerator is highly affected by the properties of operating materials.

Usually the characterizing parameters for the surface aeration are mainly the achieved oxygen mass transfer, the agitation extent and the power consumption. Some of these general parameters are comprised in more detailed characterizing parameters such as impeller pumping number and other parameters of Froude number and Reynolds number.

Many modifications on the surface aerators were made to improve the performance. Numerous trials have been performed to enhance the operation efficiency by either of increasing the mass transfer rate  $k_1a$  or by reducing the power consumed in the operation. To evaluate these mass transfer or mixing performances of the surface aeration direct experimentations with either global determination of their values or local methods determination at numerous points in the vessel were made, the second method is considered effective because for example the size of bubbles are not uniform along the vessel so the mass transfer coefficient will vary according to that.

The effect of influencing parameters can be determined with varying several parameters such as impeller rotational speed, impeller and tank geometry and fluid properties. Various models were derived to relate the important dimensionless numbers such flow number (pumping number)  $N_{Qp}$ , (which contains flow rate effect, impeller rotational speed), Froude number ( $Fr$ ), (the ratio of inertial forces to

gravitational forces), the related gas measurements (circulated and dispersed) and the vortex regions characteristics around the impeller if it exists, and other geometric dimensionless factors for the aeration system. These dimensionless factors were proposed to characterize the performance of the surface aerators. The power consumption is usually presented as the dimensionless number of Power number, ( $N_p$ ), which depends on the type of the aerator and also depends on the Reynolds number of the system. Usually the power number is between 0.4 - 1 according to the type of the surface aerator impeller implemented for consumed power per unit volume that varied between 20-50 W/m<sup>3</sup> (Heduit and Racault, 1983a).

The effect of gas hold-up (air flow in the tank) on the rotational speed can be identified as more gas holdup exists that results in more difficulties to recirculate the air bubbles in the tank due to longer circulation paths for liquid because of gas voids presence and the separation of the gas from liquid in the upper region of the tank, these effects can be accounted by using the gas flow rate measurements (Nienow, 1997).

The relation between the interfacial area, gas holdup and bubble diameter is commonly determined by employing gas dispersion approaches, which is achieved by using the equation of continuity and motion with bubbles population balance including bubble size and concentration distribution, bubble coalescence and dispersion mechanism (Tatterson, 1994).

Most likely with agitated aerated tanks systems two sets of experiments are done to evaluate the system potentials, first the experimental run in a lab-scale or in a pilot plant system to calculate power consumption, liquid hydrodynamics, flow patterns and mass transfer coefficient. And the second is determining same parameters in the same configurations with resort to CFD to specify the opportunities to gain better efficiency of the system by relocating or changing the geometrical positions of the system components (Tatterson, 1991).

### **III. Dissolved Oxygen Concentration Gradient Calculation Methodology**

The dissolved oxygen concentration transfer principle for surface aeration process has been studied and investigated by many papers taking into account the factors that affect the transfer of oxygen from the air to wastewater and the contained activated sludge.

To model the oxygen mass transfer toward the water direction there are many theories that describe the oxygen gas concentration gradient such as the two film theory, penetration model, film-penetration model, surface renewal-damped model and turbulent diffusion model.

The two film model was found more simple and close to simulate the occurred process in our case, where it presumes that two laminar films for gas and liquid exist regardless of the turbulent condition (Taricska et al., 2009).

The oxygen gas transfer to water (liquid phase) is generally represented by two mass coefficients of gas and liquid side,  $k_g a$  and  $k_l a$  respectively, with assuming that Sherwood numbers  $k_g L/D_{if}$ ,  $k_l L/D_{if}$  are same for both sides, where  $k_l$  and  $k_g$  change as a characteristic length,  $L$  and the diffusivity changes,  $D_{if}$  (Taricska et al., 2009).

For aeration system, the high diffusivity in gas film (oxygen) and low diffusivity in liquid film (water) leads to assume the mass transfer with concentration gradient in gas phase is negligible, so the  $k_l a$  become the most important coefficient in the aeration process (Tatterson, 1991).

The principal model that commonly used for oxygen mass transfer in the aeration operations depending on the mentioned assumptions is:

$$dC/dt = k_l a (C_s - C) \quad (1.1)$$

Where,  $C$  and  $C_s$  represent the concentrations at any time and at saturation state respectively

(Stukenberg et al., 1977) investigated the effects of biomass presence parameter in wastewater treatment on the final determination of the oxygen mass transfer performance model that presented by equation 1.1; they modified this principal model that commonly used for oxygen by adding the oxygen transfer correction factor  $\alpha$ , and oxygen saturation correction factor  $\beta$ , as shown in equation 1.2, where  $dO/dt$  represents oxygen concentration change with time.

$$dC/dt = \alpha k_l a (\beta C_s - C) - dO/dt \quad (1.2)$$

While, (Dudley, 1995) has derived a new oxygen mass transfer model that represent the surface aeration process. He suggested that the previously used models couldn't represent the true condition of oxygen distribution inside the entire aerated tank. (Dudley, 1995) derived the following model:

$$dC/dt = \alpha k_l a (\beta C_s - C) - r MLSS - u_s (dC/dz) \quad (1.3)$$

Where,  $MLSS$  is the mixed liquor suspended solids (the water with containing microorganisms);  $r$  is the specific respiration rate;  $z$  is the length of each stage and  $u_s$  is the liquid velocity. The modified model takes in account the correction from water conditions to mixed liquor. This general model proposes a relative improvement in the oxygen mass transfer coefficient ( $k_l a$ ), but it still didn't reach the required true value depending on standard operation conditions. (Ju and Sundarajan, 1992) found in their studies on the oxygen transfer in surface aerated bioreactors with containing microorganisms that the presence of the biomass showed no effect on the oxygen transfer rate to water because of their formed film adjacent to the gas-liquid film is

extremely small. So its resistance to oxygen transfer is considered negligible and the correction factor  $\alpha$  can be set to 1 when experimental investigations are made on the oxygen mass transfer to simplify the calculation and to prevent over estimation of the biomass effect on the calculated  $k_L a$ .

The previous oxygen mass transfer model that applied to calculate  $k_L a$  had been modified by (McWhirter et al., 1995) for surface aerator. They had divided the mass transfer process zone into two essential zones: the first is for the droplets projection from aerator turbine blades tips till it impinges the liquid surface, where they derived a new model for this purpose by considering the liquid droplets traverse in continuous infinite atmospheric air (gas) phase, the overall oxygen concentration distribution within the two zones was:

$$C_L = (A C_d^* + B C_{LS}^* / A + B) + (C_S - (A C_d^* + B C_{LS}^* / A + B)) \exp(-(A+B)t) \quad (1.4)$$

Where,  $A = Q E_{md} / V_L$ ;  $B = k_{LS} a_s$ ;  $C_d^*$  and  $C_{LS}^*$  are the saturated concentrations in the droplet and water respectively and  $E_{md}$  is Murphree efficiency for the operation.

(Oliveira and Franca, 1998) modified the previously developed model for oxygen transfer by (McWhirter et al., 1995) to represent the surface aeration for the turbines that placed in water sub-surface position. They tried to simplify the model by applying boundary initial condition and other considerations and assumptions to eliminate the low effecting parameters, so they found the following model for oxygen mass transfer coefficient with certain conditions:

$$dy/dz = -A_t / G k_L a (C_L^* - C_L) K_2 \quad (1.5)$$

With applying Henry's law and rearranging the equation the found following model was:

$$C_L^* = C_{st}^* (1 + y_o / y_o) [(P_b - P_v + \rho_L g (Z_s - Z) / 1 - P_v) y / y + 1] \quad (1.6)$$

$$C_{st}^* = 32 \rho / 18 H (1 - P_v) (1 + y_o) / y_o \quad (1.7)$$

Where  $C_{st}^*$  is the standard DO level;  $P_b$  is the barometric pressure;  $P_v$  is the vapor pressure;  $G$  is the gas flow rate;  $K_2$  conversion factor;  $A_t$  is the tank cross-sectional area;  $C_L^*$  represents the true bulk liquid DO level;  $y_o$  is the oxygen concentration in the bubbles at ( $z = 0$ ); and  $H$  is Henry's law constant. (Oliveira and Franca, 1998) tested these models with the previous models experimentally, where they found that acceptable fitting between the experimental and theoretical results, where the dissolved oxygen at equilibrium state is decreased with increasing the temperature, the highest oxygen transfer is noticed with low temperature values.

(Stukenberg et al., 1977) have studied the probability of the calculation errors with several types of aeration equipment including the surface aeration. They studied the

procedure conducted to determine the dissolved oxygen concentration in the tanks for different test durations and various effects on the exact results values of the concentration and they compared between the theoretical and experimental results for the achieved saturated dissolved oxygen and the mass transfer coefficient. They made a comparison made between two methods. They called them the direct and conventional of mass transfer coefficients, where they found that the different is by the way of calculation. They investigated practically the evaluating important parameters of the aeration in details like the methods to determine the dissolved and saturated and  $\alpha$ , was discussed with suggesting the most correct results can be obtained.

#### IV. Surface Aeration Oxygen Mass Transfer

It is very hard to classify the investigations and studies that made for the surface aeration, as the influence of the relevant parameters is very merged and blended. So it is quite tricky to identify what is criterion for the classification among the affecting parameters when describing mass transfer operation or hydrodynamics in surface aeration. The guidelines for this classification in this literature depend on the main axes those were followed by the achieved studies in this domain.

(Heduit and Racault, 1983b) made a general assessment of the oxygen mass transfer coefficient and aeration efficiency for the various surface aerators types that operate in field. Among their study they found that about 85% of 111 tested low speed surface aerator aeration efficiencies were between 1.2-1.9  $\text{kgO}_2 / \text{kWh}$ , and the average aeration efficiency for all low speed turbines were 1.49  $\text{kgO}_2/\text{kWh}$  as shown in the Fig. 1.13.

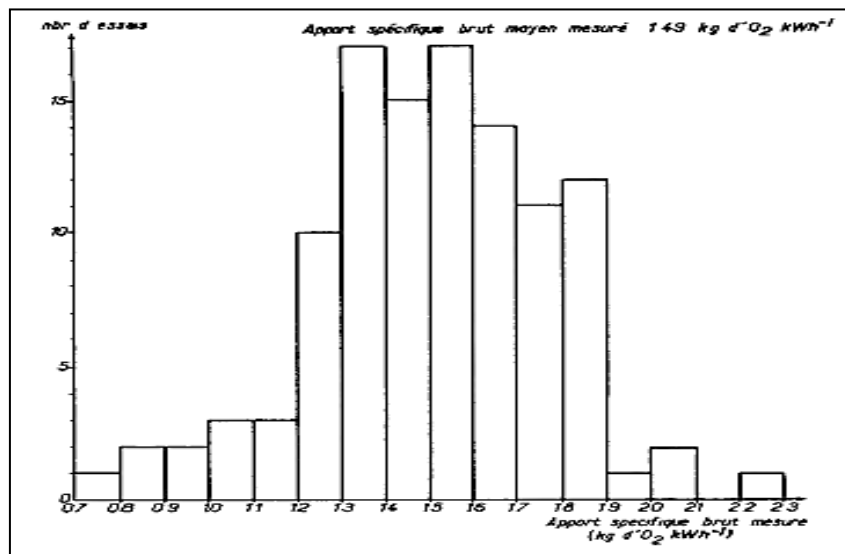


Figure (1.13): The histogram distribution of measured aeration efficiency for (111) low speed surface aerators in field, the average is 1.49  $\text{kgO}_2/\text{kWh}$ , (Heduit and Racault, 1983b).

(Fan et al., 2010) considered the surface aeration mass transfer operation is consisting of three zones, they have created CFD model for a system of high speed surface aerator. They found the most effective one is the mass transfer during the water spray in the air and they assumed the ratio of re-aeration or air entrainment by water droplets when impinging the liquid surface is not effectual. (Fan et al., 2010) employed a single phase three- dimensional CFD model for fluid flow simulation to represent the flow and dissolved oxygen distribution inside the tank and they depended on the experimental results of dissolved oxygen in two positions in the tank and the overall mass transfer coefficient, where the difference between them was quite little.

(Patil et al., 2004) derived a general correlation for the surface aerators process mass transfer depending on the previous works in the same field. They related oxygen mass transfer coefficient with the effect aerator geometry and the operation condition and power consumption in one model, the range of volumetric power consumption range for this model is  $90 < P/V < 400 \text{ W/m}^3$ .

$$k_L a/N = 7 * 10^{-6} N_P^{0.71} Fr^{0.48} Re^{0.82} (h/D)^{-0.54} (V/D^3)^{-1.08} \quad (1.8)$$

#### IV.1. Operational Condition Effects

(Zlokarnik, 1979) has related the mass transfer performance for different aerator types with the operational parameters such Froude number and Reynolds number and other geometrical factors with changing the numbers and forms of impellers blades. He formulated a dimensionless formulation that combines all the surface aerator efficiency term (E) with aeration number and Froude number with what he called sorption number (Y), which is a dimensionless number and represents the oxygen transfer, the model was developed for the ratio  $h/D = 1.0$ ,

$$E^* = Y N e^{-1} Fr^{-3/2} = \frac{G D^{0.5}}{P \Delta c} \rho (v^2 g^5)^{1/6} \quad (1.9)$$

Where,  $Y = G/\Delta c d^3 (v/g^2)^{1/3}$ ; G represents the oxygen uptake rate.

##### A. Rotational Speed Effect

The status of surface aeration changes due to the increasing the rotational speed as founded by (Albal et al., 1983) in their investigations with the effect of operational conditions. At low speed the oxygen gas transfer occurs only by diffusion at the oxygen-water interface. With increasing the speed the oxygen mass transfer rate is developed by creation convective forces inside the liquid, where velocity of air bubbles increased, with further rotation speed increasing that leads to higher air bubbles entrapped into the water bulk. (Backhurst et al., 1988) found out same

relation between the rotation speed and surface aeration efficiency with pilot and full scales.

A critical rotational speed of the surface aerator (starting with this speed the aeration efficiency or the oxygen transfer begins increasing relatively) can be observed when the effect of rotational speed and the geometric parameters on the oxygen transfer efficiency were tested as presumed by. The bubbles were created when the water droplets hitting the water surface, in consequence the liquid bulk circulation and the air entrainment are forming. (Takase et al., 1984) derived a model to represent the standard aeration efficiency for the critical rotation speed higher in square tank:

$$SAE = 6.6 * 10^{-6} (ND)^{-0.1} (D/W_T)^{0.4} (D/h + W_T)^{0.5} \quad \text{for } D/W_T = 0.24, h/D = 2.5 \quad (1.10)$$

Where;  $W_T$  is the square tank width.

### B. Number of Impellers Effect

(Veljković and Skala, 1989) have investigated the number of impellers that implied for surface aeration process. They reached to the conviction of utilizing two impeller gives higher oxygen transfer rates than using one impeller for turbine impeller type and same rotation speeds, where the position of upper impeller at the water surface enhances the intensity of surface aeration.

While a system of surface aeration consists of three immersed impellers may have better operation performance for the gas holdup and dispersion consideration inside the liquid as proposed by (Li et al., 2009). They examined several groups of three impellers systems for the flow pattern, mass transfer coefficient. They found that the three impeller system had very important effects on the gas distribution inside the tank. They also found from results the best impellers combination was Rushton disk turbine RTD, Techmix 335 hydrofoil impeller up-flow TXU and half elliptical blade disk turbine HEDT distributed from above to bottom respectively.

### C. Liquid Level Effect

The controlling factor that influences more the oxygen transfer is the liquid level beside the rotation speed as founded by (Thakre et al., 2009) from their experimental results. They have developed a correlation model for the oxygen mass transfer coefficient in the oxidation ditches by applying curved rotor aerator, where these relevant parameters presented in the developed model.

$$k_L a = 0.000746 [(N)^{1.768} (h/D)^{1.038} (\alpha)^{0.031}] \quad (1.11)$$

Where:  $\alpha$  is the blade tip angle. This model is applied within these ranges of  $Re * 10^3$  (50-84) and  $S/D$  (0.17-0.25).

D. Clearance and Submergence Effect

(Backhurst et al., 1988) examined the effect of blade submergence on the oxygen transfer rate for different impeller types. Their results showed that there is an optimum submergence (starting with submergence an efficient aeration is noticed) for all tested impellers as illustrated in the Fig. 1.14.

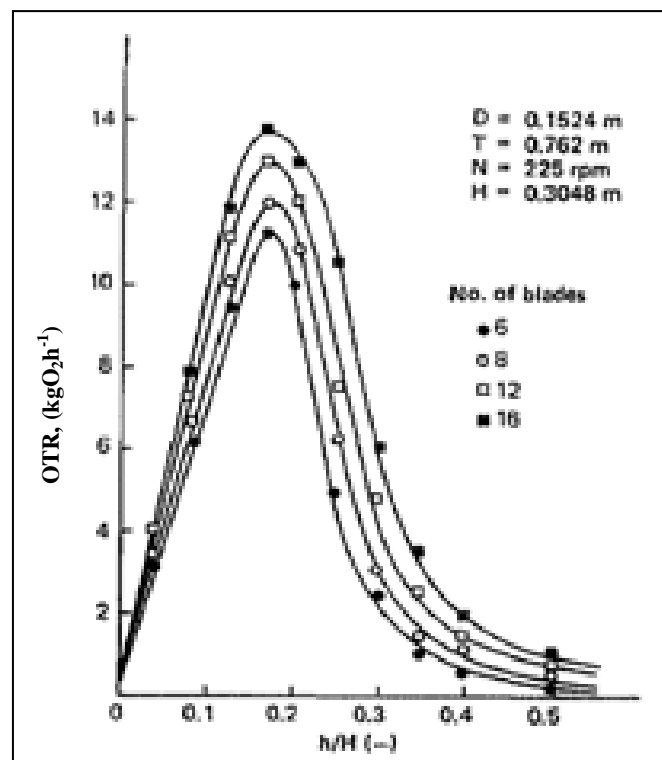


Figure (1.14): The relation between surface aeration impeller blades submergence and oxygen transfer rate for different blades number, (where H is the liquid level in the tank) (Backhurst et al., 1988).

The clearance of surface aerator impeller in the treatment tank is commonly defined as the distance between the lowest point of surface aerator and the tank bottom. While the submergence is defined as the distance the water surface level and the specific point on surface aerator blade. (Patwardhan and Joshi, 1998) concluded that with increasing the submergence of surface aerator impeller the intensity of surface aeration, oxygen transfer rate and gas hold up are decreased. They explained that the amount of energy reaching the liquid surface is decreased. That also agrees with the results obtained by (Backhurst et al., 1988). It is better always to set the impellers in closer position to the liquid surface to enhance the reached energy to the liquid surface and increase the gas holdup. This persuasion was found by (Deshmukh and Joshi, 2006) by testing three types of surface aerators impeller of PBTU, PBD and

DT. In their experimental work (Deshmukh and Joshi, 2006) examined each type by varying the rotational speed with submergence for each type of impeller.

For these three different types of impellers that applied for surface aerator; PBTD, PBTU and DT impellers, (Patil et al., 2004) found that an optimum submergence position for PBTD can be found. Where best mass transfer coefficient was reached with submergence ( $S/D$ ) that equals 0.2 and rotation speed of (2.5 1/s) for tank diameter 1.5 m. (Patil et al., 2004) studied the positions for three types of the impellers; pitch blade turbine up-flow PBTU, pitch blade turbine down-flow, PBTD and disc turbine, DT, where for all effective operations the impellers were located near the liquid surface. They found that generally with increasing the submergence the number of eddies at gas-liquid contact area were decreased, also the maximum jet size accomplished by the impeller blades location at just near in the water. The maximum value of  $k_L a$  was at the submergence ratio of 0.12D that was accomplished by PBTU type. The other types didn't have the same ability to project the liquid in the air. (Patil et al., 2004) determined the effect of impeller clearance, where the tests were conducted with keeping the submergence constant where for impeller diameter that equals  $T_v/3$  it was found that optimum  $k_L a$  found at the clearance of (1.98D), but for the impeller diameter that equals  $T_v/5$  the  $k_L a$  was noticed decreasing constantly with increasing the clearance.

### IV.2. Geometry Effect

It is so difficult to categorize the most important geometric parameters in surface aeration for various techniques that implied in the surface aeration (Kumar et al., 2010b), but generally it is found that there are frequent parameters that can affect performance for the majority of the surface aeration as following:

#### A. Tank Geometry

The surface aeration for water treatment is usually performed in cylindrical shape tanks or basin, which are the most usual among the used tanks, but the geometry of these cylindrical tanks may vary between plate bottom shape to curved and conical shape (with  $15^0 - 30^0$  degree angle depending of the existed activated sludge properties). The volume of the tank is commonly related with the height of the liquid in the tank (Jakobson, 2008). Square or rectangular shape are also used but in very limited way and for special uses. On the whole, the water treatment tank volume that equals height of the liquid is considered as standard geometric ratio for design considerations.

(Rao and Kumar, 2007b) have derived a model for circular shape aeration tank, where the derived model relates the mass transfer coefficient of oxygen,  $k_L a$ , with circular

tank on the basis of theoretical power input to the system. The mass transfer coefficient used for theoretical power per volume, for baffled tank is:

$$k = (3.26 \exp[-0.56/X] + 0.21 - 0.426 \exp[-0.47(X - 0.878)^2]) 10^{-6} \sqrt{X} \quad (1.12)$$

Where X represents the theoretical power/ liquid volume ( $Fr^{4/3}/Re^{1/3}$ ) and  $k = k_{La20}(v^2/g)^{1/3}$ , the model is developed for the geometric ranges;  $h/D = 1.0$ ,  $S/W = 1.26$  and  $W/D = 0.24$ .

The experimental results of (Rao and Kumar, 2007a) showed that the square tank aeration was also effective in surface aeration process, where higher values of mass transfer coefficient k are achieved in shorter duration (that doesn't agree with previous works where the square shape not preferred because the formation of dead angles exist) but in the power requirement point of view the circular aeration tanks were more effective for less amount of power was required to reach the value of mass transfer coefficient with keeping the other conditions constant during the experiment. For square tanks, (Rao and Kumar, 2007a) verified a correlation that was developed earlier in the previous work (Rao, 1999), which represents the mass transfer and power measurement on electrical measured basis. The general correlation found by (Rao, 1999) was for the mass transfer parameter k (where  $k = k_{La20}(v^2/g)^{1/3}$ ), as a function of geometric and physical properties that referred as, X, the ratio of the Froude Number Fr, to Reynolds No., Re, for a baffled tank:

$$k = [17.32 \exp(-0.3/X^{1.05}) + 3.68 - 0.925 \exp(-750 X - 0.057)^2] 10^{-6} \sqrt{X} \quad (1.13)$$

Where; X is ( $Fr^{4/3}/Re^{1/3}$ ). This model is applicable within X range of (0.01 – 8.0) and it is developed for the geometric and operational ranges;  $h/D = 1.0$ ,  $S/W = 1.26$  and  $W/D = 0.24$

(Fuchs et al., 1971) have studied the surface aeration performance by examining the effect the volume of the aeration tank according to volumetric power provided to the operation, where they tried to keep the mass transfer coefficient constant during the tests. (Fuchs et al., 1971) founded that the oxygen mass transfer coefficient was generally increased as the volume of aeration tank is decreased for large volume tanks, a satisfactory results found for high levels of provided power per volume ratios

### B. Baffles Effect

Baffles are commonly used in the water treatment tank, where they are fixed near the walls of the tank to reduce or prevent the formation of vortex that are generated because of the centrifugal force created by impeller rotation especially when cylindrical vessels used and when the impellers are centrally positioned in the vessel

(Jakobson, 2008). In general the baffles are considered as vertical blades works to divide the primary motion into axial and radial movements according to the model used. The number of baffles that used may vary according the method of use, but generally the numbers between two and four are advocated (to do their mission perfectly) because one is not enough to prevent the formation the vortex. It is very necessary to put them in symmetrical form and it is advised to choose the number of the baffles same with the number of the blades of the used impeller for reducing the symmetrically mechanical stress on the shaft. The width of the baffles usually chosen as  $(T/10)$ , are not touched (affixed) to the walls, the distance between the baffles and the walls is usually  $(T/50)$ , and the long of the baffles is generally exceed the surface of the liquid and reaches tank bottom (Treybal, 1980; Xuereb et al., 2006).

(Lines, 2000) has used a dual impeller surface aeration system to find the effect of three types of baffles on the aeration with changing impeller speed and liquid height. With angle-blade turbine and six flat-bladed discs turbine, the highest mass transfer was obtained with 4-half height wall baffles and the gas-liquid mass transfer coefficient was decreased with increasing the liquid height.

(Rao and Kumar, 2007b) investigated the effect of the baffles in circulated shape tanks for wastewater treatment aeration process. They tested the performance of the system by calculating the  $k_L a$  for both ratios of actual and the theoretical power per unit volume. They applied a simulation of oxygen transfer coefficient in the two cases. They deduced that the baffled system is more efficient in the treatment process but it also more power consumer so they recommended using un-baffled system for long duration treatments, where the power consumption will be more important. The baffled circular shape tank system can be used for short duration treatment or in rapid aeration process, where power consumption was less importance. They derived two models for un-baffled and baffled tanks. For un-baffled as shown in following equation:

$$10^5 k = 7.38 P_V \exp(-0.189/P_V) + 0.33(P_V)^{0.5} \quad (1.14)$$

For baffled tank:

$$10^5 k = 3.95 P_V \exp(-0.85/P_V) + 0.15(P_V)^{0.5} \quad (1.15)$$

Where,  $P_V$  = actual or measured power/ volume and  $k = k_L a_{20} (v^2/g)^{1/3}$ . These models are developed for the geometric and operational ranges;  $h/D = 1.0$ ,  $S/W = 1.26$  and  $W/D = 0.24$ .

### C. Draft Tube Effect

Draft Tubes are used some times with the surface aerators to centralize the return flow to the impeller and to centralize the direction and velocity to the suction region (inward) of the aerator turbine.

It is needed to modify the surface aeration systems by adding draft tube to prevent vortex formation or to enhance flow patterns. (Kirke and El Gezawy, 1997) in their investigations have tested the effect of draft tube presence on the impeller function. They found out the flow profile is improved and axial velocity rate was higher with using the draft tube.

(White and De Villiers, 1977) have investigated the relation between the presence of the draft tube and its effect on the aerated agitated tank oxygen mass transfer performance. They found that it has remarkable effect on the aeration number  $N_A$ , where they observed the increasing in applied pressure and reduction of hydrostatic head of water was maintained by the existence of draft tube.

### D. Surface Aerators Geometry

Many types of aerators are used in the surface aeration; the design characteristics changes due to the required operations. There is wide diversity of the impellers that can be implemented in the surface aeration according the needs for each specific case. The axial and radial impellers are used with many shapes and forms depending on the particular conditions of the operation and the aim of the process. The most used axial impellers types are the pitched-blade propeller and hydrofoil propeller. There are numerous types of turbines that used in surface aeration. The number and the shape of blades can be changed to curved, pitched and inclined blades if there are needs for special performance. The turbines can participate to generate homogenous flow inside the tank and prevents the air bubble rise to the surface of the liquid and they are able to form a shear due to the force gradient of the velocity which is essential for the systems of gas-liquid, where it improves the oxygen mass transfer as a result of this shear that localized in reduced zone and by this the turbulent intensity was increased (Roustan, 2003; Tatterson, 1994; Xuereb et al., 2006). It is important to know that not all the turbines can act as successful aerator for all cases, where there are specific impellers types that are suitable to perform the surface aeration correctly for each case, as (Roustan et al., 1975) figured out by comparing several types of aeration systems.

(Cancino, 2004a) made a comparison of the performance of several types of axial flow surface aerator that conducted in (Cancino et al., 2004), where he tried to compare between these configurations in depending on factors such (water splashed flow/ power consumption ratio,  $Q/P$ ) and mass transfer coefficient with changing the aerators geometric configurations like blades shapes and their types with inlet and outlet angles of the water flow. He found that not always the increasing of aeration efficiency is accompanied with increasing mass transfer coefficient because other important factors may affect the aeration like the types of blades, inlet and outlet angle and pattern of water projection in the air (i.e. the droplets that well dispersed). In his assessment he preferred to take the ratio ( $Q/P$ ) than using  $Q$ , itself because the behavior of aeration efficiency with water flow is not clear where it is affected by the

power consumption. The best global mass transfer coefficient at 10 °C yielded was (3.249 1/h); best standard aeration was SAE (1.805 kg O<sub>2</sub>/kWh) for the flat propeller type.

In depending upon of the work of (Cancino, 2004a; Cancino et al., 2004),(Cancino, 2004b) investigated the best configuration of aerators groups in order to develop a model by applying the dimensional analysis. He has chosen the most important geometrical parameters that affect the process beside other parameters to characterize two different aerators, the flat and pitched blade (PB) types. The results and application of correlation equation showed difference in accuracy between the types of aerators used, where the equation was about 80.3% close to the experimental results for the flat propeller type, while it was about 56.5% accuracy to the experimental results for other types. The general model he for flat blade impellers:

$$AE = (\rho Q/P)^{-0.0461} (DN)^{-0.9345} (Re)^{0.003778} (Fr)^{1.3696} (\beta_2)^{-0.598} (D/S)^{0.039} \quad (1.16)$$

AE is the aeration efficiency (it is defined as the transferred oxygen mass rate to the liquid per the power consumed at actual condition).

For pitched blade impellers

$$AE = (\rho Q/P)^{-0.02678} (DN)^{-5.7148} (Re)^{-0.3388} (Fr)^{4.8695} (\beta_2)^{-0.3676} (D/S)^{-0.1256} (\beta_1)^{0.2} \quad (1.17)$$

Where Q is the water flow splashed by the aerator;  $\beta_1$  is 1/Inlet angle of paddle (rad<sup>-1</sup>);  $\beta_2$  is 1/Outlet angle of paddle (rad<sup>-1</sup>). The model is developed for impeller blade submergence (58% - 228%).

For paddle wheel surface aerators performance, (Moulick et al., 2002) established a general model by finding a modified standard aeration efficiency termed SAE'. They verified the model by performing several set of experiments with varying the geometric configuration for each one with SAE' to reach the optimal geometric parameter, where they varied the paddle width / impeller diameter ratio, liquid volume/ impeller diameter, impeller pitch/ impeller diameter and horizontal projection of bent length / impeller diameter and bent angle. The correlated general equation was:

$$SAE' = [-147 \times e^{(0.151X)} + 0.176(X)^{3.13} + 178.48 + 33.84X - 9.03 \times \ln(67.51X)] \times 10^{-5} \quad (1.18)$$

Where (SAE') = (SAE) (v/g<sup>2</sup>)<sup>1/3</sup> (Δc)<sup>-1</sup> .ρ .N<sup>3</sup> . D<sup>2</sup> and X= Fr<sup>4/3</sup>/Re<sup>1/3</sup>. The ranges of this model are; Re (2×10<sup>5</sup> - 8×10<sup>5</sup>), Fr (0.05 – 0.25) and (S/D)<sub>paddle wheel</sub> (0.025-0.225).

(Zlokarnik, 1979) compared between different surface aerator types with respect to the oxygen mass transfer. He found that the surface aeration is highly influenced by several geometric ratios. The investigation he made was as a function of aerator type and their geometrical specification with other operational parameters like Froude

number and Reynolds number for different aerator types with changing the numbers and forms of impellers blades (See Figure 1.15).

(Patil et al., 2004) found out the surface aerator with the PBTU type was the best in the general in comparison between the impellers for surface aerator; PBTU, PBTU and DT impellers within the tested range of system configuration with respect to the values of mass transfer coefficient achieved by these aerators.

(Deshmukh and Joshi, 2006) have tested the impeller geometry effects on the liquid flow profile for the surface aeration system with impeller placed in water sub-surface position. They tested different impeller types PBTU, PBTU and DT. The results showed that the performance of PBTU was the worst between the impellers according flow patterns in the tank with increasing the rotation speed, where the created flow was unsatisfactory and didn't cover all parts of the tank in contrary to the rest two impellers PBTU and DT.

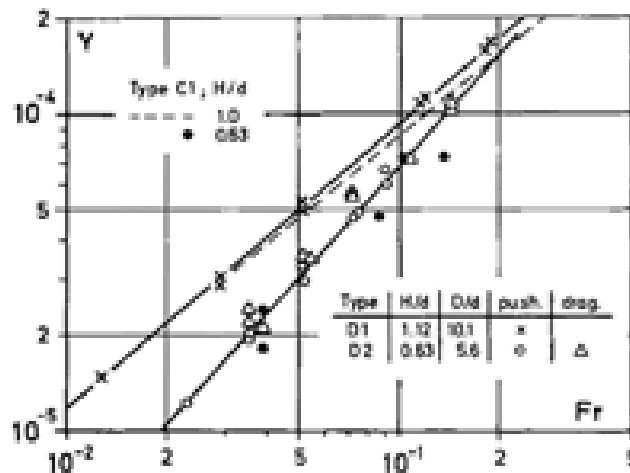


Figure (1.15): Relation between sorption number (Y) with the Froude number (Fr) for the conical shape turbine surface aerator (Zlokarnik, 1979).

(Backhurst et al., 1988) built a correlation for the OTR (The oxygen mass transfer rate to the liquid during the aeration (kgO<sub>2</sub>/h)) with affecting factors like the geometric parameters, the flow and water surface conditions in the surface aeration system:

$$OTR=10^{-3}(DC_s D_m) Re^{1.90} Fr^{0.15} (D/h)^{0.2} (S/h) (n/n_8)^{0.20} (T_w/D)^{0.05} \quad (1.19)$$

Where n is the number of turbine blades; D<sub>m</sub> is the oxygen diffusivity coefficient in water at 20°C; and C<sub>s</sub> is saturation concentration, the specification for the tested surface aerator of this model are illustrated in Figure 1.14.

### D.1. Surface Aerator Diameter

Surface aerator impeller diameter is usually related to the tank dimension, for example a minimum turbine diameter should be corresponded to the tank diameter (i.e. for circular shape tanks,  $T_v/5$ ) and to the depth of the tank to minimize the risk of dead zone existence and that occurs more in the lower part of the treatment tank. It is important for radial surface aerators diameter to keep the  $D/T_v$  ratio in a particular range in order to keep the energy consumption within accepted range (Oldshue, 1983; Tatterson, 1994; Treybal, 1980; Xuereb et al., 2006).

(Patwardhan and Joshi, 1998) figured out after reviewing many papers of various surface aeration processes of air entrainment from free surface that the surface aeration intensity, the oxygen mass transfer coefficient and suspension ability of biomass are increased with increasing the impeller diameter due to increasing surface turbulence and high velocity performed inside the liquid bulk. They tested the effect of impeller diameter on surface aeration efficiency for both laboratory and industrial scales.

The effect of the aerator diameter has been tested by (Patil et al., 2004), the ratio of  $(P/V)$  (consumed power per liquid volume) had considered as distinguishing factor for different aerator impeller diameters, where for  $(P/V < 100 \text{ W/m}^3)$  the impeller diameter that equals  $T_v/5$  exhibit in some kind more higher mass transfer coefficient but for range  $(P/V > 150 \text{ W/m}^3)$  the impeller diameter that equals  $T_v/3$  showed higher values of mass transfer coefficient.

## IV. Temperature Effect

Since the solubility of the oxygen in the water is highly temperature dependent factor. The temperature effect is very limiting factor when the calculations are made for the oxygen mass transfer to the water in the surface aeration. The calculated oxygen transfer coefficient should always be corrected to standard temperature condition to allow a meaningful understanding and assessment of this coefficient which in turn helps to characterize the surface aeration efficiency of the concerned process.

The oxygen transfer rate can increase with temperature increasing, as the viscosity of biomass in treatment tank is reduced with temperature elevation so the surface mobility increased as proposed by (Cumby, 1987a).

The temperature has contradictory effects on oxygen mass transfer, where the mass transfer coefficient is decreased with temperature increasing in the droplets while it slightly increased with increasing the temperature in liquid bulk as founded by (Chern and Yang, 2004) in their investigation for the performance of aeration system by spraying the water droplets through the atmospheric air and then re-impinging with the surface liquid bulk. They studied the distribution of dissolved oxygen concentration in the droplets and inside liquid bulk and the turbulent flow created by

the impinging of droplets with the surface of liquid. Beside the different effects on the system liquid like the height of droplets, recirculation rates of droplets and liquid depth; (Chern and Yang, 2004) examined the effect of air condition, like temperature and humidity on the oxygen transfer. (Chern and Yang, 2004) derived a general model of oxygen mass transfer coefficient in the water droplets including the temperature effect. They verified the results experimentally and found the equation (1.20) can predict the behavior of the system with identical conditions used into experimental work:

$$(k_l a)_s = k_3 Q^{k_4} Y^{k_5} h^{k_6} \theta^{T_w} \quad (1.20)$$

The mass transfer operation in their work is considered as two divided zones as it proposed by (McWhirter et al., 1995). Where  $(k_l a)_s$  is the volumetric mass transfer coefficient in the surface mass transfer zone;  $\theta$  is the temperature correction factor; and  $T_w$  is the bulk liquid temperature,  $k_3$ - $k_6$  are equation constants.

(Wichterle, 1994) figured out that the heat transfer is scale dependent, this effect is more clearly noticed with surface aeration process when is compared with other operation on the basis of same rotational speed is used especially for smaller tanks. (Wichterle, 1994) has developed a generalized correlation for surface aeration temperature effect by depending on the laminar boundary layer concepts. He related the heat transfer process at wall tanks with other dimensionless numbers Reynolds number, Prandtl number and other operational parameters by depending on with the flow velocity and pattern for aerated agitated baffled tank.

$$Nu = A Re^\alpha Pr^{1/3} V_i^{1/4} \quad (1.21)$$

Where, A is a constant that depends on tank geometry; Nu is Nusselt No.; Pr is Prandtl No.;  $V_i$  is the viscosity ratio ( $\mu_{\text{bulk}}/\mu_{\text{wall}}$ ) and  $\alpha$  is the heat transfer coefficient. The model was developed within the ranges A (0.3-1.2) and Re (250-235×10<sup>3</sup>).

## V. Hydrodynamics

### V.1. Flow Patterns

#### A. Flow Patterns Characterization

The flow pattern and circulation inside of surface aeration in the wastewater tank has a very crucial importance to ensure distribution and efficient mixing for the dissolved oxygen, the homogenization and suspension of the mixed liquor that contains the activated sludge (Roustan et al., 1984).

Most of the agitation and mixing means that used for the surface aeration are operating with including impellers or turbines that are placed on a turning shaft. There are many of these impellers that can be characterized according to the generated pattern flow. These impellers accomplish two main flow types. The axial flow

promotes a circulation toward down and top of the tank creating self-looping patterns of circulation. The propeller is the most known device used in this type of operation (Leng et al., 2008). For the radial flow, there are many types of impellers that all have the characteristics of pushing the water in the radial form in perpendicular way to the rotation shaft. The turbines are the principle agitators (impeller) that are used for radial movement turbines in general imply a horizontal disc or cone on which the paddles are fixed but there are numerous forms of modified turbines (Leng et al., 2008; Nagata, 1975; Tatterson, 1994; Xuereb et al., 2006).

For the surface aeration systems, the axial flow may be produces in up-ward or down-ward directions by the impeller and then the flow will be redirected to the impeller intake region by the tank walls in closed circulation profile.

In general the discharge flow that moves and hits the vessel walls, entrains liquids from other parts outside its circulation field. The axial flow may invert to radial flow during its general axial flow.

The generated radial flow by impellers blades moves always toward the vessel wall and then the it is redirected by the wall for both upper and lower directions to goes back toward the impeller (Nagata, 1975).

In the turbulent regime the flow patterns of various agitator speeds usually are considered similar for each type of impeller (radial or axial). It is assumed that the absolute flow velocity increases in proportion to the impeller speed, the flow pattern is very important as a function of various geometrical and operational parameters such as impeller diameter, tank diameter and Reynolds number (Tatterson, 1991).

The flow field in the aerated wastewater tank is dominated by the energy sources of aeration and mixers, where the flow development in aerated tank with the presence of bubbles is controlled by the buoyancy effects (Gresch et al., 2011).

The flow pattern of the water droplets impingement at the water surface plane was examined by (Okawa et al., 2008). They noticed the generated liquid column on the water surface after the water droplets collision is depending on the angle and conditions of collision were convenient. When the angle wasn't too large, the breakup of the liquid column led to the production of secondary drops. The number of secondary drops depends on different factors like droplet diameter, the surface tension, density, viscosity and impact velocity, where they are referred by dimensionless parameters that called (k-number) that may control the number and size of secondary drops.

(McWhirter et al., 1995) illustrated that the flow parameters of surface aerators with water projection include an important modification that due to a new occurring mass transfer zones concept. They found out the most important factor in the process is the total liquid discharge velocity that refers to all the water droplets that propelled by the turbine, which is very dependable on the geometry of the turbine. The discharge

velocity contains three component, two of them are constant the radial  $V_R$  and tangential  $V_\phi$  but the third one the vertical axial velocity  $V_{oy}$  is changing with time and it has a maximum value at a certain point and after this point it decreases which is the first velocity that gets out at the upper tip of blades.

### B. Vortex Formation

The depth and the form of formed vortex has the predominate effectiveness on the process of un-baffled surface aerator. (Rao et al., 2009) built a general correlation for specific configuration with emphasizing on the vortex forms. In order to correlate the relevant parameters of the process with depending on previous work of (McWhirter et al., 1995) to describe the formation and performance of vortex especially, the role of critical speed of the impeller and other effective parameters in the system.

(Rao et al., 2009) performed experimental runs to deduce the mass transfer coefficient related with vortex formation and they found that the mass transfer coefficient at standard condition increase sharply near or above the critical speed. The general modified correlation for scale-up purposes was:

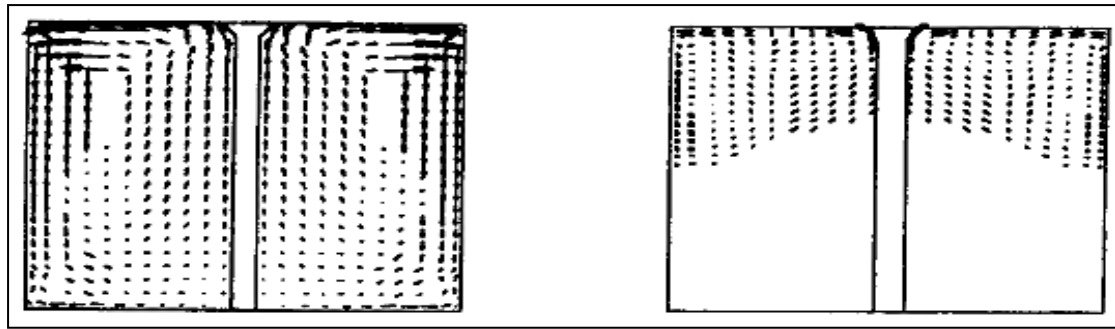
$$h_v / D = 43.2 F_r (0.1 - G_a^{-0.18}) (h - C_u - W/L)^{-0.16} \quad (1.22)$$

Where  $h_v$  is the depth of the vortex;  $C_u$  is the turbine blade clearance (in this case it represents the distance between the horizontal bottom of the tank and the top of the blades);  $L$  represents blades length;  $G_a = Re^2 / Fr$ . The model was developed within the ranges  $h_v / D$  (0.003-0.2) and  $Fr$  (0.005-0.02).

### V.2. Air Bubble Size Distribution and Hold-up

When suitable impeller diameter and rotational speed are employed, with proper bubble size distribution and residence time an improved oxygen transfer coefficient was achieved as founded by (Lee et al., 2001). They studied the bubble distribution inside a surface aeration for water treatment tank with turnover conical turbine, as shown in the Figure (1.16) the air bubble distribution delivered by the axial impeller blade rotation is homogeneously distributed in the entire tank and reaches the bottom.

While (Barigou and Greaves, 1992) have performed various tests on the aerated tank to measure local bubble size distribution with changing the position. They found out that there is a variation in the bubble size distribution within the tank and this variation was related to other parameters variations like the rotational speed and gas flow inside liquid bulk. The size of bubbles was lower at high rotation speed (these results agree with those performed by (Kawecki et al., 1967), the location of bubbles, they observed that bubbles size was changed especially between the vertical plane coinciding with baffles and the mid-plane between two baffles location.



(a)  $D/T_v=1/3$

(b)  $D/T_v=1/5$

Figure (1.16): Bubble distribution of surface aerator system of rotation speed  $N=110$  rpm, liquid level  $h=0.66$  m. (Lee et al., 2001).

(Deshmukh and Joshi, 2006) pointed out that the gas holdup plays an important role on the velocity field in the impeller region for the surface aeration system, which in turn is affected by the impeller design, submergence and rotational speed of the impeller.

These observations were noticed by (Sun et al., 2006). They found that the air bubbles holdup profile was non-uniform in the surface aerated agitated tank, the bubbles holdup was high in two regions, first close the liquid surface and second in the impeller region. The weakest gas holdup region was under the impeller region. The air bubbles holdup was measured at different operation conditions; the impeller was Rushton disc turbine with surface baffle used.

### V.3. Mixing Time

#### A. Mixing Time Characterization

The mixing time is generally considered as an indicating factor for perfect accomplished mixing potentials in surface aeration, where it is necessary to achieve the homogenization and effective mixing of dissolved oxygen inside the treatment tank with maintaining the desired operation conditions for suspension and distribution of activated sludge and biomass particles. Mostly the mixing time in aerated conditions is less than non-aerated conditions, (Guillard and Trägårdh, 2003) reached to same persuasion by examining the mixing time for both aerated and non-aerated condition for disc turbine impeller. The mixing time usually referred as dimensionless number called mixing number ( $t_m N$ ), which is very dependent on the turbulence flow regime, where is always has lower values with turbulent flow than other flow for gas-liquid systems (Hadjiev et al., 2006).

The mixing time is always decreased with increasing the impeller rotational speed as seen in the Fig. 1.17, when the system consists in two impellers with the upper clearance is set at the liquid surface as figured out by (Kang et al., 2001) in their studies the influence of rotation speed effect on the mixing time for surface aerator system, where they tested the effect of rotation speed on the mixing time for different geometric configurations.

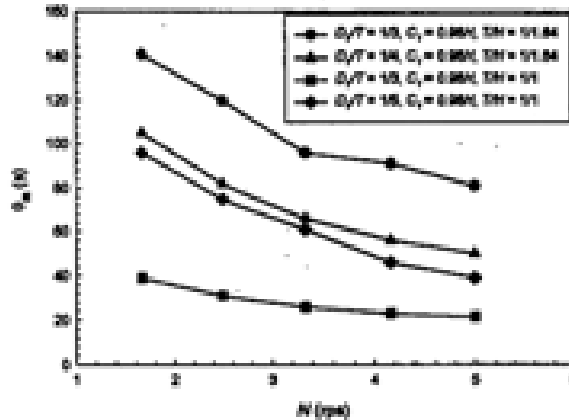


Figure (1.17): The relation between the rotation speed and mixing time for surface aeration dual impeller system, (Kang et al., 2001).

(Guillard and Trägårdh, 2003) found out the general approach is difficultly applicable in actual sized tanks and they deduced that the mixing time under aerated condition is longer than non-aerated and depends on the tracer injection position also. They used tracers by pouring pulses of concentrated acid; the injection was in three different positions in the tank then the concentration gradient determined by PH electrode.

### B. Mixing Time Modeling

(Hadjiev et al., 2006) developed a model to correlate the dimensionless mixing number with the most important geometrical parameters and liquid flow and water surface condition for the aeration systems:

$$Nt_m = [-13.981(S/D)^2 + 27.972(S/D) - 4.1327] (S_p/D)^{-0.54} Re^{0.275} Fr^{0.275} F_g^{-0.04} \quad (1.23)$$

Where, S is the upper impeller submergence, and  $F_g$  is the modified aeration number, which equals  $G/(Nd^3n_{im})$ . The model was developed within the ranges  $S_p/D = 2.12$ ,  $Re (2.0 \times 10^3 - 14 \times 10^3)$ ,  $D/T_v = 0.16$  and  $h/T_v = 3.5$ .

For micro- mixing in surface aeration process, (Rao and Kumar, 2009) derived a model for mixing time by depending on the basis of theoretical power per unit volume to simulate the process time with  $X = Fr^{4/3} Re^{1/3}$ , the ranges for the model are same in equations 1.14 and 1.15.

$$k_l a_{20} t_m = [6.5e^{-4.61X^{0.1}} + 0.03 - 4 \times 10^{-6} e^{0.84(X-3.6)^2}] \sqrt{X} \quad (1.24)$$

### **V.4. Air Bubbles Entrainment**

The flow inside the water treatment tank is produced indirectly by the turbine rotation, the splashed water droplets are plunged in the water surface in tank. These plunged water droplets entrain the atmospheric air as bubbles and go downward inside the tank. Air bubbles are formed at the water surface when the turbulent kinetic energy is strong enough to break the stabilizing effects of surface tension and gravity (Bhattacharya et al., 2007). (Chanson, 2003) defined the air entrainment by the water spray plunging as the entrainment or entrapment of un-dissolved air bubbles and air pockets that are carried away within the flowing fluid.

(Biń, 1993; Ohkawa et al., 1986; Qu et al., 2011) have reached the persuasion that the penetration depth of the entrained air bubbles is highly controlled by the water spray velocity or flowrate in depending on combined experimental and numerical study of the flow. (Kusabiraki et al., 1990) have added the water velocity distribution at the impact position as effecting factor on the air bubbles entrainment as a results of their experimental studies on the gas entrainment rate in a jet aeration system. The importance of the water spray velocity is explained by (Ohkawa et al., 1986) is to overcome the buoyancy forces of the air bubbles produced by the water spray jet.

Usually an impeller is coupled with surface aerator turbine in order to produce significant shearing stresses in the mixing zone which enables air bubbles entrainment from the surface (Heim et al., 1995).

### **V.5. Surface Aeration Power Consumption**

In the surface aeration system, with the occurred agitation in the treatment tank it is very indispensable to identify the necessary energy needed in the process. The power or energy consumption in the surface aeration is the energy that is delivered from the shaft to the surface aerator turbine and then to the water. Or it is simply can be defined as the energy that leaving the impeller and entering the liquid in the tank. Because of many variables can affect the energy consumption, identifying a general characterization for the power consumption in surface aeration is so complicated, where the power consumption here may influenced by the whole system variables of the surface aeration, the chemical and physical properties of water and included solid contents and the operational conditions like the rotation speed, gravity and water level in the tank and other parameters.

There are many methods to measure the power consumption in the agitated tanks such as the widely used electrical and torque-meters gauges are used for large scale tanks (Ascanio et al., 2004) considered the torque-meter as an accurate method.

The power consumption is related of surface aerator and tank geometries and operation conditions. It is quite clear that it will be influenced when different number of impeller used, but it is not always dependent on these impellers equally, the

position and the bubbles flow profile around each impeller has its different effect (Cui et al., 1996).

#### A. Operational Condition Effect

(Takase et al., 1982) have investigated the power consumption of surface aeration system with aerator impeller (6 blade disc turbine, DT) positioned at the water surface for different conditions of treated liquid with clean water and with two different activated sludge mixed liquids, they found out the different conditions didn't consume similar energy with surface aeration process, but their impact on the power number were almost same for same operation condition and experimental equipment (See Figure 1.18).

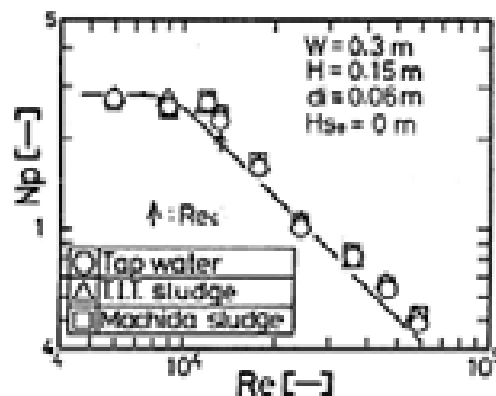


Figure (1.18): The relation between the Reynolds number and power number for three different liquid conditions, clean water and two types of activated sludge mixed liquid (Takase et al., 1982).

#### B. Power Consumption Relation with Oxygen Mass Transfer

When comparing two surface aerators with same diameter and rotational speed, the one that consumes more power has higher oxygen transfer efficiency (Ognean, 1997). For each surface aeration process according to the power consumption there will be three characteristic affecting parameters: the active volume, that identified by the volume created by the aerator within the energy transferred to the liquid, the energy transfer area and the mass transfer area; for certain operation condition and active volume an optimum oxygen mass transfer can be achieved as supposed by (Ognean, 1993b).

(Ognean, 1993b) built a model that correlates the power consumption for the surface aeration and the relevant dimensionless parameters with the aeration modified sorption number  $Y_N$  at the maximum oxygen transfer condition. This model can be

applied to compare the different surface aerator types, where subscript m represents maximum condition; G is the mass-transfer rate (oxygen uptake).

$$(Y_N)_m = (OTR/P)_m (1/P_m^{1/2})(D^3 N^{3/2})_m (g^{5/6} \rho^{3/2} v^{1/3} \Delta c^{-1}) \quad (1.25)$$

$$Y_N = G \left( \frac{v}{g^2} \right)^{1/3} / \Delta c d_e^3 \quad (1.26)$$

Where  $d_e$  is the geometric equivalent dimension ( $d_e = \left( \frac{P}{\rho g N D^2} \right)^{0.5}$ ),  $c$  is dissolved oxygen concentration in the water (mg/l).

(Ognean, 1993b) proposed models of dimensionless numbers for various types of surface aerators by correlating the oxygen transfer efficiency with power consumption and other affecting parameters like geometric ratios of the system. For an optimum condition the maximum values for these parameters are correlated in the model. For vertical shaft aerator, the maximum aerator diameter used was always considered as relevant factor when trying to reach maximum aeration efficiency  $(AE)_m$ .

$$(AE)_m = K_1 P^{1/2}_m (D^3 N^{3/2})_m \quad (1.27)$$

$K_1$  is the equation constant

While for horizontal shaft aerator he proposed another model, where (Ognean, 1993a) considered  $d_c$  as a characteristic length of the horizontal surface aerator and depends on the contact area between the aerator and the water.

$$(AE)_m = K_2 P^{1/2}_m (N^{3/2} D^{3/2} d_c^{3/2})_m \quad (1.28)$$

$K_2$  is the equation constant. The models 1.25 to 1.28 were developed within the ranges  $D / T_v = 0.125$ ,  $h/D = 3.0$ ,  $N_p$  (1.0-3.0) and  $Fr$  (0.05-4.0).

## VI. Contact Time between Water Droplets and Atmospheric Air

(Cancino et al., 2004) modified a model for the water spray droplets contact time with the atmospheric air in the surface aeration process within the development of theoretical design of the axial flow surface aerator. The model relates the time,  $t_e$ , with the height of water droplets,  $H_d$ , in air and gravitational acceleration:

$$t_e = \sqrt{8H_d/g} \quad (1.29)$$

(Cancino et al., 2004) deduced that it is required to increase the contact time of water droplets in the air to enhance the mass transfer operation and this can be done in the way of increasing the height of water spray that projected or by increasing the dispersion of the water droplets (decrease the size of the droplets). (Cancino et al., 2004) demonstrated that to achieve these objectives it is required to increase also the projected water flow rate to power consumption ratio (Q/P). (Cancino, 2004a)

declared that according to design consideration of surface aerator turbine it should be made with considering that largest amount of water should be projected with largest distance for droplets flight pattern should match the contact time within the limit of lowest power consumed with regard to the fact that inlet and outlet angles of water for the blades were well chosen.

### VII. Environmental Effects

The performance of projected water and wastewater droplets as a spray in the atmospheric air and the concerning process can produce undesirable emitted aerosols causing air pollution, further it can be a source of unwanted odors (Cumby, 1987b).

(Chern and Chou, 1999) have studied the surface aeration but in different way, they covered in their study the other sides of mass transfer of volatile organic compounds that stripped from waste water to the air during the treatment operation, they divided the mass transfer area into two zone for both continuous and batch aerations in order of developing a general model to estimate the emission mass transfer for (VOC) in the air, for the liquid spray zone for VOC emission rate the following equation was derived:

$$VOCER = k_l a_{voc} V_L \left( C_{voc} - \frac{C_G}{H_c} \right) \quad (2.30)$$

For the surface re-aeration zone the emission rate was:

$$VOCER_s = k_{ls} a_{svoc} V_L \left( C_{voc} - \frac{C_G}{H_{cs}} \right) \quad (2.31)$$

Where VOCER and VOCERs represent VOC emission rates;  $C_{voc}$  is the dissolved VOC concentration in the bulk liquid;  $H_c$  and  $H_{cs}$  are Henry's law constant of VOC at water and air wet-bulb temperatures respectively; and  $C_G$  represents VOC concentration in the air.

Water and wastewater treatment plants that implement surface aeration are well known as sources for noise pollution, so it is recommended to build these plants away from urban zones.

### 1.3. Conclusions

In this chapter a brief presentation was made for the present day aeration systems for the water and wastewater treatment with introducing the types and efficiencies for each system. The surface aeration for water treatment was described somehow in detail.

It is found that; many modification essays are made on the surface aerators to improve the performance. There are many trials have performed to enhance the operation efficiency by either of increasing the mass transfer rate or by reducing the power

consumed in the operation. In order to achieve these objectives there are many studies are made concerning with the various operation variables like hydrodynamic of the system (gas hold-up, bubble size distribution), the flow pattern for gas and water, the properties of working mediums (air and water), rotational speed of the aerators, the circulation time (mixing and aeration time), power consumption, geometric configurations (i.e. number of impellers, types of impellers, geometric ratios), oxygen mass transfer rate in the water and scale up, modeling process for the aeration system.

Form the literature review it can be presumed that in general the limiting factors for successful surface aeration can be resumed as; the turbulent regime should be ensured in the entire water treatment tank that contains sufficient dissolved oxygen entrained from atmospheric air. The generated water flow by axial or radial surface aerators must be sufficient to reach all parts of the treatment tank. The aeration process accomplished the axial or radial impellers must be accompanied by mixing and agitation performance to ensure an efficient distribution of the dissolved oxygen, these constrains can be overcame by an appropriate surface aerator with suitable pumping capacity to handle efficiently and effectively the large quantities of water.



**CHAPTER TWO**  
**EXPERIMENTAL SETUP AND**  
**CACULATION METHODS**



## Chapter Two

### Experimental Setup and Calculation Methods

#### 2.1. Introduction

The experimental design and setup for surface aeration runs depend on many important influencing factors, that generally can be classified as the geometric configuration of the system, the operation conditions, the theoretical assumption that describes the occurred process during the experimentation such as the models of the transferred oxygen mass in water, the flow pattern of the air-water flow inside the tank and at water surface, the physical and chemical properties for both water and air used. The economic factor is an important factor that should be taken into account.

The experimental work was performed to interpret the important aims: the energy or power consumed by the surface aeration system, the oxygen mass transfer coefficient in water bulk  $k_{l,a}$  and in the water spray (droplets)  $k_{l,a,d}$ , the impeller configurations and operational influences on the oxygen mass transfer and power consumption. Where, the experimental runs can be classified into two main categories, the mass transfer and hydrodynamics.

#### 2.2. Experimental Installation and System Description

The surface aeration system was built in the laboratory and is the perfect scale-down representation of the industrial system (MOS, Biotrade)(FR Patent Demand, 2012); the surface aeration and mixing are achieved by employing the turbine (conical overturned shape with 15° pitched blades) placed at the water surface with mixing assembly positioned lower the turbine (See Figure 2.1). The turbine body is made of PVC; while their blades are made of stainless steel adhered to the turbine body. The mixing assembly is composed of reversible twisted pitched RTP propeller of four blades with 45° pitch angle at the propeller hub (Milton Roy Mixing HPM204D) fixed inside a draft tube (See Figure 2.2) to enhance the performance of the system. Three baffles are fixed inside the draft tube (See Table 2.1).

The experimental runs are carried out in a cylindrical flat bottom vessel with dimensions of 600 mm height and 800 mm in-diameter placed in a larger cubic vessel. All the vessels are made of fibre glass (Perspex) except the front face of cubical vessel, which is made of glass for easy cleaning and to eliminate causing scratches during the cleaning and in order to avoid the laser beam diffraction, for the crossing laser beams for (Laser Doppler Velocimetry) LDV and (Particle Image Velocimetry) PIV application. The reason for the second vessel is to provide a compatible medium for the laser beams in both inside and outside the pilot plant. The schematic diagram of the system for both aeration and mixing is shown in figure 2.3 a, b.

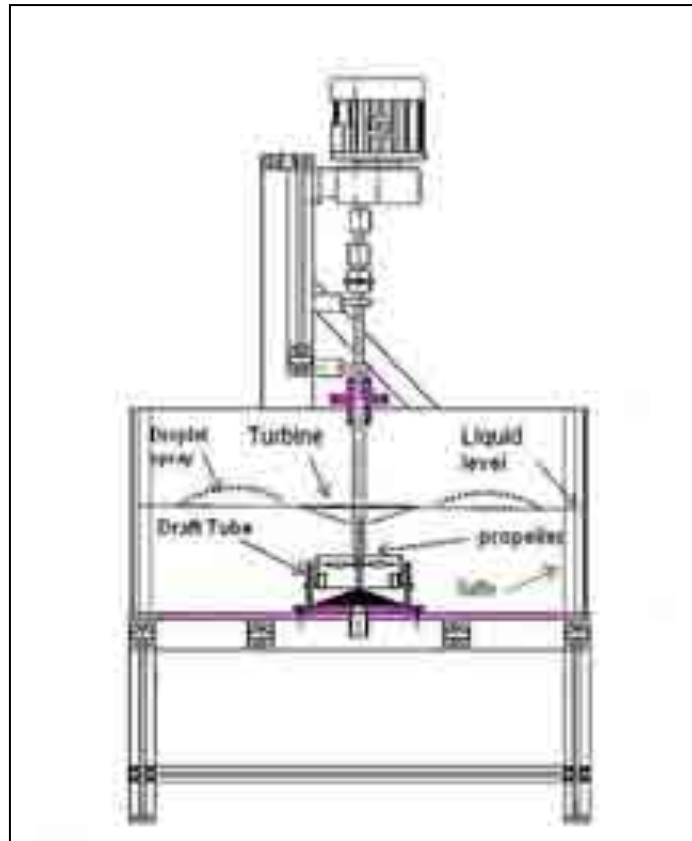


Figure (2.1): The schematic diagram of the experimental apparatus.



Figure (2.2): The turbine, propeller and draft tube.

Three baffles were used in order to prevent or lessen the tangential circulatory flow created by the system, (the baffles have the same height of the vessel see Table 2.1). A cone is positioned at the vessel flat bottom exactly beneath the draft tube to improve the inlet flow by preventing secondary eddies formation and dead zones under the propeller. As it is noticed the geometrical ratio for the propeller ( $d_{pr}/T_v$ ) = 0.15, where that is lower than the general applied ratio ( $d_{pr}/T_v$ ) for axial flow impellers (0.2 - 0.7) in classical agitated tanks.

## Chapter Two: Experimental Setup and Calculation Methods

Table (2.1): Geometrical configuration details

	Diameter (m)	Clearance	Height (m)	Width (m)	Blade width (m)	No. of blades	Numbers
Vessel	0.8 ( $T_v$ )		0.6				
Turbine	0.19 (D)	$T_v/3.13$			0.024	12	
Draft tube	0.15 ( $d_f$ )	$T_v/10$	0.1				
Propeller	0.12 ( $d_{pr}$ )	$T_v/5.13$			0.018	4	
Cone	0.15		0.06				
Baffles			0.6	$T_v/10$			3
Draft tube baffles			0.06	$d_f/8$			3
Impellers spacing			0.076				
Water height			0.28				

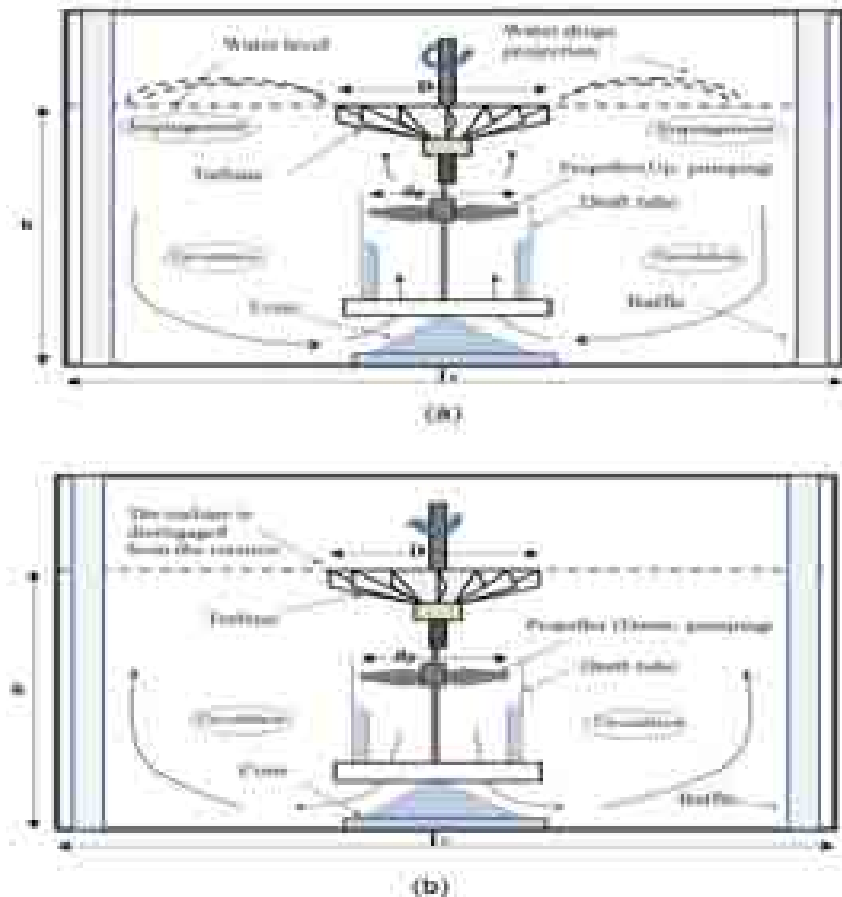


Figure (2.3): Schematic diagram of experimental apparatus; (a) Up pumping flow (Aeration mode), (b) Down pumping flow (Mixing mode).

### 2.3. The Measurement of Power Consumption

The consumed power by the surface aeration system was calculated by torque measurements, which is applied for both the surface aerator turbine and lower propeller. This measurement is achieved by two steps. First, the torque is measured in empty vessel to determine the frictional mechanical loss due to air resistance during the impellers and shaft rotation. Second the torque is measured with the rotation in filled vessel with testing liquid (water). The actual consumed power is the difference between the calculated powers in both filled and empty vessel by applying the following equation:

$$P = 2\pi N (T_o - T_{oe}) \quad (2.1)$$

Where,  $T_o$ , and  $T_{oe}$ , are the measured torques in filled and empty vessel respectively in (Nm). The torque meter used with a torque capture transducer all are made by (HBM). A motor (LEROY SOMER), (LS90SL, rated power 1.1 kW, max. rated speed 1420 rpm) utilized to achieve the desired rotation speed.

### 2.4. Hydrodynamics and Mean Velocity Measurements Techniques

In order to determine the velocity profiles and the occurred flow pattern inside the tank, the mean values of the different velocities are measured by both the LDV (Laser Doppler Velocimetry) and PIV (Particle Image Velocimetry). With LDV technique it is the yield from set of velocity measurements for one or more of velocity vector components on the same time (Mavros et al., 1998), while the PIV is used to study of the instantaneous flow field for both single phase and multiphase (Aubin et al., 2004).

#### 2.4.1. Laser Doppler Velocimetry (LDV)

##### I. LDV Apparatus Description

The LDV (Laser Doppler Velocimetry) is non-intrusive technique. The laser source consists of two beams (514.5 nm green- 488 nm blue wavelengths) Dantec fibre flow device. The measurement of the occurred velocity depends on the reflected scattering beams by added tracer particles to the water. The light laser source is a 4 W Argon ion of laser stability 2017 (Spectra Physics) with a focal length of 600 mm (See Figure 2.4). The measurement that performed by the LDV is usually made in regular plans inside the fluid bulk. The LDV measurements are carried out with a Dantec fiber flow system is operating in back-scattering mode. The Doppler signal is transmitted to a 58N20 flow velocity analyser (Dantec) for the signal processing. The cooling is achieved by water medium that is circulated with pumping pressure of (5 bar). The employed software is BSA flow (version 4.5).



Figure (2.4): The Laser Doppler Velocimetry (LDV) testing apparatus, (1) Laser source. (2) Traverse system, (3) Tested tank, (4) Flow velocity analyser.

## II. Tracer Particles Seeding

In order to accomplish flow measurements with LDV the vessel is filled with operating fluid (in our case is tap water) and seeded with small amount of tracer particles of Iridium 111 Rutile stain particles (Merck) ; the diameter of these particles,  $d_p$  is about 15  $\mu\text{m}$ .

## III. Measurement Principals

The device operating concept depends on the reflected scattering beams by previously added tracer particles to the water. The LDV device is equipped with a traverse system for the purpose of moving the laser source to have the necessary flexibility of reaching all the parts inside the tank easily; the coordinates of the traverse system matches the actual lab coordinates.

Two laser beams are crossed and formed an interference fringe pattern, where this area of interference is called the volume of measurement. This volume is consisting of equally spaced interference fringe planes parallel to the bisector of the angle between the two laser beams (See Figure 2.5). The model that indicates the set of parallel fringe planes is equally spaced by a certain distance.

The equally distance between the fringes  $\Delta y$ , can be determined by the following equation (Costes and Couderc, 1988):

$$\Delta y = \lambda_0 / 2 \sin(\theta/2) \quad (2.2)$$

Where:  $\lambda_0$  is the laser beam wave length.

When the tracer particles move through the region of interference fringes, they scatter the light of the two laser beams, with modulated intensity corresponds to its movement through the fringes. The phenomena is called the Doppler effect, where the basic principle of the effect is the scattering of the two light beams by the particles, which is propagating in a direction represented by a unit vectors with certain frequency and wavelength to form an aggregate beam with a frequency different to the two incident beams, the diffused light by the particles has a frequency relative to the first light beams. The frequency of the modulated intensity at which the light is scattered is called the Doppler frequency that is directly related to the components of the particle velocity perpendicular to the interference fringes .

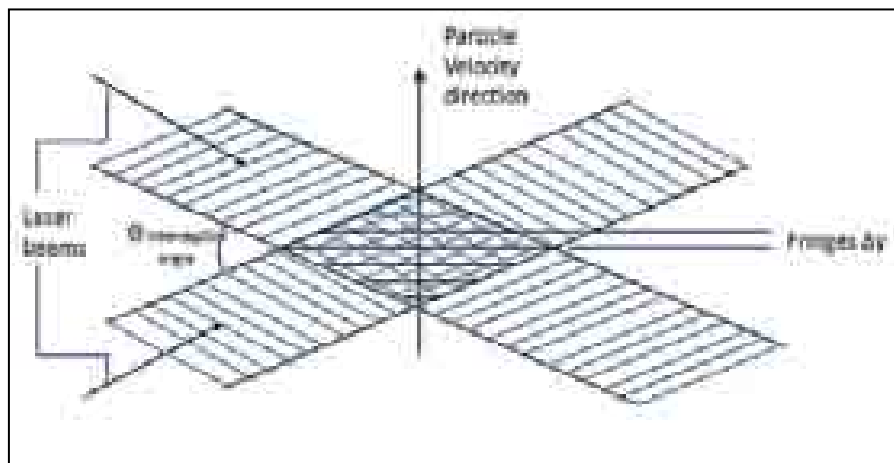


Figure (2.5): The LDV measuring volume fringe planes.

The quality of the LDV results depends on the size of the ellipsoidal measuring volume formed at the beam intersection point and the number of the interference fringes in this volume. The size is refined as much as possible in order to avoid the presence of too many particles with different velocities and thus a random out of phase signal. At the same time the number of interference fringes must be kept maximized in order to maximize the precision of the frequency of the signal (Aubin, 2001).

The dimensions of the measuring volume can be determined as (See Fig. 2.6):

$$2a_v = d_p / \sin(\theta/2) \quad (2.3)$$

$$2b_v = d_p / \cos(\theta/2) \quad (2.4)$$

$$2c_v = d_p \quad (2.5)$$

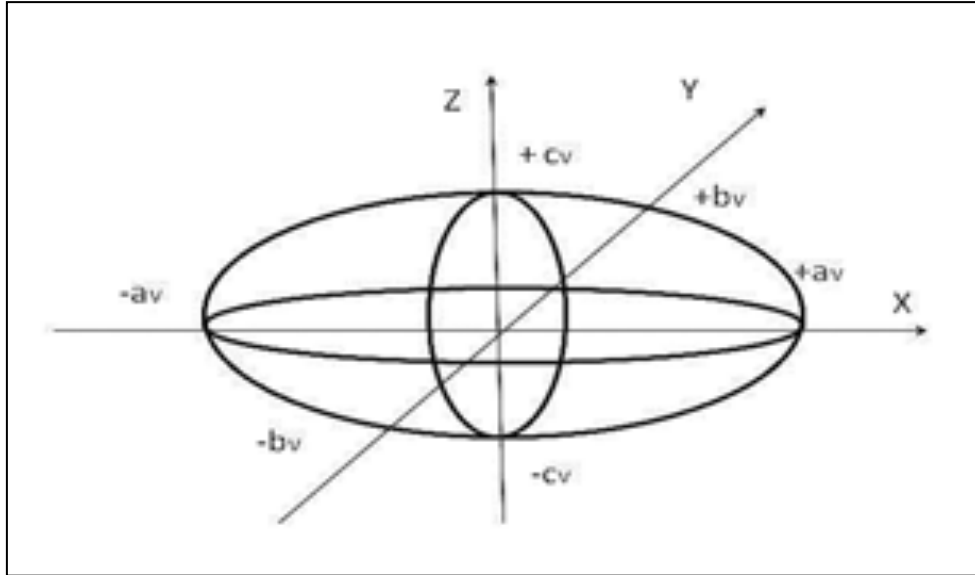


Figure (2.6): The measuring volume.

The two velocity components  $v_r$  and  $v_z$ , are measured by changing the position of the laser beams in the vessel. To measure the velocity component, the laser beams was oriented such that they are in the same plane as the component and the bisector of the angle formed by the two beams is perpendicular to it. Aligning the beams in a horizontal plane allows the radial velocity component,  $v_r$  to be measured and when in a vertical plane the axial velocity component,  $v_z$  can be determined. So, the measured velocity components by the LDV laser beams are the axial and radial components only. The other component of the flow velocity that the tangential is not measured, especially the measurement concerned area applied by the LDV is the propeller vicinity and the draft tube inlets, where the majority of occurred velocities are the axial and the radial, where the laser beams should move in a direction perpendicular to the optical axis (See Fig. 2.7).

#### IV. Signal Post-Processing

A Dantec burst spectrum analyzer (BSA) for time-resolved measurements is used as the LDV signal processing, where the signal from the photomultiplier that contained in the apparatus was filtered to remove the undesired low and high frequencies then amplified by a variable gain. The number of samples required to achieve statistically independent results depends on the flow field. It was found that at least 300 samples

were convenient for local turbulence intensity occurred in the testing area. The BSA was also interfaced to a PC controlled by software installed in the PC. The BSA was operated in Burst mode, that is, only one measurement was performed per detected burst, where the frequency data are transformed to velocity data by the used software (Lee and Yianneskis, 1998).

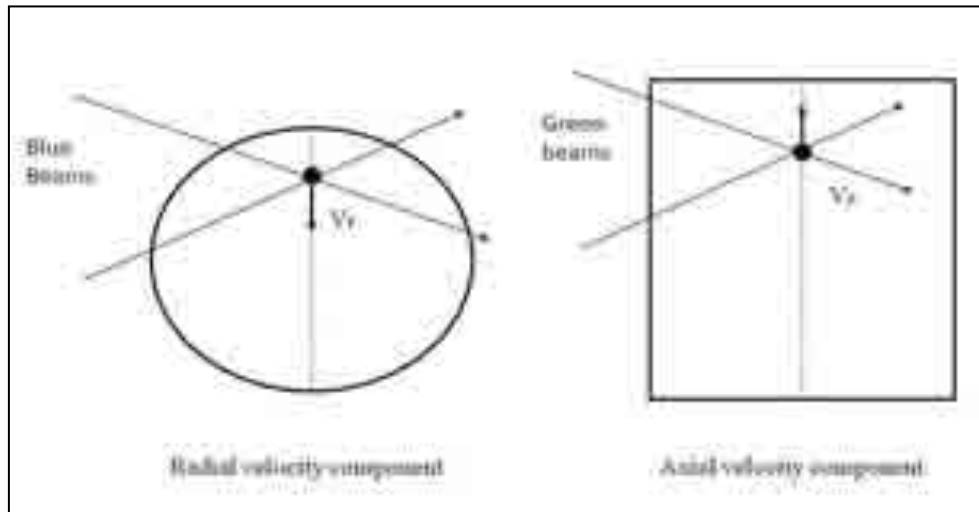


Figure (2.7): The LDV laser beams positions.

### 2.4.2. Particle Image Velocimetry (PIV):

#### I. Theory

The PIV technique is now widely used in the agitated tank flow field acquisitions because of its convenience to obtain the full characteristics for the measured field (Li et al., 2011). The PIV is applied to measure the instantaneous velocity field using the images of tracer particles in the fluid flow (See Figure 2.8), where the PIV technique provides a quantitative, instantaneous, whole-field visualisation and two dimensional description of the flow (Udrea et al., 1997). The displacement of tracer particles is measured through the analysis of the images that produced during the illumination of these particles by pulsed sheets of light at precise time intervals and recorded on film or a video camera array (Adrian, 1991). The average displacement is measured when high image density of large particle concentration is applied (Keane and Adriane, 1992). The usual used PIV type is the two dimensional, where it can be applied to acquire only both the radial and axial flow velocities components in the stirred tanks, where the laser sheet is positioned vertically inside the vessel.

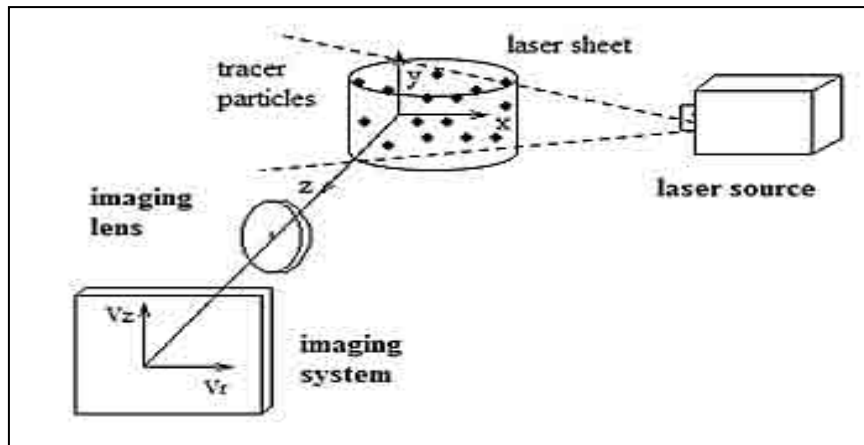


Figure (2.8): Schematic diagram of the PIV

## II. Tracer Particles Seeding

The PIV experimental setup is generally consist of the addition of tracer particles to the investigated flow stream. Tracer particles are small enough to ensure a good tracking of fluid motion due to the difference in density between the fluid and the tracer particles and in same time to ensure not they will not interact with the flow being measured, they can frequently to be the order of 50-100 nm, their diameters are then (1/10) to (1/5) the wavelength of green,  $\lambda_{green}=532$  nm. Seeding of the tracer particles is made in order to achieve sufficient image contrast, where seeding can easily be done by suspending solid particles into the fluid and mixing them to ensure a homogenous distribution.

## III. PIV Principles

After the addition of tracer particles, these particles are illuminated for detected plane within the target flow for several times during short time interval. The displacement of particles images between the light pulses determined by the evaluation of the recording for the light scattered by these particles, which is recorded by high quality lens of CCD cameras, where a post-processing then is applied to deal with these collected data (Raffel et al., 2007). The main parts of PIV system are illustrated in Figure 2.9.

## IV. Scattered Light

The light scattered by the small tracer particles is a function of the ratio of the refractive index of the particles to that of the surrounding medium, the particles size, and their shape orientation, polarization and observation angle (Raffel et al., 2007).



Figure (2.9): The Particle Image Velocimetry (PIV) testing apparatus, (1) Laser source, (2) Recording camera, (3) Tested tank.

The light is not blocked by the small particles but it spread in all directions, so massive multi-scattering occurs when sufficient number of tracer particles exists inside the light sheet, where the light scattered by more than one particle is imaged so the recorded light by the lens is not only because of the direct illumination but also because of the fraction of the light (See Figure 2.10).

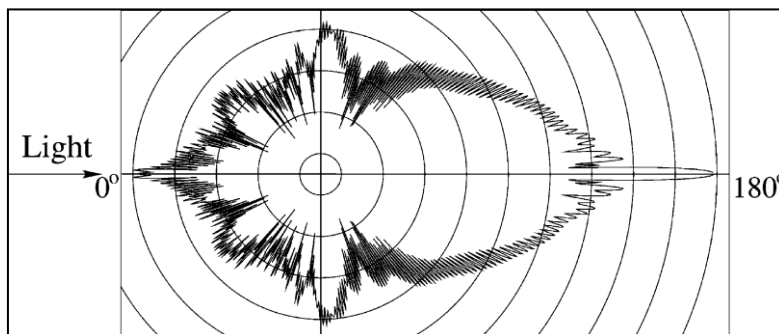


Figure (2.10): Light scattering by the (10  $\mu\text{m}$ ) glass particles in the water (Raffel et al., 2007).

### V. Laser Source

The laser is used in the PIV process is related to their ability to emit monochromatic light with high energy density, where it easily can be bundled into light sheet for illuminating and recording the tracer particles.

The laser device in the PIV consist of three main components: (a) the laser material, which it in turn consists of an atomic or molecular gas, (b) The pump source; that excites the laser material by the introduction of electro-magnetic or chemical energy, (c) The mirror arrangement; i.e. the resonator allows an oscillation within the laser materials (Keane and Adriane, 1992).

The used laser beam is usually Argon-ion laser ( $\lambda= 514\text{nm}, 488\text{nm}$ ), which is a laser gas, where this type of laser is characterized by the very high current is achieved for the ionization process. For this type the laser mirrors that used is produce an emission at several wavelengths, where specific wavelength can be selected in the laser resonator, in such a manner that the individual wavelengths can be adjusted by rotating the prism in the laser mirror. In general this type is used for the liquid fluid mechanics.

The light sources are also used in the PIV flow investigation with laser sheet. For the spectral output of the light source may suit for specific cameras. For the similarity in the spectral sensitivity and that offer a repetition rate that matches the video rate. Optical fiber bundles are used to link the light sources in order to achieve short pulse separation times, where the generated light is simplified when the outputs of the fibers are arranged inline. Generally three types of the lens are used to generate light source, in which can be set in different combination of the various shapes used. The fiber bundles can be used for the combination of two sources for shorter pulse separation time (Hecht and Zajac, 2001).

### **VI. Recording Techniques**

For each recorded frame of PIV, it represents a freeze of the flow in time. The successive images average time can be applied to build flow maps that characterize the impeller and the vessel configuration. For each frame, it can be considered as a transient image of the flow, which exhibits the non-stationary phenomena, like flow instabilities (Mavros, 2001).

In the PIV, the recording methods are achieved by either photographic or digital recording. The recording process can be implemented in two ways: first the capture of the illuminated flow with a single frame and then provide a single illuminated image for each illumination pulse (single frame / single-exposure PIV) or for several illumination pulses (single frame / multi-exposure PIV), the second way is the capture of the illuminated flow on a multi frames and then provides a multi illuminated image for each illumination pulse (multi-frame / single-exposure PIV). The (single frame / multi-exposure PIV) recording was first used in conjunction with photography, as it doesn't retain information on their temporal order of the illumination pulse, which cause a directional ambiguity like what is called image shifting , while the second way of recording preserves this temporal order of the particle motion(Raffel et al., 2007).

The digital CDD (Charge coupled device) cameras in PIV recording are used because they provide high repetition rates that needed for high pulse energy lasers. In CDD cameras the individual pixels are grouped into a rectangular array to form a light sensitive area, in which the array should to be read out sequentially in a two-step process, that the accumulated charge shift vertically one raw at a time after exposing CDD sensor into a masked off analog shift register on the lower edge of the sensor's active area.

### **VII. Image Analysis Method**

In order to extract the needed information for target displacement from the recording, the interrogation methods are applied on the selected images to tracking the individual particles from exposure to exposure (Agüí and Jimenez, 1987). The process is implemented by image processing computer software. The processing step of the images is depend on the dividing the complete image into the squared interrogation areas (Escudie and Line, 2003).

The image evaluation by the experimental data with the results of numerical calculation requires high density images or medium concentration of the images of the tracer particles. The experimental applications for the image analysis are dependent on the type of these experiments. For example for the air-liquid system, gas bubble distribution, a careful arrangement of camera and light sources are needed to avoid the over exposure of bubbles and the optical distortions from vessel wall (Laakkonen et al., 2005).

### **VIII. The Cross-Correlation Calculation**

The evaluation of the PIV recordings is made by the cross-correlating for two frames of single exposure of the tracer particles. For each interrogation area with the cross-correlation application, the calculation for most of the probable tracer displacement is attained. With choosing the adequate time interval between the two successive images, the instantaneous flow field inside the vessel can be calculated (Escudie and Line, 2003).

(Raffel et al., 2007) demonstrated that the cross-correlation calculation can be represented as assuming the displacement is constant  $D_{dsp}$  (See eq. 2.7) of all the particles inside the interrogation volume, so the particle location during second exposure during second exposure at time ( $t'= t+\Delta t$ ) is:

$$Xi' = Xi + D_{dsp} \quad (2.7)$$

The particle image displacement is represented as:

$$d_{dsp} = \begin{pmatrix} MD_{dsp}x \\ MD_{dsp}y \end{pmatrix} \quad (2.8)$$

Where M: is the magnification factor. The image intensity field for the time of the second exposure:

$$I'(x, \Gamma) = \sum_{j=1}^N V'_o(X_j + D_{dsp}) \tau(X - X_j - d_{dsp}) \quad (2.9)$$

Where,  $V'_o$ : is the volume of the interrogation during second exposure. So the cross-correlation function of the two interrogation areas will be:

$$R_{II}(s, \Gamma, D_{dsp}) = 1/a_I \sum V_o(X_i) V_o(X_j + D_{dsp}) \int_{a_I} \tau(X - X_i) \tau(X - X_j + S - d_{dsp}) dX \quad (2.10)$$

The comparison between the PIV and LDV techniques showed good agreement between them for the quantitative comparison of the radial and axial velocities (Myers et al., 1997).

### 2.4.3. Other Flow Related Measurements Parameters

The mean velocity measurements that performed by the LDV and PIV are used to calculate the flow rate or the pumping rate at the turbine and propeller vicinity or in the entire vessel area. The calculated flow rate is necessary for example to compute the pumping number and other flow related factors.

#### I. Mixing Time ( $t_m$ )

The mixing time  $t_m$ , experiments were performed for the system in aerated and non-aerated modes.

In aeration mode, the tested configurations consist in the turbine with RTP propeller and the draft tube, the turbine, RTP propeller and the draft tube and for the turbine alone in order to determine the mixing performance of each configuration and elucidate its influence on the mixing time.

The mixing time in non-aerated vessel (the turbine is removed) was investigated for both up and down pumping modes.

The injection position was kept for same position at the water surface for all tests to eliminate the effect of injection variation on the results obtained.

The mixing time was determined by applying the colorization-decolorization method. It consists in colouring the water with 10 ml iodine solution and then in decolorizing it with 10 ml sodium thiosulfate solution with a slightly exceeded volume to insure completely decolorizing the iodine solution. The decolorization reaction occurs progressively from yellowish brown colour to clear water (Brown et al., 2004; Xuereb et al., 2006). The detailed mixing time experimental results are discussed in separated chapter

### II. The Pumping Number ( $N_{Qp}$ )

It is also called flow number. Each type of impellers has its own pumping number. It is defined as a dimensionless number refers to the pumping capacity of the impeller by relating the flow discharged by the impeller blades to its diameter and rotational speed as presented in equation 2.11.

The liquid velocity that leaves the impeller blade tips could be tangential, axial and radial and this depends on the geometry of the impeller such as the number of blades and pitch angle for the blades (Brož et al., 2004). To compare between the geometrically similar impellers, the pumping number is frequently used as a characterization factor. Generally the axial velocity is generated by the propellers and radial flow is generated by the turbines.

Impellers pumping number can be represented as:

$$N_{Qp} = \frac{Q_p}{\rho ND^3} \quad (2.11)$$

Common types of propellers have the pumping numbers around 0.5. For ordinary flat blade turbines and blade turbines are 1.3 and 0.87 respectively (Roustan, 2005).

The pumping number,  $N_{Qp}$ , for the propeller is obtained in depending upon the radial and axial flow balance; the total inflow should equal the total outflow. The discharge flow,  $Q_p$ , is generated from propeller blades rotation is calculated from the measured values of axial and radial velocities at known distance from propeller blades within a determined volume calculated by equations 2.12a, 2.12b (See Figure 2.11). At propeller vicinity the axial flow,  $Q_{pz}$ , is calculated by measuring the axial velocities at a distances of 1 mm above and below from the propeller edges, where these distances are usually depend on the rotation position of the propeller. To calculate the radial flow,  $Q_{pr}$  the outer radial borders was taken at 1 mm from propeller edges side. The formula of pumping rate calculation is depending on the velocity component occurred within the controlled area as it explained with following equations (Sardeing et al., 2003):

$$Q_{pr} = \pi D \int_{z^-}^{z^+} V_r(z) dz \quad (2.12a)$$

$$Q_{pz} = 2\pi \int_{r=0}^{r=R} r V_{z^-}(r) dr + 2\pi \int_{r=0}^{r=R} r V_{z^+}(r) dr \quad (2.12b)$$

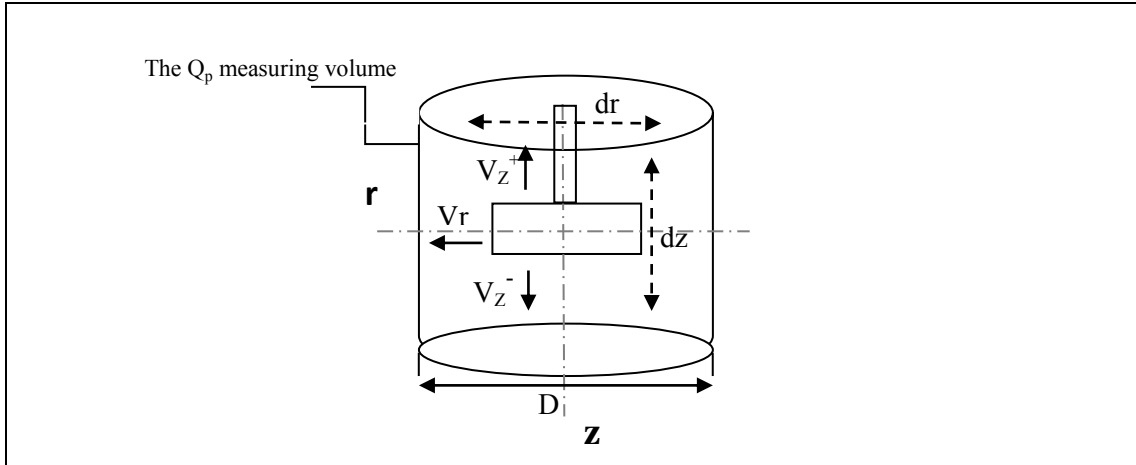


Figure (2.11): The pumping number and pumping flowrate measuring volume.

To evaluate the impellers efficiencies, sometimes instead of using the pumping number another dimensionless group was employed and called the discharge efficiency. This efficiency is varied according to the impeller type and the flow profile created by the impeller. The discharge efficiency relates with the power number to pumping number of the impeller. When the ratio  $N_p/N_{Qp}$  is large the impeller is considered that has less efficiency and when the ratio  $N_p/N_{Qp}$  is small, the impeller is considered as it has more efficiency, which is called also the circulation efficiency (Tatterson, 1991).

### III. Circulation Number and Circulation Flowrate

The overall circulated volumetric flowrate in the vessel that generated by the implemented impeller is characterized by the circulation flowrate  $Q_c$ . The calculation principle for the circulation flowrate is same as pumping the axial flowrate  $Q_{pz}$  as shown in the equations 2.12b, except that the limits of the integration are larger, where the upper limit extends to the main circulation loop center in the vessel (Aubin et al., 2001; Mishra et al., 1998).

$$Q_c = 2\pi \int_{r_{cent}}^r (r(v_z)_{z=z_{cent}}) dr \quad (2.13)$$

The maximum occurred axial flowrate in the vessel is assumed to be equal to the maximum radial flowrate (Jaworski et al., 1996). The circulation flowrate is normalized by dividing by  $ND^3$  and known as circulation number.

$$N_{Qc} = \frac{Q_c}{ND^3} \quad (2.14)$$

Since the circulation number presents the overall flowrate entrained by the impeller in the vessel, therefore the  $N_{Qc}$  is commonly greater than  $N_{Qp}$  (Jaworski et al., 1996).

#### IV. Agitation Index ( $I_g$ ) and Flow Quantification

The agitation index was derived by (Mavros and Baudou, 1997) to evaluate and compare the agitation quality of different impellers for the mixing process in stirred vessels. The agitation index calculation depends on the measured mean velocities in the r-z plane positioned on the posterior baffle (angle =  $0^\circ$ ). The agitation index is a dimensionless parameter as a percentage ratio of the total mean velocity to the impeller tip velocity:

$$I_g = \frac{v_m}{v_{tip}} \times 100\% \quad (2.15)$$

The 3-D flow inside the stirred vessel can be represented by the corresponding 2-D velocities for each volume grid that related to the vessel dimensions (See Figure 2.12), where the volume weighted average 2-D velocities can be used to compare the agitation indices. These velocities are determined in assuming that each composite mean local 2-D velocity ( $v_{ij}$ ) corresponds to a 3-D cell liquid volume and related to the grid coordinates (Garcia-Cortes et al., 2006; Mavros and Baudou, 1997). The volume weighted velocity for the vessel is calculated as:

$$v_m = \frac{\sum_i \sum_j V_{Lij} v_{ij}}{\sum_i \sum_j V_{Lij}} \quad (2.16)$$

The cumulated volume summation ( $\sum_i \sum_j V_{Lij}$ ) represents the vessel volume except the volume swept by the impellers and the volume occupied by the cone and baffle edges, the liquid volume calculations details were carried out as determined in (Mavros and Baudou, 1997).

The 2-D composite mean local velocities was calculated for each grid point in depending on the measured mean velocities in the r-z plane performed by the PIV, as following (Garcia-Cortes et al., 2006; Mavros and Baudou, 1997; Mavros et al., 1997):

$$v_{ij} = (\sum_k v_{ij,k}^2)^{1/2}, k = r, z \quad (2.17)$$

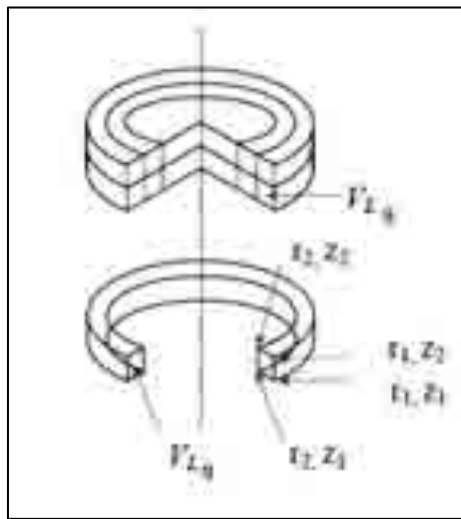


Figure (2.12): The 3-D liquid volume cell and the vessel volume grids, (Garcia-Cortes et al., 2006).

## 2.5. Mass Transfer Experimental Setup and Calculation Methods

### 2.5.1. Oxygen Probe Description

The employed oxygen probes in the experimental runs are of two types, the polarographic probe and optical probe. The polarographic probe is Inpro 6000, series O<sub>2</sub> sensors, (Mettler-Toledo), type s-96 with DO-meter of Mettler-Toledo, transmitter O<sub>2</sub> type 4100. The function of the polarographic probe depends in its measurements on the polarographic Clark electrode (i.e. electron transfer reaction principles). The polarographic probe contains two electrodes, a cathode of platen and an anode made of mercury immersed in the saline electrolyte of (PH=13). This probe requires a voltage input from the meter to polarize the electrodes. The oxygen probe has a thin membrane covering a layer of the electrolyte and the two metal electrodes (See Figure 2.13). The oxygen diffuses through the membrane at a rate proportional to its partial pressure. The oxygen meter measures the current as the oxygen is reduced at the cathode and more oxygen diffuses through the membrane, where the meter measures

the concentration of the dissolved oxygen by converting the current into concentration units. The dissolved oxygen measurement is achieved in depending on the oxygen partial pressure with correction for the affecting factors such as the temperature. The concentration units are expressed in milligrams of oxygen per liter of water (mg/l).

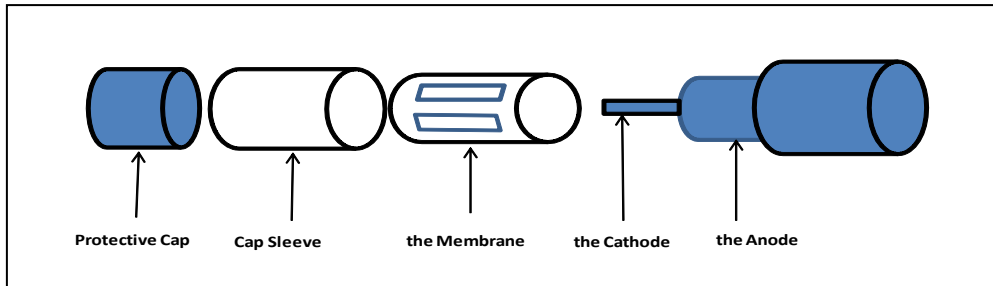


Figure (2.13): The schematic diagram of the polarographic probe.

The optical probe (HACH, LDO type) and the dissolved oxygen meter (HACH, type HQ 10 (OENODEN)) were used. With this probe, the recalibration is not necessary and the operation principle depends on the fluorescence properties of the electrode. The amount of dissolved oxygen is determined from zero concentration to the saturation. The probe includes blue LED, red LED, filter, lens, photo detector and oxygen preamble foil. The concentration of the dissolved oxygen depends on the delay by the oxygen molecules held back on the gas permeable foil in the probe cover cap for the emitted light by blue LED inside the probe. The returning signals are detected by a photo detector. This shifting or delay between the returning red light and the blue excitation is measured to determine the dissolved oxygen quantity in water (see fig. 2.14). The average percentage error of probes readings was calculated by least squares best fit between experimental and theoretical readings. Average percentages error were (3.49 %) and (4.8 %) for polarographic and optical probes respectively.

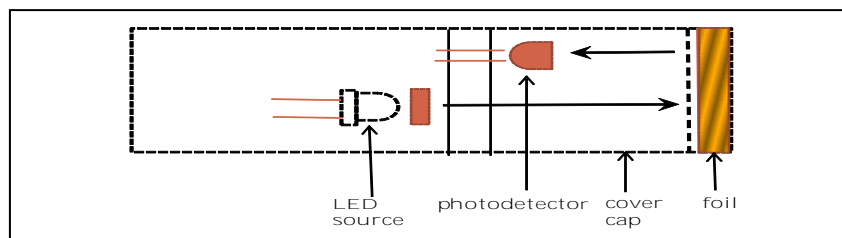


Figure (2.14): The schematic diagram of the optical probe.

### 2.5.2. Mass Transfer Coefficient

The mass transfer during the surface aeration process is occurred mostly at the water droplets surface and inside the vessel. So the operation of the oxygen transfer is assumed to be divided into two main essential mass transfer zones: first, the water spray (droplets) zone that is generated at the water surface by the impeller rotation in the encircling area around turbine. The second mass transfer zone is the water bulk zone at the water subsurface near the vessel wall and in the remaining zone inside the vessel (See Figure 2.15). The principals of oxygen mass transfer that occurs within these two zones are clearly different due to the distinct way of gas-liquid contacting. Mass transfer by surface aeration was previously identified only by the water bulk zone, whereas the little attention has been paid for the droplet zone despite of oxygen transfer is predominantly in the water droplets zone.

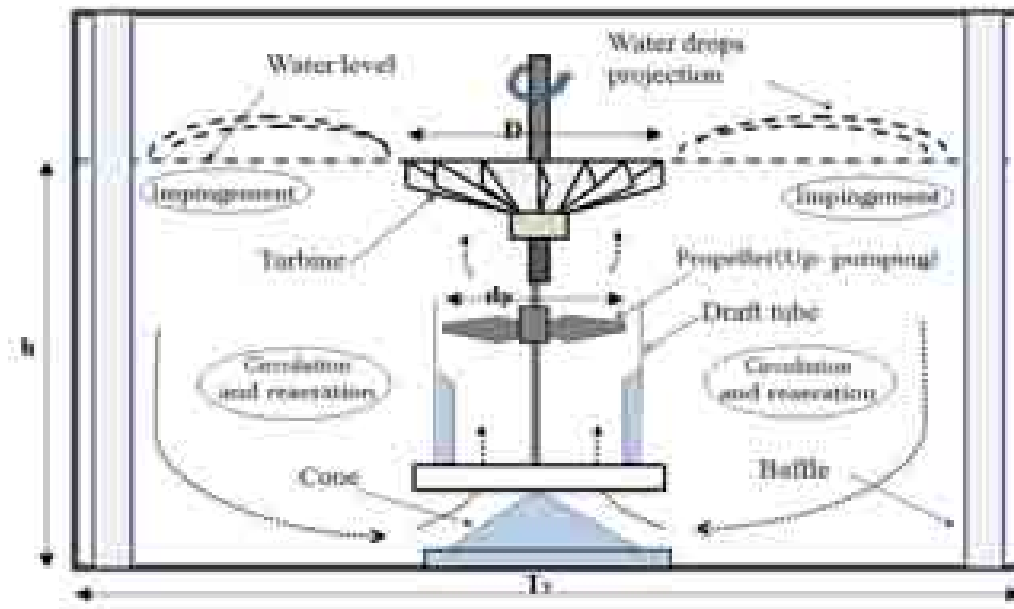


Figure (2.15): The schematic diagram of oxygen mass transfer zones.

## I. Liquid Bulk Oxygen Mass Transfer Zone

### I.1. Introduction

As the oxygen mass transfer is divided into two mass transfer operation zones of water spray and bulk zones (See Figure 2.15), it will be two occurring oxygen transfer coefficients in these two zones (McWhirter and Hutter, 1989). Our concern in this section is the water bulk mass transfer coefficient  $k_L a$ . The zone will be discussed in next section. The oxygen transfer in water bulk zone is related with many parameters, such as water level, tank and impeller geometry, rotation speed, number of impellers used and aeration rate and other operational conditions (Bandaiphet and Prasertsan,

2006; Nakanoh and Yoshida, 1980; Yatomi et al., 2008; Yoshida et al., 1960). The oxygen transfer in water bulk occurs directly after the water droplets impinge the water surface and then they plunge within water bulk; due to that air bubbles are created and are entrained inside water bulk, in a manner that they are redistributed and dispersed in whole tank.

The theory of oxygen transfer in water bulk is related to the mixing performance of the implemented impellers. The mixing process that occurs within the tank and around the propeller has been implemented widely in aeration processes in order to enhance contact area between water and air phases (Van't Riet, 1979). As the resistance to oxygen mass transfer is only considered in the water with neglecting all other resistances in the system, the oxygen mass transfer coefficient in the water,  $k_L a$  was regarded as an indicator for mass transfer rate beside the oxygen concentration profile (Shluter and Decker, 1992). The available interfacial contact area for oxygen mass transfer in aeration tank is essential for the rational design of a variety of gas liquid equipment (Dehkordi and Savari, 2011). The interfacial contact area in the liquid bulk during surface aeration depends essentially on the entrained air bubbles size (El-Temtamy et al., 1984). The applied method to determine the volumetric mass transfer coefficient  $k_L a$  in water phase is the dynamic method since the tested aeration tank is batch system, wherein the initial concentration of dissolved oxygen is close to zero. The water then is saturated by direct contact with air as a batch-wise manner (El-Temtamy et al., 1984).

The water surface re-aeration oxygen mass transfer at the water surface is counted within the water bulk zone, as the boundary of this zone begins directly where the spray zone ends. The water surface re-aeration is actually not a part of water bulk oxygen transfer, where at the water surface the atmospheric air is entrained into the water as result of turbulent condition formed by the falling water droplets.

The re-aeration operation at water surface is more convenient to be included in the spray mass transfer zone but it is so difficult to consider the surface re-aeration as separate zone from bulk zone because of its boundaries are so hard to be identified clearly as they are highly combined with water bulk transfer zone due to flow profile and mixing effects take place in the tank.

The proposed model that represents the occurred oxygen transfer operation in all parts (surface re-aeration and bulk inside) of liquid (water) bulk mass transfer zone is the two-film theory (Atkinson et al., 1995).

The water bulk zone experiments were carried out with the turbine and the 4-bladed reversible twisted pitched RTP propeller was mounted to the rotation shaft below the turbine. The draft tube is installed around of the RTP propeller.

The water bulk zone experiments were conducted with the system configuration of  $D/T_v = 0.238$ ,  $C/T_v = 0.313$ ,  $d_{pr}/T_v = 0.15$ ,  $C_{pr}/T_v = 0.2$ ,  $h/T_v = 0.35$ ,  $d_f/T_v = 0.188$ , but these ratios were changed as several geometrical parameters are tested.

### **I.2. Bulk Zone Oxygen Mass Transfer Calculation Methodology**

Since the whole resistance to the mass transfer is occurred in the liquid phase, the oxygen mass transfer coefficient in the gas phase is neglected. It is assumed that no other mass transfer occurs during the operation for the other constituents from the air toward the water and also for the used nitrogen gas during the deoxygenating process.

The implemented calculation for the oxygen mass transfer,  $k_{1a}$  in the experimentation was also based on several general assumptions: the vessel is efficiently mixed; subsequently the  $k_{1a}$  values throughout the vessel can be represented as one value. Also the saturated dissolved oxygen can be represented as one value, the other mass transfer may occur that are related to other constituents from the air toward the water as well as the nitrogen gas -during the deoxygenating process are neglected. Weak heat gradient occurred during the aeration; in that manner the accompanied heat transfer is ignored.

### **I.3. Testing Different Probe Positions in the Vessel**

It is assumed that the liquid is well mixed and the variation in  $k_{1a}$  measured values should not exist. In order to verify this, seven different positions for the oxygen probes are tested. The measured  $k_{1a}$  for the seven different positions were close, where the  $k_{1a}$  is changing about  $\pm 2.5\%$  of the value  $4.1 \times 10^{-3} \text{ 1/s}$  in all tested points of the tank (See Figure 2.16, a). The difference could be due to various affecting factors like the accumulation of oxygen bubbles on the probes, the difference of time lag for the two probes. The measurement of the dissolved oxygen is carried out by both optical and polarographic probes placed in two different positions inside the vessel (See Figure 2.16, b).

Because the measured  $k_{1a}$  for seven different positions is close and the difference noticed is very small, the assumption of well mixed tank can be verified for the used probes accuracy and for applied experimental conditions (Philichi and Stenstrom, 1989).

**I.4. Repeatability of Experimental Results**

The experimental results repeatability were tested by repeating each time two experimental runs for same geometric configuration of same probe and for the two used oxygen probes. The results were close for all the cases, as it can be noticed from the figure 2.17 (the results obtained at a clearance of 0.10 m, from vessel bottom, where the  $k_{l,a}$  was about  $(2.4 \times 10^{-3} \text{ 1/s})$  for both cases at  $N=2.08 \text{ rps}$ ).

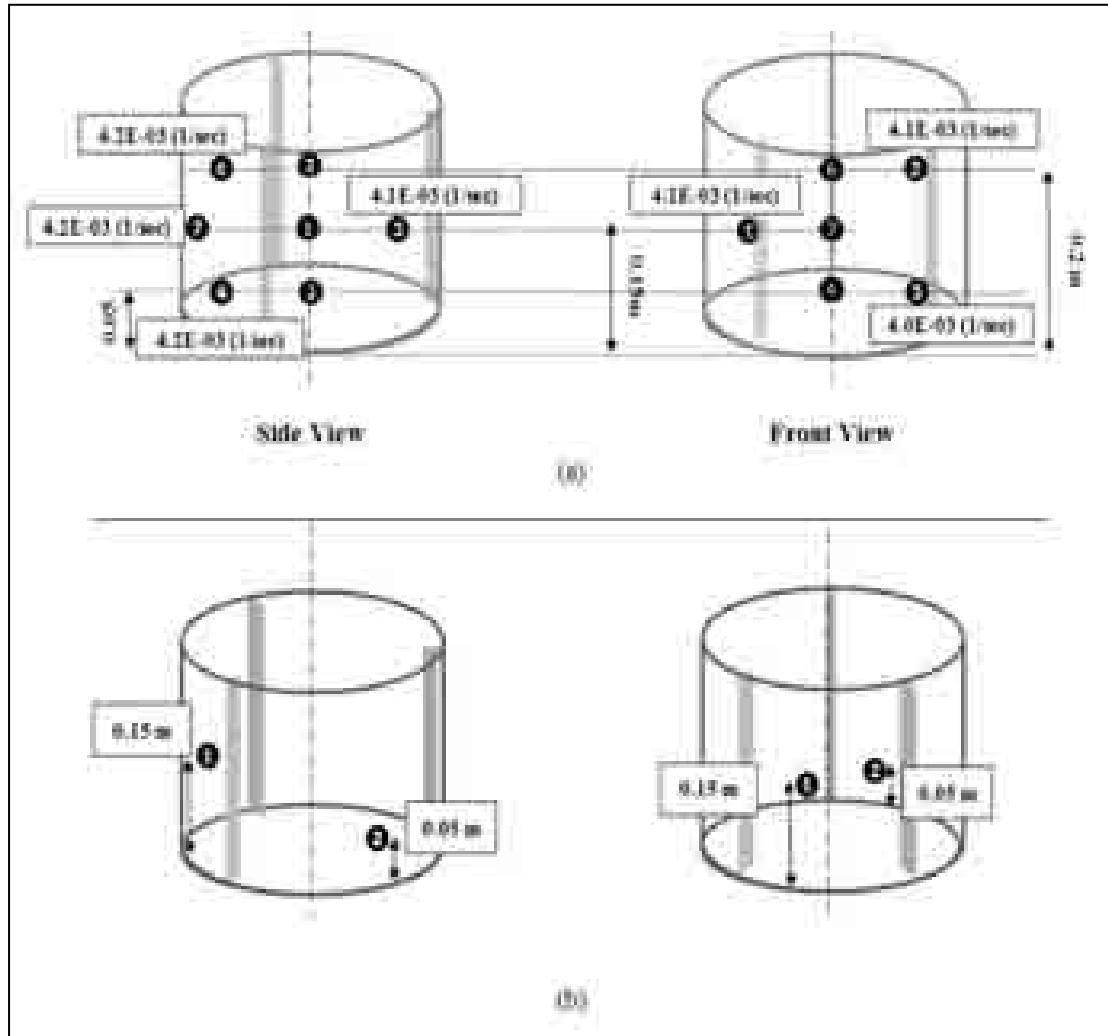


Figure (2.16): (a) Experimental oxygen probes positions in the liquid volume, (b) Experimental oxygen probes positions in the liquid volume,  $N=2.5 \text{ rps}$ ,  $(h/T_v) = 0.35$ .

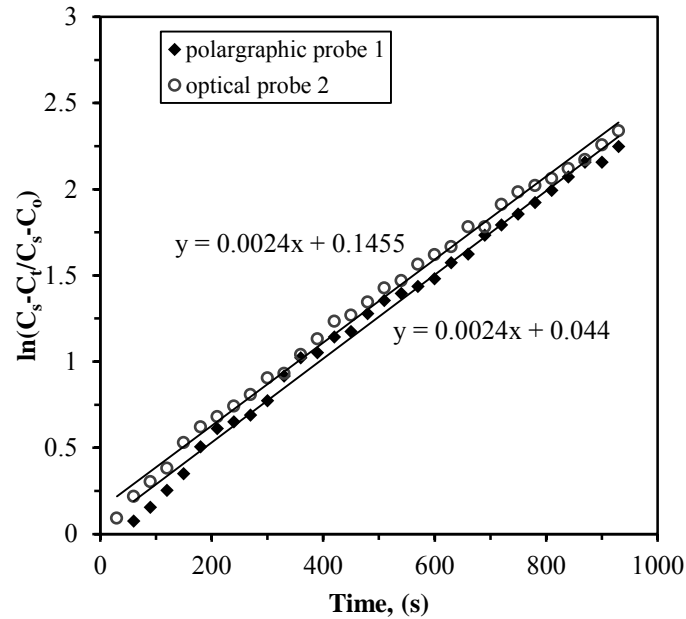


Figure (2.17): The repeatability of the mass transfer ( $k_1a$ ) experimental results for both oxygen probes, ( $N= 2.08$  rps).

### 1.5. De-oxygenation and Re-oxygenation Processes

In order to perform the oxygen mass transfer coefficient experimental runs, it is necessary to apply the de-oxygenation of the water, the implemented technique of deoxygenating is accomplished by bubbling the nitrogen gas through the water inside the vessel until it reaches the lowest possible dissolved oxygen concentration level DO ( $\leq 0.5$  mg/l) within reasonable time period (1/2 hr.). The operating fluid during all experimental runs is tap water. To determine the oxygen mass transfer coefficient during the surface aeration, direct measuring of DO is applied by the immersed probes.

### 1.6. Oxygen Probe Response Time Measurement Verification

The response time for each of the used probes (polarographic and optical) in the experimentation is determined by depending upon both the experimental and theoretical results of dissolved oxygen. The theoretical values of the dissolved oxygen are determined by equation (3.11), (Merchuk et al., 1990; Mueller et al., 1967):

$$C_t = C_s - (C_s - C_o) e^{-t/\tau} \quad (2.18)$$

While the experimental DO values are determined directly during the experimental measurements of the probes response time through the direct changing from the zero DO level solution (prepared by passing the Nitrogen gas through the water), then into

100% saturated solution (prepared by passing the air through into the water for sufficient time), where the DO concentration were measured each 3 seconds until reaching the saturation concentration level for the DO.

The  $\tau$ , response time is determined by identifying the lowest difference value between the experimental and the theoretical value that is calculated by equation (2.18) of dissolved oxygen values which matches the highest value of the R-squared for the least square method application, as it shown in the (Figure 2.18 and Figure 2.19). The response time for the polarographic probe (Inpro 6000) is (9.2 sec) and for the optical probe (HACH, LDO type) is (8.8 sec).

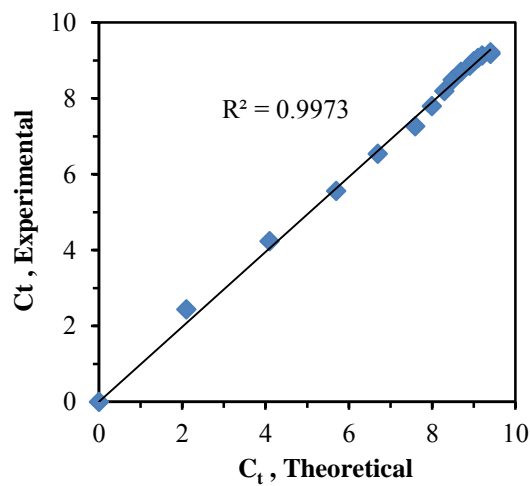


Figure (3.18): Optical probe response time verification

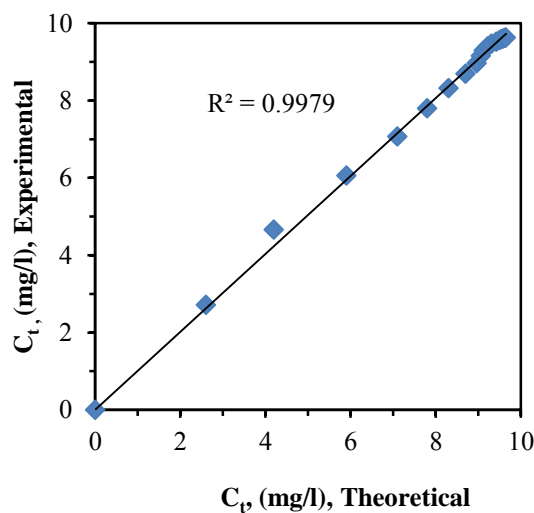


Figure (2.19): Polarographic probe response time verification.

### **I.7. Determination Model of the Bulk Zone Oxygen Mass Transfer Coefficient ( $k_1a$ )**

The relationship between the DO with the time during the surface aeration process with taking in account the effect of probe response time can be represented as the following equation (Arjunwadkar et al., 1998; Chern and Yang, 2003; Puthli et al., 2005):

$$\frac{dC_l}{dt} = k_1a(C_s - C_l) \quad (2.19)$$

By applying the boundary condition at  $t=0$ ,  $C_l=C_0$  and at  $t=t$ ,  $C_l=C_t$ :

$$C_t = C_s - (C_s - C_0) e^{(-k_1at)} \quad (2.20a)$$

By rearranging equation (2.20a):

$$\ln \frac{(C_s - C_t)}{(C_s - C_0)} = k_1a \cdot t \quad (2.20b)$$

On the other hand, the effect of probe response time on the dissolved oxygen concentration measurement for aeration processes is identified according to the following equation (Sardeing et al., 2005):

$$C_t = C_s + \frac{C_s - C_t}{C_s - C_0} (k_1a \cdot \tau e^{-t/\tau} - e^{-k_1at}) \quad (2.21)$$

To evaluate the probe response time effect on the experimental results and the calculated mass transfer coefficient  $k_1a$ , a comparison was made for same experimental and calculated conditions. The dissolved oxygen concentrations in both experimental and theoretical that calculated by equation (2.21) for the polarographic and optical probes respectively are shown in the figure (2.20) and (2.21). The oxygen mass transfer relation with time with considering the probe response time was implied in the applied mass transfer equation that represents the experimental runs to take in account the experimental errors that are produced due to that. The oxygen mass transfer coefficient is calculated theoretically with applying equation 2.21, where the effect of time lag constant for the oxygen probes are implied in our calculations of oxygen mass transfer in water bulk zone  $k_1a$ .

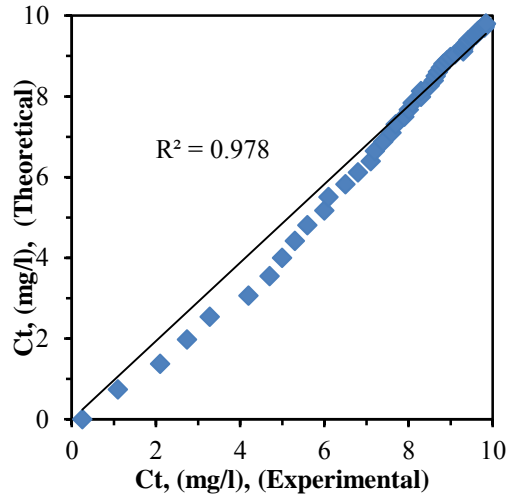


Figure (2.20): The probe response time relationship verification for both theoretical and experimental DO values for the optical probe.

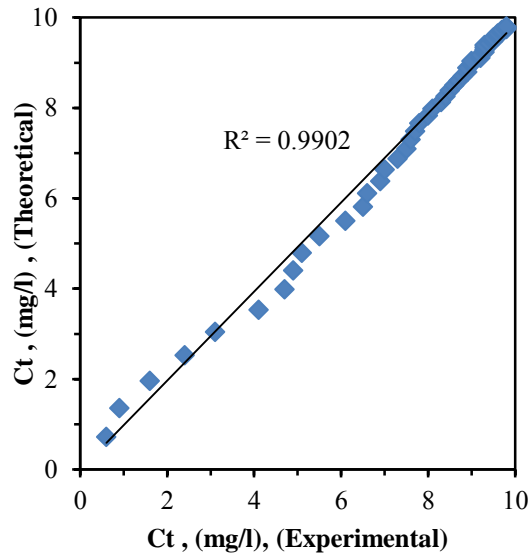


Figure (2.21): The probe response time relationship verification for both theoretical and experimental DO values for polarographic probe.

### I.8. Measurement Procedure for the Bulk Zone Oxygen Mass Transfer Coefficient

At the beginning of the experimental runs, the water volume was de-oxygenated by the bubbling of Nitrogen gas through it for at least 15 minutes until DO concentration becomes below (0.5 mg/l). The DO measurements were conducted directly by the two probes that situated in their positions as shown in the Figure (2.16), where the dissolved oxygen was measured each 30 seconds till reaching the saturated level, where run was terminated. The operation parameters and geometric configuration

were considered as variables according to the purpose of the experiments to identify their influence.

### **I.9. Temperature Correction for the Oxygen Mass Transfer Coefficient**

To calculate the necessary parameters for standard oxygen transfer rate and the standard aeration efficiency its needed to correct the measured oxygen transfer coefficient in the liquid to the standard conditions, where the following (Van't- Hoff, Arrinuous) equation was applied (Capela et al., 2004):

$$(k_l a)_{10^{\circ}C} = 1.024^{(10-T)}(k_l a)_T \quad (2.22)$$

The volumetric coefficient of oxygen mass transfer is derived by depending on the all the resistances in the water to oxygen transfer. The volumetric coefficient of oxygen transfer,  $(k_l a)_T$  is measured at operation temperature T, and corrected to standard temperature here usually T=10 °C or 20 °C by the equation 2.22 (Roustan, 2003).

### **I.10. Oxygen Transfer Rate for the Bulk Mass Transfer Zone ( $OTR_b$ )**

The oxygen transfer rate (OTR), which is the transferred mass of oxygen rate at experimental condition in the total volume of the filled vessel with water.

$$OTR = k_l a C_{LS} V_L \quad (2.23)$$

To have complete view for oxygen mass transfer for all surface aeration process and to realize the contribution of droplets spray mass transfer zone in the oxygen mass transfer operation, oxygen mass transfer rate in other side of water bulk re-aeration mass transfer zone  $OTR_b$  is needed to be calculated.  $OTR_b$  was determined by applying the following relation, which is modified to be agreeable for implemented system depending upon mass transfer expression derived by (Chern and Yang, 2004):

$$(OTR_b) = k_l a (C_{LS} - C_{Lt}) V_L \quad (2.24)$$

### **I.11. Standard Oxygen Transfer Rate for the Bulk Mass Transfer Zone ( $SOTR_b$ )**

The standard oxygen transfer rate ( $SOTR_b$ ) is the transferred mass of oxygen rate at standard condition in the total volume of tank filled with water. The  $SOTR_b$  is the standard criterions that employed to determine the surface aeration performance

beside the standard aeration efficiency  $SAE_b$  (Cancino et al., 2004; Sardeing et al., 2005).

$$(SOTR_b) = (k_l a)_{10^{\circ}C} (C_s)_{10^{\circ}C} V_L \quad (2.25)$$

### I.12. Standard Aeration Efficiency for the Bulk Mass Transfer Zone ( $SAE_b$ )

The standard aeration efficiency ( $SAE_b$ ) sometimes it called the overall transfer efficiency which represents the mass of oxygen transferred to the water per the consumed power (Cancino et al., 2004; Sardeing et al., 2005)

$$(SAE_b) = \frac{(3.6 \times 10^6) \cdot (kla)_{10^{\circ}C} \cdot (C_s)_{10^{\circ}C} \cdot V_L}{P} \quad (2.26)$$

## II. Spray Oxygen Mass transfer Zone

### II.1. Introduction

The oxygen mass transfer coefficient at the water surface, which is identified as spray (droplets) zone oxygen transfer coefficient  $k_{lad}$  is investigated in details in this study. The spray zone begins with the creation of the water droplets thrown into the atmospheric air rapidly as a projection (spray) at the water surface by the turbine through the annular surrounding peripheral space until they impinge the water surface at the end of their flight, where with this point the second zone of water bulk occurs (See Fig. 2.15). The oxygen that transferred at this step mostly takes place at the wall of these droplets, where for this kind of gas-liquid contacting is considered as a single stage zone. The droplets are the dispersed liquid phase into the virtually infinite continue gas phase with constant oxygen concentration in the atmospheric air. The gas phase is considered as completely mixed of constant atmospheric air composition with plug flow of dispersed liquid phase for water droplets (McWhirter et al., 1995). It is assumed that any other possible secondary mass transfer can be occurred is neglected such as the possibility of the Nitrogen gas transfer contained in the atmospheric air toward water droplets. Since the mass transfer resistance is exist merely at the liquid phase side, so the water mass transfer toward the gas phase is neglected.

## II.2. Spray Zone Oxygen Mass transfer Coefficient Calculation Methodology

The occurred operation within and around the water droplets during their flight is not only the oxygen mass transfer, other parameters as well accompany the operation like the heat transfer or the water evaporation. The heat transfer that combined with the mass transfer has very important effect on the water droplets air surface temperature, and it is not the same with the water bulk inside the vessel. The employed saturation level here is considered as the wet bulb temperature of the air,  $C_{ds}$  (Huang et al., 2009). The basis used for this assumption is depending on the fact that the path of water droplets in the atmospheric air follows its own conditions of constant air composition, humidity and temperature which is completely different from those existed in the water bulk. As a result the higher equilibrium oxygen concentration can be reached theoretically for the droplet is the air wet-bulb temperature. The constraining factor controls how deep the wet-bulb temperature goes inside the droplet is depending on the droplet flight time, (which is too short in our case). Consequently the wet-bulb temperature prevails only at water droplet surface, while the inner droplet part temperature is highly effected by the relative high droplet velocity in the air and high heat transfer caused by this velocity, it remains generally at lower level than the surface temperature, while due to the inner motion the oxygen mass transfer inside the droplets is enhanced (Sirivasan and Aiken, 1988).

## II.3. Determination Model for the Spray Zone Oxygen Mass Transfer Coefficient ( $k_1a_d$ )

The representative model for the spray zone that explains the oxygen mass transfer during the travel of the droplets in the atmospheric air from turbine blades tips until their impingement points at the water surface. The droplets trajectory are determined by the following unsteady state oxygen mass balance equation (McWhirter et al., 1995):

$$V_d (dC_d/dt_f) = k_l A_d (C_{sd} - C_d) \quad (2.27)$$

In equation (2.27) several assumptions are made to facilitate the explanation of the oxygen transfer process for the intended zone. Each water droplet is assumed to be completely mixed; the dissolved oxygen distribution is uniform within the droplets at any time when they traverse the atmospheric air until their impingement points at water surface with no back mixing might take place during this flight. The dissolved oxygen concentrations at the limits of the droplet zone are related with other presented zones, where at the zone inlet the concentration at any time is the same of the well mixed liquid bulk for the dissolved oxygen concentration level inside the

vessel. The dissolved level at the outlet of the droplet zone (when the spray hits the water surface) for the oxygen gas is considered as  $C_{dt}$ . The dissolved oxygen at outlet of droplets zone,  $C_{dt}$  is the average of concentrations level for all the droplets at the end of water droplets spray zone. If the droplets volume and the mass transfer coefficient with the droplets oxygen saturated concentration are considered constant, the equation (2.27) can be integrated and resolved as follows:

$$C_{dt} = C_{ds} - (C_{ds} - C_{Lt}) \exp(-k_l A_d t_f / V_d) \quad (2.28)$$

Equation (2.27) is a distinguishing equation that is built to explain especially the droplet spray oxygen mass transfer zone; the oxygen behavior is well described particularly for this step on the contrary for the equation (2.19), which is a general equation that can be applied for the mass transfer zones but with the limited ability to identify the actual mass transfer path that happens in each step. Equation (2.28) shows that it is preferred to keep the droplets volume at the minimum during the surface aeration process to reach possible highest dissolved oxygen level. For the same reason the droplets should stay as long as possible in the atmospheric air before they fell down into the liquid bulk and go inside the vessel.

In order to evaluate the efficiency for gas-liquid contacting systems, it is common to apply a known indicating factor called (Murphree contacting efficiency  $E_{md}$ ) for various mass transfer operations (Baylar and Bagatur, 2000b; Chisti and Jauregui-Haza, 2002; Sharma, 2007). In the surface aeration water spray zone and in other similar processes, the implemented criterion for indicating the progressive oxygen mass transfer that takes place is the Murphree contacting efficiency or it is called in our case the spray mass transfer zone aeration efficiency,  $E_{sp}$  (Toombes and Chanson, 2005; Vouk et al., 2005).

Equation (2.28) is rearranged to express the contacting efficiency is dependent on the fraction between the actual and the theoretical oxygen transfer in the droplets spray:

$$E_{md} = \frac{C_{dt} - C_{Lt}}{C_{ds} - C_{Lt}} = 1.0 - \exp\left(\frac{-k_l A_d t_f}{V_d}\right) \quad (2.29)$$

Equation (2.29) shows that the contacting efficiency can be varied from its minimum value (0.0) (no mass transfer occurred) to its maximum value of (1.0), which is an ideal condition that can be reached at infinite time when equilibrium is achieved between the water droplets and the atmospheric air (McWhirter et al., 1995). The equilibrium level for the dissolved oxygen at the droplets outer surface depends on the

air humidity is less than the saturation level in the water bulk. So the saturation level at this condition is better represented by the wet bulb temperature than the normal dissolved oxygen saturation level in the water bulk; the presence of related heat transfer takes place, as the air temperature here differs from the water bulk temperature.

Rearranging equation (2.29) and re-writing it in the term of water spray zone surface aeration efficiency gives us the following:

$$E_{sp} = \frac{C_{dt} - C_{Lt}}{C_{ds} - C_{Lt}} = 1.0 - \exp(-k_l a_d t_f) \quad (2.30)$$

In the equation (2.30), the definition of Murphree contacting efficiency relates the boundary levels for the actual and theoretical oxygen concentration gradients that take place from water droplets propelling position to the impingement with water surface location. In order to facilitate the calculation of the oxygen mass transfer results, the previous equation (2.30) is rearranged in more appropriate correlation form (Baylar and Bagatur, 2000a; McWhirter et al., 1995):

$$C_{dt} = (1 - E_{sp})C_{Lt} + E_{sp} C_{ds} \quad (2.31)$$

From equation (2.31) it can be estimated that the plot between the resulted oxygen concentrations at the droplets impingement point with water surface at the corresponding recorded water bulk dissolved oxygen gives a straight line with a slope of  $(1 - E_{sp})$ , and the intercept with y-axis will be  $(E_{sp} C_{ds})$ .

Same as the surface aeration the similar efficiency calculation technique is applied in other aeration processes like the aeration by weirs (Baylar et al., 2006; Kim and Walters, 2001), where it is required to find a uniform basis for comparison purposes between the obtained results, which can be achieved by normalizing the calculated efficiencies to standard condition.

#### II.4. Temperature Correction for the Spray Mass Transfer Zone

The spray mass transfer zone aeration efficiency,  $E_{sp}$  is corrected to the standard temperature condition, mostly of 20 °C by applying, the widely applied temperature correction relation is the Arrhenius type of water temperature correction. The following relationship is developed by many previous work, (Baylar et al., 2010; Gulliver et al., 1998; Khudenko, 1983; Nakasone, 1987; Wormleaton and Soufiani, 1998):

$$1 - (E_{sp})_{20} = (1 - E_{sp})^{(1-f)} \quad (2.32)$$

Where the  $(E_{sp})_{20}$  is the spray aeration efficiency at 20 °C, and  $E_{sp}$  is spray transfer aeration efficiency at the water bulk temperature,  $f$  is the exponent determined by the following equation:

$$f = 1.0 + 0.02103(T - 20) + 8.261 \times 10^{-5}(T - 20)^2 \quad (2.33)$$

### II.5. Oxygen Transfer Rate in the Spray Mass Transfer Zone ( $OTR_{sp}$ )

It is necessary to take in account the relative humidity of the air when this approach of  $OTR_{sp}$  is applied if a remarkable change is occurred with the relative humidity during the experimentation because the saturation level that used at the air wet-bulb temperature is also depends on the air relative humidity.

Another important factor in the oxygen transfer in the water droplets spray zone is the oxygen transfer rate  $OTR_{sp}$ , which beside the standard aeration efficiency depends on the water volumetric flow rate discharged by the turbine blades (Chern and Yang, 2004; McWhirter et al., 1995):

$$(OTR_{sp}) = Q(C_{at} - C_{Lt}) = QE_{sp}(C_{ds} - C_{Lt}) \quad (2.34)$$

### II.6. Spray Zone Mass Transfer Coefficient ( $k_{ia_d}$ ) - Measurement Procedure

The measurements performed are similar to the mass transfer coefficient inside the liquid bulk except that in this case it is needed to measure the dissolved oxygen at the end of water droplets spray zone before they go inside the vessel,  $C_{ds}$ . The implemented measurement technique in this case for the given surface aeration operation conditions and geometric configurations are depending on the dissolved oxygen level in the droplets during their flight. In order to achieve the accurate investigations it is needed to apply sampling for the droplets at nearest point above the water surface prior to their clash with the surface and enter inside the bulk. The available way for this sampling is collecting these droplets by narrow neck bottle provide with rubber cup to prevent further contact with air after the appropriate amount is collected (the collected water quantity was in the neck bottle for each reading was approximately between 20 to 25 ml). Then an immediate measurement is applied by an optical oxygen probe. The measurement is repeated periodically each (60 seconds). At the same time, the dissolved oxygen level inside the water bulk is measured also by the polarographic oxygen probe positioned inside the vessel; the dissolved oxygen is registered with same time interval for each (60 seconds) (See Figure 2.22).

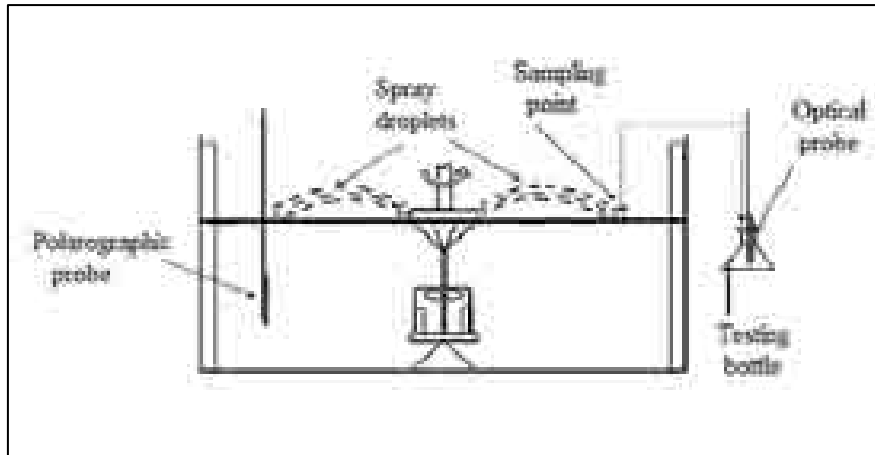


Figure (2.22): The droplets zone mass transfer coefficient ( $k_{1a_d}$ ) measurement.

### 2.6. Water Droplets Flight Time ( $t_f$ )

In order to calculate water spray zone oxygen mass transfer coefficient  $k_{1a_d}$ , it is necessary to be determined the droplets flight time. The droplets flight time is calculated in function of the directly measured maximum droplets height  $Y_m$  and the height of apparent turbine blade above water surface  $H$  (See Figure 2.23), as it shown in the following equation (McWhirter et al., 1995):

$$t_f = \sqrt{2(Y_m - H)/g} + \sqrt{2Y_m/g} \quad (2.35)$$

Equation (2.35) is derived principally from Newton's second law of motion, where the initial vertical velocity of the water droplets has a changeable value during droplets throwing operation (as it will be seen in next section). The droplets flight time is affected by its trajectory, which in turn is affected by many parameters beside rotation speed that act as lift force on droplets, like gravity, buoyancy and drag force (Matsuura et al., 2003).

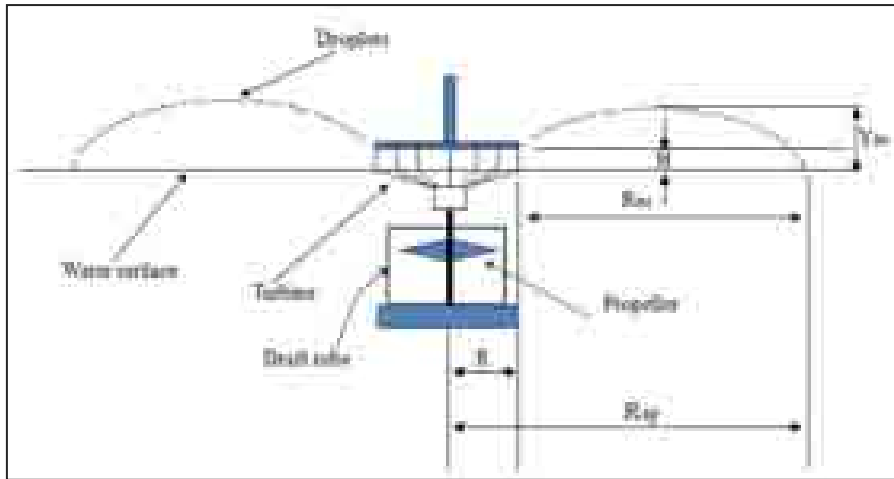


Figure (2.23): Schematic diagram illustrates the surface aeration water droplets spray from turbine blades till the impingement point with some important relevant dimensions.

### 2.7. Water Droplets Velocity and Volumetric Flow Rate

The water droplets are discharged with a considerably high velocity  $V_{sp}$  according to turbine rotation speed used. The water droplets velocity is regarded as an essential step for further droplets spray zone related calculations. Determining  $V_{sp}$  by directly measuring turbine discharge velocity is somehow complicated. The alternative way is applying the measurements to droplets flight path, where these projected droplets are considered as free falling objects following physical laws that used in similar cases. In order to simplify  $V_{sp}$  calculation, several assumptions are applied; (i) no friction losses due to droplets flight in the atmospheric air, (ii) regardless to droplets projection position by turbine blades above the static water surface, and (iii) maximum droplets height during their trip is considered constant that equal to  $Y_m$  that corresponds to maximum spray radius  $R_m$  that fulfilled by droplets impingement at the water surface. The total water spray droplets velocity can be feasibly represented by one value, wherein in turn the three components of the spray droplets velocity are constant. The spray droplets velocity is consisting of three components; vertical, radial and tangential velocities, where their relationship can be represented by the following equation (Huang et al., 2009; McWhirter et al., 1995):

$$V_{sp}^2 = V_y^2 + V_r^2 + V_\theta^2 \quad (2.36)$$

Droplets vertical velocity propelled by the turbine in contrast to radial and tangential velocities is determined by its initial velocity because at a certain point it begins to change pursuant to acceleration of gravity; ( $V_{oy}^2$ ) is determined by measuring the spray maximum height (See Fig. 2.23), (Huang et al., 2009; McWhirter et al., 1995) as follows:

$$V_{oy} = \sqrt{(2g(Y_m - H))} \quad (2.37)$$

The used straight tip blade turbine propels water droplets toward radial and tangential directions in a horizontal plane, is parallel to the water surface, as it has been described in Figure 2.24. To calculate these velocities for the given applied geometry the following relationships (See equations 2.38 and 2.39) are employed (McWhirter et al., 1995) with equation (2.35) for droplets flight time:

$$(V_a)^2 = V_{\phi}^2 + V_r^2 \quad (2.38)$$

$$V_r = \frac{R}{t_f} \left[ -1 + \frac{R_{sp}}{R} \left( 1 - \left( \frac{V_{\phi} t_f}{R_{sp}} \right)^2 \right)^{1/2} \right] \quad (2.39)$$

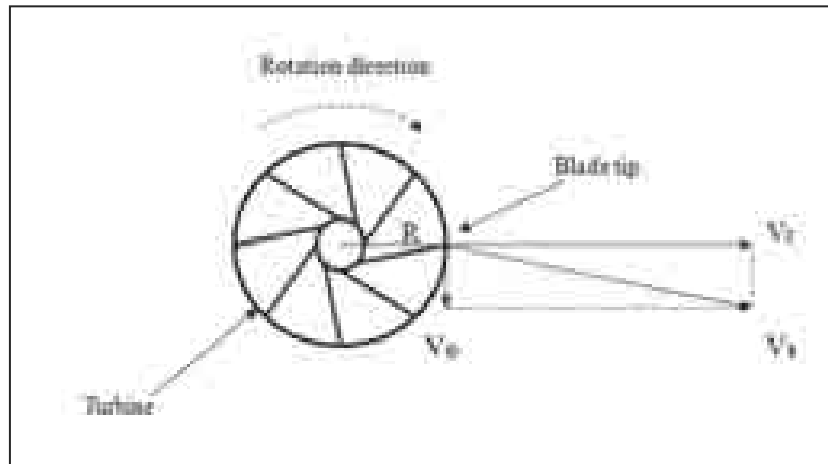


Figure (2.24): Droplets radial and tangential velocities propelled in horizontal plane by turbine blades.

The determination of  $V_r$  and  $V_\phi$  separately is very complicated, because in general they are calculated together as ( $V_a$ ). But  $V_a$  in turn is also not easy to be measured or identified, and it needs a sophisticated analysis that depends on the turbine geometric configuration. (Huang et al., 2009) tried to simplify this analysis for straight blade tip turbine. In order to have feasible value of oxygen transfer rate in the spray mass transfer zone, (Huang et al., 2009) considered it is more logical to determine this value at droplets impingement point with water free surface. The occurred velocities at impingement point are essentially the radial velocity  $V'_r$  and secondly the axial vertical velocity  $V'_y$ , when on the other hand the tangential is very weak and can be ignored or actually it disappears. So the velocities at impingement position can be calculated as follows:

$$V'_r = (R_{sp})/t_f \quad (2.40)$$

$$V'_y = \sqrt{2gY_m} \quad (2.41)$$

At the impingement position the water droplets velocity is considered approximately equal to the discharge velocity from turbine blades and the water spray droplets direction is not different evidently from radial direction. For very short droplets flight time up to (0.19 s), the energy consumed in the atmospheric air was neglected. ( $V_{sp}$ ) can be determined as:

$$V_{sp} = \sqrt{(V'_r)^2 + (V'_y)^2} \quad (2.42)$$

When the droplets spray velocity is known, the volumetric flow rate of the droplets that are propelled at turbine blades edges can be determined by applying the overall conservation of energy to surface aeration turbine and the overall power consumed through blades to project these droplets into atmospheric air. It is assumed the power consumption is delivered to the free water surface as a kinetic energy, which contributes to elevate water velocity up to discharge velocity leaving the blades as droplets thrown in the air with power conversion is 100% effectively achieved (Baylar et al., 2001). The energy balance relation gives an appropriate relation between the spray volumetric flow rate and the power consumption (Baylar et al., 2001; McWhirter et al., 1995). (Baylar et al., 2001) used in their approach the pumping power relation in weir aeration process by water droplets creation. The relation was applied within the boundaries between jet point and plunging point of droplets. In surface aeration process the previous relation can be considered as a convenient

relation that employed in similar conditions, where the better way is applied the energy conservation of converted mechanical energy to a kinematic energy within the boundaries between the inlet and outlet points along turbine blades, where for 100% energy conversion efficiency the general energy balance yields the following relation:

$$P = 1.389 \times 10^{-7} \rho Q (V_{sp})^2 \quad (2.43)$$

Where, the constant  $1.389 \times 10^{-7}$  depends on the applied geometry of the surface aerated equipment. For eliminating errors that may occur when whole system is used during the energy balance calculation, the power consumption was measured only with presence of the turbine to assure all the energy was converted to propel water droplets into atmospheric air (i. e. the power consumption by the propeller with draft tube do not have any relation with droplets generation outside the water surface but they consume power only for water bulk mixing purposes inside the tank).

### 2.8. Conclusions

The procedures for measurements and calculation methods for the oxygen mass transfer coefficients in both water bulk and water droplets spray zones, power consumption, mixing time, water spray discharge flowrate, water droplets flight time and other related parameters are represented in this chapter. These methods are applied in the experimentation to propose the results that are showed in the next chapters. The measurements of the flow field and mean velocity profiles in all parts of the tank that achieved by Laser Doppler Velocimetry LDV and Particle Image Velocity PIV are also have been described in this chapter.



**CHAPTER THREE**  
**OXYGEN MASS TRANSFER IN  
THE SURFACE AERATION**



## Chapter Three

### The Oxygen Mass Transfer in the Aeration Mode

The surface aeration system has the capacity to operate in two different operation modes; (i) Firstly, The aeration mode, where two phases (water and air bubble) condition occurs, this mode is always exist when the turbine is employed. Mode, where the single phase condition occurs, the mixing is accomplished by the RTP propeller (no oxygen mass transfer takes place in the mixing mode).

The oxygen mass transfer in the surface aeration system is divided into two main mass transfer operation zones of water bulk and spray zones according to the way of contact between the water and the air (See Figure 2.14). The two occurring oxygen transfer zones have two phases; the dispersed phase of the water droplets in the continuous phase of atmospheric air. In water bulk mass transfer zone these two phases are reversed, where the continuous phase is the water bulk and the dispersed phase is the air bubbles. For these two zones there will be two different oxygen mass transfer coefficients (McWhirter and Hutter, 1989). The water spray zone represents the oxygen mass transfer that takes between the atmospheric air and water droplets in the spray. While the water bulk zone represents the oxygen mass transfer that takes place inside aeration tank between air bubbles and water bulk. It is so hard to identify clearly the limits between the two zones. Theoretically the water bulk zone doesn't begin directly when the water droplets impinge water surface where air bubbles are created and entrained inside water bulk. Due to this impingement and the direct contact with the atmospheric air a separate mass transfer zone occurs, where a re-aeration takes place between the water surface and the atmospheric air in a manner close to that happened in the water spray zone. This water surface aeration is actually not a part of water bulk zone. But it is highly combined with water bulk transfer zone due to flow profile and mixing effects that takes place in the tank zone, so practically the effect of surface re-aeration is included in this water bulk zone.

### 3.1. Water Bulk Mass Transfer Zone

#### 3.1.1. Introduction

The measurement of the dissolved oxygen deficit carried out by utilizing both of optical and polarographic probes, they are placed in two different positions inside the vessel (See chapter 2), as it is assumed before the liquid is efficiently mixed, in this way the variation in  $k_1a$  measured values should not to be exist or to be very limited. In order to verify that, seven different positions for the oxygen probes are tested, (the measured  $k_1a$  for the seven different positions were close (the resulted  $k_1a$  was around  $4.0 \times 10^{-3}$  1/s, as illustrated in Figure 2.15), the difference noticed was very small, this gap might be caused by the simple accumulation of oxygen fine bubbles on the probes

despite of the effective circulation occurs in the vessel or due to the difference of saturated concentration levels between these positions.

### 3.1.2. The Experimental Results

#### I. Effect of Geometrical Configuration

Three geometrical configurations are examined beside the whole system configuration; (i) the turbine and propeller (draft tube elimination), (ii) the turbine alone (the draft tube and propeller elimination) and (iii) the turbine and the draft tube (the propeller elimination) (See Figure 3.1). For all the modifications it was found that the  $k_{1a}$  is relatively lower than that achieved by the whole system configuration (Figure 3.2), which indicates that with propeller and/or draft tube has a contribution in  $k_{1a}$ . It is obvious that the draft tube improves the propeller function, where the flow pattern is affected by redirecting the flow from the lower propeller towards the turbine. From Figure 3.2, it was found that neither the draft tube nor the RTP propeller can improve  $k_{1a}$  individually, where their influences appear to be combined. Figure 3.2, illustrates that the contributions of draft tube and propeller in the enhancement of  $k_{1a}$  are negligible at low impellers speeds, their effect starting to appear with impeller speed higher than 2.08 rps ( $Re = 75000$ ,  $\pi ND = 1.24$  m/s), which can be considered as critical rotation speed for the surface aeration as it will be discussed the in next section.

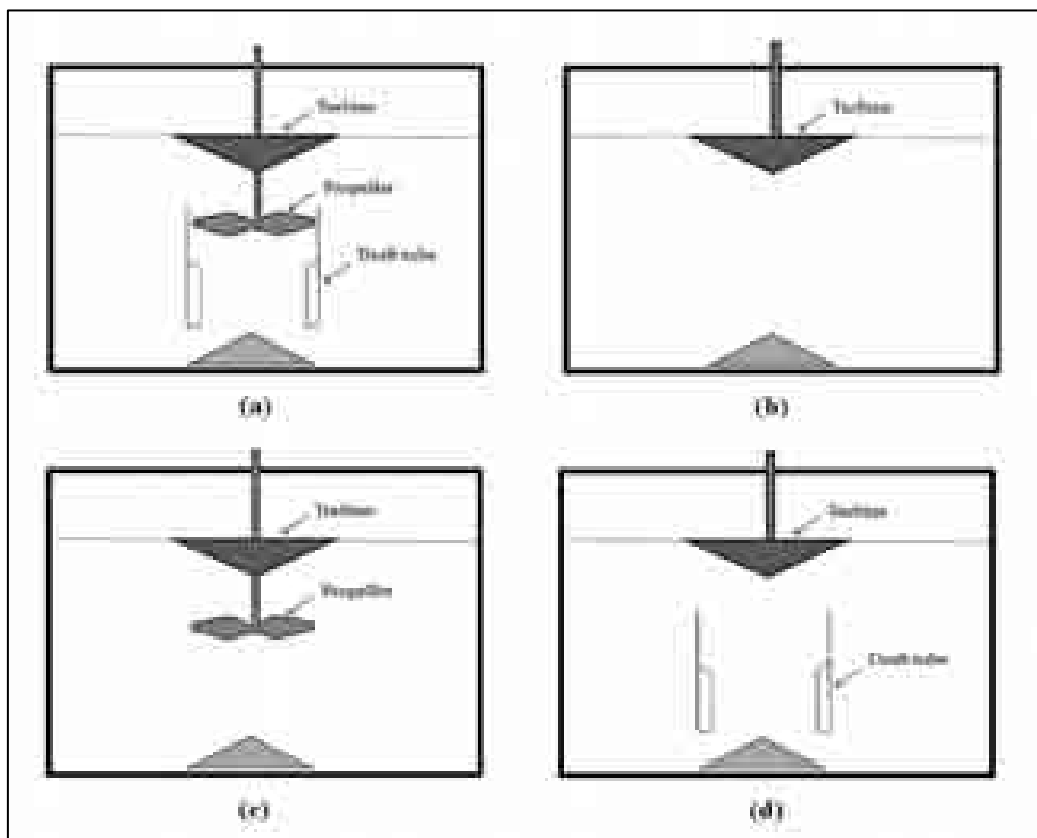


Figure (3.1): Different tested geometric configurations, (a) Whole system, (b) Turbine alone, (c) Turbine + Propeller, (d) Turbine + Draft tube.

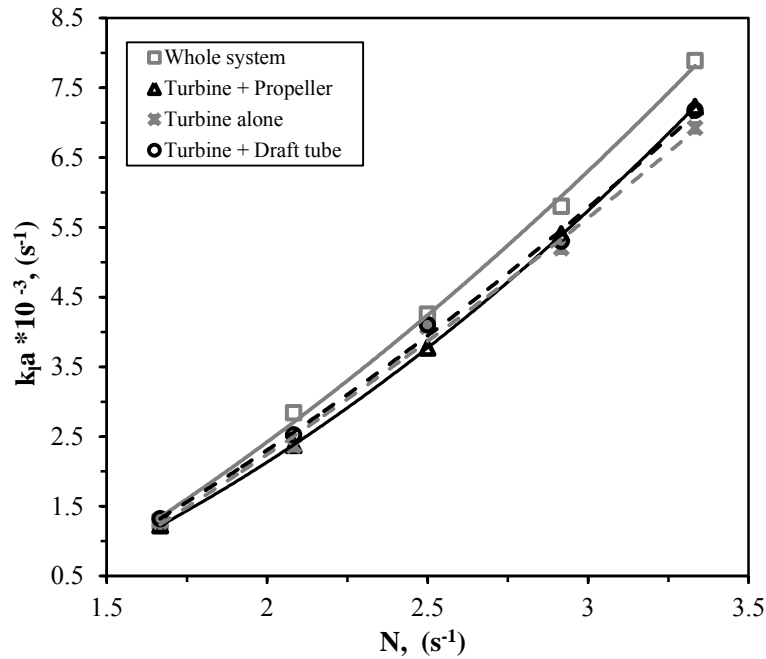


Figure (3.2): Impellers speed effect on the oxygen transfer coefficient with four different geometrical configurations; (Whole System, without draft tube, turbine alone and without propeller),  $D/T_v=0.24$ ,  $C/T_v=0.31$ ,  $h/D=1.47$ ,  $C_{pr}/T_v=0.2$ ,  $S/W=1$ .

## II. Effect of Impellers Rotational Speed

The dissolved oxygen concentration profile showed in Figure 3.3 is for the water bulk mass transfer zone with four rotation speed levels, the figure illustrates that with increasing of impellers rotation speed  $N$  the dissolved oxygen concentration increases till reaching its higher possible level near to its saturation dissolved oxygen in water. With higher impeller rotation speeds, higher energy was consumed to achieve efficient mixed condition of the dissolved oxygen in the water bulk, where the dissolved oxygen reaches its equilibrium concentration in shorter time with higher  $N$ ; for example after (500 sec) from the beginning of experiment time at ( $N = 1.67$  rps) oxygen concentration level was reached (5.0 ml/g), while at ( $N= 3.33$  rps) the oxygen concentration level was reached (9.3 ml/g).

The oxygen mass transfer coefficient,  $k_{1a}$  value depends on the dissolved oxygen DO range that implemented during the calculation in order to have the best fit of dissolved oxygen deficit term ( $\ln C^* - C_t / C^* - C_0$ ) versus experimentation time in the semi log graph and to get rid of the nonlinear parts of the plot; usually the curved parts are subject to truncations to reach this aim. As the calculated  $k_{1a}$  value is related with the applied dissolved oxygen range during the measurement depending on the way that the  $k_{1a}$  was calculated. Some authors have used linear regression of DO deficit with time to calculate  $k_{1a}$  from equation 2.20; they have taken different dissolved oxygen range (10%-70%) to (10%-90%) of the saturated oxygen concentration in water

(Boyd, 1998; Roustan, 2003), where this truncation was applied in order to find best fit between actual and measured dissolved oxygen concentrations. In our calculations we didn't use any truncations as we applied the least squares technique of nonlinear regression for oxygen deficit (ASCE, 1993) for the equation 2.21, which it seems to be more determinative for the experimentally reached mass transfer coefficient  $k_L a$  values with the best accuracy.

The rotational speed of the turbine and the propeller was tested (with keeping other parameters constant) on the oxygen transfer coefficient  $k_L a$  for the speed range of (1.67 – 3.33 rps). As shown in the Figure 3.2, an increase of the rotation speed leads to  $k_L a$  increasing, in other word the saturated oxygen condition was reached in shorter time. This relation is explained as the impellers rotation speed was increased, the amount of the water exposed to atmospheric air was increased consequently and the interfacial contact area between the air and water droplets was enlarged, the upper limit of the rotation speed for this relation 3.33 rps, after this level further increasing in the rotation speed leads to the water droplets hit the vessel wall and some of them splashed of the vessel, this situation is highly undesirable and considered as inapplicable operation.

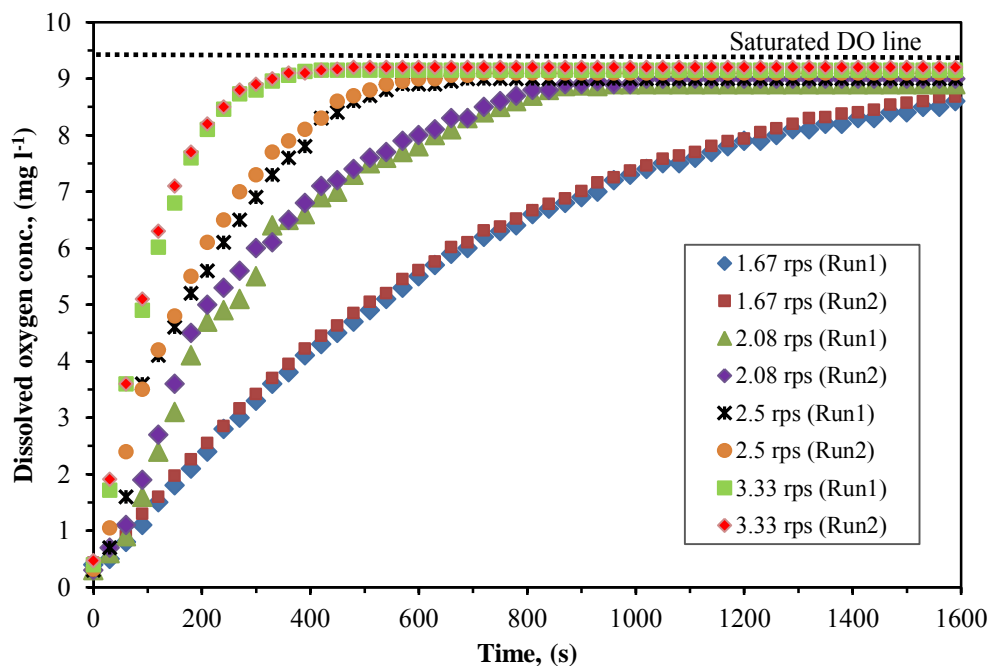


Figure (3.3): The DO profile for different rotation speeds,  $h/T_v=0.35$ ,  $C/T_v=0.313$ ,  $C_{pr}/T_v=0.2$ , temperature =15 °C.

For the different geometrical configurations tested, the oxygen transfer coefficient  $k_L a$  always shows a dependence on the impellers rotational speed, as it can be seen in the

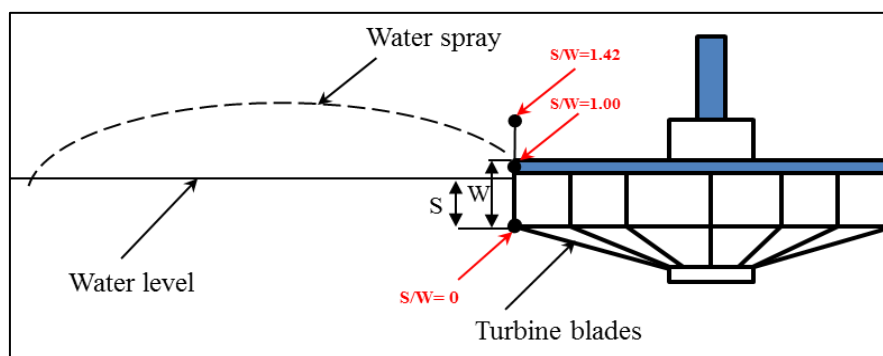
Figure 3.2, this agrees with the results obtained by (Chisti and Jauregui-Haza, 2002). Starting from  $N= 2.08$  rps, it was visually observed that the formation of air bubbles appears in the vessel due to water droplets plunging with water surface. So the rotation speed 2.08 rps can be considered as a critical rotational speed.

### III. Turbine Blades Submergence Effect

The effect of turbine blades submergence on the oxygen transfer coefficient was examined (See Figure 3.4). The turbine blades submergence refers to the distance from the water surface to the lower edge of turbine blade this effect is represented as the dimensionless geometric ratio ( $S/W$ ) as shown in Figure 3.4. This effect is also can be considered as the effect of the water spray form and water droplets properties. The turbine submergence (The distance from the tank bottom to the lower edge of the turbine) is fixed during the experimentation. When the turbine blades submergence is modified in the experimental runs, the liquid volume is modified too.

The effect of the water level inside the vessel that represented as the ratio  $h/D$  represents here the effect of the liquid volume through its relation with flow condition and circulation. It was found that the  $k_L a$  is highly sensitive to the turbine blades submergence and water level variation, this agrees with (Patil et al., 2004).

Five different turbine blades submergence are tested (0.17, 0.58, 1.0, 1.42, 1.83, and 2.25) that correspond the water levels  $h/D$  of (1.37, 1.42, 1.47, 1.53, 1.58 and 1.63) respectively, where three conditions are tested; at  $S/W < 1$  the turbine blades are partially submerged ( $h/D$  lower than 1.47), at  $S/W > 1$  ( $h/D$  higher than 1.47) the turbine blades are over submerged and at  $S/W=1$  which corresponds to 100% submergence of the blades ( $h/D = 1.47$ ) here the water level is just at blades upper tip.



(a)

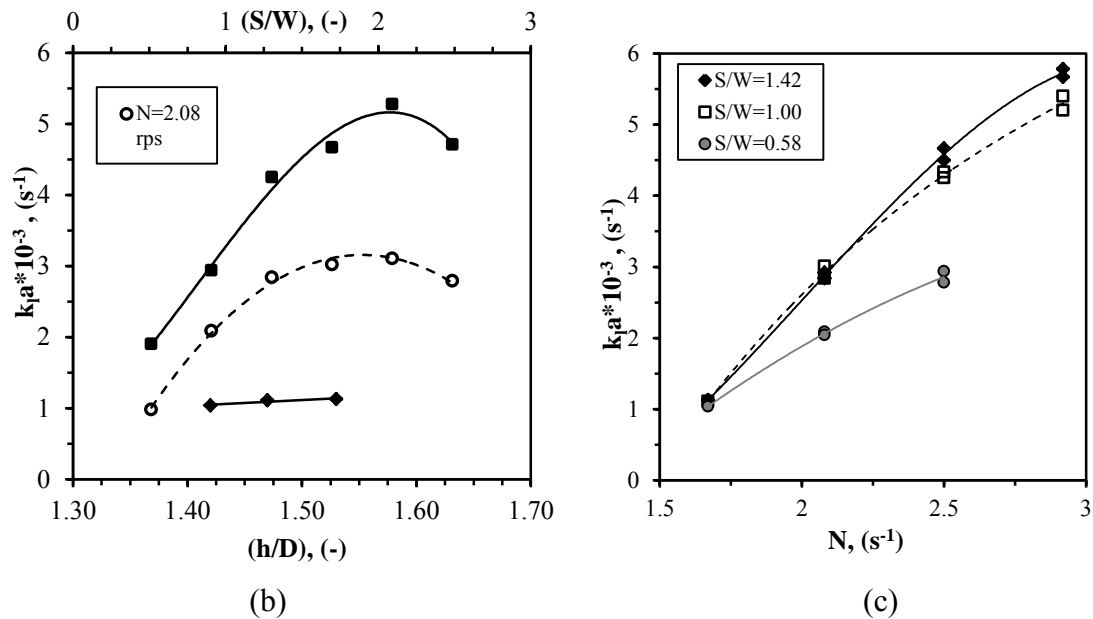


Figure (3.4): (a) The limits of the tested turbine blades submergence, (b) Mass transfer Coefficient  $k_{1a}$  relation with turbine blades submergence and water height in the liquid bulk for three levels of rotational speed, (b) Mass transfer Coefficient  $k_{1a}$  relation with the rotation speed for three levels of turbine submergence.  $D/T_v = 0.24$ ,  $C/T_v = 0.31$ ,  $C_{pr}/T_v = 0.2$ .

Figure 3.4 shows that higher  $S/W$  ratio leads to higher  $k_{1a}$  until the ratio  $S/W = 1.75$  after this point the  $k_{1a}$  values are decreased. This relation can be explained that with higher  $(S/W)$  more water droplets are thrown into the air, consequently larger interfacial area achieved between air and water and also the flight trip of these droplets goes farther, so as a result the  $k_{1a}$  mount up, but at the lower impellers speed 1.67 rps, the  $k_{1a}$  stays relatively constant despite elevation the  $S/W$  ratio.

At higher impellers speeds, further increasing with  $S/W$  higher than 1.58 the  $k_{1a}$  goes down, as illustrated in (Figure 3.4). The dropping down of  $k_{1a}$  with further increasing of water level ratio is happened, when it is noticed with higher water levels the spray begins to be deformed; the interfacial contact area is constricted. For the water levels lower that 100% submergence ( $h/D = 1.47$ ) of the aerator blades, the values of  $k_{1a}$  are moderate. This relation is depending on the desired shape of droplets spray as well as preserving interfacial area between air and water.

Figure 3.4, displays the influence of water level on the  $k_{1a}$ , as the higher  $(h/D)$  ratio leads to higher  $k_{1a}$  produced, This relation can be explained that with higher  $(h/D)$ , more efficient fluid circulation loop is accomplished in the tank, so as a result the  $k_{1a}$  is increased, but at the lower impellers speed 1.67 rps, the  $k_{1a}$  stays relatively constant despite elevation the  $h/D$  ratio.

The  $k_{ia}$  reaches a maximum with the  $(h/D)$  ratio of 1.58, with further increasing with  $(h/D)$  the  $k_{ia}$  goes down ( $2.8 \times 10^{-3}$  1/s), as illustrated in Fig. 3.4. This behavior is usual one, where the  $k_{ia}$  mount up with increasing of water level ratio turbine blade submergence ratio, in consequence more of water droplets are thrown into the air and also the flight trip of these droplets goes farther, where with  $S/W$  more than 1.75 ( $h/D$  higher than 1.58) the  $k_{ia}$  goes down, as illustrated in Figure 3.4.

#### IV. Effect of the Spacing between the Impellers

The lower RTP-U propeller in up-pumping mode (Aeration mode) was implemented to assist the surface aerator turbine performance by redirecting the flow toward the aerator intake in order to eliminate any shortage during the water projection and also the other important propeller role is achieving the homogenous distribution of dissolved oxygen in entire the vessel by ensuring the flow circulation moves through all vessel parts especially the deep lower levels in the down-pumping mode (Mixing mode), where with its presence the short circulations that may occur in the upper half of the vessel is eliminated by forcing the flow to continue its circulation down to the vessel deep bottom.

The obligatory position of the lower propeller inside the draft tube limits the choices to vary the distance between the two impeller, where the performance of the propeller is conjugated with that of the draft tube, as a result it is evident the propeller should stay inside the draft tube, on the other hand the existence of draft tube baffles prevent to push down the propeller to more lower positions (more geometric configuration are tested see next section).

From Figure 3.5 it can be noticed that the relationship between  $k_{ia}$  and rotation speed,  $N$  for two different spacing distances between the turbine and lower propeller; the reference position that is implemented in the all experimental runs of 7.6mm with lower position of 8.3 mm, where at lower rotation speed 1.67rps the lowest  $k_{ia}$  achieved, which was about  $1.3 \times 10^{-3}$   $s^{-1}$  for both configuration, while with elevating the rotation speed to 2.5 rps, higher  $k_{ia}$  accomplished of  $(5.42 - 5.8) \times 10^{-3}$   $s^{-1}$ , when  $N$  reaches its higher value 3.33 rps,  $k_{ia}$  was increased to around  $7.1 \times 10^{-3}$   $s^{-1}$  to  $7.89 \times 10^{-3}$   $s^{-1}$  for spacing 8.3 mm and 7.6 mm respectively.

From these results it is figured out with lower impellers speed (up to 2.5 rps), the achieved  $k_{ia}$  was close for both the tested spacing 8.3 mm and 7.6 mm. For higher impellers speed (higher than 2.5 rps) the  $k_{ia}$  is lower for the spacing of 8.3 mm that that of 7.6 mm, and the difference becomes wider with impellers rotation speed increasing (See Figure 3.5).

The slightly lowered  $k_{ia}$  at the lower tested position of the propeller  $S_p=8.3$  mm, compared with the standard reference position (upper position)  $S_p=7.6$  mm for higher rotation speed  $N > 2.5$  rps, comes from the fact that with lower position the inter-

action between the aerator and the propeller is weakened, since no other meaningful reasons can be developed with this small replacement, in that way the spacing has an effect on the oxygen transferred.

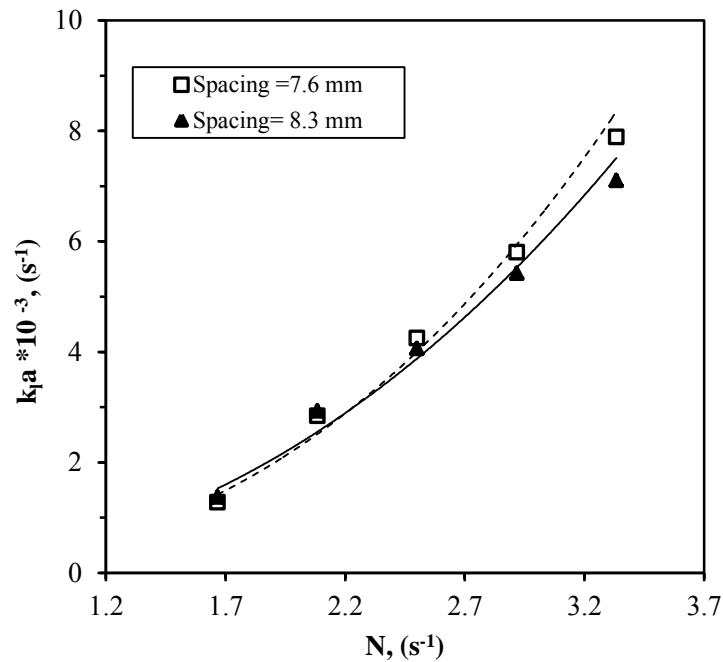


Figure (3.5): Spacing effect on the oxygen transfer coefficient,  $D/T_v= 0.24$ ,  $C/T_v= 0.31$ ,  $S_p$  (Reference) =7.6 mm.

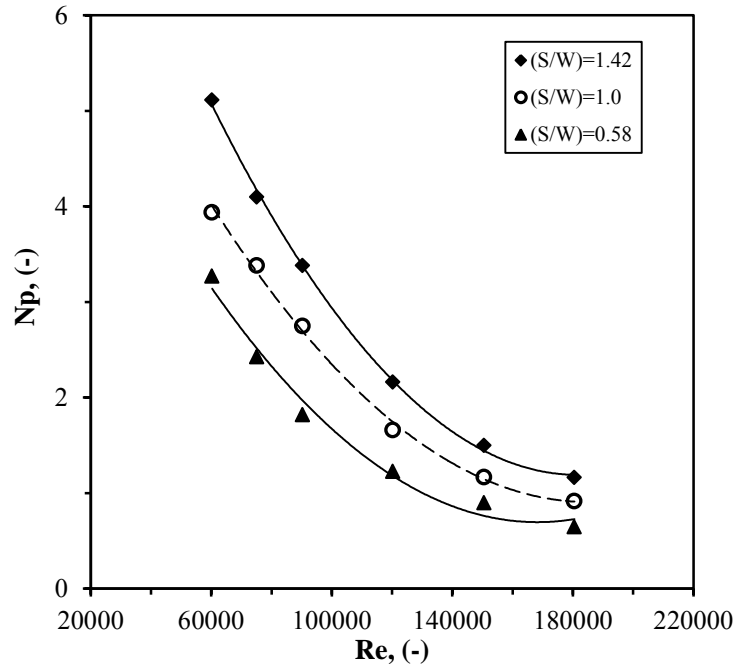
### V. Power Consumption Measurements

In the aeration mode the power consumption was studied for various turbine blades submergences ( $S/W$ ), for the spacing variation between two impellers and for the different geometrical configuration modifications (Figs. 3.6, 3.7 and 3.8).

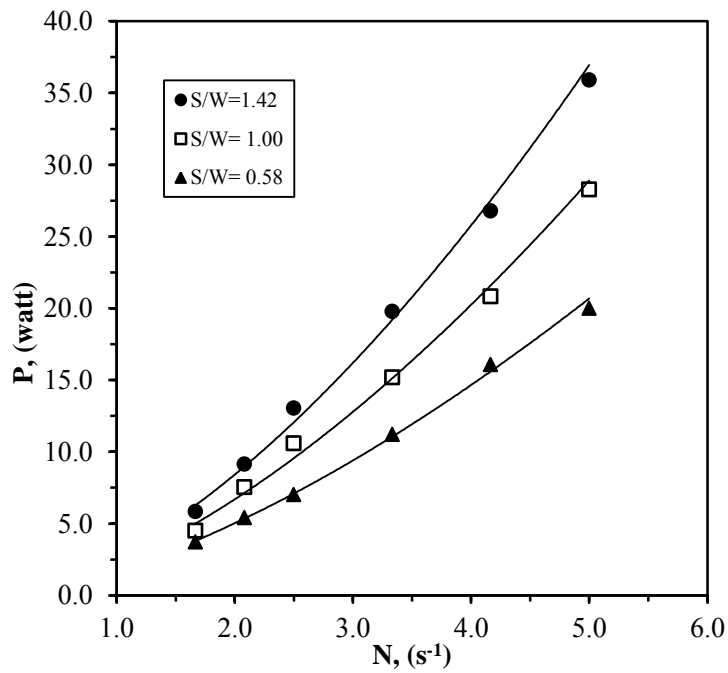
It is observed that the power consumed is changing due to all these modifications; the power consumed is highly relevant to each replacement or modification performed in different manners. The difference in power consumption was very slight for the spacing alteration and for the draft tube elimination, while it was remarkably affected by the increasing of turbine blade submergence levels.

Figures 3.6 a and b illustrate that the power consumption in aeration mode is dependent on both the Reynolds number (the diameter of the turbine  $D$ , was taken for calculating  $Re$ ) and water levels or turbine submergence. The power number decreases with increasing the Reynolds number, as higher power is consumed with higher impellers rotation speed (See Figure 3.6b). The power number increases when the turbine blade submergence increases, wherein higher power consumed with turbine blade submergence and higher water level. In the case of the water level is higher than upper tip of turbine blades  $h/D = 1.53$  with blade submergence ratio  $S/W=1.42$ , the turbine blades need more power to propel water droplets through the air. The resulted power numbers for the three turbine submergence levels are

somehow close at highest Reynolds number achieved, while the difference goes to be more widely at lowest Reynolds number  $6 \times 10^4$ .



(a)



(b)

Figure (3.6): (a) The relationship between power number and Reynolds No., for different turbine blades submergence levels  $C/T_v = 0.31$ , (b) The relation between power consumption and rotation speed,  $C/T_v = 0.31$ .

Figure 3.7, shows the power consumption in the water bulk as mentioned before, for both tested spacing (7.6 - 8.3 mm), on the other hand both spacing configurations showed close power consumption.

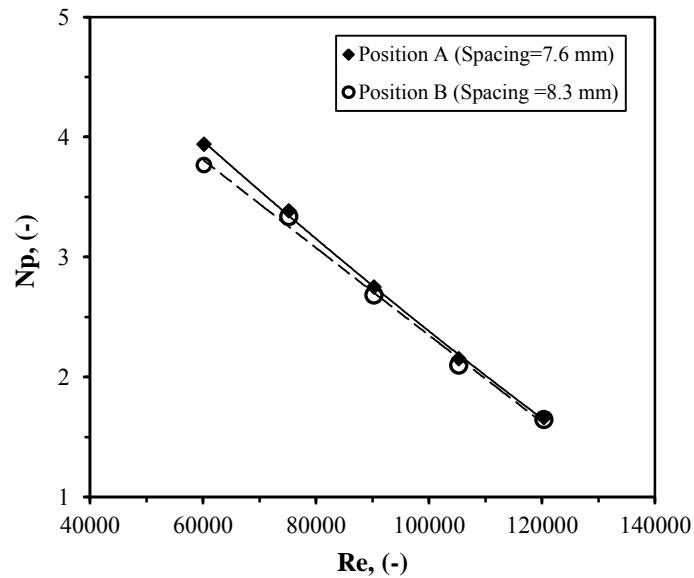


Figure (3.7): The spacing between two impellers effect on the power consumption.

Figure 3.8, shows that the power number  $N_p$  relation with  $Re$  for geometrical configuration effect on whole system, without draft tube and propeller and without draft tube configurations, where the relation appears similar behavior with Figure 3.6. It is important to explain that power consumption is less relevant to geometry modification than the water level  $h$  elevation.

Figure 3.8 illustrates the effect of the draft tube and the RTP propeller on the power number for the condition, where for all different configurations the water level is just at the upper edge of turbine blades. It points to the power consumption was slightly changed from whole system configuration for Reynolds number range ( $6 \times 10^4$  to  $18 \times 10^4$ ). The power number profile was very similar for the draft tube elimination and the turbine alone aeration mode. This refers that the presence of the draft tube and the propeller doesn't contribute to an increase of the power consumption.

Comparing the power consumption relation with mixing mode (down-pumping), the power number in that case was relatively constant and it was around 0.6. In mixing mode the RTP propeller operates only in liquid phase with low gas presence, therefore the power number has close values for different Reynolds numbers, is for that power number can be referred by one value.

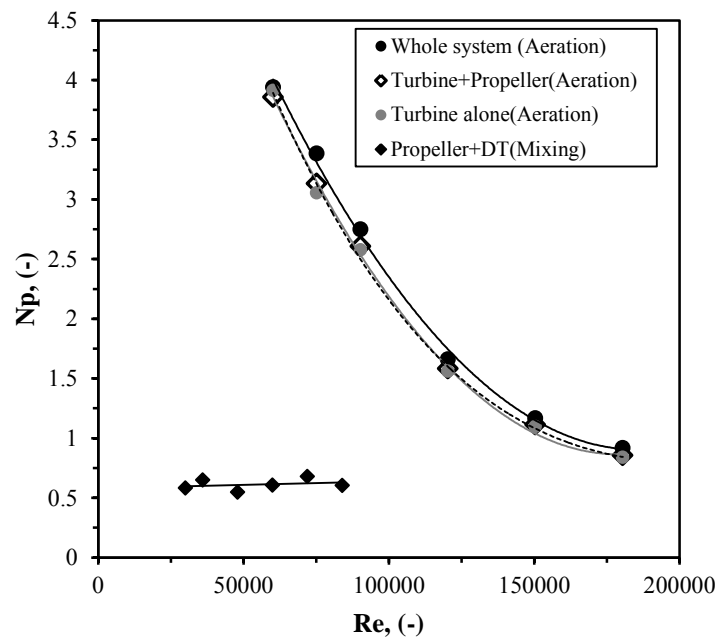


Figure (3.8): The effect of various impellers configurations on the power consumption.

### VI. Standard Aeration Efficiency ( $SAE_b$ ) and Standard Oxygen Transfer Rate ( $SOTR_b$ ) for the Water Bulk Zone

The standard oxygen efficiency of the water bulk mass transfer zone  $SAE_b$  refers to the relationship between the power consumption with achieved oxygen transfer rate and calculated by equation 2.26, the  $SOTR_b$  was calculated by equation 2.25. It is noticed that  $SAE_b$  was increased according to the elevation of rotation speed (See Figure 3.9). The  $SAE_b$  was affected by the increasing of impellers rotation speed for the different tested geometrical configurations. For the whole system configuration, when  $N$  was elevated from 1.67 rps to 3.33 rps the  $SAE_b$  value was approximately doubled this behavior was repeated for all tested geometrical configuration. Starting from  $N=2.08$  the whole system configuration shows competitive behavior with turbine alone configuration till higher  $N \geq 2.92$  rps, where it looks clearly the whole system achieves highest  $SAE_b$  this behavior can explained that the contribution of draft tube in redirecting the flow up-ward. As illustrated in Figure 3.9 the  $SAE_b$  relation with  $N$  wasn't similar for all tested configurations. At lower  $N$  levels it seems that the propeller and draft tube have no contribution in the  $SAE_b$ . With higher  $N$  levels, the turbine and propeller performance become closer to turbine alone configuration. But in general it can be notice that the draft tube presence looks somehow necessary to assist the propeller in its work of pushing more gas liquid dispersion to turbine intake region. The other advantage of draft tube is its power consumption was quite low. On the other hand it was found that the  $SAE_b$  didn't changed effectively and proportionally with the turbine blades submergence or water level variations. From Table 3.1 it was noticed that higher turbine blades submergence or higher water level leads to higher accomplished  $SAE_b$  till reaching the turbine

blades submergence ratio of  $S/W=1$ . After this ratio it is clear that the  $SAE_b$  was relatively kept its value for higher  $S/W$  ratios.  $SAE_b$  was decreased gradually with further increasing of the submergence of turbine blades by elevating the water level till it reach lowest  $SAE_b$  at  $S/W=2.25$ . The reason for this behavior is related with the shape of water spray droplets projection, as it was observed that the spray form was deformed at higher water level applied water level  $h/D = 1.63$  ( $S/W=2.25$ ) and the  $SAE_b$  value is lowered (See Table 3.1).

The achieved  $SAE_b$  with the applied surface aeration system that shown in Tables 3.1 to 3.5 are considered successful and efficient when they are compared with other surface aerators (See Tables 1.1 and 1.2), where the  $SAE_b$  for slow speed surface aerator that implement turbine is equal to  $1.5 \text{ kgO}_2.\text{kW}^{-1}\text{h}^{-1}$  (Duchene and Cotteux, 2002).

The standard oxygen transfer rate  $SOTR_b$  was increased with increasing impellers rotation speed or water level for the three examined configurations (See Tables from 3.1 to 3.6) and Figure (3.10). The obtained results of  $SOTR_b$  can be explained as same manner for  $k_1a$  results discussed before.

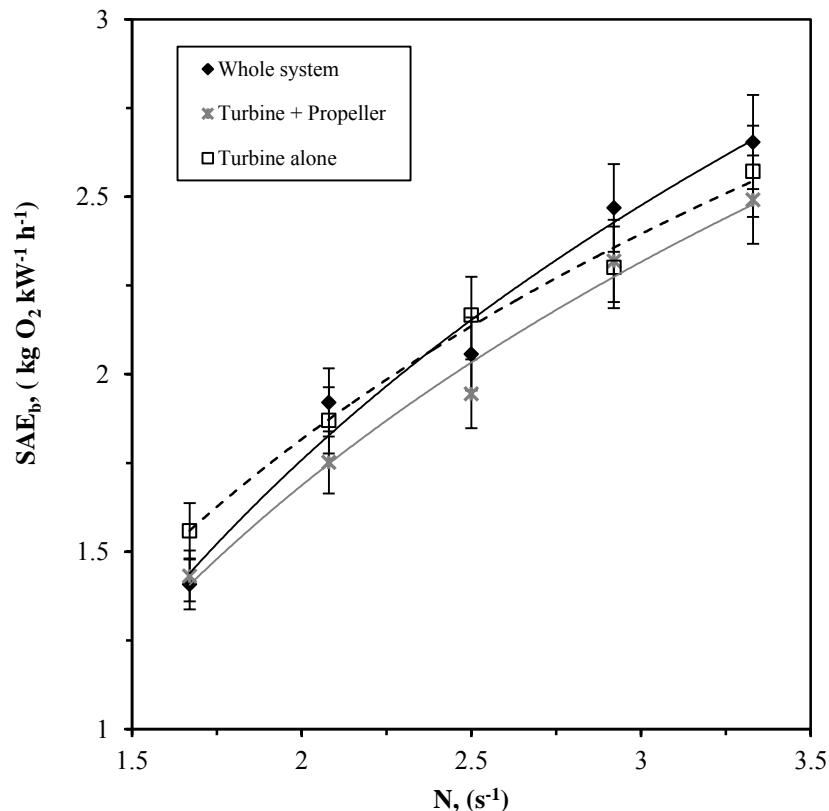


Figure (3.9): The relationship between the standard aeration efficiency  $SAE_b$  for three aeration mode configurations (Whole System, turbine + propeller and turbine alone) with the impeller rotation speed,  $D/T_v=0.24$ ,  $C/T_v=0.31$ ,  $h/D=1.47$ ,  $S/W=1$ .

Table (3.1): The  $SAE_b$  and  $SOTR_b$  for different water level ratios ( $h/D$ ) and turbine blade width to blades submergence ratio ( $S/W$ ),  $D/T=0.24$ ,  $C/T=0.31$ ,  $C_{pr}/T=0.2$ ,  $N=2.803$  rps, (Whole system Configuration).

Power (watt)	$h/D$ (-)	$S/W$ (-)	$(k_{ia})_T$ ( $s^{-1}$ )	$(k_{ia})_{10\text{ }^\circ C}$ ( $s^{-1}$ )	$SOTR_b$ ( $kgO_2 \cdot h^{-1}$ )	$SAE_b$ ( $kgO_2 \cdot kW^{-1} h^{-1}$ )
2.932	1.37	0.17	9.80E-04	8.38E-04	0.00448	1.5265
5.418	1.42	0.58	2.09E-03	1.72E-03	0.00953	1.7591
7.552	1.47	1.00	2.84E-03	2.52E-03	0.01451	1.9208
9.148	1.53	1.42	3.02E-03	2.64E-03	0.01572	1.7185
9.698	1.58	1.83	3.10E-03	2.74E-03	0.01686	1.7386
10.025	1.63	2.25	2.79E-03	2.51E-03	0.01596	1.5923

The  $SOTR_b$  and  $SAE_b$  were decreased when turbine blades submergence increased  $S/W$  from 1.83 to 2.25 (water level ratio  $h/D$  was increased from 1.58 to 1.63), where the lowest  $SOTR_b$  took place (0.01596  $kgO_2/h$ ). As turbine blades submergence was increased to  $S/W= 2.25$  (water level ratio was increased to  $h/D=1.63$ ) that will cause deformation of water spray shape created by turbine blades, so variation in contact interfacial area was available.

The standard oxygen transfer rate  $SOTR_b$  was increased with increasing impellers rotation speed or water level for the three configurations examined that can be explained as same manner for  $k_{ia}$  results discussed before (see Tables from 3.1 to 3.4). From Table 3.2, it can be observed that  $SOTR_b$  is higher when higher water height level used. Table 3.4 elucidate the relation between the experimental results of  $SOTR_b$  and with  $SAE_b$ ; where high  $SOTR_b$  was reached with high surface aeration efficiency  $SAE_b$  was achieved, but this increasing is applicable for water level ratio up to 1.58 ( $h = 0.3$  m).

Table (3.2) demonstrates that standard oxygen transfer rate for water bulk mass transfer zone  $SOTR_b$  is acted same as the standard aeration efficiency  $SAE_b$ .  $SOTR_b$  was increased according to increasing of impellers rotation speed  $N$ , when  $N$  was increased that will leads to more air bubbles entrapped into well mixed water bulk, so larger contact interfacial area between the water bulk and air bubbles is provided. In other hand water droplets propelled by turbine blades take longer travel time before reaching impingement at water surface, this meaning larger contact area between droplets and atmospheric air; as a consequence higher dissolved oxygen concentration was accomplished.

## Chapter Three: Oxygen Mass Transfer in the Surface Aeration

Table (3.2): The  $SAE_b$  and  $SOTR_b$  for different impellers speed,  $D/T= 0.24$ ,  $C/T= 0.31$ ,  $C_{pr}/T= 0.2$ ,  $h/D = 1.47$  (Whole system Configuration, Aeration mode).

Power (watt)	N (rps)	$(k_{ia})_T$ ( $s^{-1}$ )	$(k_{ia})_{10\text{ }^\circ C}$ ( $s^{-1}$ )	$SOTR_b$ ( $kgO_2.h^{-1}$ )	$SAE_b$ ( $kgO_2.kW^{-1}h^{-1}$ )
4.503	1.67	1.28E-03	1.1E-03	0.0063	1.4078
7.552	2.08	2.84E-03	2.52E-03	0.0145	1.9205
10.603	2.5	4.25E-03	3.79E-03	0.0218	2.0570
15.184	3.33	7.89E-03	7.01E-03	0.0403	2.6540

Tables (3.3, 3.4 and 3.5) are representing the  $SOTR_b$  with different impellers rotation speeds for three different configurations with the achieved oxygen mass transfer coefficient at actual and standard conditions. From Figure 3.10 and from tables 3.3, 3.4 and 3.5 it can be noticed that the  $SOTR_b$  is lowered when both the draft tube and the propeller were removed or when the draft tube alone was removed from the system. The explanation for this is similar to that mentioned earlier in this chapter for the oxygen mass transfer. The same behavior was observed for spacing changing between the two impellers and for the turbine alone implementation cases respectively. The  $SOTR_b$  was increased with impellers rotational speed (N) increasing; this is logic as with higher impellers rotation speed higher oxygen mass transfer coefficient is obtained.

Table (3.3): The  $SAE_b$  and  $SOTR_b$  for different impellers speed,  $D/T_v= 0.24$ ,  $C/T_v= 0.31$ ,  $C_{pr}/T_v= 0.2$ ,  $h/D = 1.47$  (Turbine and propeller configuration).

Power (watt)	N (rps)	$(k_{ia})_T$ ( $s^{-1}$ )	$(k_{ia})_{10\text{ }^\circ C}$ ( $s^{-1}$ )	$SOTR_b$ ( $kgO_2.h^{-1}$ )	$SAE_b$ ( $kgO_2.kW^{-1}h^{-1}$ )
4.409	1.67	1.23E-03	1.10E-03	0.00631	1.4318
6.991	2.08	2.38E-03	2.13E-03	0.01224	1.7515
10.053	2.5	3.77E-03	3.35E-03	0.01926	1.9154
14.472	3.33	7.23E-03	6.42E-03	0.03693	2.5516

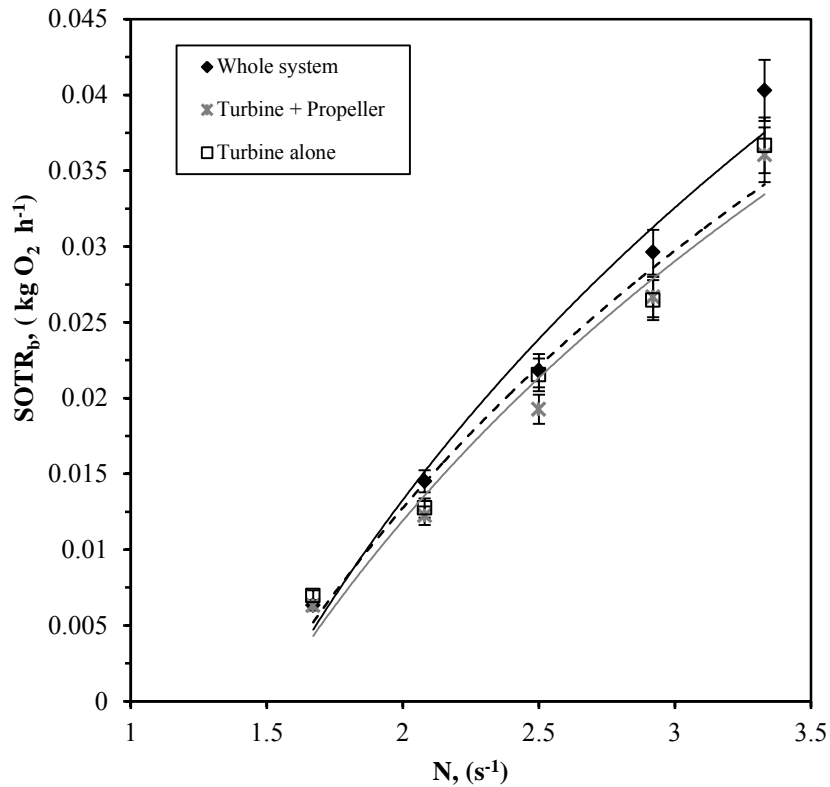


Figure (3.10): The relation between the standard oxygen transfer rate  $SOTR_b$  for three aeration mode configurations (Whole System, turbine + propeller and turbine alone) with the impeller rotation speed,  $D/T_v=0.24$ ,  $C/T_v=0.31$ ,  $h/D=1.47$ ,  $S/W=1$ .

Table (3.4): The  $SAE_b$  and  $SOTR_b$  for different impellers speed,  $D/T_v= 0.24$ ,  $C/T_v= 0.31$ ,  $h/D = 1.47$ , (Turbine alone configuration).

Power (watt)	N (rps)	$(k_1a)_T$ (s <sup>-1</sup> )	$(k_1a)_{10\text{ }^\circ\text{C}}$ (s <sup>-1</sup> )	$SOTR_b$ (kgO <sub>2</sub> .h <sup>-1</sup> )	$SAE_b$ (kgO <sub>2</sub> .kW <sup>-1</sup> h <sup>-1</sup> )
4.472	1.67	1.28E-03	1.21E-03	0.00697	1.5588
6.82	2.08	2.37E-03	2.22E-03	0.01275	1.8700
9.943	2.5	4.07E-03	3.75E-03	0.02154	2.1664
14.263	3.33	6.93E-03	6.38E-03	0.03668	2.5715

Table (3.5): The effect the spacing between impellers on  $SOTR_b$  and  $SAE_b$ ,  $D/T_v= 0.24$ ,  $C/T_v= 0.31$ ,  $h/D = 1.47$ ,  $S_p=8.3$  mm.

Power (watt)	N (rps)	$(k_1a)_T$ (s <sup>-1</sup> )	$(k_1a)_{10\text{ }^\circ\text{C}}$ (s <sup>-1</sup> )	$SOTR_b$ (kgO <sub>2</sub> .h <sup>-1</sup> )	$SAE_b$ (kgO <sub>2</sub> .kW <sup>-1</sup> h <sup>-1</sup> )
4.932	1.67	1.40E-03	1.25E-03	0.00720	1.46
7.448	2.08	2.50E-03	2.22E-03	0.01277	1.71
10.352	2.5	4.00E-03	3.52E-03	0.02024	1.96
15.038	3.33	7.20E-03	6.33E-03	0.03643	2.42

### 3.1.3. The Modeling

In order to determine and improve the oxygen mass transfer and power consumption for surface aeration systems with larger scales in depending on the obtained experimental results collected from the implemented water treatment tank model in this work. The most affecting parameters during the surface aeration process were correlated in two models that were derived for oxygen mass transfer and power consumption in the bulk mass transfer zone. The influencing parameters such as operational, property and geometrical parameters are considered as independent variables, and are related with the dependent variable of mass transfer parameter or power consumption.

It worth to mention that the number of the considered experimental points that applied to derive the models for the transferred oxygen and power consumption are actually the mean for the number of the results that obtained for the similar conditions at each point.

#### I. Mass Transfer

From the previous studies that dealt with surface aeration dimensional analysis, it was found that there are various trends to correlate different relevant variables. (Fuchs et al., 1971) have correlated the mass transfer coefficient  $k_{1a}$  with the volumetric power consumption ( $P/V$ ) for tank volumes of ( $V \geq 200$  liter). (Zlokarnik, 1979) proposed two correlation models for both mass transfer and power consumption for various types of surface aerator. The main distinction in the correlations made by (Zlokarnik, 1979) is the mass transfer parameter was represented as a dimensionless parameter that called the sorption number  $Y$ , which represents both the transferred oxygen and turbulence intensity ( $Y = k_{1a}V(\mu/\rho g^2)^{1/3}D^3$ ). (Zlokarnik, 1979) has related in his model the oxygen mass transfer with the water surface flow characteristics. (Zeybek et al., 1997) have applied the Box-Wilson method to optimize the values of mass transfer correlation for both linear and non-linear models of  $k_{1a}$  in general application of aerated agitated tanks. (Patil et al., 2004) performed various tests for different types of surface aerators and they emphasized on the geometrical configuration that affecting parameters such as liquid height and volume, tank diameter and impeller clearance. The model was for optimum values of  $k_{1a}$  with respect to impeller submergence. (Cancino, 2004; Chandrasekharan and Calderbank, 1981; Chisti and Jauregui-Haza, 2002; Deshmukh and Joshi, 2006; Kumar et al., 2010; Moulick et al., 2002; Rao, 1999) have attempted to correlate the oxygen transfer and / or the power consumption for diverse affecting variables (for the aeration process), each one of them depending on its implemented geometrical configuration and proposed relevant geometric, material and process parameters.

The mass transfer model was developed in depending on the experimental results and the previous performed studies. Normally in the surface aeration process there are geometrical, operational and materials (physical and chemical properties) parameters that govern the system performance. The operational parameters like the rotational speed, the gravity of acceleration, the water level in the tank and power consumption or many other parameters. The geometrical parameters are the turbine and tank diameters. While the parameters of the chemical and physical properties are the water viscosity and density. All these parameters may refer to the intensity of turbulence inside the tank and at the water surface. The number of these parameters is different according to each case, but generally they are the same essential parameters that work for all the surface aeration cases. For example, the operational parameter that refers to water wave action generated by the turbine or refers to flow regime. Always the effect of the gravitational acceleration force, the rotational speed and the power consumed are taken in account in the surface aeration with considering that the aerated fluid properties; the water viscosity and density are crucial for any attempt to build a surface aeration model. It is not restricted to use one normalized mass transfer parameter, but it depends on the system implemented distinction, in addition to many variables in relation with the geometrical configuration and operation condition. In accordance to experimental results, it is found the most realistic independent variables can affect the oxygen transfer are

$$(k_l a) = f(N, P, \rho, \mu, D, h, g) \quad (3.1)$$

The geometrical ratios were chosen upon the standard design ratios that generally implied in the surface aeration process. By applying Buckingham  $\pi$  theory the equation (3.1) converted to the following relation:

$$\left(\frac{k_l a}{N}\right) = K_1 \left[ N_p^a R_e^b F_r^c \left(\frac{h}{D}\right)^d \right] \quad (3.2)$$

Since the surface aeration process predominantly within the turbulent flow state, so the Reynolds No. can be ignored, where for air-water submergence aerator the value of Re is always ( $> 10^4$ ), so the Re, is considered irrelevant to the process objective (Zlokarnik, 1979).

So equation (4.5) was reformed as:

$$\left(\frac{k_l a}{N}\right) = K_1 \left[ N_p^a F_r^b \left(\frac{h}{D}\right)^c \right] \quad (3.3)$$

Equation (3.3) was solved to determine the values of the constants by applying multiple non-linear regressions. The following correlation was developed:

$$\left(\frac{k_l a}{N}\right) = 0.0322 \left[ N_p^{1.14} Fr^{1.47} \left(\frac{h}{D}\right)^{-2.52} \right] \quad (3.4)$$

For surface aeration cases the constant ( $K_1$ ) which have the value 0.0322 in equation 3.4 it normally represents the effect of the system geometry, but it in our case in all implemented geometrical configurations have the same effect because actually we have kept the essential geometry for all the tested configurations, where the turbine and tank geometries didn't changed during experimental runs.

From equation (3.4) it is noticeable that the water level has higher effect on the dimensionless mass transfer parameter ( $k_l a/N$ ) than the wave condition that represented by  $Fr$  or the power consumption that represented by  $N_p$ . This elevated value for  $h/D$  parameters shows that the oxygen mass transfer is highly related with the liquid volume and flow circulation condition in the tank

The mass transfer correlation (equation 3.4) is applicable for the three ranges, ( $P/V$ ,  $\text{watt/m}^3$ ) = (22 -100), ( $Fr$ ) = (0.054 – 0.214), ( $h/D$ ) = (1.37 - 1.58) with respect to the applied geometry in the experimentation.

The comparison between the predicted values from applying above correlation (equation 3.4) with the experimental results that obtained from 74 experimental runs showed that the coefficient of determination of (0.985), which is accepted in the frame of the error as shown in Figure 3.11a.

## **II. Power Consumption**

The power consumption parameter in the derived model for the surface aeration is related with the geometrical, material and dynamic parameters same as it was explained with oxygen transfer correlation procedure. Furthermore most of the dependent parameters are similar with that implied in the mass transfer correlation, except that they are related directly with molecular diffusivity of oxygen in water. During the past decades various attempts are developed to correlate the consumed power in aeration applications that relied on each study condition of geometric and operation specifications. (Sano and Usui, 1985) proposed several correlations for the aerated tank, he mainly considered that the power is effected by geometrical configuration, (Wu, 1995) regarded the Froude number as the main representative independent variable for the power consumed by the aerator.

The attempt was conducted to drive a power consumption correlation with looking at the experimental results as a prime source to have an idea about the affecting factors on the consumed power. It was found that the power is a function of following independent parameters can be represented as:

$$P = f(N, h, T_v, S, g, D, \rho, \mu) \quad (3.5)$$

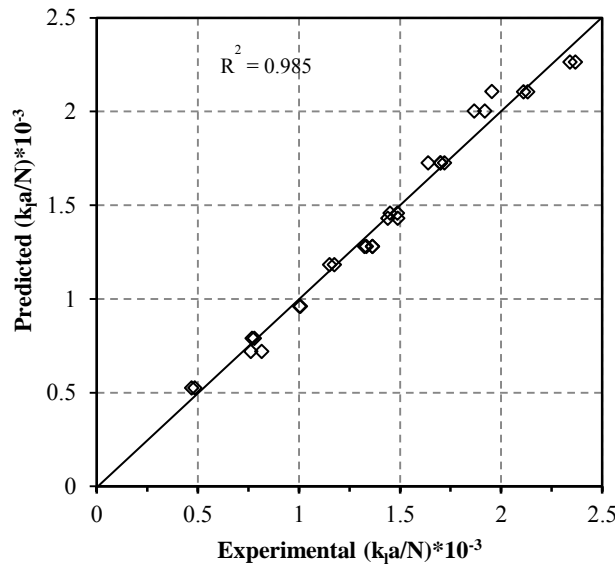
By applying Buckingham  $\pi$  theory of equation (3.5), the following correlation developed:

$$N_P = K_2 \left( F_r^a \left( \frac{T_v^2 h}{D^2 S} \right)^b Re^c \right) \quad (3.6)$$

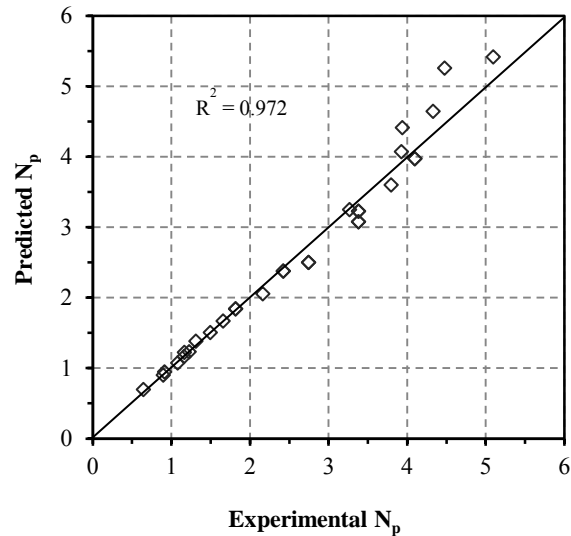
Since the flow regime is always kept in turbulent region ( $Re > 10^4$ ), the  $Re$  is considered irrelevant to the process objective same as mass transfer model. Equation 3.6 was solved to determine the values of the constants by applying multiple non-linear regressions, the following correlations developed:

$$N_P = 38.695 \left( F_r^{-0.7} \left( \frac{T_v^2 h}{D^2 S} \right)^{-0.83} \right) \quad (3.7)$$

The power correlation applicable for the ranges ( $22 < P/V$ , watt/m<sup>3</sup>  $< 100$ ), ( $1.37 < h/D < 1.63$ ) and ( $0.054 < Fr < 0.214$ ) according to the applied geometry in the experimentation. The comparison of predicted values from power consumption correlation with experimental results values obtained from 58 experimental runs found that the coefficient of determination of (0.972), (See Fig .3.11b).



(a)



(b)

Figure (3.11): (a) The comparison between the  $k_{1a}/N$ , predicted by the correlation model (Eq. 3.4) with the experimentally resulted  $k_{1a}/N$ , (b) The Comparison between the ( $N_p$ ) values predicted by the Eq. 3.7 with the experimentally resulted ( $N_p$ ) values.

## 3.2. Spray Mass Transfer Zone

### 3.2.1. Introduction

The concept of dividing the mass transfer operation in the surface aeration process into two zones above and under water surface was identified in many previous works for the surface aeration and other types of aeration (Demoyer et al., 2003; McWhirter and Hutter, 1989). As it was described in chapter two the oxygen transfer in the water spray zone is related with the droplets form and condition that created by the aeration turbine blades rotation at the water surface, where they propel the water droplets into the atmospheric air with relatively high discharge velocity. The oxygen transfer occurs with droplets creation till their clash on the water surface, wherein the second mass transfer zone boundary begins.

### 3.2.2. The Experimental Results

#### I. Impellers Rotation Speed Effect

The effect of impellers rotation speed,  $N$  was tested for the whole system configuration,  $D/T= 0.238$ ,  $C/T= 0.313$ ,  $d/T= 0.15$ ,  $C_{pr}/T= 0.2$ ,  $h/T= 0.35$ ,  $d_f/T = 0.188$ . For the whole system configuration, the turbine and the RTP propeller are mounted on the shaft and the RTP propeller is placed inside the draft tube. The impellers rotation speed effect was tested with keeping the other operational

parameters constant, in order to interpret influence of  $N$  on the water spray droplets oxygen mass transfer zone coefficient  $k_{La}$ . The  $N$  was varied between (1.67 – 3.33 rps). The applied range represents the limits where the purpose to unequivocally establish a correct and affective spray form of water droplets for the given operational conditions and geometrical configuration, where at the impeller rotation speed lower than 1.67 rps there is no spray creation, upper the limit of 3.33 rps the water spray form begins to be deformed from its regular form and part of the droplets began to hit vessel wall, wherein the benefit of droplets impingement with water surface was lost.

The repeatability of water spray zone aeration efficiency experiments was tested; two experimental runs were repeated and then to identify the calculated spray zone aeration efficiency relevant to these results (See Figures 3.13 to 3.17).

### **I.1. Aeration Efficiency for the Water Spray Zone**

Figures 3.12 to 3.15 illustrate the dissolved oxygen concentration DO profile during surface aeration in two different positions (same to that illustrated in Figure 2.15 b) in the water bulk inside the tank and in the water spray for four impellers rotation speed levels, where two experimental runs were performed for each level. It can be noticed that the dissolved oxygen concentration DO in all positions is increased progressively with the time, but in different manners. The DO concentration gradient in the droplets was occurred in a pattern that is higher than that occurred in water bulk as the saturated equilibrium DO concentration level in the droplets corresponds to the wet-bulb temperature of atmospheric air, which is higher than the saturated equilibrium DO of water bulk for the given operation conditions of water bulk temperature, air temperature and atmospheric air relative humidity.

As it is shown from the Figures 3.12 to 3.16 the DO is gradually proceed to attain the saturation level, where practically the DO isn't attained the 100% saturation due to the various limitation that hinder the theoretical DO saturated equilibrium level to be achieved. Among these limitations in the practical applications is the employed water quality, where the DO saturation level is different for different water qualities. From Figures 3.12 to 3.16 it was observed that for all impellers rotation speed levels performed for same water level ratio  $h/D$  and other geometrical parameters. The DO behavior is in the way of higher impellers rotation speed leads to shorter time needed to reach its saturation level (highest DO concentration) as seen in the results.

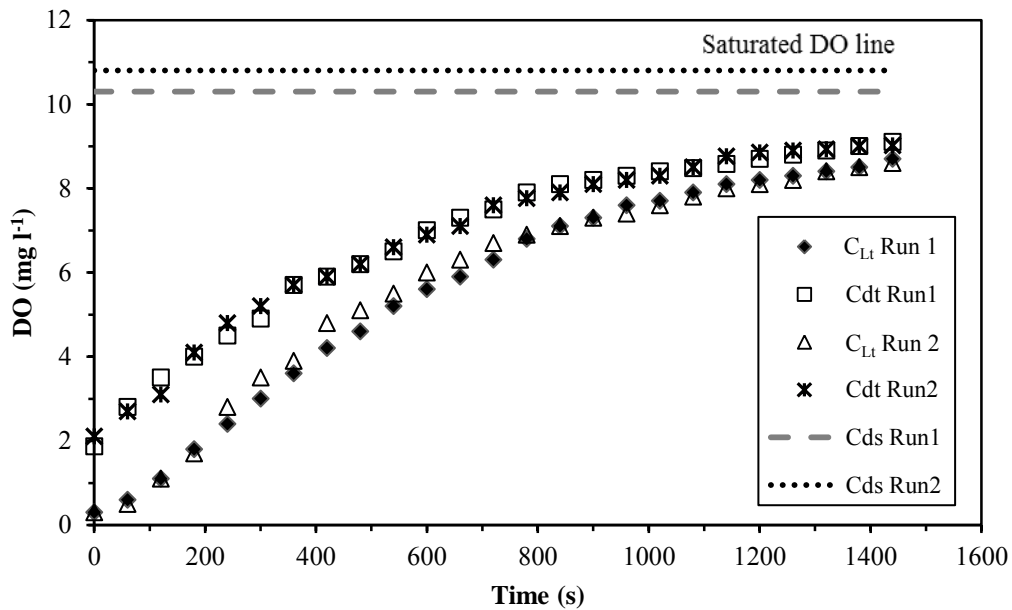


Figure (3.12): Dissolved oxygen concentration profile with time of experiment in the water bulk zone ( $C_{dt}$ ), and the water spray zone ( $C_{Lt}$ ) at  $N = 1.67$  rps for two experimental runs.

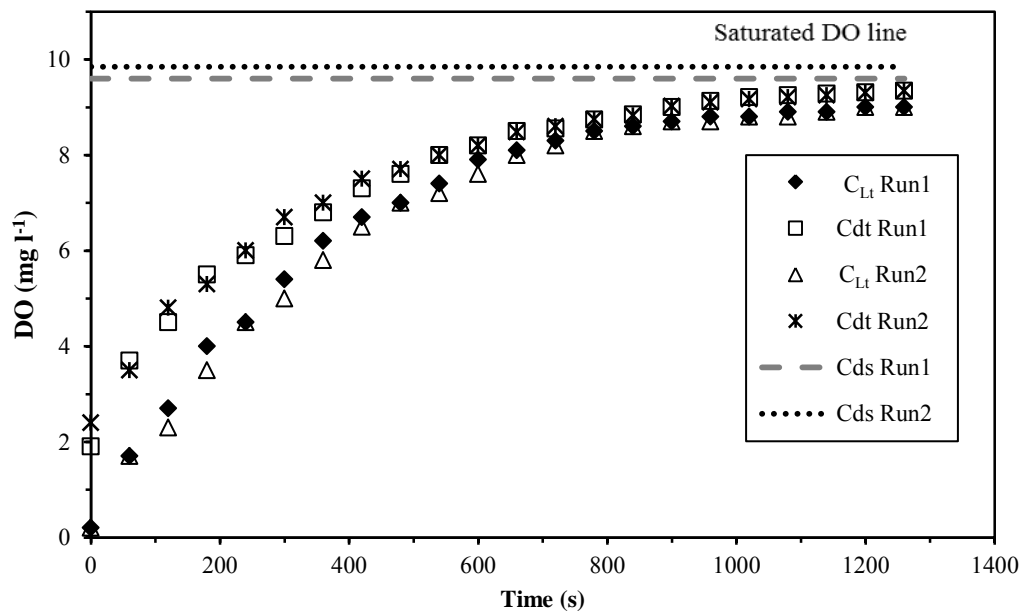


Figure (3.13): Dissolved oxygen concentration profile with time of experiment in the water bulk zone ( $C_{dt}$ ), and the water spray zone ( $C_{Lt}$ ) at  $N = 2.08$  rps for two experimental runs.

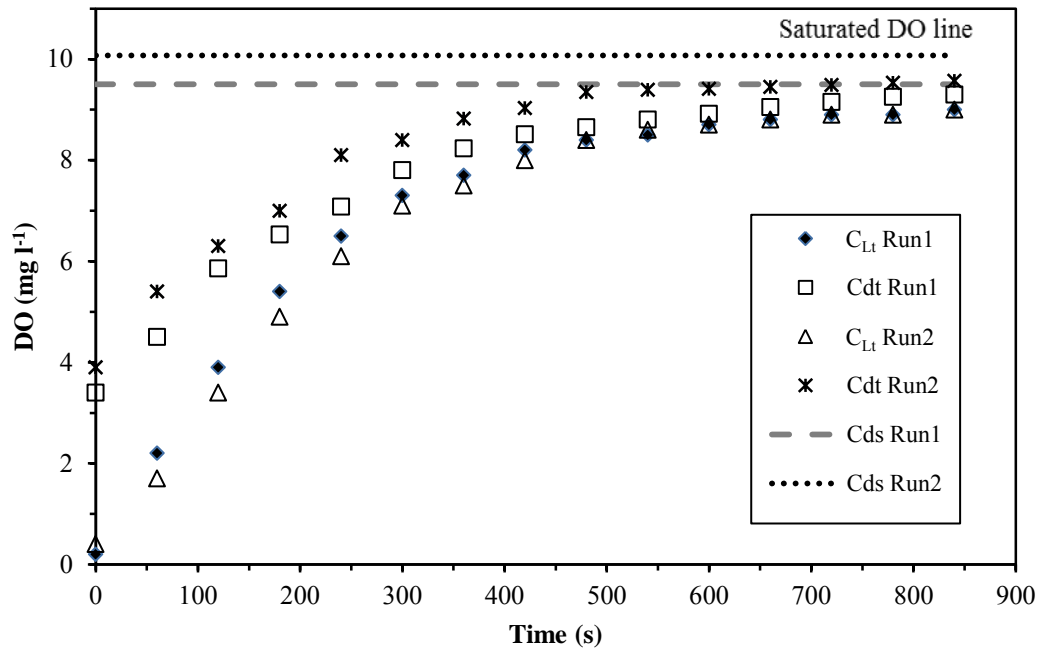


Figure (3.14): Dissolved oxygen concentration profile with time of experiment in the water bulk zone ( $C_{dt}$ ), and the water spray zone ( $C_{Lt}$ ) at  $N = 2.5$  rps for two experimental runs.

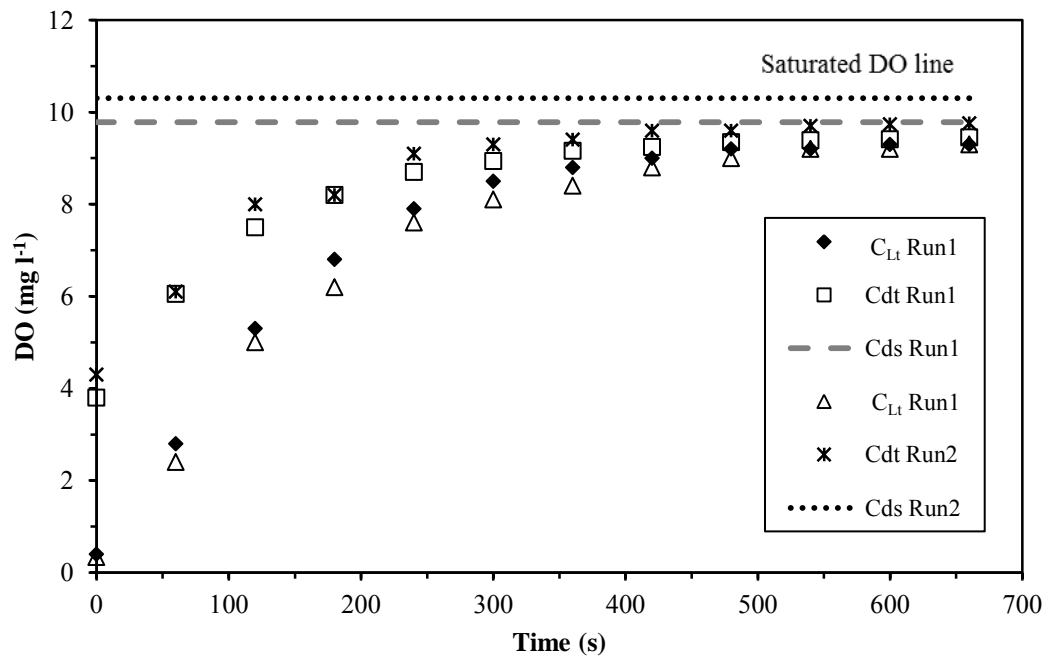


Figure (3.15): Dissolved oxygen concentration profile with time of experiment in the water bulk zone ( $C_{dt}$ ), and the water spray zone ( $C_{Lt}$ ) at  $N = 3.33$  rps for two experimental runs.

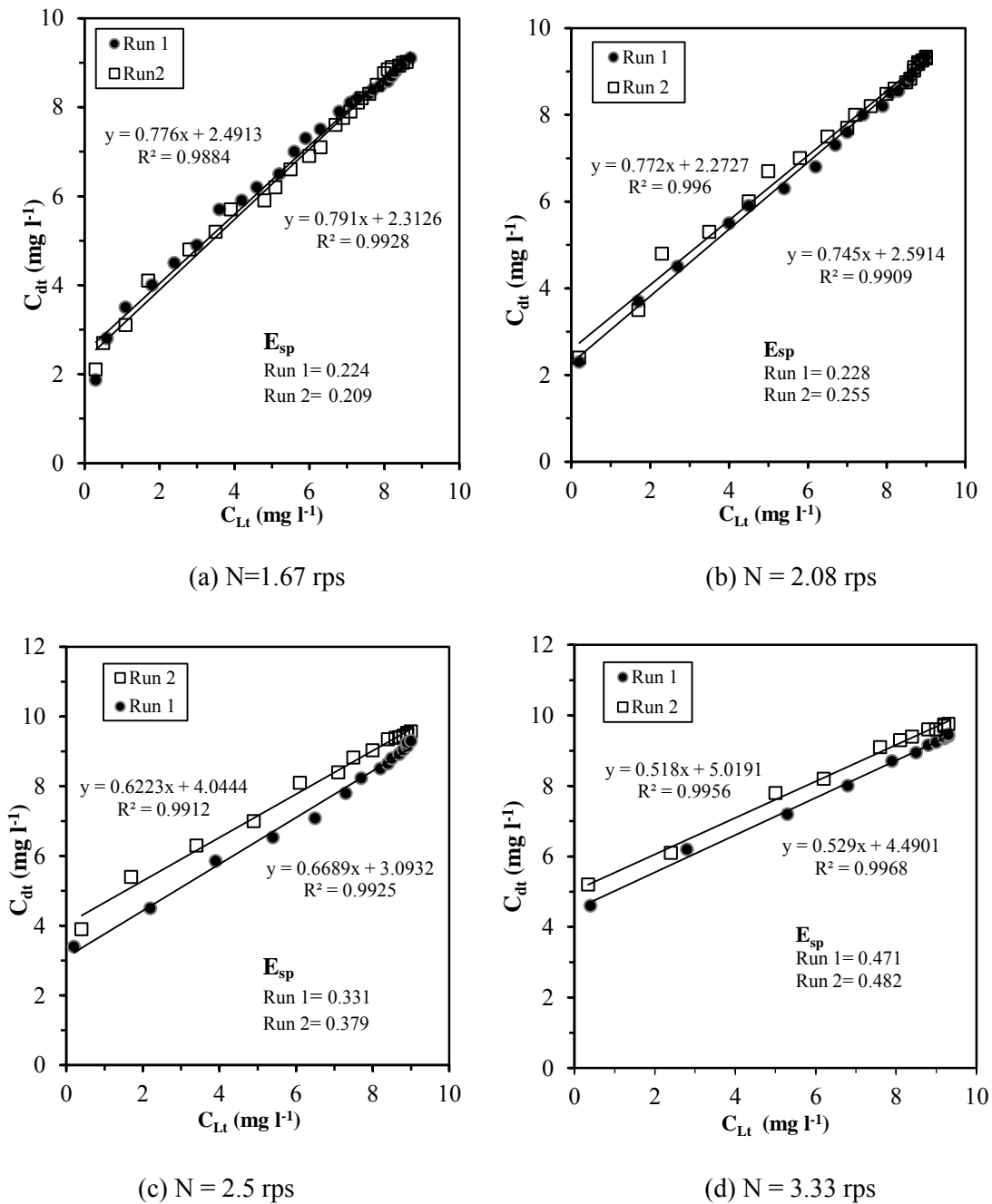


Figure (3.16): The linear regression correlation of water spray zone aeration efficiency by plotting  $C_{dt}$  versus  $C_{Lt}$  for various rotation speeds.

It is noticed from Figures 3.12 to 3.15, the impellers rotation speed gradually increasing from 1.67 rps to 2.08, 2.5 and 3.33 rps causes the increasing of oxygen mass transfer coefficient  $k_{La_d}$  in the spray zone. The increased oxygen mass transfer coefficient  $k_{La_d}$  means that the DO inside the droplets reaches its higher concentration level (nearest to air wet-bulb saturated oxygen condition) in shorter time, but in the same time the flight time for the water droplets from turbine blades to the water

surface is longer since these water droplets are thrown farther with increasing impellers rotation speed.

Figure 3.16 illustrates the linear correlation obtained by plotting the dissolved oxygen DO concentrations of the water droplets directly before they impinge water surface in function of the DO concentration of the water bulk inside the tank. Applying the least squares method of the DO concentrations best fit yields the water spray mass transfer zone aeration efficiency  $E_{sp}$  (The  $E_{sp}$  was calculated by applying equation 2.31). When the impellers rotation speed was increased from 1.67 to 3.33 rps; the water spray zone aeration efficiency increased from 0.21 to 0.48. This particular behavior depends on the fact that water droplets exposure time to the atmospheric air was prolonged and consequently the amount of oxygen transferred from the atmospheric air to the water droplets was increased too. Since the exposure time is same the flight time for the droplets, so that higher impellers rotation speed results in longer flight time, but this relation is applicable just up to 3.33 rps, after this limit desired shape of the water droplets spray begins to be deformed, as consequence the interfacial contact area between the air and water droplets is lessened.

Also Figure 3.16 shows that when the impellers rotation speed has been increased from 1.67 rps to 2.08 rps, the spray zone aeration efficiency was slightly increased where the average spray aeration efficiency was elevated from 0.215 to 0.245. With further increasing of impellers rotational speed to 2.5 rps the spray aeration efficiency was noticeably increased to its average value of 0.335. With continuation of impellers rotation speed elevation to 3.33 rps it seems the corresponding related spray mass transfer zone aeration efficiency was remained progressively increasing to its average value 0.477. From these experimental results it was found that alteration of impellers rotation speed has low effect on the water spray zone aeration efficiency up to 2.08 rps, while its effect on the water spray zone aeration efficiency was apparently remarked after this limit.

### **I.2. Spray Zone Mass Transfer Coefficient ( $k_{ja_d}$ )**

Right after droplets flight time was calculated for the four different rotation speed levels and given operation condition, the  $k_{ja_d}$  was determined by applying equation (2.30). The resulted  $k_{ja_d}$ , the droplets flight time and other related parameters for different rotation speed are shown in Table 3.6.

Table 3.6 shows at the first glance that water spray droplets zone has oxygen mass transfer coefficients  $k_{ja_d}$  much higher than of mass transfer coefficients in water bulk mass transfer zone  $k_{ja}$ . The majority of oxygen mass transfer actually happens in the spray zone (droplets) due to high interfacial area and turbulent conditions. This agrees with (Yeh and Rochelle, 2003). In the surface aeration the bulk oxygen mass transfer zone can be considered as a complementary or supplementary zone, where the

## Chapter Three: Oxygen Mass Transfer in the Surface Aeration

accompanied mixing or agitation process appears in order to accomplish distribution and diffusion of dissolved oxygen in the entire tank. From Figure 3.17 it can be found that the dependence of  $k_{l}a_d$  was increasing with impellers rotation speed  $N$  increasing for the whole system configuration.

Table (3.6): The spray droplets mass transfer zone of  $k_{l}a_d$ , flight time  $t_f$  and the related measured parameters, (of 100% submerged turbine blades,  $H = \text{zero}$ ),  $h/D = 1.47$ ,  $S/W = 1$ .

N (rps)	$T_{\text{bulk}}$ (°C)	$C_{\text{ds}}$ (mg L <sup>-1</sup> )	$Y_m$ (mm)	$R_m$ (mm)	$E_{\text{sp}}$	$(E_{\text{sp}})_{20}$	$t_f$ (s)	$k_{l}a_d$ (s <sup>-1</sup> )
1.67	15.8	10.7	15	110	0.224	0.242	0.11	2.305
1.67	15.2	10.3	15	110	0.209	0.229	0.11	2.131
2.08	16.1	9.6	20	130	0.228	0.245	0.13	2.000
2.08	15.9	9.85	20	130	0.255	0.275	0.13	2.264
2.50	16.5	9.5	35	170	0.331	0.352	0.17	2.365
2.50	16.0	10.07	35	170	0.379	0.405	0.17	2.802
3.33	16.3	9.78	45	280	0.471	0.498	0.19	3.351
3.33	15.9	10.3	45	280	0.482	0.513	0.19	3.462

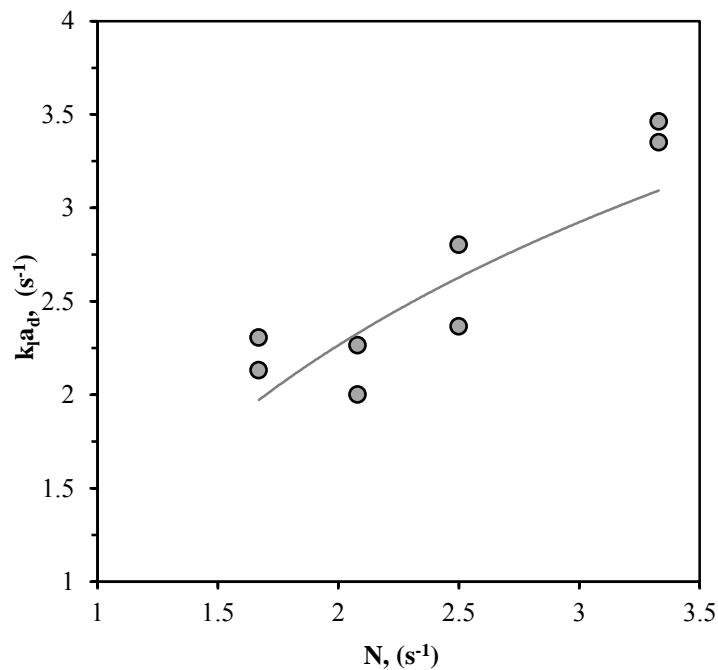


Figure (3.17): The relation between the oxygen mass transfer coefficient  $k_{l}a_d$  and impellers rotation speed and in the spray zone,  $S/W = 1$ .

### I.3. Surface Aeration Water Spray Discharge Velocity and Volumetric Flow Rate

For eliminating the errors of interpretation that may occur when the whole system was used during the energy balance calculation (i. e. the lower propeller and draft tube were placed under the turbine and their contribution in the power consumption is mainly for mixing purposes inside the tank, where that doesn't have any relation with the droplets generation outside the water surface), the power consumption was measured only with presence of the turbine to assure all the energy was converted to propel water droplets into atmospheric air. For the case of turbine alone it was noticed that spray configuration didn't changed significantly, which means the presence of propeller and draft tube doesn't have noticeable effect on the spray configuration. By applying equation (2.43) the water spray flow rates were calculated for various N levels as shown in Table 3.7.

To evaluate the accuracy of the equation 2.43, the calculated water spray flow rates by this equation were compared with those obtained by the PIV technology at the same turbine rotation speeds and it is found that the equation 2.43 can predict the flow rates with an average error less than 2.0%

Table (3.7): Water spray droplets velocity and volumetric flow rate of given operation and geometric configuration (whole system) for various rotation speed levels.

N (rps)	$Y_m$ (mm)	$R_m$ (mm)	$R_{sp}$ (mm)	$E_{sp}$	$t_f$ (s)	P (Watt)	$V_{sp}$ ( $m\ s^{-1}$ )	Q ( $L\ h^{-1}$ )
1.67	15	85	180	0.224	0.111	4.472	1.71	11010
1.67	15	85	180	0.209	0.111	4.472	1.71	11010
2.08	20	115	210	0.228	0.128	6.820	1.76	15851
2.08	20	115	210	0.255	0.128	6.820	1.76	15851
2.50	35	175	270	0.331	0.169	9.943	1.80	22094
2.50	35	175	270	0.379	0.169	9.943	1.80	22094
3.33	45	270	365	0.471	0.19	14.263	2.14	22422
3.33	45	270	365	0.482	0.19	14.263	2.14	22422

From the first glance on the results illustrated in Table 3.7, it is obvious that the droplets spray flow rate was increased when the turbine blades rotation speed was increased, this agrees with (Takase et al., 1982), this relation can be easily explained as the higher rotation speed leads to higher water droplets were projected through the air by the turbine blades. The droplets velocities in the spray at the impingement position at water surface is approximately considered equal along the water spray from turbine blades tip to plunging point and the energy consumption within water spray path was ignored since the droplets flight time is extremely short. With elevating the turbine rotation speeds it was noticed that the spray velocity was increased, this relation was achieved with higher rotation speed or in other word with higher power consumed, so higher mechanical energy was converted to a kinetic

energy and delivered into water bulk, which in turn causes that the water droplets to be discharged faster from turbine blade tip through the atmospheric air. It is worth mentioning that actually the occurred droplets velocities are slightly different according droplet position in the spray, where the droplet position in the spray depends on its projection position from blade tip. For the droplets velocity determination purposes, only the maximum spray height was considered in order to simplify the calculation since the effect of this variation generally is limited (Huang et al., 2009; McWhirter et al., 1995).

#### **I.4. Spray Zone Oxygen Transfer Rate ( $OTR_{sp}$ )**

As mentioned before the fast water droplets in the spray travel with very short flight time, where only the droplets surface has higher dissolved oxygen DO concentration, while the DO concentration becomes lower for further deeper levels inside the droplets. Despite the short flight time of droplets, a high mass transfer rate and may be also a high heat transfer rate can take place during the operation, wherein the outer surface layer temperature of the droplets becomes equal to the wet-bulb temperature. The remaining important factors for evaluating purposes in the droplet spray mass transfer zone is the overall oxygen mass transfer rate ( $OTR_{sp}$ ) that occurred along water spray by contacting droplets surface with atmospheric air. After determination of water spray discharge velocity  $V_{sp}$  and flow rate  $Q$ ,  $OTR_{sp}$  can be calculated easily by applying the equation (2.34) (Chern and Yang, 2004; McWhirter et al., 1995).

The  $OTR_{sp}$  values obtained by applying equation (2.34) are illustrated in Table 3.8; in the view of the fact that higher oxygen transfer rate takes place with higher rotation speed employed. The  $OTR_{sp}$  results agree with those obtained for  $E_{sp}$ , it is obvious that  $OTR_{sp}$  in the water droplets zone is high.

Table (3.8): Spray zone oxygen transfer rate  $OTR_{sp}$  variation with impellers rotation speed.

N (rps)	$E_{sp}$	$t_f$ (s)	$V_{sp}$ ( $m\ s^{-1}$ )	Q ( $L\ h^{-1}$ )	$OTR_{sp}$ ( $gO_2\ h^{-1}$ )
1.67	0.22	0.111	1.71	11010	25.649
1.67	0.21	0.111	1.71	11010	23.011
2.08	0.23	0.128	1.76	15851	33.972
2.08	0.26	0.128	1.76	15851	39.005
2.5	0.33	0.169	1.80	22094	68.012
2.5	0.38	0.169	1.80	22094	80.973
3.33	0.47	0.19	2.14	22422	99.050
3.33	0.48	0.19	2.14	22422	107.642

Table 3.8 and Figure 3.18 show that the oxygen transfer rate in the spray zone increases with increasing of impellers rotation speed  $N$ . Increasing  $N$  leads to the water droplets take longer time in their travel before reaching impingement position at water surface, in other word more time is available for the oxygen in atmospheric air to transfer to the water droplets. A higher dissolved oxygen DO concentration in these droplets is accomplished. The difference in the resulted  $OTR_{sp}$  of each experimental run for the same  $N$  may occur due to the variance in operation conditions such as the air and water bulk temperatures effect.

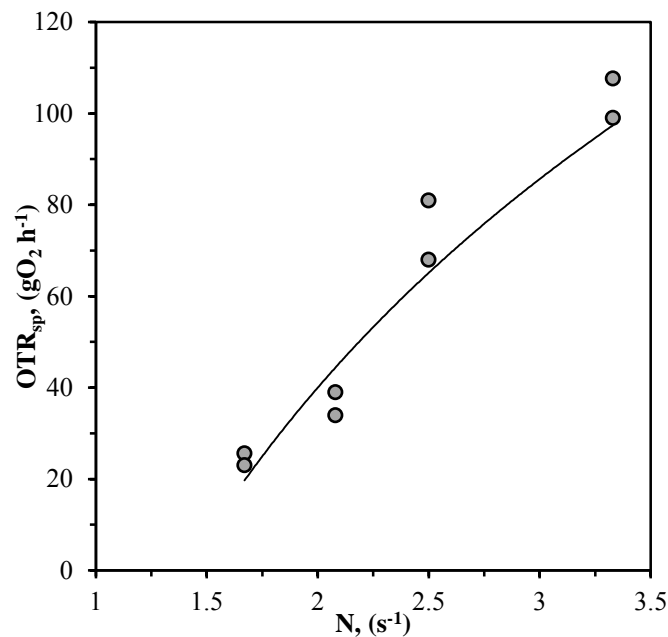


Figure (3.18): The relation between the oxygen transfer rate  $OTR_{sp}$  and impellers rotation speed and, in the spray zone,  $S/W = 1$ .

### I.5. Contribution Percentage of the Spray and Bulk Zones in the Overall Mass Transfer Operation

To have complete view for the oxygen mass transfer for all surface aeration process and to realize the contribution of spray mass transfer zone in the overall oxygen mass transfer operation, the oxygen mass transfer rate in the water bulk mass transfer zone  $OTR_b$  is needed to be calculated.  $OTR_b$  was determined by applying the equation (2.24) (See Appendix II).

## Chapter Three: Oxygen Mass Transfer in the Surface Aeration

Table (3.9): The oxygen mass transfer rates for spray and bulk zones  $OTR_b$  and  $OTR_{sp}$  with the percentage of contribution.

N (rps)	$t_f$ (s)	$OTR_{sp}$ ( $gO_2 h^{-1}$ )	$OTR_r$ ( $gO_2 h^{-1}$ )	$OTR_{sp}\%$	$OTR_b\%$
1.67	0.11	25.649	6.753	79.16	20.84
1.67	0.11	23.011	6.810	77.16	22.84
2.08	0.13	33.972	10.183	76.94	23.06
2.08	0.13	39.005	10.214	79.24	20.76
2.50	0.17	68.012	20.621	76.73	23.27
2.50	0.17	80.973	19.935	80.02	19.98
3.33	0.19	99.050	35.307	73.72	26.28
3.33	0.19	107.642	35.541	75.18	24.82

Results from Table 3.9 and Figure 3.19 show that for different impellers rotation speed, N levels (1.67-3.33 rps); the spray zone oxygen mass transfer  $OTR_{sp}$  has a contribution range between (80.02% - 73.72%) of the overall oxygen mass transferred during the operation, which is higher than the contribution of bulk mass transfer zone in the overall oxygen transfer rate. At higher N, the percentage of contribution for the oxygen mass transfer rate in the bulk zone  $OTR_b$  in the overall oxygen transfer rate stays the same although the  $OTR_b$  was increased with N elevation, where more turbulent state of water surface was occurred by water droplets at the impingement and plunging position due to more mechanical energy was converted to kinetic energy. As a consequence of this condition more air bubbles were generated and entrained into the water bulk, beside that more fine air bubbles were diffused into the tank (Ozkan et al., 2006). So the range of the oxygen mass transfer rate of the bulk zone is improved. The improvement of the  $OTR_b$  assists the bulk zone to keep its contribution somehow similar within the tested range of N. It is also important to mention that both the  $OTR_b$  and  $OTR_{sp}$  were calculated at the same water bulk temperature and ambient temperature for each run.

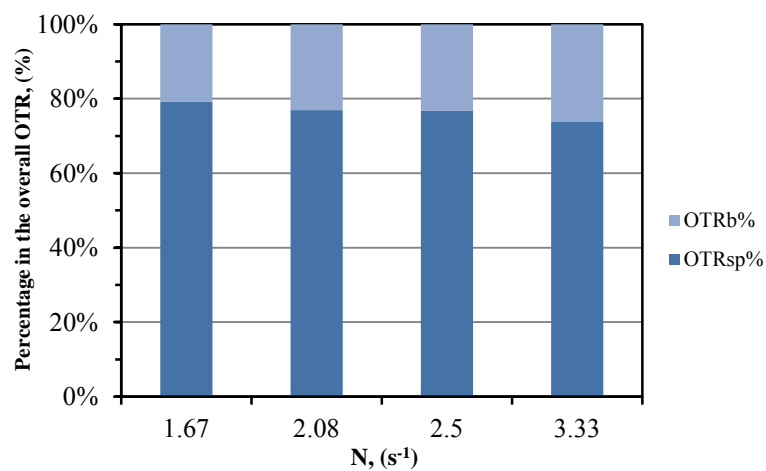


Figure (3.19): The influence of the impellers rotational speed on the spray zone oxygen transfer rate  $OTR_{sp}$  and in the bulk zone oxygen transfer rate  $OTR_b$ ,  $S/W = 1$ .

### II. The Effect of Turbine Blades Submergence

#### II.1. Water Spray Velocity and Volumetric Flow Rate

Table 3.10 illustrates that the calculated water spray flow rate  $Q$  was increased as the dimensionless turbine blades submergence ratio  $S/W$  was increased, where with higher water level higher amount of water droplets are propelled into atmospheric air by the turbine blades. As it was mentioned before, water spray droplets velocity at impingement position of water surface is approximately considered equal to the water spray discharge velocity by turbine blades tip according to physical laws for projectiles.

The energy consumption within the water spray path is ignored since the droplets flight time is extremely short. By elevating the water level it was noticed that the spray velocity remained somehow around (1.8 m/s).

For high turbine blades submergence levels ( $S/W > 1$ ) it was found that even though more power was consumed by turbine blades with increasing ( $S/W$ ) the spray velocities were relatively close. The excess power was consumed to convert the needed mechanical energy into kinetic energy and delivered into water bulk in order to overcome the excess in water amount that to be projected into atmospheric air with achieved spray velocity.

In the case of turbine blades were partially submerged in water  $S/W = 0.17$  (particularly for minimum water height used  $h/D = 1.37$ ), it was noticed at the given rotation speed ( $N = 2.5$  rps) the spray velocity is somehow lower, the reason for that may rely on the fact that a part of the mechanical energy didn't converted to kinetic energy into water bulk, and has been wasted by air resistance due to direct contact of apparent blade part above water surface, which in turn causes less discharged water droplets from turbine blade tip through the atmospheric air.

Generally the water spray volumetric flow rate is increased with increasing turbine blades submergence level, as more water droplets can be propelled when higher  $S/W$  is implemented. The spray velocities and volumetric flow rates for the water droplets were calculated by equations (2.42) and (2.43).

The values of power consumption were measured for the turbine alone condition at various  $S/W$  levels to eliminate the error in calculation because power consumed by the lower propeller and to insure that all the measured power are equivalent to the converted mechanical energy from turbine blades to kinetic energy in water bulk.

Table (3.10): The water spray velocity and volumetric flow rate for the whole system geometrical configuration with various turbine blades submergence and water levels,  $N= 2.5$  rps.

S/W (-)	h/D (-)	$Y_m$ (mm)	$R_m$ (mm)	$R_{sp}$ (mm)	$E_{sp}$ (-)	$t_f$ (s)	P (Watt)	$V_{sp}$ ( $m\ s^{-1}$ )	Q ( $L\ h^{-1}$ )
0.17	1.37	23	55	150	0.182	0.093	4.214	1.74	10021
0.17	1.37	23	55	155	0.185	0.093	4.214	1.74	10021
0.58	1.42	26	85	180	0.217	0.109	6.754	1.79	15176
0.58	1.42	26	85	185	0.223	0.109	6.754	1.79	15176
1.00	1.47	33	170	265	0.353	0.164	9.943	1.81	21850
1.00	1.47	33	170	265	0.340	0.164	9.943	1.81	21850
1.42	1.53	35	180	275	0.362	0.169	11.624	1.82	25264
1.42	1.53	35	180	275	0.360	0.169	11.624	1.82	25264
1.83	1.58	38	187	282	0.392	0.176	12.872	1.80	28602
1.83	1.58	38	187	282	0.384	0.176	12.872	1.80	28602

## II.2. Spray Zone Aeration Efficiency ( $E_{sp}$ )

The oxygen mass transfer in water spray zone is affected by various factors. Beside impeller rotation speed  $N$  it is necessary to consider the effect of turbine blades submergence or water level on the spray mass transfer zone characteristics. The turbine blades submergence primarily affects the droplets volumetric flow rate, whereas the amount of the projected droplets by turbine blades is changed due to the difference of water free surface height. The operation condition and geometrical configuration were kept constant, while the turbine blades submergence was tested as a dimensionless geometrical ratio of  $S/W$ , where the submergence of the turbine blades  $S$  has been normalized with turbine blade width  $W$ . The submergence of turbine blades  $S$  is referring to the distance from the water surface to the lower edge of turbine blade. The ratio  $S/W$  was changed for different water levels of (0.17, 0.58, 1.0, 1.42, 1.83, and 2.25) (See Figure 3.20) wherein  $N$  was kept constant at 2.5 rps. The five tested levels of the submergence ratio  $S/W$  correspond to the water levels  $h/D$  of (1.37, 1.42, 1.47, 1.53, 1.58 and 1.63) respectively. The submergences of turbine blades can be referred as submergence percentage by considering the water level at the turbine blades upper edge as 100% of submergence, the submergence percentage variation in the experimentation were (167% - 33%). At  $S/W < 1$  ( $h/D$  lower than 1.47) the blades are partially submerged, at  $S/W > 1$  ( $h/D$  higher than 1.47) the blades are over submerged and at  $S/W = 1$  ( $h/D = 1.47$ ) the water level is just at blades upper tip (See Table 3.11). All the possible conditions were covered from excessively submerged, totally submerged to partially submerged turbine blades. The repeatability of water level height experimental runs was tested also, where spray zone aeration efficiency is calculated twice for each experimental run.

Figure 3.20 shows the DO concentration profile in the water spray with the experiment time at different turbine blade submergence levels with constant rotation speed. When the turbine blade submergence increases, the DO reaches its higher possible level near to its equilibrium state within shorter time. As higher turbine blade submergence was used, more water droplets were projected into the atmospheric air, which leads to more contact area between water droplets and air was provided. In the same time water droplets were propelled farther toward the periphery space around the turbine, where these droplets travel in atmospheric air longer flight time before they impinge water surface.

From Figure 3.20 it was found that there is no noticeable difference of dissolved oxygen DO profile at high blades submergence level  $S/W = 1.42$  and  $1.83$  ( $h/D = 1.53$  and  $1.58$ ). It was noticed that from the level  $S/W = 1.42$  ( $h/D = 1.53$ ), the regular form of water spray begins to be deformed by creation of instability of its configuration during the turbine rotation. At low turbine submergence levels  $S/W < 1$  ( $S/W = 0.17$  and  $0.58$ ) it was also observed that the DO profiles are similar and the DO takes longer time to reach equilibrium level, which means with low submergence of turbine blades (33% - 67%) correspond to ( $h/D = 1.37$  and  $1.42$ ), the amount of water droplets that propelled by turbine blades is lower and flight time is shorter. In other word less contact time is achieved between water in droplets and atmospheric air, so longer time is needed to reach equilibrium DO concentration.

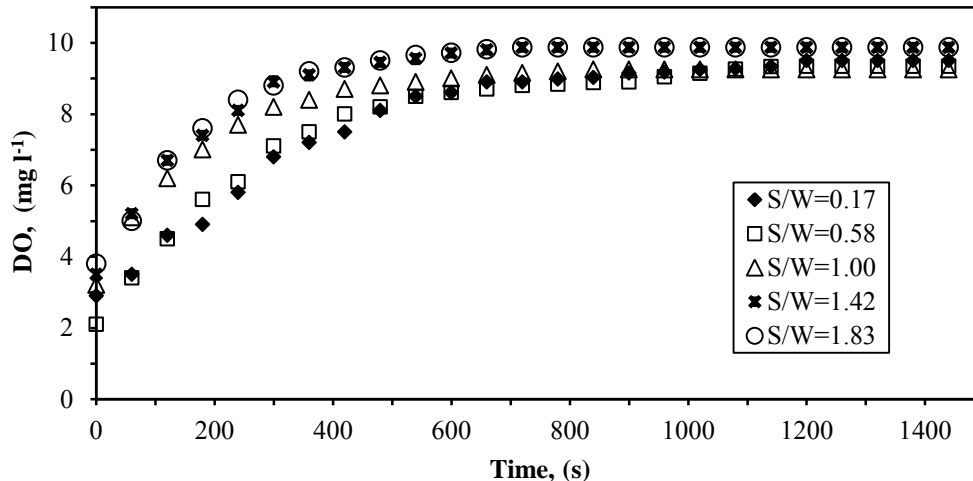


Figure (3.20) Effect of the turbine blade submergence on spray mass transfer zone dissolved oxygen concentration at rotation speed ( $N=2.5$  rps) and turbine clearance ( $C/T_v = 0.35$ ).

From Figure 3.20 it was found also that elevating  $S/W$  ratio to  $1.42$  has no enhancement on DO behavior, on the contrary higher  $S/W$  levels causes deformation of water spray, in consequence the achieved DO is lowered. In the other hand at lower  $S/W$  ratio ( $1.37$  and  $1.42$ ) it seems that DO profiles with time are close together.

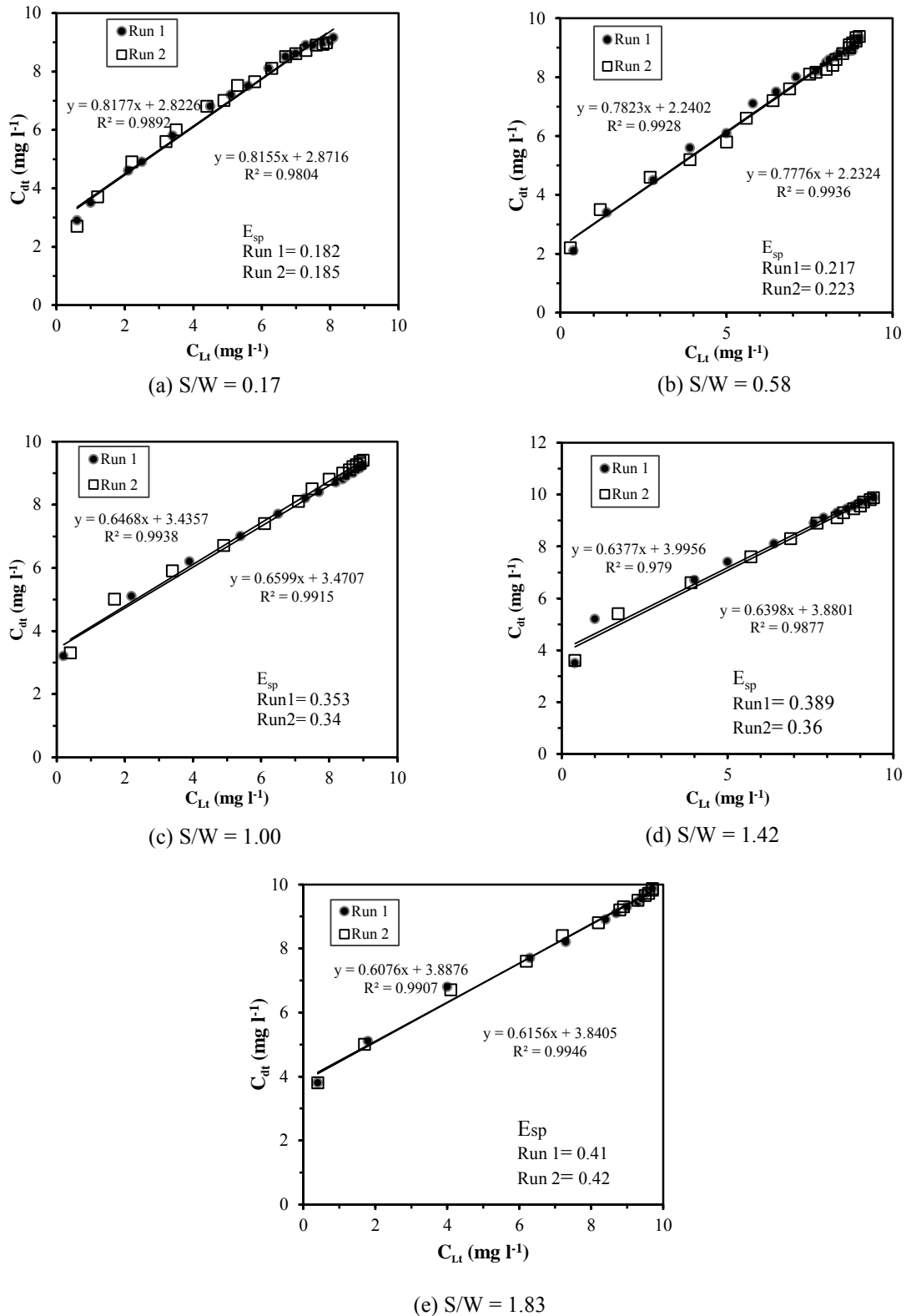


Figure (3.21): The linear regression correlation of water spray zone aeration efficiency by plotting ( $C_{dt}$ ) versus ( $C_{Lt}$ ) for various turbine blades submergence,  $N = 2.5$  rps.

Figure 3.21 shows the obtained linear regression correlations of the spray zone efficiency. The DO concentration levels of droplets before the impingement at water surface and of the water bulk inside the tank were plotted for different turbine blades submergence ratios  $S/W$  (from 0.17 to 1.83), by applying the least squares of the DO concentrations best fit to identify ( $E_{sp}$ ).

The increasing in spray zone efficiency depends as mentioned before on the fact that water droplets flight time in atmospheric air is longer, the amount of oxygen transferred from the atmospheric air to the water droplets is increased. As a consequence it can be deduced that water droplets aeration efficiency  $E_{sp}$  depends on turbine blades submergence  $S$  and the ratio  $S/W$ , so that leads to higher  $E_{sp}$  was accomplished with higher  $S/W$ .

From Figures 3.21 and Figure 3.22 it was founded that when  $S/W$  was increased from 0.17 to 0.58, the average spray zone aeration efficiency  $E_{sp}$  is increased from 0.183 to 0.22. But it is noticed that at  $S/W$  equals 1.47 the  $E_{sp}$  was effectively increased to its average value of 0.35. With further elevating of  $S/W$  from 1.00 to 1.42 and 1.83 it was found that the achieved  $E_{sp}$  was increased respectively to their average values 0.36 and 0.388. From these experimental results it seems that elevation of  $S/W$  has remarkable effect on  $E_{sp}$  for higher than 1.00, while  $S/W$  has a relative effect on ( $E_{sp}$ ) especially for the levels lower than 1.00. These experimental results show that  $E_{sp}$  is effectively lowered when the submergence level of turbine blades is less than 100% ( $S/W < 1$ ), where  $E_{sp}$  was changed from 0.346 to 0.183. The  $E_{sp}$  is relatively affected by turbine blades submergence level higher than 100% ( $S/W > 1$ ), where the  $E_{sp}$  was changed from 0.358 to 0.392. From Figure 3.20 it can be noticed as ( $S/W$ ) is increased, the water spray zone aeration efficiency is increased from 0.182 to 0.392.

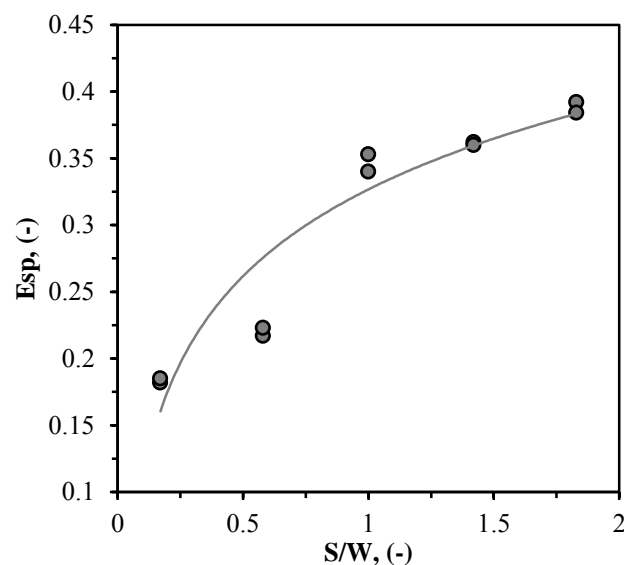


Figure (3.22): The relation between the spray zone aeration efficiency  $E_{sp}$  and turbine blade submergence ratio,  $N = 2.5$  rps.

### II.3. Spray Zone Mass Transfer Coefficient ( $k_{1a_d}$ )

Table 3.11 and Figure 3.23 show that the oxygen mass transfer coefficient in the water spray zone  $k_{1a_d}$  as mentioned before is also much higher than the mass transfer coefficients in water bulk mass transfer zone  $k_{1a}$  for different turbine blades submergence (See section 3.1 in this chapter). Table 3.11 illustrates the dependence of  $k_{1a_d}$  on turbine blades submergence for whole system configuration at given impellers rotation speed ( $N=2.5$  rps), where the  $k_{1a_d}$  was increased from 2.16 1/s to 2.827 1/s when  $S/W$  was increased from 0.17 to 1.83. It is important here to elucidate that the water spray aeration efficiency  $E_{sp}$  is relevant to  $S/W$  elevation, the  $k_{1a_d}$  showed also the same behavior as a result of enlarging the interfacial contact area and flight time elongation. The water droplets flight time was calculated by equation (2.35). The standard water spray aeration efficiency at 20 °C was calculated by the equation (2.32).

Table (3.11): The calculated water spray mass transfer zone ( $k_{1a_d}$ ), droplets flight time( $t_f$ ) and some related measured parameters and turbine blades submergence and water level, at constant rotation speed ( $N = 2.5$  rps).

S/W (-)	h/D (-)	$T_{bulk}$ (°C)	$C_{ds}$ (mg L <sup>-1</sup> )	$Y_m$ (mm)	$R_m$ (mm)	$E_{sp}$ (-)	$(E_{sp})_{20}$ (-)	$t_f$ (s)	$k_{1a_d}$ (s <sup>-1</sup> )
0.17	1.38	17.7	10.73	23	60	0.182	0.190	0.093	2.160
0.17	1.38	17.8	10.9	23	60	0.185	0.193	0.093	2.199
0.58	1.42	18.4	9.45	26	90	0.217	0.224	0.109	2.244
0.58	1.42	18.3	9.94	26	90	0.223	0.230	0.109	2.449
1.00	1.47	16.8	9.5	33	170	0.353	0.373	0.164	2.655
1.00	1.47	16.7	10.07	33	170	0.340	0.360	0.164	2.534
1.42	1.53	16.7	10.5	35	180	0.362	0.383	0.169	2.659
1.42	1.53	16.5	10.2	35	180	0.360	0.382	0.169	2.641
1.83	1.58	15.2	9.94	38	187	0.392	0.424	0.176	2.827
1.83	1.58	15.1	10.0	38	187	0.384	0.417	0.176	2.785

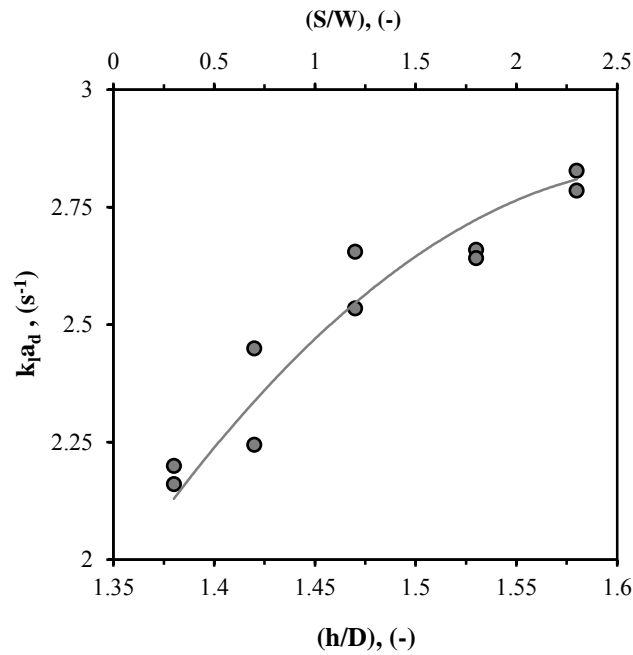


Figure (3.23): The relation between the spray zone oxygen mass transfer coefficient,  $k_1a_d$  with the turbine submergence and liquid level impellers rotation speed,  $N = 2.5$  rps.

#### II.4. Spray Zone Oxygen Transfer Rate ( $OTR_{sp}$ )

Table 3.12 and Figure 3.24 illustrate the oxygen transfer rate of the water spray zone ( $OTR_{sp}$ ) calculated by equation (2.34), where higher oxygen transfer rate takes place with higher blade submergence used. The experimental results of  $OTR_{sp}$  and  $E_{sp}$  elucidate a direct relation with them; high  $OTR_{sp}$  was accomplished as high spray zone surface aeration efficiency was obtained. It was indicated in the Table 3.12 that a higher oxygen transfer rate at droplet spray zone was reached (106.514 g/h) when the highest turbine blades submergence was used ( $S/W = 1.83$ ), while a lowest  $OTR_{sp}$  took place (16.232 g/h) with lower blades submergence level used ( $S/W = 0.17$ ). When  $h/D$  or  $S/W$  was increased that causes more water droplets to be propelled into atmospheric air, so larger contact interfacial area is available and also the longer flight time during their travel before reaching impingement position at water surface was fulfilled, so higher DO concentration in droplets is accomplished.

Table (3.12): Water spray zone oxygen transfer rate ( $OTR_{sp}$ ) variation with different turbine blades submergence and water levels, ( $N = 2.5$  rps).

S/W (-)	h/D (-)	$E_{sp}$ (-)	$t_f$ (s)	$V_{sp}$ ( $m\ s^{-1}$ )	Q ( $L\ h^{-1}$ )	$OTR_{sp}$ ( $g\ h^{-1}$ )
0.17	1.37	0.182	0.093	1.74	10021	16.232
0.17	1.37	0.185	0.093	1.74	10021	16.407
0.58	1.42	0.217	0.109	1.79	15176	29.211
0.58	1.42	0.223	0.103	1.79	15176	30.424
1.00	1.47	0.353	0.164	1.81	21850	71.346
1.00	1.47	0.340	0.164	1.81	21850	67.975
1.42	1.53	0.362	0.169	1.82	25264	85.511
1.42	1.53	0.360	0.169	1.82	25264	85.221
1.83	1.58	0.392	0.176	1.80	28602	106.514
1.83	1.58	0.384	0.174	1.80	28602	104.340

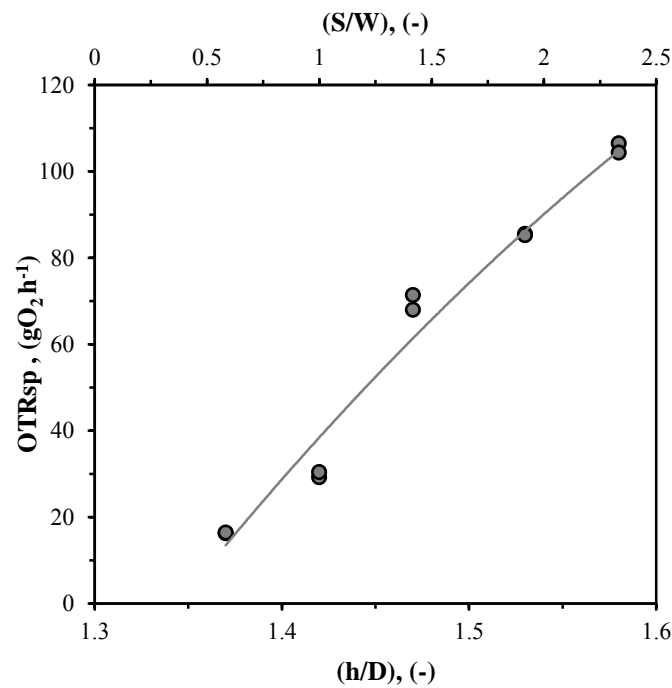


Figure (3.24): The relation between spray zone oxygen transfer rate  $OTR_{sp}$  with the turbine blades submergence and liquid level,  $N = 2.5$  rps.

### II.5. Contribution Percentage of the Spray and Bulk Zones in the Overall Mass Transfer Operation

Table 3.13 and Figure 3.25 show the results for the comparison between the oxygen transfer rates for both bulk and spray mass transfer zones in order to have a general understanding on the overall oxygen mass transfer occurred in the system and its distribution in the zones. At low turbine blades submergence ( $S/W=0.17$ ) or low water level ( $h/D = 1.37$ ) the resulted spray mass transfer zone  $OTR_{sp}$  has a contribution range between (60.1% - 61.12%), which is higher than the contribution of occurred re-aeration in water bulk mass transfer zone  $OTR_b$  in the overall oxygen transfer rate.

At moderate turbine blade submergence ( $S/W=0.58$ ) or the water height level ( $h/D=1.42$ ), the contribution percentage of the spray oxygen mass transfer rate  $OTR_{sp}$  in overall oxygen transfer rate is higher and reaches (66.56%). With elevated turbine blade submergence level  $S/W \geq 1$  ( $h/D = 1.47$  and higher), the contribution of  $OTR_{sp}$  was high and reaches (78.86%) but it stays close to this value even though the  $h/D$  was increased, which means that further elevation in water level for totally immersed turbine blades doesn't affect the contribution of water spray mass transfer zone in the overall oxygen mass transfer in the system.

The oxygen mass transfer rate for water spray (droplets) mass transfer zone  $OTR_{sp}$  and bulk (re-aeration) mass transfer zone  $OTR_b$  are calculated according to equations (2.34) and (2.24) respectively.

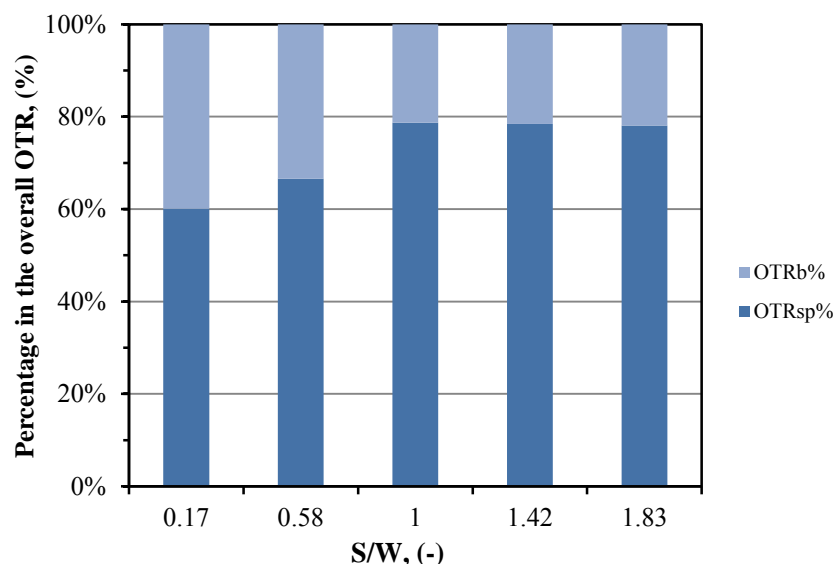


Figure (3.25): The influence of the turbine submergence on the spray zone oxygen transfer rate,  $OTR_{sp}$  and in the bulk zone oxygen transfer rate  $OTR_b$  contributions the overall transfer rate  $OTR$ ,  $N = 2.5$  rps.

Table (3.13): Oxygen mass transfer rate and percentage of contribution for both water spray and bulk (re-aeration) zones, ( $N= 2.5$  rps).

S/W (-)	h/D (-)	$t_f$ (s)	$OTR_{sp}$ ( $g\ h^{-1}$ )	$OTR_b$ ( $g\ h^{-1}$ )	$OTR_{sp}\%$ (%)	$OTR_b\%$ (%)
0.17	1.37	0.093	16.232	10.778	60.10	39.90
0.17	1.37	0.093	16.407	10.437	61.12	38.88
0.58	1.42	0.109	29.211	14.673	66.56	33.44
0.58	1.42	0.103	30.424	16.607	64.69	35.31
1.00	1.47	0.164	71.346	19.319	78.69	21.31
1.00	1.47	0.164	67.975	20.578	76.76	23.24
1.42	1.53	0.169	85.511	23.540	78.41	21.59
1.42	1.53	0.169	85.221	22.841	78.86	21.14
1.83	1.58	0.176	106.514	29.969	78.04	21.96
1.83	1.58	0.174	104.340	30.157	77.58	22.42

### III. Effect of Propeller and the Draft Tube

The function of the propeller and the draft tube that positioned below the turbine is mainly to enhance the distribution of dissolved oxygen in the water bulk. The investigation of the effect propeller and draft tube presence on the water spray mass transfer characteristics was performed by the determination of oxygen mass transfer coefficient, aeration efficiency, surface aeration water velocity, volumetric flow rate and oxygen transfer rate for the water spray mass transfer zone with turbine alone geometrical configuration in order to find out if there will be any preliminary difference occurred. The way to recognize the relative effects consider in testing the mentioned parameters for turbine various rotation speeds,  $N$  for constant water level ratio  $h/D=1.47$  and turbine blades submergence ratio  $S/W = 1.00$ . The other operation condition and geometrical configuration are also kept constant.

#### III.1. Spray Zone Aeration Efficiency ( $E_{sp}$ )

The dissolved oxygen DO concentration profile in the water spray during surface aeration of turbine alone configuration at four rotation speed levels is shown in Figure 3.26. As it was found in the whole system configuration, with turbine rotation speed,  $N$  increasing the DO increases till it reaches its saturation level at wet-bulb of atmospheric air. With higher  $N$  applied, more water droplets were propelled into the atmospheric air and at the same time the water droplets DO concentrations are close to those obtained in the whole system configuration, where DO reaches the equilibrium concentration in shorter time with higher  $N$  used.

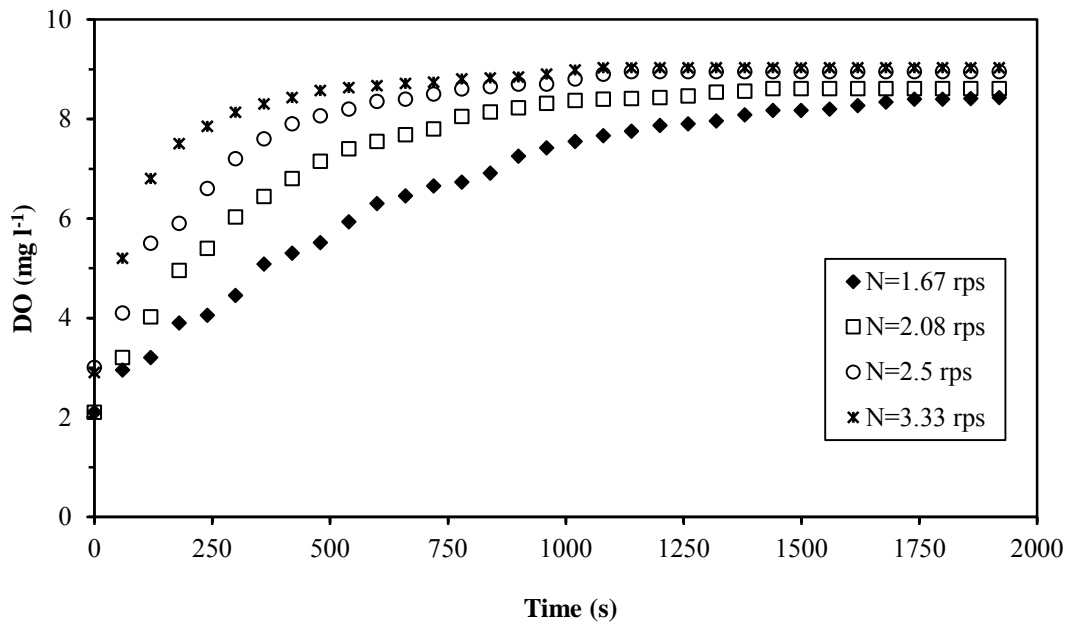


Figure (3.26): The effect of the turbine rotation speed on the spray mass transfer zone dissolved oxygen concentration at  $h/D=1.47$  and  $C/T=0.35$ , (Turbine alone configuration).

The spray zone aeration efficiency  $E_{sp}$  for the turbine alone configuration was calculated by the linear regression for the  $C_{dt}$  versus  $C_{Lt}$  plot. Aeration efficiency  $E_{sp}$  was determined for the four different rotation levels by applying best fit with the least squares method. The results are shown in Figure 3.27.

As in the whole system configuration, with higher  $N$ , higher water spray zone aeration efficiency  $E_{sp}$  is achieved. Figure 3.26 shows that when  $N$  was increased from 1.67 rps to 2.08 rps; the  $E_{sp}$  was increased from 0.183 to 0.206. At moderate  $N=2.5$  rps, the aeration efficiency  $E_{sp}$  was noticeably elevated to 0.292. At relatively elevated  $N=3.33$  rps, the  $E_{sp}$  was found to be 0.356. From Figures 3.27 and 3.28 it is found that the  $E_{sp}$  is remarkably lowered when the propeller and the draft tube are removed.

The  $E_{sp}$  values are relatively lower than the whole system configuration aeration efficiencies for all tested  $N$  levels, for  $N= 1.67$ rps, the  $E_{sp}$  was lowered from 0.21 to 0.183, while for  $N= 3.33$ rps, the  $E_{sp}$  was lowered from 0.471 to 0.356. From these comparisons it can be deduced that the presence of the propeller and draft tube has a relative influence on the water spray efficiency  $E_{sp}$  especially at higher rotation speeds.

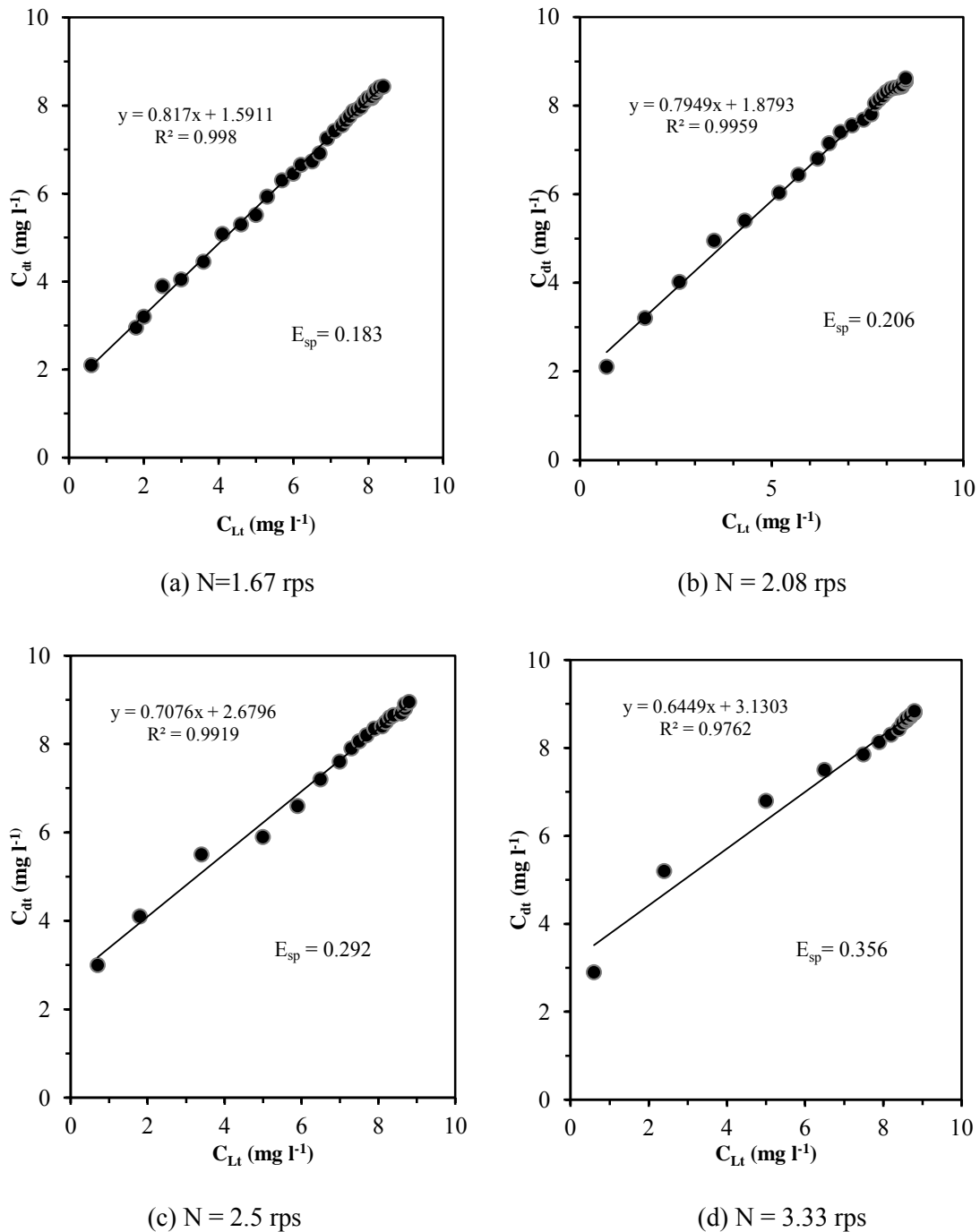


Figure (3.27): The linear regression of the spray zone aeration efficiency of the plot ( $C_{dt}$ ) versus ( $C_{L_t}$ ) for various rotation speeds, (Turbine alone configuration).

The performances of both the draft tube and the propeller are to enable the system to obtain an efficient mixing condition of the DO in the water bulk mass transfer zone inside the aeration vessel, which has also a relative effect in the enhancing of the aeration efficiency  $E_{sp}$  in the spray mass transfer zone through increasing the dissolved oxygen DO in the liquid bulk. The water bulk here is considered in the same time as the intake of water spray droplets.

For this configuration it can be said that each zone of the two existed spray and water bulk mass transfer zones is regarded as complementary to other zone and each zone cannot be evaluated separately from the other one.

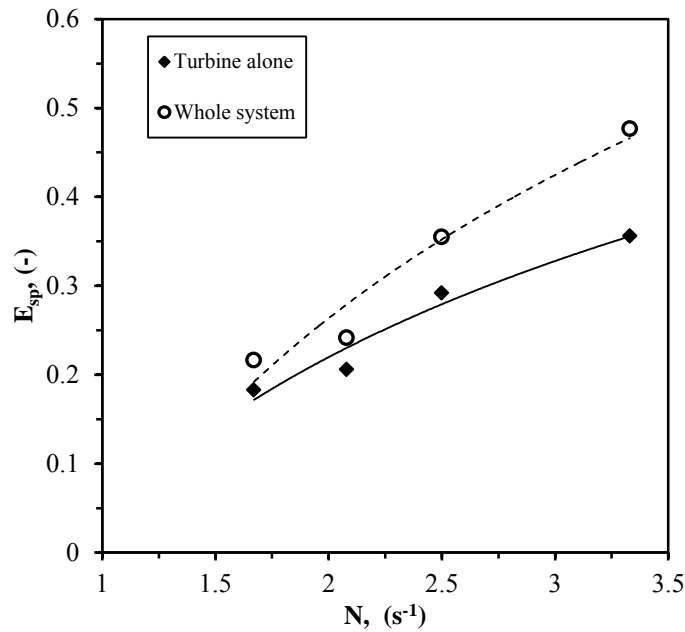


Figure (3.28): The relation between the impellers speed  $N$  and the spray zone aeration efficiency  $E_{sp}$  for both turbine alone and whole system configurations,  $S/W = 1.0$ .

### III.2. Spray Zone Mass Transfer Coefficient ( $k_{1a_d}$ )

The water spray zone oxygen mass transfer coefficients ( $k_{1a_d}$ ) for turbine alone configuration is illustrated in Table 3.14. The occurred  $k_{1a_d}$  values are slightly lower than the  $k_{1a_d}$  values for the whole system configuration as shown in Figure 3.29.

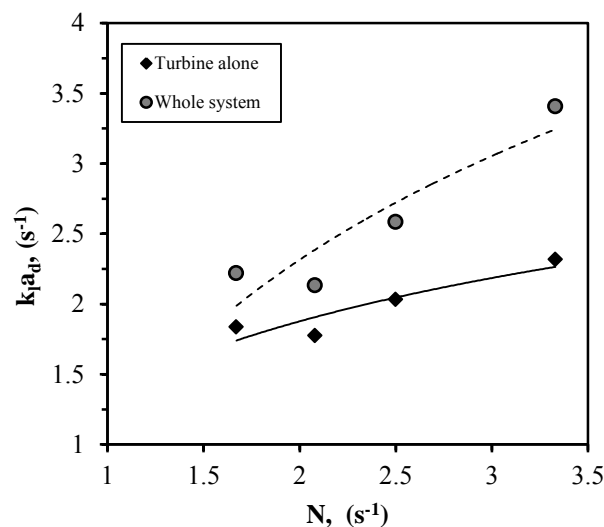


Figure (3.29): The relation between  $N$  and the oxygen mass transfer coefficient  $k_{1a_d}$  for both turbine alone and whole system configurations,  $S/W = 1.0$ .

## Chapter Three: Oxygen Mass Transfer in the Surface Aeration

Table 3.14 and Figure 3.29 show that the  $k_{ia_d}$  was higher for the rotation speeds 2.5 and 3.33 rps ( $k_{ia_d} = 1.837$  1/s) than of low rotation speed (1.67 and 2.08 rps), where the  $k_{ia_d}$  was increased to 2.316 1/s. The  $k_{ia_d}$  showed same behavior as spray aeration efficiency  $E_{sp}$ , where their values are decreased when the draft tube and propeller are removed. As a result of that the water bulk DO concentration is reduced inside the water bulk. It was found that the accomplished water spray maintains its dimensions for both whole system and turbine alone configurations. The water droplets flight time is calculated by equation (2.35), while  $k_{ia_d}$  is calculated as mentioned in chapter 2.

Table (3.14): The spray mass transfer zone ( $k_{ia_d}$ ), flight time ( $t_f$ ) and some related measured parameters,  $S/W=1.00$ ,  $h/D=1.47$ , (Turbine alone configuration).

N (rps)	$T_{bulk}$ (°C)	$C_{ds}$ (mg L <sup>-1</sup> )	$Y_m$ (mm)	$R_m$ (mm)	$E_{sp}$ (-)	$(E_{sp})_{20}$ (-)	$t_f$ (s)	$k_{ia_d}$ (s <sup>-1</sup> )
1.67	19.6	8.85	15	110	0.183	0.184	0.11	1.837
2.08	20.8	8.74	20	130	0.206	0.203	0.13	1.774
2.5	21.0	9.28	35	170	0.292	0.287	0.17	2.031
3.33	19.7	9.01	45	280	0.356	0.358	0.19	2.316

### III.3. Water Spray Velocity and Volumetric Flow Rate

The water spray flow rate  $Q$  as well as the water spray velocity  $V_{sp}$  for the turbine alone configuration match those in whole system configuration, since both the  $Q$  and  $V_{sp}$  depend in their calculations on the shape of water spray which it is identical in both cases. Table 3.15 shows the  $Q$  and  $V_{sp}$  in the turbine alone configuration and elucidates the relation between the water spray dimensional values with the generated spray. Same as the whole system configuration both the spray velocity  $V_{sp}$  and spray flow rate  $Q$  increase with rotational speed increasing. Equations (2.40), (2.41), (2.42) and (2.43) are applied to calculate water spray discharge velocity  $V_{sp}$  by the turbine blades tip according to physical laws for projectiles and water droplets spray flow rate  $Q$ . It was found that when the turbine rotation speed was elevated from 1.67 rps to 3.33 rps the achieved spray flow rate  $Q$  was approximately doubled from 11010 g/h to 22422 g/h. The increasing in  $N$  higher than 2.5 rps didn't produce a noticeable rising in the projected water droplets spray flowrate  $Q$ .

Table (3.15): The spray velocity and volumetric flow rate for various turbine rotation speed (Turbine alone configuration).

N (rps)	$Y_m$ (mm)	$R_m$ (mm)	$R_{sp}$ (mm)	$E_{sp}$ (-)	$t_f$ (s)	P (Watt)	$V_{sp}$ (m s <sup>-1</sup> )	Q (L h <sup>-1</sup> )
1.67	15	85	180	0.183	0.111	4.472	1.71	11010
2.08	20	115	210	0.206	0.128	6.820	1.76	15851
2.5	35	175	270	0.292	0.169	9.943	1.80	22094
3.33	45	270	365	0.356	0.19	14.263	2.14	22422

**III.4. Spray Zone Oxygen Transfer Rate ( $OTR_{sp}$ )**

Table 3.16 and Figure 3.30 show that a higher oxygen transfer rate  $OTR_{sp}$  was produced with higher water rotation speed  $N$ . It was noticed in turbine alone configuration the  $OTR_{sp}$  and  $E_{sp}$  water spray efficiency are related in direct relation, where higher  $OTR_{sp}$  is obtained as high  $E_{sp}$  is achieved. From Table 3.15 it was founded that at the highest employed rotation speed ( $N=3.33$  rps), the maximum oxygen transfer rate was reached (67.131g/h). The lowest  $OTR_{sp}$  (16.622 g/h) was occurred with lower  $N$  used ( $N=1.67$  rps). Table 3.15 shows that as higher  $N$  causes more water droplets to be projected into atmospheric air as consequence larger contact interfacial area is available. The calculated  $OTR_{sp}$  is by applying equation (2.34). The important of the  $OTR_{sp}$  calculation for this case is to compare this performance with that obtained for whole system configuration in order to understand the effect of the draft tube and the RTP propeller on the achieved  $OTR_{sp}$  for the system as it is explained in the next section IV.

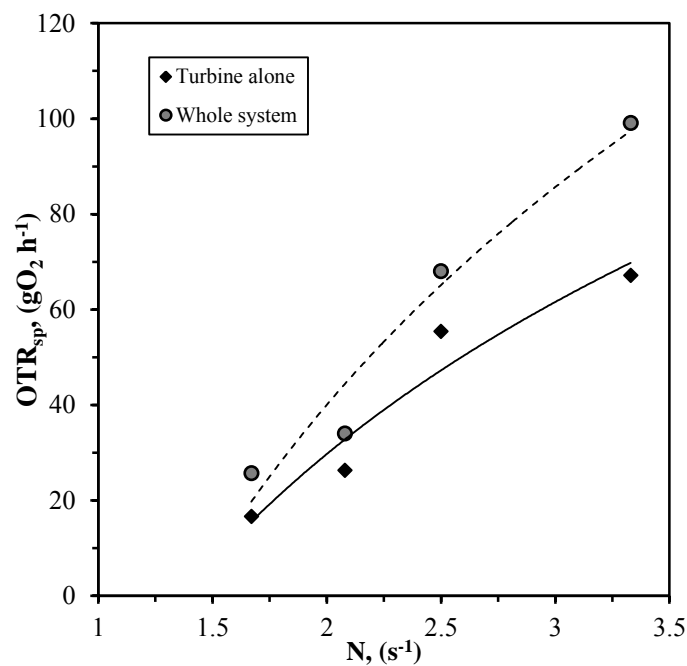


Figure (3.30): The relation between spray zone oxygen transfer rate with the rotational speed for the whole system and turbine alone configurations,  $S/W = 1.0$ .

Table (3.16): The Spray zone oxygen transfer rate  $OTR_{sp}$  for different rotation speed levels, (Turbine alone configuration).

N (rps)	$E_{sp}$ (-)	$t_f$ (s)	$V_{sp}$ ( $m\ s^{-1}$ )	Q ( $L\ h^{-1}$ )	$OTR_{sp}$ ( $g\ h^{-1}$ )
1.67	0.183	0.111	1.71	11010	16.622
2.08	0.206	0.128	1.76	15851	26.253
2.5	0.292	0.169	1.80	22094	55.353
3.33	0.356	0.19	2.14	22422	67.131

#### IV. Comparing the $OTR_{sp}$ for the Whole System and Turbine Alone Configurations

To find out the effect of the RTP propeller and draft tube presence on oxygen mass transfer rate in spray mass transfer zone  $OTR_{sp}$ , a comparison was made between the calculated  $OTR_{sp}$  in both whole system and turbine alone configurations. It is found that  $OTR_{sp}$  in whole system configuration has moderately higher values than the turbine alone configuration as illustrated in table 3.17 and Figure 3.31. The improvement in  $OTR_{sp}$  when propeller and draft tube placed under the turbine is generally has an excess percentage around (30 %). The experimental results showed that  $OTR_{sp}$  is always greatly depending on the aeration efficiency for various conditions tested in this work as seen in Table 3.16. The excess in the oxygen mass transfer rate for the spray mass transfer zone,  $OTR_{sp}$ , when the RTP propeller and the draft tube are positioned in their places is due to the improvement of the mass transfer rate in the tank as a result of flow pattern improvement which is highly related to the oxygen mass transfer in the spray zone since the initial concentration of the DO in the spray zone is in the same time the final concentration of DO in the bulk zone.

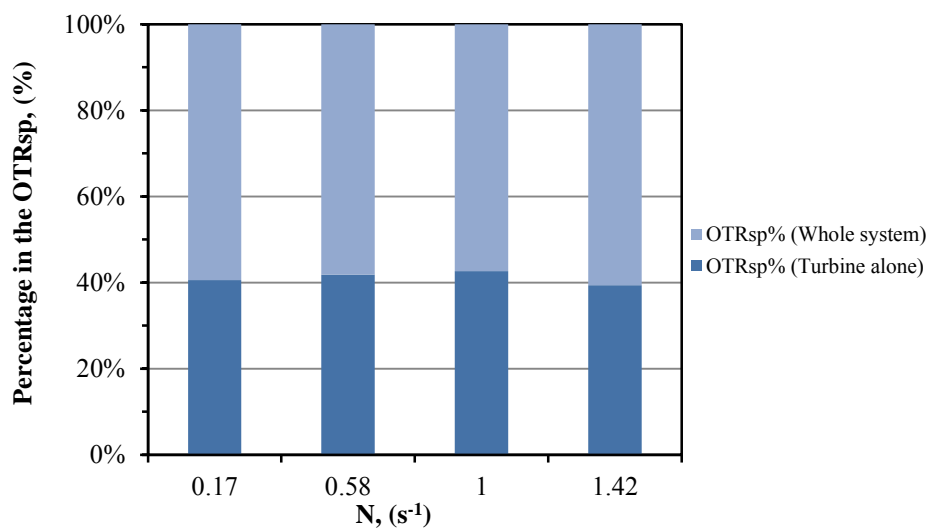


Figure (3.31): The influence of the tank internals (Propeller and draft tube) on the spray zone oxygen transfer rate,  $OTR_{sp}$  contribution the overall transfer rate OTR,  $S/W = 1.0$ .

Table (3.17): The Comparison for the spray zone oxygen transfer rates  $OTR_{sp}$  between the whole system and turbine alone configurations,  $S/W = 1.00$ ,  $h/D = 1.47$ .

N (rps)	Q (L h <sup>-1</sup> )	$OTR_{sp}$ (g h <sup>-1</sup> ) Turbine alone	$OTR_{sp}$ (g h <sup>-1</sup> ) Whole system	$OTR_{sp}$ Excess percentage (%) (Whole system)
1.67	11010	16.622	24.330	31.68
2.08	15851	26.253	36.488	28.10
2.5	22094	55.353	74.493	25.69
3.33	22422	67.131	103.346	35.04

### 3.2.3. The Modeling

In order to characterize the oxygen mass transfer rate achieved in the spray zone by the turbine through propelling water droplets in the air and to determine the optimum process condition. A model of the water spray mass transfer zone efficiency was developed depending on applied works in the same field of investigation and the obtained results from the experimental results. The model is built to interpret the oxygen mass transfer operation to water droplets, where have considered the standard water spray efficiency  $(E_{sp})_{20}$  as the dependent factor instead of  $(k_L a/N)$  that applied in the model for bulk (re-aeration) mass transfer zone (See equation 3.4), (Kim and Walters, 2001; Kucukali and Cokgor, 2009; Watson et al., 1998) have also considered the  $(E_{sp})_{20}$  as the independent parameter in their models. Same as the water bulk mass transfer zone, the most affecting independent parameters during the surface aeration process are related with the dependent mass transfer parameter but here for the parameter  $(E_{sp})_{20}$ , these independent parameters represent the important objectives achieved through the experimentation. A total of 47 experimental runs were conducted for determining the standard water spray mass transfer zone efficiency of surface aerators at 20 °C,  $(E_{sp})_{20}$ . At the experimental run temperature,  $E_{sp}$  spray zone efficiency coefficient was calculated using the equation 2.30. The equations 2.32 and 2.33 are applied to convert the calculated spray mass transfer zone efficiency  $E_{sp}$  to standard spray mass transfer zone efficiency at 20°C  $(E_{sp})_{20}$ .

The spray zone oxygen mass transfer depends on various relevant geometric, dynamic (process) and materials (property or physical) parameters. The most important parameters are shown in the following list:

Geometrical Parameter:	Turbine diameter	D
	Turbine blades width	W
Material Parameters:	Density	$\rho$
	Viscosity	$\mu$
Process Parameters:	Gravitational constant	g
	Turbine speed	N
	Turbine blades submergence	S

The spray zone standard efficiency varies noticeably with the turbine rotation speed. The standard spray efficiency depends also on the submergence level of the turbine blades, where the turbine blades submergence  $S/W$  showed also a remarkable effect on the standard spray zone efficiency.

As a primary essay to correlate the standard efficiency of the spray mass transfer zone with the influencing parameters in the same way that applied for the water bulk zone as represented in the equation 3.1.

$$(E_{sp})_{20} = f(N, \rho, \mu, D, g, S, W) \quad (3.8)$$

Equation 3.8 is solved to determine the values of the constants by applying Buckingham  $\pi$  theory equation (3.8) was converted to the following correlation:

$$(E_{sp})_{20} = f(Fr, \frac{S}{W}) \quad (3.9)$$

Solving equation 3.9 by multiple non-linear regressions, the following model is obtained:

$$(E_{sp})_{20} = 1.235 Fr^{0.616} \left(\frac{S}{W}\right)^{0.355} ; \quad Fr=0.54-0.215 \quad (3.10)$$

$S/W=0.17-1.83$

Where Reynolds number  $Re$  was ignored because it is considered irrelevant to the process objective  $(E_{sp})_{20}$  according to the multiple non-linear regressions, as the spray flow is predominantly turbulent the value of  $Re$  is always  $> 10^4$  (Zlokarnik, 1979). The plot of the predicted values of spray zone standard efficiency calculated from equation 3.9 with the experimental values showed a coefficient of determination of (0.9095) as shown in Figure 3.32.

Equation 3.10 means the correspondences  $(E_{sp})_{20} \propto (N)^{1.23}$  or  $(E_{sp})_{20} \propto (S/W)^{0.355}$  are achieved when the turbulent regime was prevailing ( $Re > 10^4$ ) and within indicated ranges of  $Fr$  and  $S/W$ .

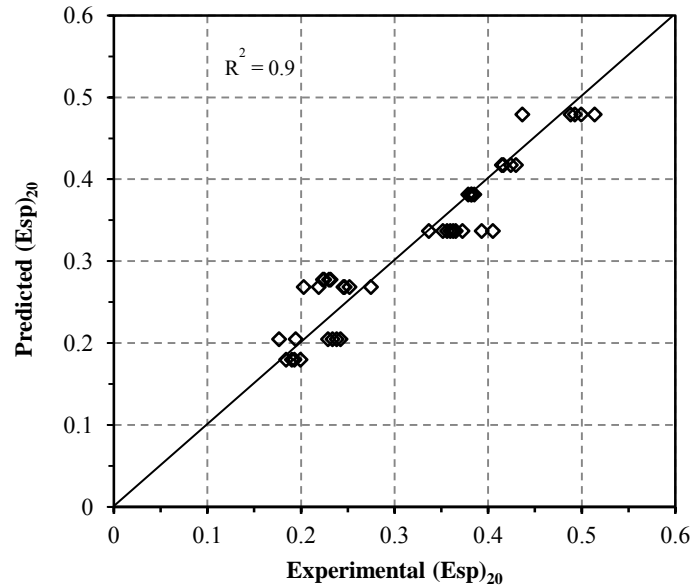


Figure (3.32): The Comparison between the  $(E_{sp})_{20}$ , Predicted by the Correlation model (Eq. 3.10) with the experimentally resulted  $(E_{sp})_{20}$ .

From the earlier works (Baylar and Bagatur, 2006; Baylar et al., 2010; Nakasone, 1987; Tarshish et al., 2000; Wormleaton and Soufiani, 1998), they have found that the form of the water spray standard efficiency correlation is more complicated than the power law correlation applied in equation (3.10). For the same influencing parameters as shown in equation (3.8), this was solved by applying multiple non-linear regressions and least square method. The following model was derived:

$$(E_{sp})_{20} = 1 - [1 + 0.345R_e^{0.198} Fr^{0.867} \left(\frac{S}{W}\right)^{0.535}]^{-1} \quad (3.11)$$

This means the target quantity  $(E_{sp})_{20}$  increases in a correspondence to  $(S/W)^{0.535}$  within same indicated ranges in equation 3.10. The plot of the predicted values of spray zone standard efficiency calculated from equation 3.11 with the experimental values showed a coefficient of determination of (0.9025) as shown in Figure 3.33. The range of  $Re$  in equation is (60000-120000). While the range for  $Fr$  and  $S/W$  are same in equation 3.10.

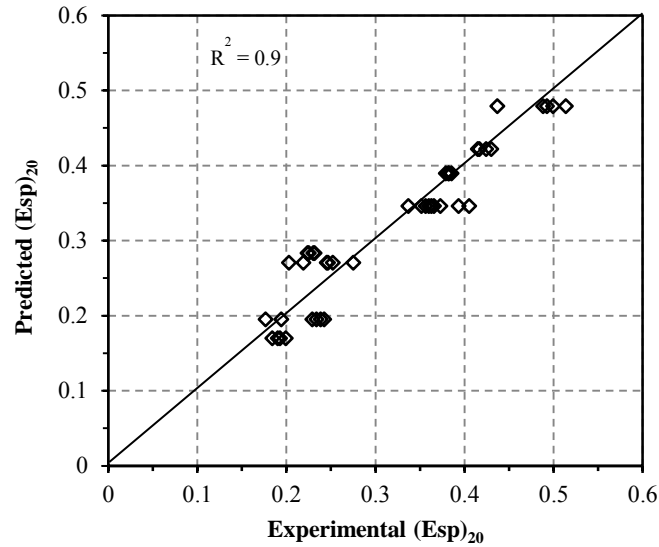


Figure (3.33): The Comparison between the  $(E_{sp})_{20}$ , Predicted by the Correlation model (Eq. 3.11) with the experimentally resulted  $(E_{sp})_{20}$ .

(Baylar and Bagatur, 2006; Nakasone, 1987; Wormleaton and Soufiani, 1998) developed a model of weir type aeration, where they showed that spray discharge flow rate and droplets height involves the effects on the standard spray zone efficiency.

(Tarshish et al., 2000) have built a model for the achieved oxygen mass flow rate by the surface aeration in the wastewater treatment tank, they showed the oxygen mass flow parameter in the model is affected by power consumption and jet flow rates of waste water and activated sludge. (Wormleaton and Tsang, 2000) studied the aeration behavior in weirs with. For the spray zone, they derived the model of standard spray aeration in terms of a spray Froude number and Reynolds number.

The effect of spray discharge flow rate and droplets height included in the previous models are not considered separately here, but they are implicated in more general dimensionless parameters.

In dependence on experimental results and earlier studies, it is found that standard spray zone efficiency for the surface aeration, it is considered that the target quantity of standard spray zone efficiency  $(E_{sp})_{20}$  for the given process conditions (the discharge spray flow rate/spray radius,  $q_{sp}$  and the maximum height of the spray  $Y_m$ ) depends on the turbine blades submergence  $S$ , turbine blades width  $W$ , gravitational constant  $g$ , and kinematic viscosity of the water  $\nu$ . The following relevance list is:

$$[(E_{sp})_{20}; q_{sp}, Y_m; W, S; g, \nu] \quad (3.12)$$

## Chapter Three: Oxygen Mass Transfer in the Surface Aeration

---

As mentioned earlier the various relevant variables included in equation 3.12 are not considered separately and are implicated in more general dimensionless parameters. Thus, dimensionless parameters for standard spray zone efficiency coefficient can be taken as function of the dimensionless parameters of Reynolds, Froude and power numbers. The equation (3.12) converted to the following relation:

$$(E_{sp})_{20} = f \left[ R_{sp} F_{sp} \left( \frac{S}{W} \right) \right] \quad (3.13)$$

$$Re_{sp} = \frac{q_{sp}}{\nu} \quad (3.14)$$

$$Fr_{sp} = \frac{gY_m^3}{q_{sp}^2} \quad (3.15)$$

The spray Reynolds number is calculated by equation (3.14), the spray Froude number is calculated by the equation (3.15). Equation (3.13) was solved to determine the values of the constants by applying multiple non-linear regressions and least square method. The following correlation was developed:

$$(E_{sp})_{20} = 1 - [1 + 0.056 Re_{sp}^{0.263} Fr_{sp}^{0.357} \left( \frac{S}{W} \right)^{0.250}]^{-1} \quad (3.16)$$

The mass transfer model (equation 3.16) is applicable within the ranges,  $(Re_{sp} * 10^{-3}) = (22.1 - 46.2)$ ,  $(S/W) = (0.17 - 1.83)$ ,  $(Fr_{sp}) = (0.044 - 1.80)$  and (water spray maximum height  $Y_m/D) = (0.08 - 0.24)$ .

Equation 3.16 shows that the determined powers for the three parameters are somehow close and they are proportionally related the spray zone standard efficiency. This means the effect of these parameters have close effects on the objective parameter  $(E_{sp})_{20}$ . For example the equation 3.16 refers that the standard spray zone efficiency  $(E_{sp})_{20}$  increases by the factor 1.3 when the turbine blade submergence ratio  $(S/W)$  was altered from 0.17 to 0.58.

The standard error of estimation for the equation is 0.0215, which indicates a 98% probability that the equation 3.16 will predict  $(E_{sp})_{20}$  within  $\pm 0.01$  of its true value. The correlation coefficient for this equation is  $R^2 = 0.9568$ . The measured  $(E_{sp})_{20}$  values are compared with those predicted by the equation 3.16 are given in the Figure 3.34. An acceptable agreement between the measured values and the values computed from the predictive equation is obtained.

From Figure 3.33 it can be found that the points with higher error compared with the experimental values are the points of lower spray Reynolds number with the ratio of  $S/W=1$ .

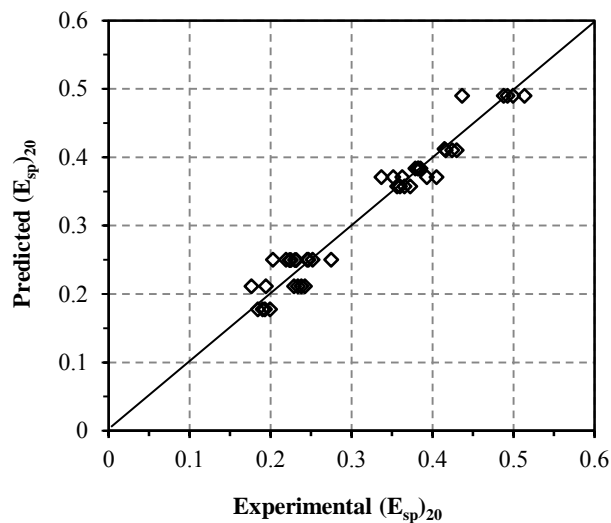


Figure (3.34): The Comparison between the  $(E_{sp})_{20}$ , Predicted by the Correlation model (Eq.3.16) with the experimentally resulted  $(E_{sp})_{20}$ .

### 3.2.4. Conclusions

With the totality of experimental runs performed for the power consumption in water bulk zone, it was found that the power consumed is related with rotation speed and water height level (turbine blades submergence) variations more than other parameters occurred in aeration mode.

For the given impellers rotational speed range, it was observed that the desirable performance of the aeration mode and flow patterns in the bulk zone is achieved starting with impellers rotation speed of 2.08 rps, the formation of air bubbles appears in the vessel due to plunging water droplets with water surface, so the impellers rotational speed 2.08 is considered as the critical speed to accomplish aeration process.

At the given water level ratios and turbine blades submergence, the water bulk zone oxygen mass transfer coefficient  $k_a$  was increased with the rotation speed  $N$ . It was observed that the  $k_a$  was highly dependent on the impellers rotation speed, however this relation is limited: the outer edge of the spray should not colloid the vessel wall what can be observed with rotational speed  $N$  lower up to 3.33 rps.

An optimum water height level came across from the water bulk zone surface aeration experimental testing and it depends on a satisfactory formation created by the aerator turbine blades. Where, neither too low nor too high blade submergence is preferred.

## Chapter Three: Oxygen Mass Transfer in the Surface Aeration

---

The spacing between the impellers affects slightly the water bulk zone oxygen mass transfer coefficient  $k_{1a}$ . This influence stays related with the obligatory of remaining the lower propeller inside the draft tube. The reliance of the  $k_{1a}$  on the spacing is conjugated with the interaction between the propeller and the draft tube.

Through the four tested different geometrical configurations of the water bulk zone, the highest  $k_{1a}$  was achieved when all the aerator system parts exist together (the turbine with both the draft tube and RTP propeller).

Upon the calculated water bulk zone standard aeration efficiency  $SAE_b$  values, it seems the  $SAE_b$  is more sensitive to rotational speed variation, while on the other hand the  $SAE_b$  didn't show same response toward water height level variation.

For the whole system configuration it is found that at the spray mass transfer zone both the oxygen transfer rate  $OTR_{sp}$  and spray zone efficiency  $E_{sp}$  are highly dependent on the impellers rotation speed  $N$ , dimensionless turbine blade submergence ratio  $S/W$  and dimensionless water level ratio  $h/D$ .

The majority of oxygen mass transfer is achieved in the spray zone due to high interfacial area and turbulent mass transfer occurred in this zone

The discharge flowrate of the water spray (droplets)  $Q$  is increased when impeller rotation speed or water level are increased for the given turbine blades submergence.

The  $OTR_{sp}$  in whole system configuration is slightly higher than  $OTR_{sp}$  for the turbine alone configuration.

Two models are developed for water bulk zone oxygen transfer coefficient  $k_{1a}/N$  and power consumption, applicable in specified range. A model is developed for surface aeration spray zone, standard oxygen transfer efficiency coefficient; the model is applicable for specified limits.



# **CHAPER FOUR**

**HYDORDYNAMICS IN THE SINGLE  
PHASE NONAERATED AGITATED  
TANK FOR UP AND DOWN  
PUMPING DIRECTIONS MODES**



## Chapter Four

### Hydrodynamics in the Single Phase Non-Aerated Agitated Tank for Up and Down Pumping Directions Modes

The investigated surface aeration system consists in two agitation tools; the turbine positioned at liquid surface which propels droplets into atmospheric air, thus forming the water spray. The second tool is the mixing assembly (RTP propeller and draft tube) placed below the turbine. The proposed function of the mixing assembly is to improve mixing capability of the surface aeration system by enhancing air bubbles distribution inside the vessel and redirecting the flow toward the upper turbine. The mode of mixing assembly employment is either individual or conjugated with turbine, where mixing assembly operates separately from the turbine when it's needed to achieve well-mixed condition inside the vessel, when sufficient dissolved oxygen is accomplished but without satisfying distribution of dissolved oxygen throughout the liquid bulk.

In this chapter the turbulent flow regime in liquid phase generated by the reversible twisted pitched, axial 4-bladed and 45° pitched blade propeller (RTP) (Milton Roy Mixing HPM204D) is investigated to determine velocity field for different areas of propeller vicinity, inside the draft tube and in the vessel, whereas the upper turbine is not combined. Thus there is only the liquid phase and very few gas bubbles are entrapped inside the liquid bulk can be neglected. Comparison between flow patterns resulting from up-pumping and down-pumping operation modes of RTP propeller is made. The up-pumping condition is performed ordinarily with surface aeration system; so the propeller turns in same manner than the upper turbine and pushes the fluid upward. The down-flow is applied mainly when propeller and draft tube are used separately aiming that mixing objectives are to be fulfilled for the liquid bulk.

#### 4.1. Experimental Aspects

Both PIV and LDV (details for the devices are shown in chapter two) are applied to measure mean velocity fields. The pumping capacity of the propeller is calculated for all tested flow conditions at different positions inside the draft tube. In order to achieve LDV and PIV measurements the cylindrical tank is placed inside another square tank with front face made of glass to eliminate laser distortion that may affect the measurements. The outer tank is filled with water in order to avoid refraction and deflection of laser beams at cylindrical and square tanks walls.

All flow patterns tests were conducted in the baffled vessel. At the beginning un-baffled vessel was examined to find out its compatibility for given experimental runs.

## Chapter Four: Hydrodynamics in the Single Phase Non-Aerated Agitated Tank for Up and Down Pumping Directions Modes

Un-baffled vessel seems not to be suitable because of oscillation occurred at water surface resulting from agitation due to impellers rotation.

The LDV and PIV measurements were applied for the flat bottom cylindrical vessel ( $T_v = 0.8$  m) provided with three transparent baffles their width are equal to ( $b = T_v/10$ ). A draft tube ( $d_f = 0.15$  m,  $L_f = 0.1$  m) was positioned in the tank with clearance ( $C_{DT} = 0.1$  m) and was removed for some of the measurements. The four  $45^\circ$  pitched and twisted blade propeller RTP was studied at clearance ( $C_{pr}/T_v = 0.2$  m) with rotation speed was ( $N = 5$  rps) to ensure staying always in turbulent regime for created flow field ( $Re = 72000$ ), where the LDV measurements were focused on the core of the tank where draft tube is settled to measure the flow pattern, the mean velocity field and the liquid flow rate created by the propeller inside draft tube in different planes that cannot be reached by the PIV.

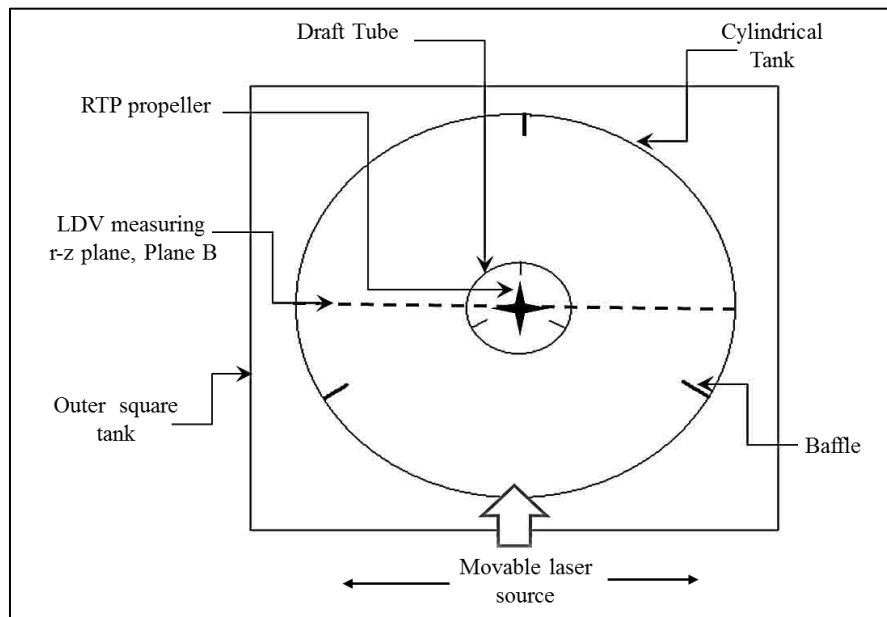


Figure (4.1): LDV implementation for measuring velocity in a (r-z) plane, (Plane B).

The LDV is a Dantec Fiberflow system with two green and blue laser beams, wavelengths of 514.4 nm and 488nm respectively. The laser source in the LDV is 4-W Argon with a focal length of 600 mm (Spectra Physics). The LDV measurements were performed through an r-z plane (Plane B) at ( $90^\circ$ ) to posterior baffle and ( $30^\circ$ ) to two lateral baffles (See Figure 4.1), where for each measurement, about (4000 to 5000) samples are applied with a maximum measurement time of 300 seconds. The tracer particles that were used to seed the liquid are (Iridium 111) ( $d_p = 15\mu\text{m}$ ).

The PIV were performed in order that flow patterns can be determined for all vessel areas. the vessel dimensions are considered somehow large in comparison with same kinds of experimentations, so it is preferred to conduct flow field measurements by

## Chapter Four: Hydrodynamics in the Single Phase Non-Aerated Agitated Tank for Up and Down Pumping Directions Modes

PIV for time and effort saving. PIV creates a laser sheet which allows us to inquire flow and velocity profile at various spatial parts inside the vessel. LDV provides detailed information for single points with good temporal resolution while with PIV we can get detailed spatial information for different instants of time (Atkinson et al., 2000).

The obtained PIV measurements detailed information depends on the number of interrogation areas that divides the simultaneous images taken by used CDD camera after seeding tested liquid bulk with (Rhodamine) red fluorescent tracer particles ( $d_p=15 \mu\text{m}$ ). In the experiments the laser sheet created by used Nd: YAG laser source is placed in the middle of vessel, where r-z measurement plane was positioned directly on posterior baffle ( $0^\circ$ ) and at ( $60^\circ$ ) from the two lateral baffles from front face (see figure 4.2). (32% $\times$ 32%) with (50% overlap) is applied for velocity measurements. The number of image pairs was (300) and exposure time delay ( $\Delta t$ ) between each two sequent images was (1000  $\mu\text{s}$ ) depending on operation condition such as propeller tip velocity and image scale factor adapted during the acquisition.

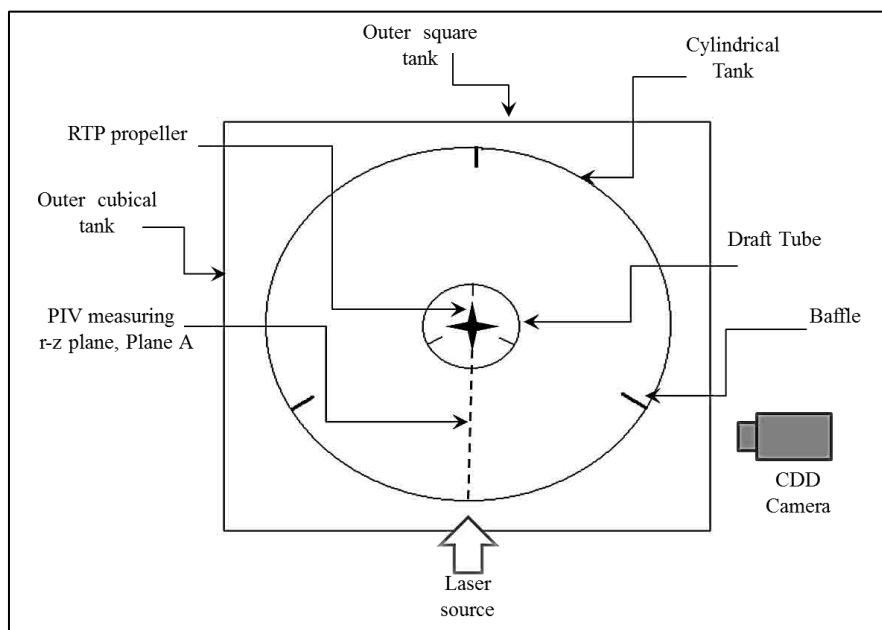


Figure (4.2) PIV implementation for measuring velocity in a (r-z) plane, (Plane A)

For single (liquid) phase flow the used propeller rotation speed was kept at (5 rps) to ensure reasonable vector displacement between two frames and since upper limit of rotation speed due to turbine presence and consequence droplets impingement position does not exist. The applied software for acquisition system is (DaVis 8.0.5 flow master), while image processing is (PIV imager pro x2M system).

## 4.2. Mean Velocity Field and Flow Pattern

In order to obtain a good knowledge of the flow profiles inside the vessel in mixing mode, it is needed to examine both the up-pumping and down-pumping flow generated by the axial 4-bladed, 45° pitched blade RTP propeller (See Figure 4.3) with or without draft tube. The flow is discharged from propeller axially in up-ward direction when the shaft is rotated in its normal direction, while it is discharged in down-ward direction when the shaft is rotating in reverse mode. Since the propeller blades are twisted and made in a symmetrical way, the propeller can be settled upside down, the blades always push the fluid in same direction. The propeller is placed inside a draft tube, the presence of draft tube having theoretically noticeable effects on the generated flow (Aeschbach and Bourne, 1972; Brož et al., 2004; Kumaresan et al., 2005; Tsui and Hu, 2008). A part of the discharge flow from the propeller goes in radial direction and needs to be redirected toward axial direction. Few studies were made for a down-pumping flow generated by an axial pitched blade propeller with draft tube presence; on the contrary many studies were made for this configuration for the airlift and bubble column reactors.



Figure (4.3): The axial 4-bladed, reversible 45° pitched and twisted blade propeller RTP propeller (HPM204D, Milton Roy Mixing)

### 4.2.1. Down-Pumping Condition:

#### I. Propeller and Draft Tube Configuration

The time averaged velocity field in the taken r-z middle plane of the vessel at (30°) from the two lateral baffles (Plane A) performed by the PIV (See Figure 4.2) is shown in the Figure 7.4, where the flow is produced by the reversible twisted pitch blade RTP-D propeller with draft tube ( $L_f = 0.1$  m) in down-pumping direction mode.

## Chapter Four: Hydrodynamics in the Single Phase Non-Aerated Agitated Tank for Up and Down Pumping Directions Modes

---

From Figure 4.4 it is noticed that one general circulation loop is formed in the entire vessel, that begins just below propeller blades and goes downside in axial pattern and then toward vessel wall in radial pattern along the vessel bottom, the circulation loop continues in upward before it returns to impeller inward flow region. The flow returns to impeller region and discharges axially due to draft tube. A part of the circulated liquid flows axially to the vessel base in the region between the draft tube wall and the middle of radial distance to the vessel wall without being entrained by the RTP-D propeller, this is occurred because the low ratio of  $d_{pr}/T_v = 0.15$  as the low pressure inflow region generated by RTP-D propeller blade rotation isn't significant enough to entrain all the returned downward flow into this RTP-D propeller inflow region.

As shown in Figure 4.4, two secondary circulation loops are produced; one of them is directly below the RTP-D propeller. This secondary loop has been also observed by (Kumaresan et al., 2005) for hydrofoil impeller (HF4 type) with draft tube in down-pumping mode, with  $(C_{imp}/T_v = d_{imp}/T_v=0.33)$  and length of draft tube ( $L_f=0.167$  m). (Kumaresan et al., 2005) found that the axial flow created by impeller (HF4 type) was increased in the core of the vessel in presence of a draft tube.

The third circulation is formed beside the RTP-D propeller blades; this circulation is actually the radial discharged flow from the RTP-D propeller redirected by the draft tube upward to the RTP-D propeller inward flow volume.

The mean axial velocities are more intense at vessel core and are significantly smaller with moving away from vessel core toward the radial direction except in the region near the vessel wall, where higher axial velocities are achieved due to the interaction with vessel wall. The low mean velocities near the water free surface should be taken into account carefully because of the error that may occur due to the reflection from the free surface. The distribution mean average velocities are presented more clearly in the contour map (See Figure 4.5) of the r-z time averaged velocities in down-pumping mode (Mixing mode).

The highest downward axial velocity below the blades of the RTP-D propeller is of the order  $0.27V_{tip}$ , whilst the highest downward velocity above the impeller is  $0.22V_{tip}$ . In the inflow region above the RTP-D propeller the value of downward axial velocities are of the order  $0.1V_{tip}$ . In the secondary loop beside RTP-D propeller blades inside the draft tube, the highest upward axial velocity in the vessel is found  $0.34V_{tip}$ , this loop is actually in the discharge flow from the impeller in radial direction but it has been redirected by the draft tube as an upward axial velocity. In the central part of the vessel exactly in the mid-planes between the draft tube and vessel wall, predominate velocity is the downward axial velocity with the order of  $0.02-0.03 V_{tip}$ ; these values are of the order  $0.02-0.04 V_{tip}$  in the upper part of the vessel. For the RTP-D propeller the maximum radial velocity is found also in the secondary loop beside impeller blades, this maximum radial velocity is of the order  $0.22V_{tip}$ , which moves toward the impeller blades. In the intake flow region above the

## Chapter Four: Hydrodynamics in the Single Phase Non-Aerated Agitated Tank for Up and Down Pumping Directions Modes

---

RTP-D and the maximum radial velocity in this region is of the order  $0.06V_{tip}$ . The highest radial velocity in the primary loop is produced in the discharged flow from RTP-D propeller inside the draft tube. The maximum radial velocity in this region is of the order  $0.2V_{tip}$ . The discharged flow below the impeller becomes mainly radial when it approaches the vessel bottom. This flow pattern is achieved with aid of the cone placed at the vessel bottom below the draft tube. The highest radial velocity in this zone is of the order of  $0.16V_{tip}$ . Radial velocities are clearly found in both the upper and lower part of the vessel and have highest radial velocities of the order  $0.12V_{tip}$  and  $0.06V_{tip}$  respectively.

The observed low axial and radial values in the upper, central and near the vessel wall regions indicates the weak mixing and flow pattern in these parts, the main cause for this performance is the small ratio of  $d_{pr}/T_v=0.2$ , where weak interaction between the discharged liquid flow by the impeller and the liquid bulk in these regions as mentioned earlier. Although the influence of applied impeller diameter to tank diameter ratio causes a poor circulation especially in farer regions from the core of the vessel, it is preferred to keep this ratio because the main purpose of mixing mode is maintain an acceptable mixing condition for the already aerated and mixed tank contents and the mixing mode should be accomplished with minimum power consumption in order to prevent any additional cost for the treatment operation; this cannot be done when higher  $d_{pr}/T_v$  is used.

The values of axial velocities with those obtained by (Kumaresan et al., 2005) for three pithed blades with the angle  $35^\circ$  and twist in the tip region, with 3 blades hydrofoil impeller of (HF4 type) with two different draft tube lengths ( $L_f = 0.125$  and  $0.167$  m) in down-pumping mode, with ( $C_{imp}/T_v = d_{imp}/T_v=0.33$ ). The axial velocities below the impeller were of the order  $0.335 V_{tip}$  and  $0.274$  for the longer and shorter draft tubes respectively, whilst they were of the order  $0.22 V_{tip}$  and  $0.18 V_{tip}$  for the longer and shorter draft tubes respectively. Compared with the velocities produced by the axial HPM204D-D impeller, the order of the axial velocity above the impeller the RTP-D is approximately than HF4 for the longer draft tube and smaller than HF4 with shorter draft tube. For the axial velocities in the discharge flow below the impeller, the order of the axial velocity for RTP-D is approximately the same than with HF4 for the longest draft tube and greater than HF4 with the shortest draft tube.

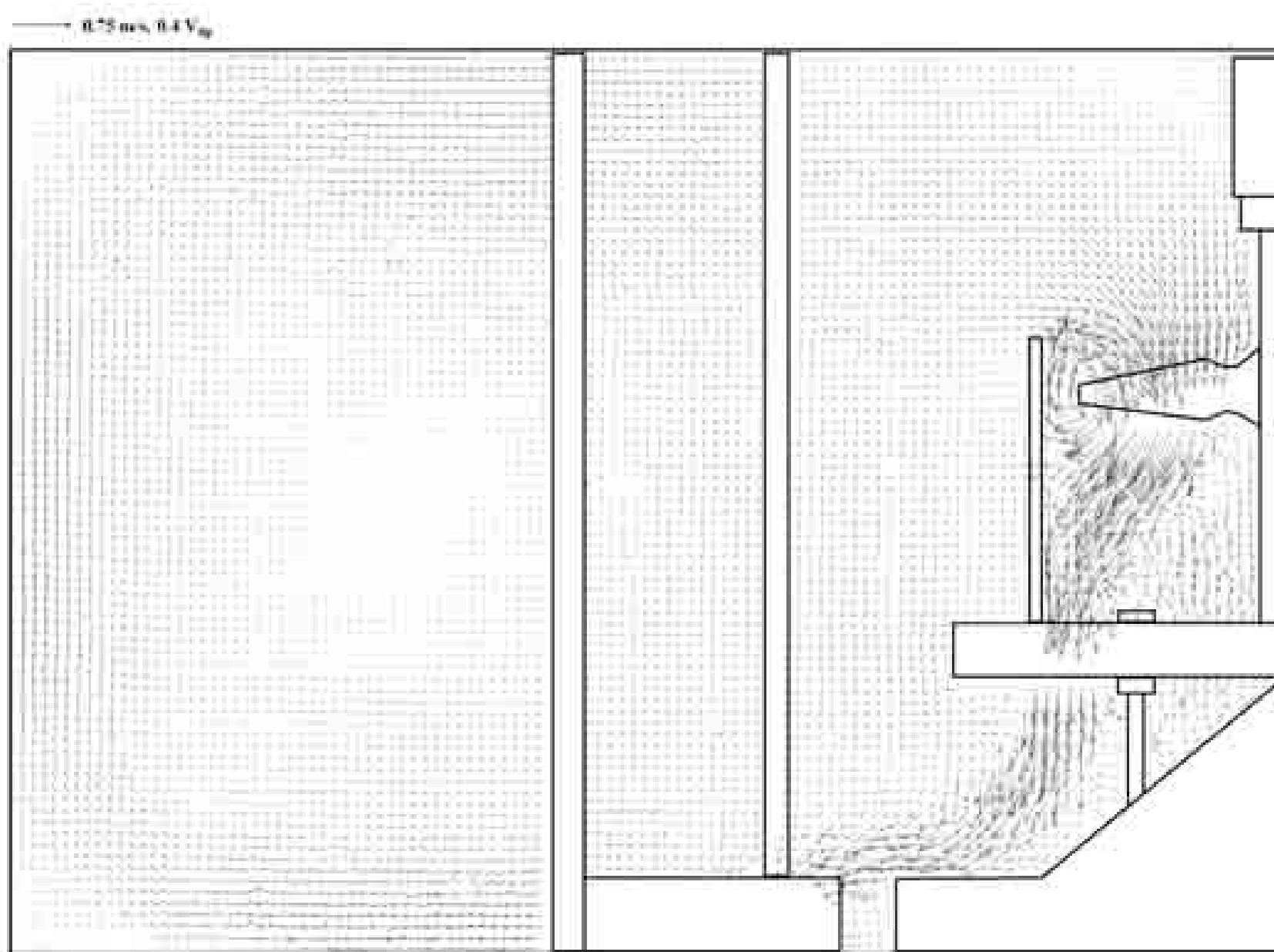


Figure (4.4): The (r - z) flow field map for the RTP-D propeller with draft tube configuration in the entire vessel.



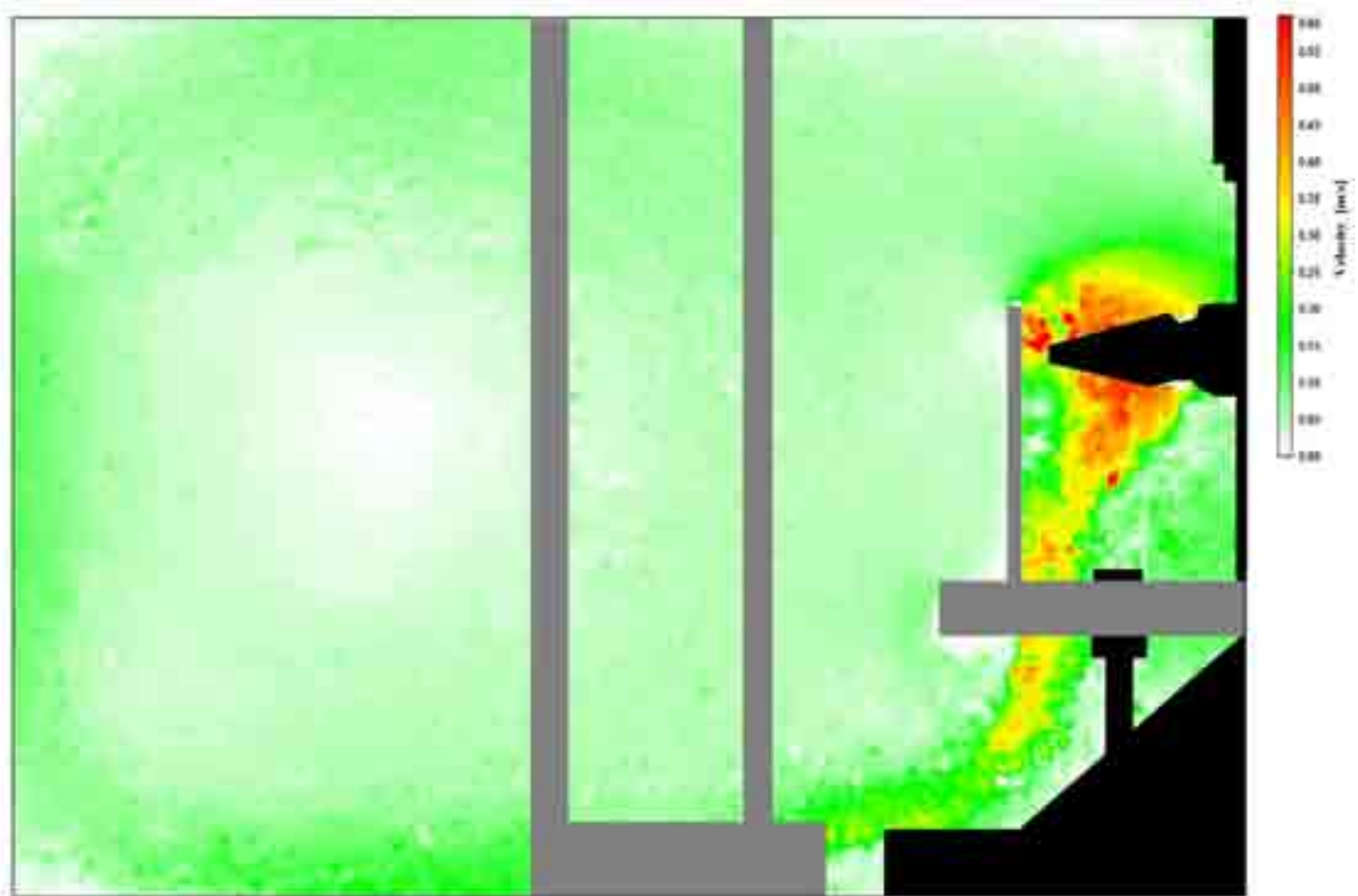


Figure (4.5): The (r - z) velocities contour map for the RTP-D propeller with draft tube configuration in the entire vessel.



More mean velocity field measurements were performed in the core of the vessel as this region was found more significant in terms of efficient circulation and mixing according to the measurements made by the PIV. As the draft tube is baffled with three half-length baffles the velocity field generated by the RTP-D propeller was measured from different planes. This was performed by LDV in the r-z plane (Plane B) at (90°) to posterior baffle and (30°) to two lateral baffles (See Figure 4.1).

Figure (4.6) shows the quantitative analysis of the velocities in the down-pumping (Mixing mode) as a radial profile for the normalized axial velocity inside the draft tube, above and below the impeller in the two different measurement planes (A at 0° and B at 90° from the posterior baffle). Above the RTP-D propeller the highest axial velocity are of the order  $0.23V_{tip}$  and  $0.25V_{tip}$  in the planes A and B respectively, whilst below the PTBD impeller in the discharge region the highest axial velocities are of the order  $0.27V_{tip}$  and  $0.16V_{tip}$  in the planes A and B respectively.

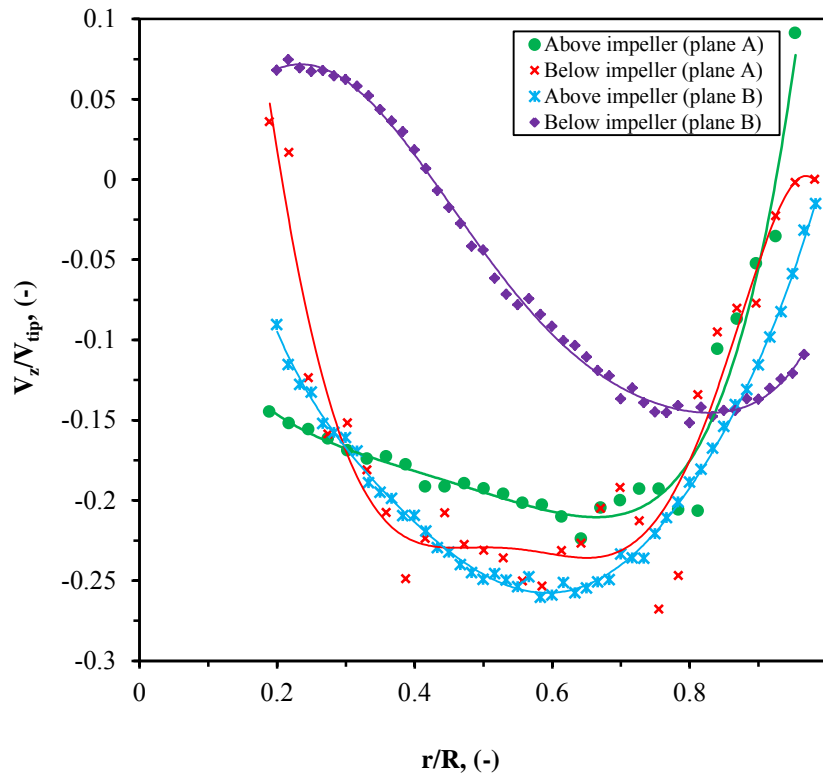


Figure (4.6): Dimensionless axial velocity profile at different liquid levels (below impeller  $z/h=0.55$ , above impeller  $z/h=0.62$ ) for RTP-D with draft tube,  $C_{pr}/T_v=0.2$ ,  $N=5$  rps in two different measuring planes; plane A at 0° and plane B at 90° from the posterior baffle respectively.

The axial velocity in the discharge region of the impeller looks higher in the measurement plane A than those in plane B and also it has a different profile more than in inward region above the impeller. This difference is due to the effect of the

## Chapter Four: Hydrodynamics in the Single Phase Non-Aerated Agitated Tank for Up and Down Pumping Directions Modes

---

draft tube baffle position, where in plane A the discharge flow is surrounded by two close baffles at  $45^\circ$  each side, when on the other hand in the plane B only one of the baffles is close at  $45^\circ$  and the other is at  $90^\circ$ . The effect of the draft tube baffles on the discharge flow will be confirmed with repeating this quantitative analysis for propeller alone configuration.

### II. Propeller Alone Configuration

Figure 4.7 shows the time averaged velocity fields in the taken r-z middle plane in same position that performed by PIV for the previous propeller and draft tube configuration, where the flow is produced by the axial 4-bladed,  $45^\circ$  pitched twisted blade propeller (RTP-D) alone in down-pumping mode. The flow pattern and mean velocity profile measurements were focused on the vessel core as it was observed in previous section for the propeller and draft tube configuration with down pumping; this region is more active in terms of generated mean velocity profiles. The effect of the propeller on the produced flow pattern was weaker near the walls as the interaction between the tank wall and the propeller is quite low ( $d_{pr}/T_v = 0.15$ ).

The downward discharge flow by the RTP-D propeller is predominantly axial and the secondary loop that was observed beside the impeller blades edges in the propeller and draft tube configuration has disappeared here. This confirms that this secondary loop was due to the presence of the draft tube.

The discharge flow shown in Figure 4.7 (a, and b) is pushed intensively downward in a regular manner. This observation somehow disagrees with that noticed by (Armenante and Chou, 1996; Tatterson et al., 1980) where (Tatterson et al., 1980) observed that the  $45^\circ$  pitched blades impellers PBT (Chemineer HTD-2,  $d_{im}/T_v = 0.35$ ) push the flow downward in a chaotic way of two different manners; a high speed jets and low speed flow, (Tatterson et al., 1980) also remarked trailing vortices formed at the blades tips, they assumed the created downward flow profiles by axial pitched blades impellers is changing due to tank and impellers geometric ratios. The produced discharge flow is similar with (Ranade and Joshi, 1989) observation The observed discharge flow agrees with that by (Ranade and Joshi, 1989) for PBT impellers ( $30^\circ - 60^\circ$  pitch angle,  $d_{im}/T_v = 0.25 - 0.5$ ), where they found that an intense axial flow pushed downward especially at impeller vicinity with negligible radial flow at this region, they reported that the velocity profile under the impeller was relatively changed with impeller clearance variation, for the tested clearance range ( $C = h/2 - h/6$ ). (Armenante and Chou, 1996) found out that the down flow in impeller region induced by 6 blades PTD ( $45^\circ$  pitched angle) had a contrary flatter form to other studies; (Armenante and Chou, 1996) imputed the non-convergence of down flow under impeller blades to the geometry and PTD clearance applied ( $d_{im}/T_v = 0.876$ ,  $C_{im}/T=0.33$ ). It is worth mentioning that the observations on the flow pattern created

## Chapter Four: Hydrodynamics in the Single Phase Non-Aerated Agitated Tank for Up and Down Pumping Directions Modes

by axial pitched impellers were made for  $d_{im}/T_v$  ratio higher than that performed in this work  $d_{im}/T_v=0.2$ , where the interaction between the flow generated by acting axial pitched propeller with the vessel bottom and walls was stronger than the measurements in larger vessel.

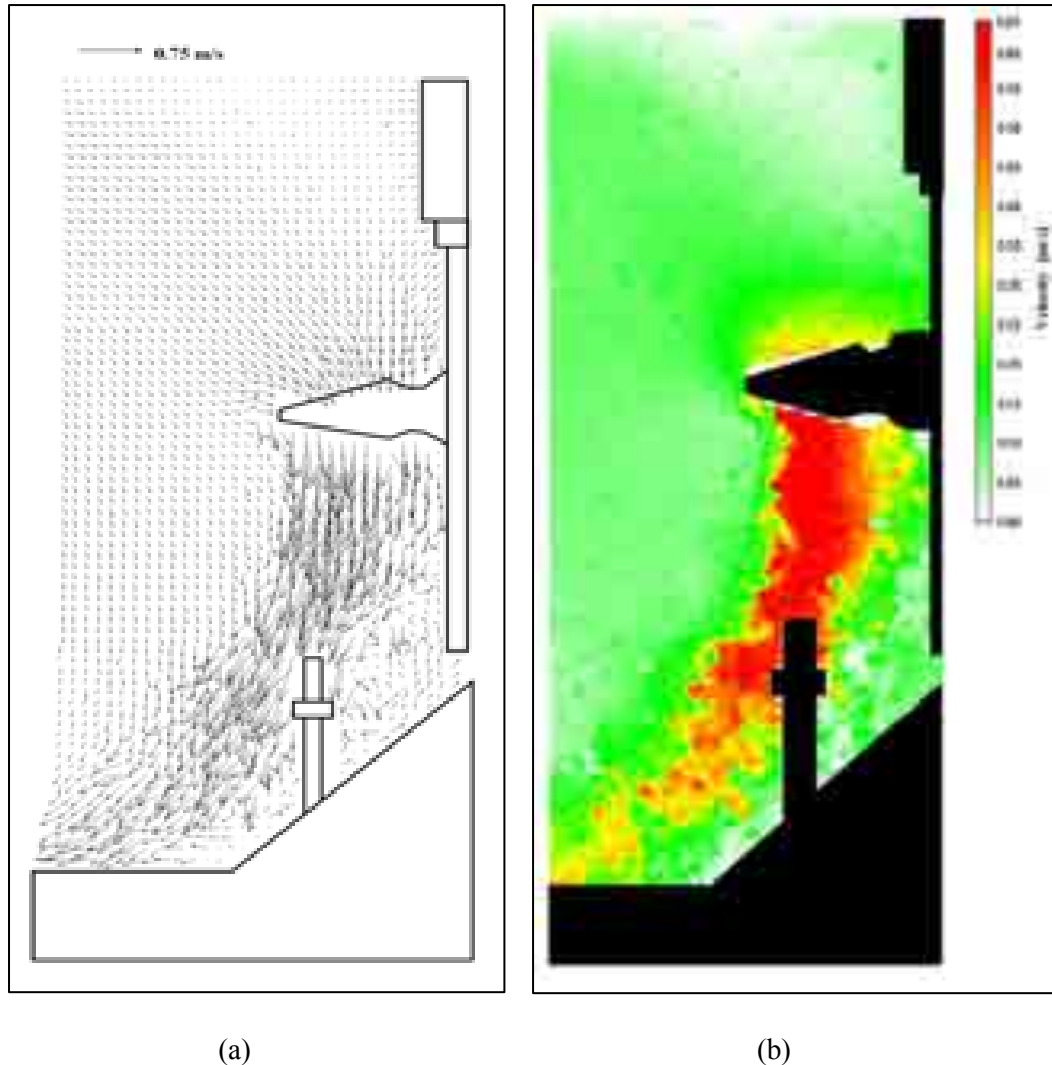


Figure (4.7): (a) The (r - z) flow field map for the RTP-D propeller without draft tube configuration in the vessel core, (b) The (r - z) velocities contour map for the RTP-D propeller with draft tube configuration in the vessel core.

As a result of the presence of the cone at the base of the vessel, a radial flow in the discharge stream begins to appear relatively and gradually, where the majority of the discharge flow is radial near the bottom. The other secondary circulation below the impeller exists as in the propeller and draft tube configuration but with less intensity. (Mavros et al. 2002) reported a close observation for pitch blade impeller (Mixel TT

## Chapter Four: Hydrodynamics in the Single Phase Non-Aerated Agitated Tank for Up and Down Pumping Directions Modes

---

type); where a downward flow jet has been released by the impeller blades and then the flow continues its circulation as a general loop through the vessel and also a small reversible circulation is created at the area below impeller and near the vessel center. The observation by (Mavros et al., 2002) was confirmed with the CFD simulation applied by (Khopkar et al., 2004).

In the Figure 4.7a, the highest axial velocity in the discharge bulk and directly below the impeller blades is  $0.345V_{tip}$ ; this is greater than that produced in the propeller and draft tube configuration by 18%. In the upper part above the impeller the highest axial velocity in the inward flow bulk is about  $0.1 V_{tip}$ , which is same in the propeller and draft tube configuration, while at above the RTP-D propeller the highest downward velocity is  $0.21 V_{tip}$ , this value being close to that produced in the propeller and draft tube configuration. For the reversible secondary loop below the RTP-D propeller beside the shaft, higher upward axial velocities are produced in both propeller and draft tube configuration and propeller alone configuration and are of the order  $0.11V_{tip}$ .

The main zone for the radial velocities in the vessel core is the lower part near the vessel bottom and beside the cone, the value of radial velocity in the discharged flow in this part is of the order  $0.11V_{tip}$ , comparing it with the propeller and draft tube configuration achieved velocity for the same zone, the highest radial velocity that obtained with propeller alone configuration is of the order  $0.217 V_{tip}$  and it is greater than that obtained in the propeller alone propeller and draft tube configuration by 7%. Above the RTP-D propeller in the inward flow region, the highest radial velocity is of the order  $0.09V_{tip}$ . This dropping in the radial velocity value illustrates the effect of draft tube presence on the flow pattern in this region clearly.

Comparing the downward axial discharge velocity produced by the RTP-D propeller with the other observations for the induced velocities by down-pumping axial impellers, (Bittrof et al. 2000) reported that the highest downward axial velocity in the discharge flow below a PBD impeller (4-bladed,  $45^\circ$  pitched angle,  $C_{im}/d_{im} = 1.5$  and  $d_{im}/T_v = 0.19$ ) is of the order  $0.1V_{tip}$ . While a highest downward axial velocity is of the order  $0.5V_{tip}$  in the discharge zone below a three-bladed  $45^\circ$  pitched blade HF impeller ( $15^\circ$  twisted blades,  $d_{im}/T_v = 0.27$ ) has been reported by (Kumaresan & Joshi 2006). (Khopkar et al. 2004) reported that the maximum axial velocities are of the order  $0.4V_{tip}$  and  $0.2V_{tip}$  respectively at below and above a  $45^\circ$  Mixel TT impeller ( $d_{im}/T_v = 0.5$ ).

A reversible secondary circulation is created below the RTP-D propeller beside the lower part of the shaft and the cone. This circulation without the draft tube is smaller and do not reach the lower edges of impeller blades. The highest upward velocity in this secondary circulation is of the order  $0.1V_{tip}$  which is same for propeller with draft tube configuration. A similar observation has been reported by (Aubin et al., 2001)

## Chapter Four: Hydrodynamics in the Single Phase Non-Aerated Agitated Tank for Up and Down Pumping Directions Modes

---

for six-bladed PBT impeller ( $d_{im}/T_v=0.5$ ), but they found the highest velocity in the secondary circulation was of the order of  $0.07V_{tip}$ .

From Figure 4.8 the radial profile of the normalized axial velocity above ( $z/h= 0.62$ ) and below ( $z/h=0.55$ ) the RTP-D propeller in the two different measurement planes A and B is plotted. The divergence for the two planes is small. The convergence of the normalized axial velocities values below the propeller without the draft tube shows clearly the effect of the draft tube and of its baffles ( $L_{bf}/L_f = 0.6$ ) on the produced discharge flow below the RTP-D propeller. A light difference still exists between the two planes, which may be due to the different measurement techniques PIV and LDV.

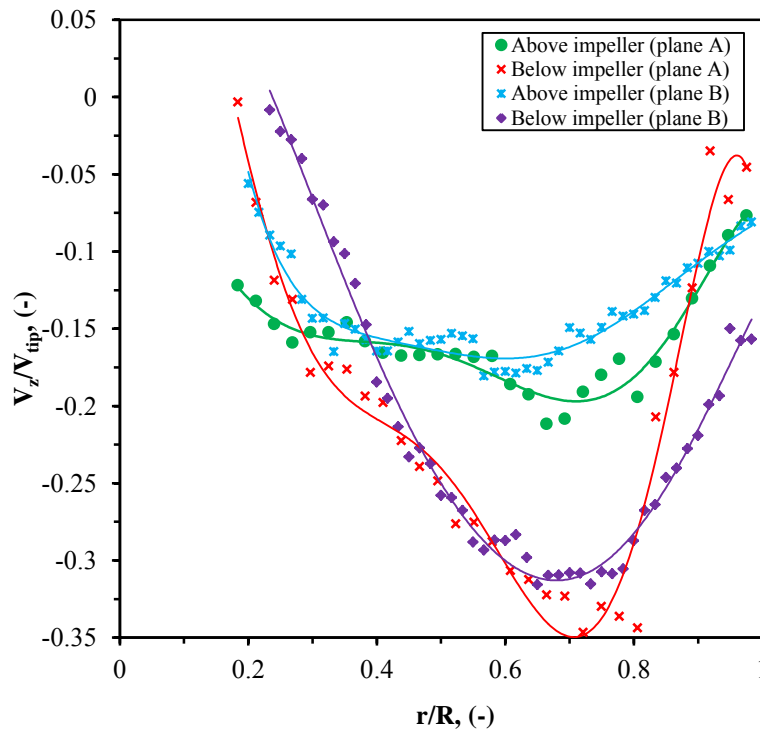


Figure (4.8): The dimensionless axial velocity profile at different liquid heights for RTP-D propeller without draft tube (below impeller  $z/h=0.55$ , above impeller  $z/h=0.62$ ),  $C_{pr}/T_v = 0.2$ ,  $N= 5$  rps in two different measuring planes; plane A at  $0^0$  and plane B at  $90^0$  from the posterior baffle respectively.

It has to be mentioned also that for the propeller alone configuration, sometimes with the rotational speed  $N=4.6$  rps, a swilling appears from the liquid surface and extends to the impeller blades tips (See Fig. 4.9). This phenomenon becomes more continuous starting from 5.8 rps, where the vortex is formed for the implemented geometry. Despite of using the baffled tank, this vortex occurs because of low ratio of  $d_{pr}/T_v = 0.15$  is implemented, where the baffles ( $L_{bf}/T_v=0.1$ ) are somehow far away

## Chapter Four: Hydrodynamics in the Single Phase Non-Aerated Agitated Tank for Up and Down Pumping Directions Modes

---

from the impeller to prevent forming this vortex above the impeller as it can be observed in the Figure 7.9. With the down-pumping direction for the propeller and draft configuration no swirling was formed despite the elevation of the impellers rotation speed higher than 6rps.



Figure (4.9): The creation of vortex in the down-pumping mode with draft tube.

### 4.2.2. Up-Pumping Mode

#### I. Propeller and Draft Tube Configuration

The flow patterns and mean velocity fields measurements were performed by the PIV in the same plane that applied for the down-pumping. Figures 4.10 a and b show the  $r$ - $z$  vector plot and velocity contour plot of the flow pattern generated by the RTP-U propeller with draft tube presence ( $L_f = 0.1$  m) for up-pumping direction mode in the vessel core. It is observed that beside the main circulation loop, two secondary circulations are formed one above the impeller near the shaft which extends to the water surface, the other one which is a small one formed beside the lower edge of the draft tube.

Compared with the down-pumping mode the upper secondary circulation loop seems that it is formed with the discharge flow generated of the by the RTP-U propeller and the position of this loop is changed upward or downward according to the pumping direction of the impeller. The flow returns to impeller region and discharged axially due to draft tube presence.

The recirculation beside the impeller blades tip has disappeared in the up-pumping mode. In the inward flow region of the impeller inside the draft tube the flow is entrained predominantly as an axial flow, whilst the flow is clearly propelled upward with increasing radial component progressively moving toward the liquid surface.

## Chapter Four: Hydrodynamics in the Single Phase Non-Aerated Agitated Tank for Up and Down Pumping Directions Modes

The RTP-U propeller discharges high upward axial velocities with the maximum velocity of the order  $0.315V_{tip}$  above the impeller. The upward axial velocities drawn by the impeller are distinguished with their elevated axial values inside the draft tube in the inward zone below the impeller as observed in Figure 4.10(a and b). The highest upward velocity below the RTP-U propeller is  $0.28V_{tip}$ ; (Brož et al., 2004) have measured the axial velocity field in the vicinity of 4-bladed PBT up-pumping impeller (pitch angle  $45^\circ$ ,  $d_{im}/T_v=0.2$ ,  $h/T_v=1.2$ ,  $C_{im}/T_v=1.0$ ) with a longer draft tube  $L_f = 0.54$ . The draft tube had four baffles placed in the upper part at the discharge side of the impeller; they found that upward axial velocity below the impeller was of the order  $0.45V_{tip}$ . The highest downward velocity in the secondary loop above the impeller was of  $0.15V_{tip}$ . With respect to the secondary loop that localized in the lower part of the draft tube and close to its wall it is found the highest downward velocity is of  $0.13V_{tip}$ .

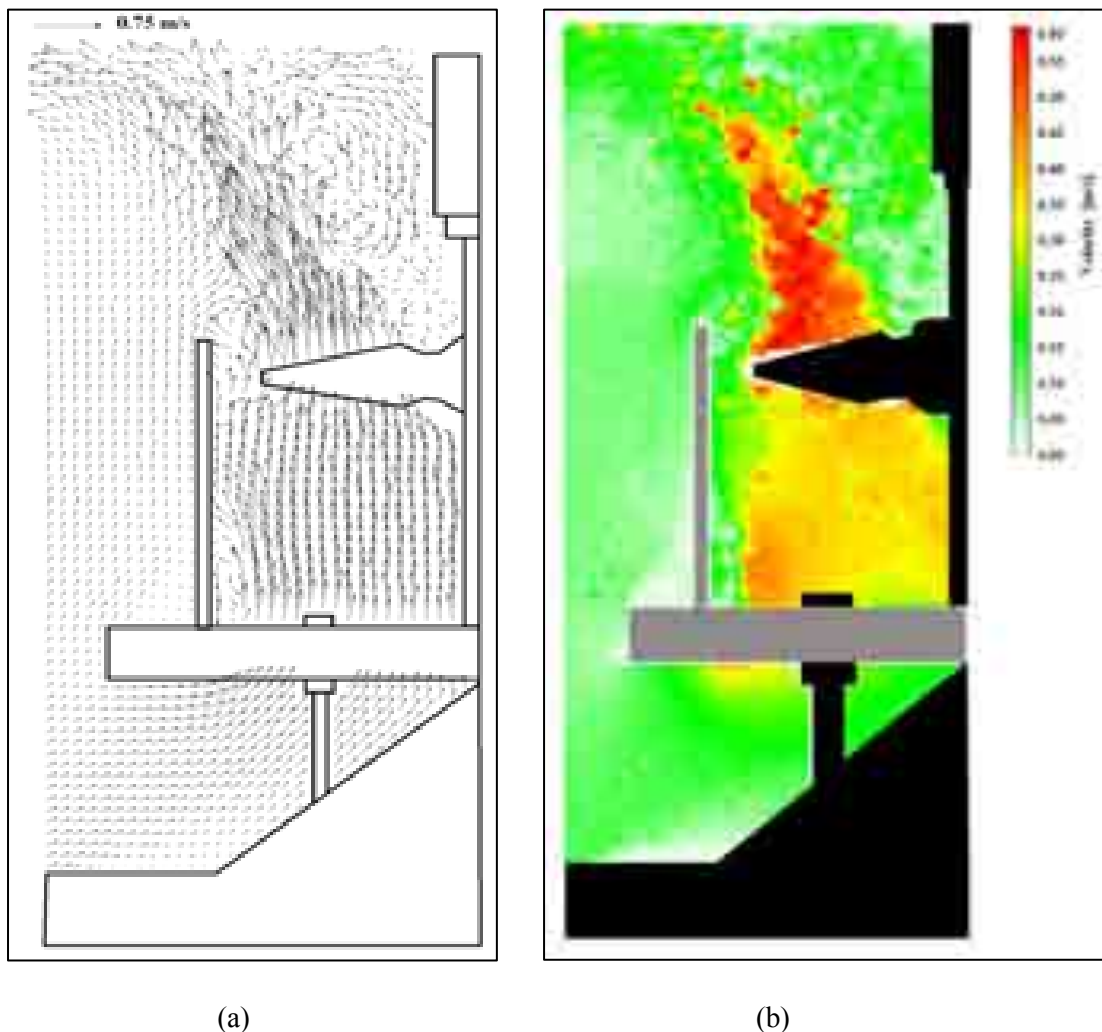


Figure (4.10): (a) The (r - z) flow field map for the RTP-U propeller with draft tube configuration in the vessel core, (b) The (r - z) velocities contour map for the RTP-U propeller with draft tube configuration in the vessel core.

## Chapter Four: Hydrodynamics in the Single Phase Non-Aerated Agitated Tank for Up and Down Pumping Directions Modes

---

The radial velocities are found mainly in the discharge zone above the RTP-U with highest value of the order  $0.22V_{tip}$  and noticeably in the intake flow zone in the lower part of the vessel core below the draft tube with the highest radial velocity of the order  $0.19V_{tip}$ .

The maximum radial velocity produced in the upper part secondary loop near the liquid surface of  $0.15V_{tip}$ . With respect to the radial velocities that achieved in the down-pumping flow mode with propeller and draft tube configuration these values are slightly higher by 9% and 15% in the discharge and inward zones by the RTP-U propeller respectively.

Figure 4.11 illustrates the quantitative analysis of the normalized axial velocities above and below the up-pumping RTP-U propeller with the draft tube in the two r-z measurement planes A and B as explained before.

As it is observed the presented radial profiles for the axial velocity above the impeller are relatively similar, with the highest generated velocities of the order of  $0.315V_{tip}$  and  $0.3V_{tip}$  for both the planes A and B. Whilst below the impeller an obvious divergence appears between the achieved axial velocities between the two measurement planes A and B, where the normalized axial velocities in plane A are much higher than the axial velocities when the normalized propeller radius is less than 0.5.

It seems that the draft tube baffle presence in this part affects the up-flow and reduces the entering flow to swept volume of the impeller in the plane B. For  $r/R > 0.5$  the velocity field profile in plane B becomes relatively higher but with clear difference of the velocity values in plane A.

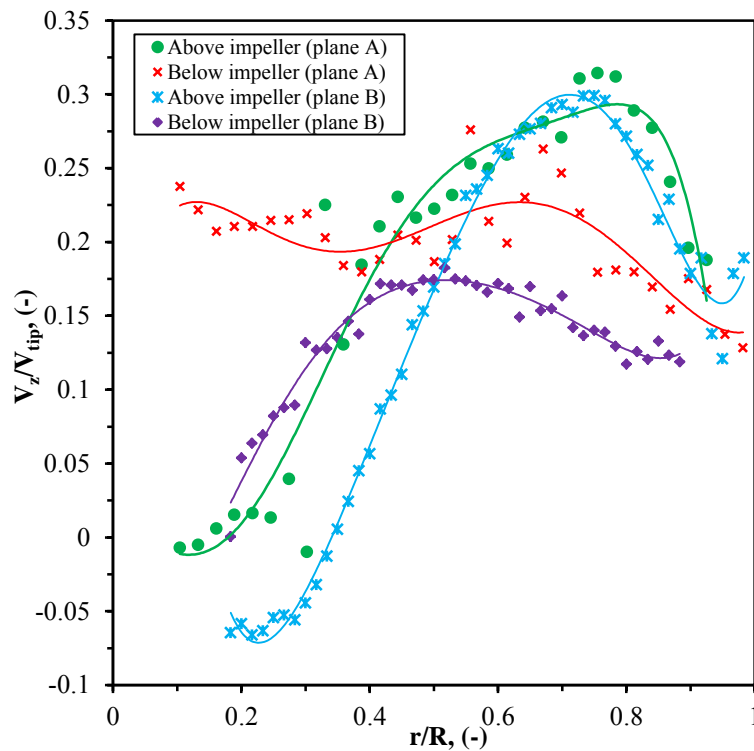


Figure (4.11): The dimensionless axial velocity profile at different liquid heights for RTP-U propeller with draft tube (below impeller  $z/h=0.55$ , above impeller  $z/h=0.62$ ),  $C_{pr}/T_v=0.2$ ,  $N=5$  rps in two different measuring planes; plane A at  $0^\circ$  and plane B at  $90^\circ$  from the posterior baffle respectively.

Similar to the propeller and draft tube configuration in down-pumping direction, the effect of the draft tube baffles appears and alters the velocities in the inward zone below the impeller and inside the draft tube, but on contrary of down-pumping condition the alteration occurs in the discharge zone. Beside the fact that the divergence is due to the difference of the measurement planes A and B cannot be neglected.

## II. Propeller Alone Configuration

The vector plot and velocity contour map of the  $r$ - $z$  plane are shown in Figure 4.12 (a) and (b) respectively. The flow pattern of the up-pumping direction without the draft tube in the vessel core generally is not different from the propeller and draft tube configuration with up-pumping direction, but the propeller alone configuration is distinguished by the fact that the flow in the inward zone below the RTP-U propeller is less intensive and has more radial component than that produced with draft tube presence. The small secondary recirculation below the impeller has vanished in this case. The upper down-ward secondary recirculation loop is occurring even without the draft tube, but it doesn't extend to the upper side of the RTP-U propeller as the propeller and draft tube configuration. The RP-U propeller pushes the flow up-ward

## Chapter Four: Hydrodynamics in the Single Phase Non-Aerated Agitated Tank for Up and Down Pumping Directions Modes

---

axially, but with moving up this axial flow tends to be relatively radial till reaching the zone near the liquid surface; here the flow becomes totally radial. In the lower part of the vessel core a noticeable radial flow is observed also, where the effect of the cone placed at the vessel bottom appears by preventing any possibility of secondary loop formation or drawing the flow axial by the impeller, so no axial flow have been seen in this area.

Comparing with other types of pitched blade impellers, (Gabriele et al., 2011) reported that up-pumping 6-bladed PBT (pitch angle  $45^\circ$ ,  $d_{im}/T_v=0.54$ ,  $C_{im}/T_v=0.33$ ) generates two distinct circulation loops one in the upper part of the vessel and one in lower part, while (Mishra et al., 1998) have reported same observation for a flow created by the APV-B2 hydrofoil 4-bladed impeller ( $d_{im}/T_v=0.45$ ,  $C_{im}/T_v=0.43$ , solidity ratio =1), beside a secondary small loop formed below the impeller. For both the PBT and APV-B2 impellers the flow enters axially into the swept volume from the inflow zone below the impeller, with a considerable flow that is entrained radially to the swept volume near the impeller lower tip. The discharge flow by the RTP-U is mainly axial when it leaves the blades and then it moves gradually in radial direction till it becomes fully radial near the liquid surface, whilst (Gabriele et al., 2011; Mishra et al., 1998) reported the outward flow is pushed radially from upper tip of the blades. This is the main cause of generating two distinct loops in upper and lower part of the vessel.

Considering the axial velocities in this case the highest upward velocity is observed in the discharge flow above the RTP-U propeller. It is of the order  $0.305V_{tip}$ , where the produced velocities above the impeller are mainly axial. The highest achieved upward axial velocity below the impeller is of the order  $0.22V_{tip}$ . The highest downward axial velocity in the upper secondary is  $0.15V_{tip}$ . Comparing these velocities with those reported by (Gabriele et al., 2011; Mishra et al., 1998), (Gabriele et al., 2011) found the highest axial velocities above and below the PBT are of the order  $0.3V_{tip}$  and  $0.12V_{tip}$  respectively, whilst (Mishra et al., 1998) found the highest axial velocities above and below the APV B-2 are of the order  $0.3V_{tip}$  and  $0.2V_{tip}$  respectively. It is obvious that the axial velocity below both the impellers PBT and APV B-2 have smaller values than that produced by RTP-U. The flow is mainly entrained into the swept volume by the RTP-U in an axial way from the inflow zone, when on the other hand an important ratio of the flow enters the swept volume for both PBT and APV B-2 radially and from above the impeller.

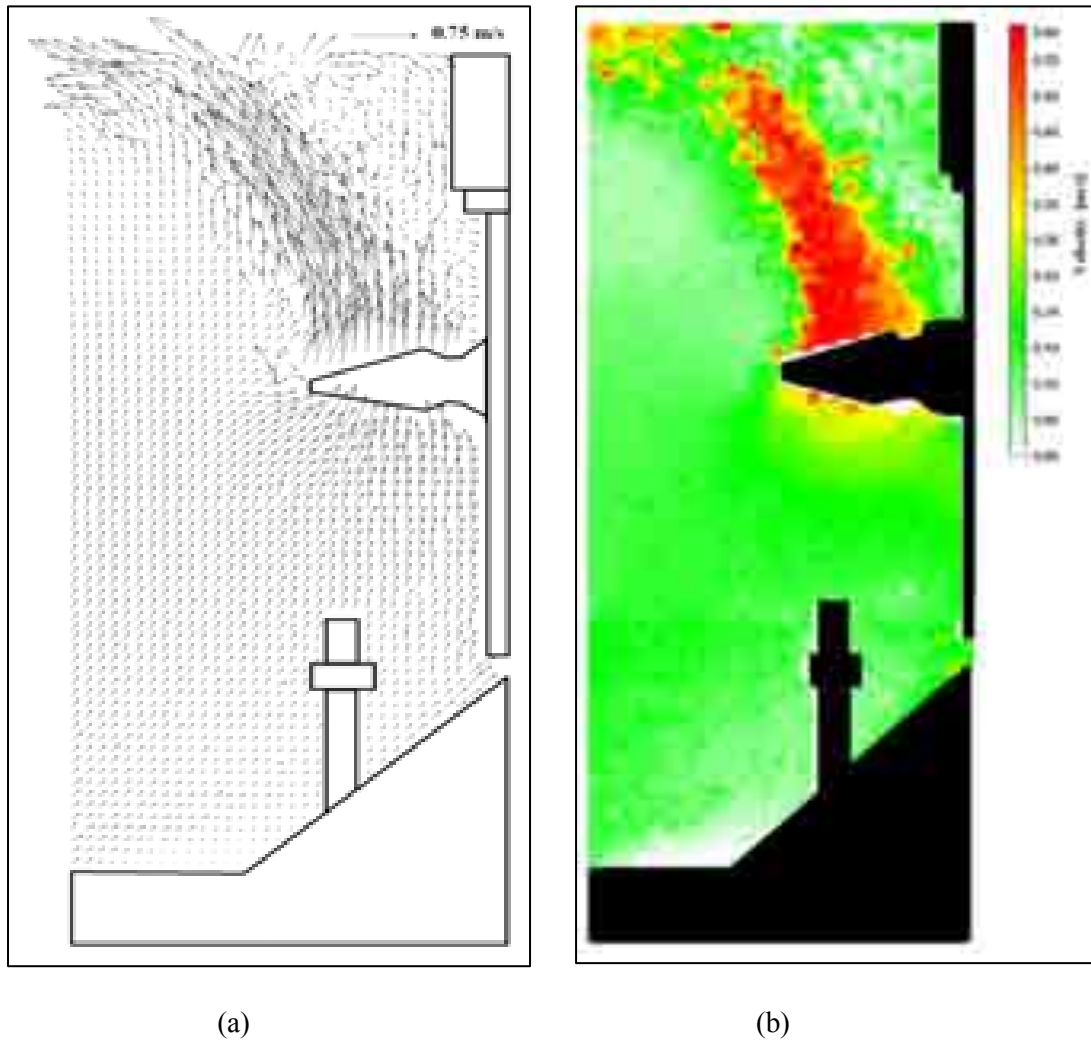


Figure (4.12): (a) The (r - z) flow field map for the RTP-U propeller without draft tube configuration in the vessel core, (b) The (r - z) velocities contour map for the RTP-U propeller with draft tube configuration in the vessel core.

The up-pumping RTP-U propeller alone generates high radial velocities in the discharge flow especially of the upper part of the vessel core near liquid surface. The maximum radial velocity in this part is  $0.3V_{tip}$ , whilst in the lower part of the vessel core the radial velocities are of the order of  $0.156V_{tip}$ . These values are relatively close to those reported by and (Mishra et al., 1998) for the APV B-2 of  $0.3V_{tip}$  in the impeller discharge and  $0.15V_{tip}$  in the lower zone below the impeller, while the reported radial velocities are higher than of those reported by (Gabriele et al., 2011) for PBT of  $0.15 V_{tip}$  in the discharge flow and  $0.12V_{tip}$  in the lower zone below the impeller.

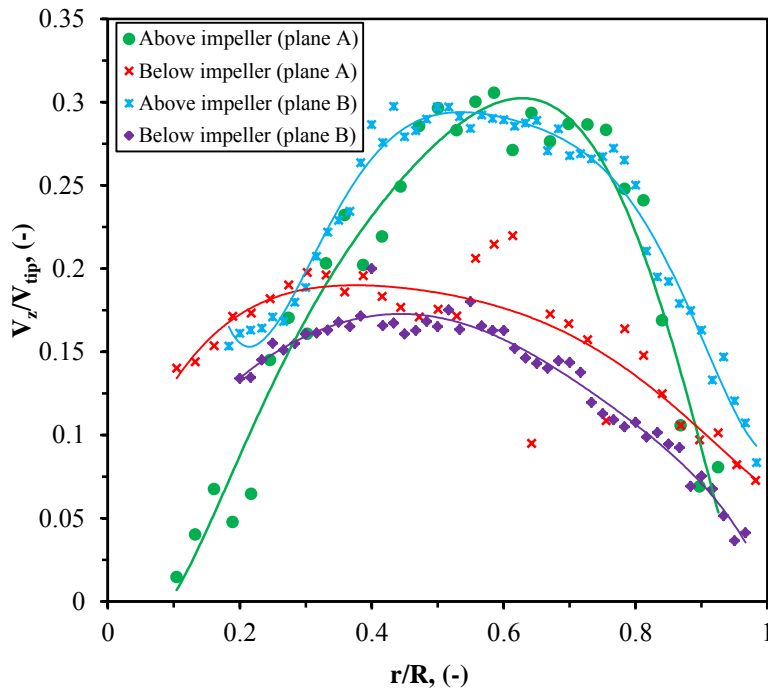


Figure (4.13): The dimensionless axial velocity profile at different liquid heights for RTP-U propeller without draft tube (below impeller  $z/h=0.55$ , above impeller  $z/h=0.62$ ),  $C_{pr}/T_v=0.2$ ,  $N=5$  rps in two different measuring planes; plane A at  $0^\circ$  and plane B at  $90^\circ$  from the posterior baffle respectively.

Figure 4.13 illustrates the quantitative analysis of the normalized axial velocities above and below the up-pumping RTP-U propeller without the draft tube in the two  $r$ - $z$  measurement planes A and B at the vertical heights of  $z/h=0.62$  and  $z/h=0.55$  respectively. As it is noticed the axial velocities profile above and below the propeller in the planes A and B are generally similar, with highest axial velocities above the impeller of the order  $0.31V_{tip}$  and  $0.3V_{tip}$  in the planes A and B respectively. These values are close to those of propeller and draft tube configuration. Below the RTP-U propeller the highest axial velocities are of the order of  $0.21V_{tip}$  and  $0.2V_{tip}$  respectively for the planes A and B. With these values of the axial velocities it is quite clear in this case where the draft tube effect no longer exists, that the produced velocities especially in planes below the impeller are relatively similar. The axial velocities below the RTP-U propeller are significantly different from those in the propeller and draft tube configuration case, where maximum axial velocities of  $0.27V_{tip}$  and  $0.18V_{tip}$  are achieved for the planes A and B respectively.

### 4.3. Power Consumption

Table 4.1 shows the power numbers measured for different configurations in this work or in the literature; the power number seems in the down-pumping mode higher than up-pumping mode approximately by 25%, and the presence of the draft tube

## Chapter Four: Hydrodynamics in the Single Phase Non-Aerated Agitated Tank for Up and Down Pumping Directions Modes

doesn't have any effect of the power number. The power number in the up-pumping mode is slightly higher without draft tube configurations. The measured power number for different types of pitch blades impeller are generally agree with the reported values of RTP propeller, In other word the power number with down-pumping is higher than up-pumping except that found by (Aubin et al., 2001) for PBT.

Table (4.1): The RTP propeller and several pitched blade impellers power numbers with different configurations and pumping modes.

Impeller Type	$C_{im}/T_v$	$d_{im}/T_v$	$N_p$ (With DT <sup>*</sup> )	$N_p$ (Without DT)
RTP-U ( $L_f = 0.1m$ )	0.2	0.15	0.53	0.54
RTP-D ( $L_f = 0.1m$ )	0.2	0.15	0.61	0.61
HF <sup>a</sup> -D	0.50	0.27	--	0.40
	0.33			0.41
	0.20			0.46
PBT <sup>b</sup> -U	0.3	0.25	--	1.3
		0.33		1.2
		0.5		1.1
PBT <sup>c</sup> -D	0.33	0.5	--	1.93
PBT <sup>c</sup> -U				2.58
APV-B2 <sup>d</sup> -D	0.25	0.45	--	0.95
APV-B2 <sup>d</sup> -U	0.43	0.45	--	0.91
MTT <sup>c</sup> -D	0.33	0.5	--	0.74
MTT <sup>c</sup> -U				0.67
EE <sup>c</sup> -D	0.25	0.45	--	2.1
EE <sup>c</sup> -U				1.7
PBT <sup>f</sup> -U ( $L_f = 0.54 m$ )	1.16	0.18	1.4	--
HF4 <sup>g</sup> -D ( $L_f = 0.125$ ) ( $L_f = 0.167$ )	0.33	0.33	0.3	--
			0.35	
Propeller <sup>d</sup>	0.33	0.33	--	0.89

\* DT : Draft tube ; <sup>a</sup> Kumaresan and Joshi (2006); <sup>b</sup> Chapple et al. (2002) ; <sup>c</sup> Aubin et al. (2001)

<sup>d</sup> Mishra et al. (1998); <sup>e</sup> Zhu et al. (2009); <sup>f</sup> Broz et al. (2004); <sup>g</sup> Kumaresan et al. (2005)

Table 4.1 illustrates clearly that the power characteristics for all types of pitched blade impellers are very dependent on the impeller to tank diameter ratio or and on the off-bottom clearance to tank diameter. As observed, the power number changes for the same pitched blade impeller when the geometry is changed, so it is difficult to compare the power characteristic between the pitched blade impellers with different geometrical ratios. This agrees with (Chapple et al., 2002) who found that the power number for pitched blade impellers is highly related to impeller position in the tank. (Chapple et al., 2002) explained this changing as the flow at the impeller interacts strongly with the proximity of the tank walls, so changes in the position of the

## Chapter Four: Hydrodynamics in the Single Phase Non-Aerated Agitated Tank for Up and Down Pumping Directions Modes

impeller in the tank can have a significant impact on the power number due to changes in the flow patterns. The power number for RTP propeller is generally smaller than that of other impellers except for HF impeller which has lowest power number in down-pumping mode. It seems that the draft tube presence has very little effect on power number.

### 4.4. Pumping Capacity

The pumping capacity can be determined by the pumping number  $N_{Qp}$  (Flow number) and circulation number  $N_{Qc}$  of the impeller. They are calculated according to equations 2.11 and 2.14. The pumping numbers and circulation numbers of RTP propeller and several pitched blade impellers determined in previous works are presented in Table 4.2 for up-pumping and down-pumping modes and for both with and without draft tube configurations.

Table (4.2): The RTP propeller and several pitched blade impellers pumping and circulation numbers with different configurations and pumping modes.

Impeller Type	$C_{im}/T_v$	$d_{im}/T_v$	$N_{Qc}$	$N_{Qp}$ (With DT*)	$N_{Qp}$ (Without DT)
RTP-U ( $L_f = 0.1m$ )	0.2	0.15	1.186 (With DT)	0.56	0.51
RTP-D ( $L_f = 0.1m$ )	0.2	0.15	1.22 (With DT)	0.55	0.495
HF <sup>a</sup> -D	0.50	0.27	--	--	--
	0.33		0.96	--	0.59
	0.20		--	--	--
PBT <sup>c</sup> -D	0.33	0.5	0.91	--	0.75
PBT <sup>c</sup> -U			1.82	--	0.68
APV-B2 <sup>d</sup> -D	0.25	0.45	1.19	--	0.83
APV-B2 <sup>d</sup> -U	0.43	0.45	0.975	--	0.58
MTT <sup>c</sup> -D	0.33	0.5	1.13	--	0.67
MTT <sup>c</sup> -U			1.35	--	0.61
EE <sup>e</sup> -D	0.25	0.45	--	--	0.73
EE <sup>e</sup> -U			--	--	0.72
PBT <sup>f</sup> -U ( $L_f = 0.54 m$ )	1.16	0.18	--	0.5	--
HF4 <sup>g</sup> -D ( $L_f = 0.125$ ) ( $L_f = 0.167$ )	0.33	0.33	0.67	0.41	--
			0.89	0.65	--
Propeller <sup>d</sup>	0.33	0.33	1.3	--	0.73

\* DT : Draft tube ; <sup>a</sup> Kumaresan and Joshi (2006); <sup>b</sup> Chapple et al. (2002) ; <sup>c</sup> Aubin et al. (2001)

<sup>d</sup> Mishra et al. (1998); <sup>e</sup> Zhu et al. (2009); <sup>f</sup> Brož et al. (2004); <sup>g</sup> Kumaresan et al. (2005)

For the RTP propeller the pumping numbers in the up-pumping mode are slightly higher than those in the down-pumping mode for both configurations with and

## Chapter Four: Hydrodynamics in the Single Phase Non-Aerated Agitated Tank for Up and Down Pumping Directions Modes

---

without draft tube. Similar observations were reported for the rest except for APV-B2<sup>d</sup>, where the down-pumping has higher pumping and circulation numbers. The pumping numbers are slightly elevated with draft tube, but this elevation is not always led to elevation of the discharge flow because part of the discharge flow is redirected upwards as seen in the down-pumping mode. Same thing may exist in the up-pumping mode but in a different way, as much flow participates to the secondary loop above the impeller for propeller and draft tube configuration.

The RTP propeller pumping numbers are relatively close the HF impeller, but comparing with the others, the RTP propeller has lower pumping number for the up-pumping and down-pumping modes. The pumping numbers for the pitched blade impellers show a noticeable dependence on the flow direction and the impeller position in the tank, as the observed pumping numbers data are slightly affected with changing geometry and impeller position.

Despite the low  $C_{im}/T_v$  applied in this work, the down-pumping circulation number for the RTP-D propeller appears close to the reported range of circulation number for the MTT<sup>c</sup>-D and APV-B2<sup>d</sup>-D circulation numbers, and RTP-D are higher than those reported for the PBT and HF impellers.

The circulation numbers are strongly related to pumping numbers. As a consequence the up-pumping mode seems to have higher circulation numbers than in the down-pumping mode, the only exception is with MTT<sup>c</sup>, which shows a reversible behavior with the pumping number. Generally for the propellers the circulation numbers are between 1.2 and 1.5 to their pumping numbers. In this work the circulation number are 2.12 and 2.22 for up and down pumping modes respectively. The slightly elevated values of circulation numbers are due to the effect of the draft tube.

### **4.5. Agitation Index and Liquid Volume Quantification for the Down-Pumping Mode with Draft Tube Configuration**

The mixing index for the RTP propeller in the down-pumping mode and with draft tube configuration was calculated according to the equations (2.15 to 2.17). Table 4.3 shows the agitation indices values (the volume-weighted average velocity) for RTP-D and for several pitched blade impellers that have been determined in previous works (Aubin et al., 2001; Mavros and Baudou, 1997). The agitation index for the RTP-D propeller is noticeably lower than the agitation indices for pitched blade impellers. This low agitation index is due to low impeller to tank diameters ratio ( $d_{pr}/T_v=0.15$ ) rather than the applied grid area applied in this work. Comparing with pumping number, the agitation index didn't show an important dependence on the pumping direction mode: it is higher for PBT-U than PBT-D and it is of the same order for MTT-D and MTT-U (Aubin et al., 2001).

## Chapter Four: Hydrodynamics in the Single Phase Non-Aerated Agitated Tank for Up and Down Pumping Directions Modes

---

Table (4.3): The agitation Index for RTP-D and various pitched blade impellers, (this work and literature).

Impeller Type	$C_{im}/T_v$	$d_{im}/T_v$	N (rps)	$I_g$
RTP-D ( $L_f = 0.1m$ )	0.2	0.15	5	3.47% (With DT*)
PBT <sup>a</sup> -D	0.33	0.5	5	16.0%
PBT <sup>a</sup> -U				22.5%
MTT <sup>a</sup> -D	0.33	0.5	5	14.1%
MTT <sup>a</sup> -U				13.7%
MTT <sup>b</sup> -D	0.33	0.5	6.7	12.0%
Lightnin A310 <sup>b</sup> -D	0.33	0.5	6.7	8.0%

\* DT : Draft tube ; <sup>a</sup> Aubin et al. (2001) ; <sup>b</sup> Mavros and Baudou (1997)

The liquid volume quantification or distribution for the down-pumping mode with the draft tube is illustrated in the Figure 4.14, where the liquid volumes distribution in the vessel is related to determine ranges of the composite mean local 2-D velocities in the vessel. The composite mean velocities are illustrated as a 3-D surface chart as seen in Figure 4.14; the liquid volume movement is elucidated in the vessel except in the swept volume of the impeller, in the volume of the cone at the vessel base, and in the one of the shaft and baffles edges. From figure 4.14 it is found that in the majority of the liquid volume, the mean velocity is low, smaller than of the order  $0.11V_{tip}$  except in three zones. The most elevated is the discharge and intake zone of the RTP-D where mean velocity is less than  $0.34V_{tip}$  excluding a very small part in this with mean local velocities of the order between  $0.34V_{tip}$  and  $0.45V_{tip}$ . The other two zones near the vessel bottom and walls have lower local velocities less than  $0.23V_{tip}$ ; these two zones are generated due to the interaction of the flow induced by the RTP-D propeller with both the vessel bottom and walls.

### 4.6. Mixing Time

#### 4.6.1. The Effect of RTP Propeller Rotational Speed

The mixing time  $t_m$  experiments are performed for different RTP propeller rotational speed levels, N, of (1.67 - 5 rps) to determine the mixing performance for two configurations with and without draft tube. The system is operated without the turbine at the top. The flow regime is always kept in the turbulent state. The mixing time measurements are conducted by the colourisation-decolouration method.

The investigations are applied for two modes of agitation: up-pumping and down-pumping, to understand the effect of draft tube in both configurations with and

## Chapter Four: Hydrodynamics in the Single Phase Non-Aerated Agitated Tank for Up and Down Pumping Directions Modes

---

without draft tube (See Figure 4.15). The injection position of the decolorizing solution is always the same at the surface of water in order to measure correctly the mixing time achieved due to the circulation of air bubbles entrapped from the water surface, as the position of the injection may cause difference in (Kawase and Moo-Young, 1989).

Figure 4.15 illustrates the effect of RTP propeller rotation speed  $N$  on the mixing time  $t_m$  in a single liquid phase (water) of both down-pumping and up-pumping modes for the two configurations with and without draft tube. From the results it is found that the mixing time  $t_m$  is reversely related with the RTP propeller rotation speed for all tested runs. This agrees with (Bouaifi and Roustan, 2001; Hadjiev et al., 2006; Houcine et al., 2000).

Figure 4.15 shows also that the mixing time for the up-pumping mode with draft tube configuration is slightly higher than the down-pumping with and without draft tube configurations, that agrees with (Patwardhan and Joshi, 1999) for impeller clearance ratio of  $C_{im}/T_v < 0.33$ . The mixing time  $t_m$  for down-pumping mode without draft tube condition is higher than with draft tube; (Aeschbach and Bourne, 1972; Houcine et al., 2000; Kumaresan et al., 2005; Tatterson, 1982) reported similar behaviour in their works. (Kumaresan et al., 2005) used a longer draft tube ( $L_f = 0.167m$ ).

From Figure 4.15 it can be observed for up-pumping mode, the mixing time is lower without draft tube at moderate propeller speeds, this can be explained by the fact that the up flow is enhanced due to the presence of a cone at the vessel bottom, which contributes to redirect the flow upward to propeller intake and also to remove the dead zone below the propeller, (Nere et al., 2003) have presented similar performance for PBT impeller. It is noticed also that at higher rotation speed for down-pumping mode with draft tube lowest mixing time is achieved.

The low values of mixing time in single phase condition are due to low ratio of ( $d_{pr}/T_v = 0.15$ ), where this ratio leads to weak flow interaction between the RTP propeller and the walls and the bottom of the vessel.



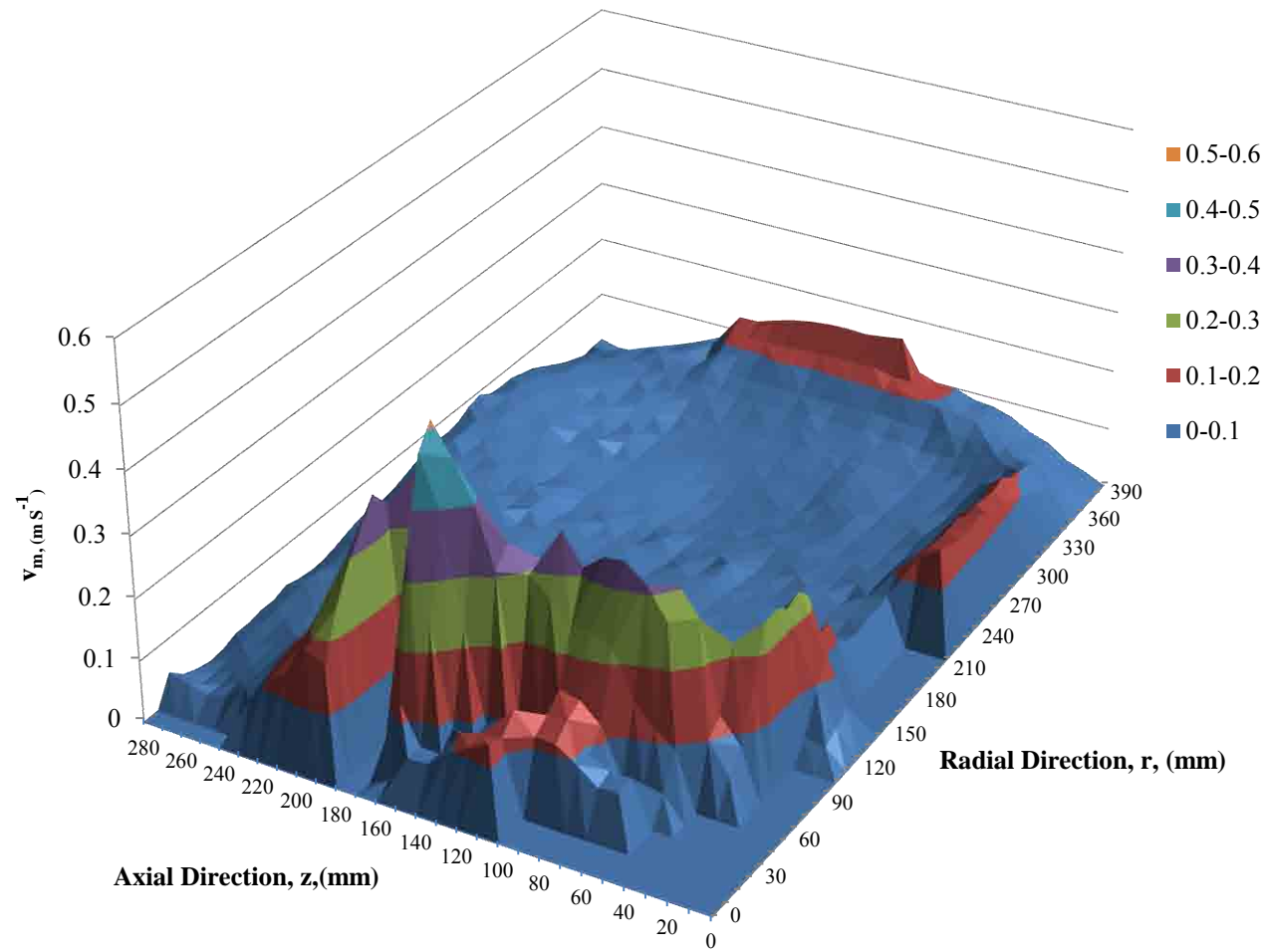


Figure (4.14): The distribution of the liquid volume in the vessel related with mean local composite velocity ranges for RTP-D propeller with draft tube configuration.



## Chapter Four: Hydrodynamics in the Single Phase Non-Aerated Agitated Tank for Up and Down Pumping Directions Modes

---

Comparing the achieved mixing times for the given rotation speed of up and down pumping modes with and without draft tubes as shown in Figure (4.15) with the investigated flow patterns for each case shows that, for up-pumping mode the shorter mixing time is accomplished without draft tube complies the fact that the radial discharge flow without the draft tube is more intensive. The highest radial velocity in this zone without the draft tube is greater by 18%. For the down-pumping mode the shorter mixing time with the draft tube is in compliance to the fact that the radial discharge flow with the draft tube near the vessel bottom and beside the cone is more intensive. The highest radial velocity in this zone with the draft tube is greater by 30%.

For the given impeller rotation speed ( $N = 5\text{ rps}$ ) and with draft tube configuration, the higher circulation number for the down-pumping mode produced by RTP-D propeller ( $N_{Qc} = 1.22$ ) agrees with the shorter mixing time ( $t_m=30\text{s}$ ) for this mode when compared with up-pumping mode that produced by RTP-U propeller, with lower mixing index ( $N_{Qc} = 1.186$ ) and longer mixing time ( $t_m=40\text{s}$ ) are achieved, as shown in Figure 4.15.

In the decolourization step, the colour was disappearing in a similar manner for down-pumping mode and for up-pumping mode with and without draft tube. The colour was disappearing gradually first near the bottom and the walls for the down-pumping, whilst it was disappearing first near the water surface zone for the up-pumping mode. For the down-pumping mode, the last zone where the colour was disappeared and delaying the good mixing is the zone that corresponds to the centre of principal circulation as shown in Figure 4.3, for the other configuration same behaviour was observed.

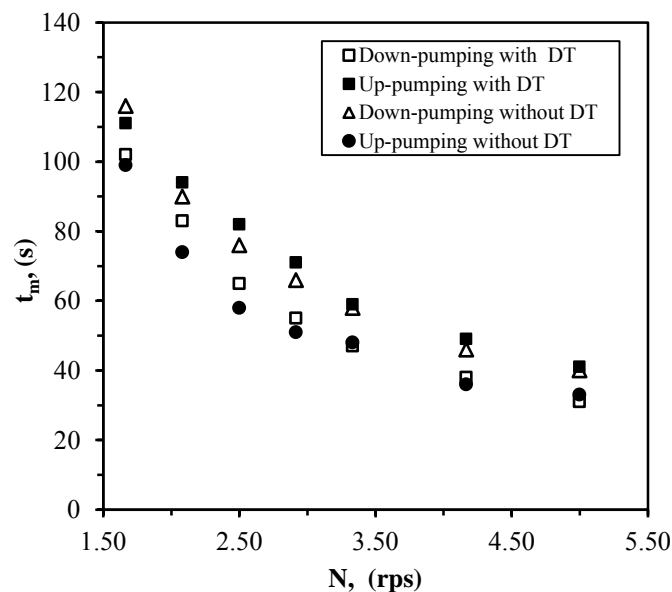


Figure (4.15): The effect of RTP propeller rotational speed on the mixing time for different flow and geometry conditions,  $h/d_{pr}=1.47$ ,  $C_{pr}/T_v = 0.2$ .

## Chapter Four: Hydrodynamics in the Single Phase Non-Aerated Agitated Tank for Up and Down Pumping Directions Modes

---

Figure 4.16 presents the dimensionless mixing time number relation with propeller Reynolds number. The mixing time appears to be not very effected by the elevation of  $Re$ . As a consequence this indicates that the dimensionless mixing time number  $Nt_m$  in a single phase (non-aerated) condition can be fairly determined apart from the occurred flow pattern and the bubble presence in the liquid phase for adapted rotation speed (1.67 -3.33 rps). From Figure 4.16 it is observed that the dimensionless number mixing  $t_m N$  stays relatively close for each flow modes and vessel configurations, this indicates that these configurations and flow modes can be characterized by their mixing number.

For the entire tested configuration, it is important to mention here that the low mixing time numbers means that efficient mixing for the given geometrical configuration is achieved.

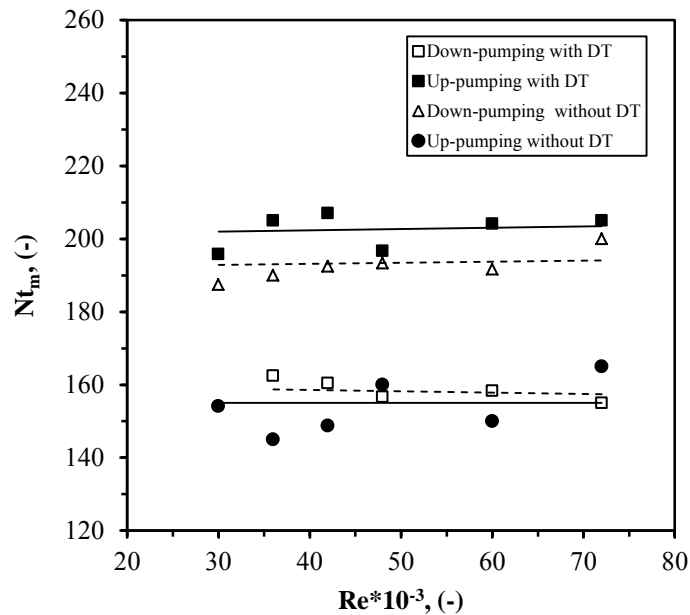


Figure (4.16): The relation of Reynolds number with the dimensionless mixing time for different pumping modes and geometry configurations,  $h/d_{pr} = 1.47$ ,  $C_{pr}/T_v = 0.2$ .

### 4.7. Conclusions

In this chapter the flow patterns and r-z velocity vector fields and contour maps in a single phase for the RTP propeller agitated vessel were measured by applying both PIV and LDV for up-pumping and down-pumping operation modes with and without draft tube configuration. The LDV measurements were restricted inside the draft tube and in the measurement plane at  $90^\circ$  from the posterior tank baffle.

For the down-pumping mode, mainly one recirculation loop is generated with RTP-D propeller with two notable secondary loops; one below the propeller and the second

## Chapter Four: Hydrodynamics in the Single Phase Non-Aerated Agitated Tank for Up and Down Pumping Directions Modes

---

beside the propeller blades. When the draft tube is removed the flow field did not show an important change in the vessel core, except that one of the two secondary loops has disappeared. For the up-pumping mode in the vessel core an overall circulation loop is generated beside that, one important secondary loop is formed above the propeller. Similar velocity vector map is observed when the draft tube is removed. The quantitative analyses were made for the axial velocities for both planes at  $0^\circ$  and  $90^\circ$  from the posterior baffle of the tank. The results showed that the velocity profiles are different for these two planes with draft tube presence especially in the region near draft tubes (i.e.) below the propeller. This difference is lessened when the draft tube is removed. Starting with propeller rotation speed 4.6 rps, a surface vortex appears and extends to the propeller blade tip in the down-pumping mode without draft tube configuration, this phenomena is created.

Generally the pumping number is found very dependable on the flow direction. The pumping capacity of the RTP propeller doesn't exhibit a great change when the draft tube is placed. The up-pumping mode shows a slight elevation for the pumping number compared with the down-pumping mode for both configurations with and without draft tube. The power consumption for the RTP propeller has a relative dependence on the flow configuration, as in down-pumping mode a limited increase in power consumption is observed compare to up-pumping mode.

The down-pumping mode agitation index showed low mean local velocities with respect to those in the previous works for pitched blade impellers. These low mean velocities are due to the influence of the low propeller diameter to vessel diameter ratio  $d_{pr}/T_v = 0.15$ .

Mixing time shows an obvious dependence upon the variation of rotation speed in the single phase conditions with different influence intensity. The mixing time is increased by 20% without the presence the draft tube in the up-pumping mode. For the down-pumping mode the mixing time is enhanced by 15% when the draft tube is placed around the RTP-D propeller. From these observations it is very difficult to clarify that one of the RTP configurations and pumping modes has an apparent influence to improve the RTP propeller performance. In summary with respect to RTP propeller pumping capacity, power consumption and mixing time for the various tested configurations and operation modes, it is found that no general approach can be recommended to improve the performance of the RTP propeller that is more efficient than the already approved down-pumping mode with draft tube.



# **CHAPTER FIVE**

## **HYDRODYNAMICS AND FLOW PATTERN IN AERATED AND AGITATED TANK**



## Chapter Five

# Hydrodynamics and Flow Pattern in Aerated Agitated Tank

### 5.1. Introduction

In this chapter the flow patterns and velocity fields for the aerated vessel have been investigated. Two phases air-water are occurring since the water droplets are sprayed in the air and then with their impacting at the water surface a sufficient amount of air bubbles are entrapped and entrained inside the water bulk. To evaluate the aeration performance of the system and to estimate the contribution of each element (Turbine, RTP propeller and draft tube) on the process different experimental sets were performed.

The PIV measurements for the flow pattern and mean velocity were carried out in the r-z plane (Plane A) same as described in chapter four, where r-z measurement plane was positioned directly on posterior baffle ( $0^\circ$ ) and at ( $60^\circ$ ) from the two lateral baffles from front face (See Figure 4.1). The number of image pairs was (300) and exposure time delay ( $\Delta t$ ) between each two sequent images was ( $2500 \mu s$ ) depending on operation condition such as upper turbine tip velocity and image scale factor adapted during the acquisition. A pixel interrogation of ( $32\% \times 32\%$ ) with ( $50\%$  overlap) was applied for the velocity measurements.

The conical shape turbine was placed at the water surface level ( $C/T_v=0.313$ ,  $D/T_v=0.238$ ,  $h=0.28m$ ). The used vessel is the 3-baffled cylindrical vessel as described earlier ( $T_v=0.8 m$ ). The four  $45^\circ$  pitched and twisted blade propeller RTP effect was studied at clearance ( $C_{pr}/T_v = 0.2 m$ ) with and without the draft tube ( $d_f=0.15 m$ ,  $L_f=0.1 m$ ) that was positioned in the vessel with clearance ( $C_f = 0.1m$ ). The RTP propeller and the draft tube were removed in a part of the measurements. The measurements were performed with turbine rotation speed of ( $N= 2.08 rps$ ) to ensure staying always in turbulent regime for created flow field ( $Re = 75000$ ) and prevent excessive air bubbles presence with higher rotation speed, which leads to miscalculation of r-z mean velocities vector plot by PIV due to the high reflection of laser beam occurred by these bubbles. The PIV measurements were performed in the entire tank to identify the effect for the both the draft tube and/or RTP propeller configurations on the produced mean velocity field and liquid flow patterns.

### 5.2. Flow Pattern and Mean Velocity Field in the Aerated Tank

The flow pattern and mean velocity fields in the aerated tank for the whole system is illustrated in the Figures 5.1 and 5.2. From these Figures the time average velocities vector plot and contour inside the aerated tank at the r-z plane at  $0^\circ$  of the posterior

baffle shows that a main circulation loop occurs in the tank. This circulation is mainly generated by the turbine, where the falling water droplets at the water surface creates a strong radial stream of the water and air bubbles near the water surface toward the walls, which then this flow is redirected by these walls down-ward to the tank bottom. The circulation node is approximately positioned in the mid-distance from the tank bottom to the water level and closer to the walls than the tank center ( $r = 270\text{-}290\text{mm}$ ,  $z = 110\text{-}130\text{mm}$ ). A part of the returning upward flow in the main recirculation loop is induced radially without passing through the turbine intake region, as this flow is induced partially due to the impingement and the plunging of the water droplets in the subsurface water area so a significant amount of the circulation flow returns to the plunging position without being induced by the turbine. The part of the flow that drawn by the turbine blades is propelled as water droplets through the atmospheric air mostly by the vertical side of the turbine blades and especially from the blades upper tip; these droplets then falls down at the water surface and plunges in the water subsurface zone and creates the main recirculation loop. The air is entrained with the droplets impingement at the water surface as air bubbles and then is dispersed in the tank by the liquid recirculation loop.

One secondary recirculation loop is generated in the central region of the tank above and below the RTP-U propeller. The discharged flow above the propeller and below the turbine is mainly drawn by the turbine blades except that some of the liquid is moved toward the shaft and then goes down to the intake zone of the propeller and forming the secondary loop. The flow in the secondary recirculation loop extends down till the upper part cone, where the cone assists to redirect the liquid flow upward to the propeller.

As shown in Figures 5.1 and 5.2 there are three high velocity zones in the tank; the first one is at the tip of the turbine blade. The second high velocity zone is the water impingement and plunging position at the water surface and subsurface. The third zone is near the tank wall, where the generated descending flow from the water droplets plunging zone has relatively kept its high velocities due to the interaction with the tank wall. The liquid flows in the third zones losses its high velocity gradually with going down toward the bottom of the tank. Very few studies concerning the mean velocities profile and flow pattern measurements have been made of the aerated water inside the vessel for similar surface aeration configuration, but generally the studies were performed for the stirred aerated tanks with air supply sources. (Lee et al., 2001) have performed CFD simulation for the flow profile that generated by the spray impingement at the water surface for a tank that aerated by surface aerator turbine, whilst (Kang et al., 2001) have carried out CFD simulation for similar tank that used by (Lee et al., 2001) but for two impellers, where an impeller was added below the turbine at the same shaft. The flow pattern with that determined by (Kang et al., 2001) for the dual impeller configuration ( $D/T = 1/3$ ,  $T/h = 1/1.84$ ) of the conical type turbine at the water surface and a PBTD impeller in the liquid has two distinct circulation loops for each impeller, the upper one is similar to that occurs in our system, the down pumping PBTD impeller apparently produces the lower loop,

where the flow comes from the upper loop is pushed down-ward and returns to the impeller intake zone above the impeller.

The produced time average velocity in the aerated tank as shown in Figure 5.2 has the highest axial velocity in the droplets plunging water subsurface zone and is of the order  $0.415V_{tip}$ . The highest generated radial velocity exists in the same zone is of the order  $0.64V_{tip}$ , which is greater than the highest radial velocity that produced in the in the tested case of the agitated vessel with the up-pumping RTP-U propeller and draft tube only (See chapter four)by 66%.

In the high flow zone near the vessel wall the highest axial velocity in the downward flow bulk is about of the order  $0.4V_{tip}$ , which is close to the highest axial velocity that produced in the high flow zone near the vertical side the turbine blades that of the order  $0.42V_{tip}$ . In this zone a high radial velocity is achieved of the order  $0.47V_{tip}$ . The upward axial velocity in the discharge flow zone of the RTP-U propeller which is in the same time the intake zone of the upper turbine is of the order  $0.17V_{tip}$ , while this velocity is raised to the order  $0.32V_{tip}$  just below the turbine blades, the radial velocity just below the turbine blades reaches  $0.08V_{tip}$ .

### 5.3. The Effect of the Propeller and Draft Tube

#### 5.3.1. Flow Pattern and Mean Velocity Field in the Aeration Tank

The vector plot and velocity contour map of the r-z plane when both the RTP propeller and the draft tube were removed are illustrated in the Figures 5.3 and 5.4 respectively. The flow pattern in the aerated vessel without the RTP propeller and the draft tube shows a slight difference with that obtained in the previous section 5.2. The only difference is in the region near the shaft, where the secondary recirculation loop is not distinguished as it was for the whole system configuration, where a weak flow zone is presented in this region and it extends downward to the cone. From the Figure 5.3, it seems that the propeller and the draft tube presence results in a slightly more intensive flow than that produced by the turbine alone.

Figure 5.4 confirms that the generated flow by both the turbine and propeller with draft tube is slightly more intensive. Figure 5.4 shows also that the high flow zone near the vertical side of the turbine blades is disappeared. The other two high flow zones near the vessel wall and at water subsurface regions are relatively smaller.

Considering the axial velocities when the propeller and draft tube are removed, the highest downward velocity is observed in the high flow zone near the vessel wall is of the order  $0.377V_{tip}$ . The highest generated upward axial velocity below the turbine blades is of the order  $0.288V_{tip}$ . The highest upward axial velocity in the zone near the vertical side of the turbine blades is of the order  $0.17V_{tip}$ . The upward velocity in the intake zone for the turbine is around the order  $0.16V_{tip}$ ; this velocity is slightly smaller

than that produced with the presence of the propeller and the draft tube at the same region by 5%.

The radial velocities in the case of the turbine alone configuration shows same behavior as the axial velocities, where their values are slightly lower than the whole system configuration. The highest radial velocity generated in the water subsurface zone is of the order  $0.6V_{tip}$ .

Whilst below the turbine blades the highest radial velocity is of the order  $0.29V_{tip}$  and the generated radial velocity near the vertical side of the turbine blades is of the order  $0.294V_{tip}$ , which is less than that obtained in the whole system configuration by 35%.

### 5.4. The Effect of the Draft Tube

#### 5.4.1. Flow Pattern and Mean Velocity Field in the Aeration Tank

The generated flow by the RTP-U propeller and the turbine without the presence of the draft tube as presented in the Figure 5.5 is generally similar to the produced flow that presented in the whole system and the turbine alone configurations. A weak flow region near the shaft exists same as the turbine alone configuration. Figure 5.6 shows the flow pattern in the aerated vessel has two distinguished high flow zones at the water subsurface region and near the vessel walls, whilst the high flow region near the vertical side of the turbine blades is mostly disappeared. From Figure 5.6 it can be found that the produced flow when the draft tube was removed is slightly less intensive than the induced flow with the draft tube as seen in Figure 5.2.

The maximum axial velocity that produced by both the RTP-U propeller and turbine without draft tube presence is of the order  $0.367V_{tip}$ , this velocity exists in the downward high flow zone near the vessel wall and it is less than that generated at the same region in the whole system configuration by 7%. The highest upward velocity just below the turbine blades is  $0.32V_{tip}$ , whilst this velocity is of the order  $0.17V_{tip}$  in the turbine intake zone or in other word this zone is the RTP-U propeller discharge zone, which is similar to the produced velocity in the whole system configuration. The highest axial velocity in the zone near the vertical side of the turbine blade is of the order  $0.32V_{tip}$ .

With respect to the radial velocities that achieved here, these velocities are found slightly lower that induced in the whole system configuration, in the zone localized near the vertical side of the turbine blades a highest radial velocity of  $0.147V_{tip}$  is achieved, while in the water subsurface zone that created due to the falling droplets plunging into the liquid bulk the highest generated radial velocity is of the order  $0.54V_{tip}$ , these radial velocities are lower by 16.5% and 31% than the radial velocities that achieved with draft tube presence respectively. The maximum radial velocity that produced at the lower edge of the turbine blades is of the order  $0.05V_{tip}$ .

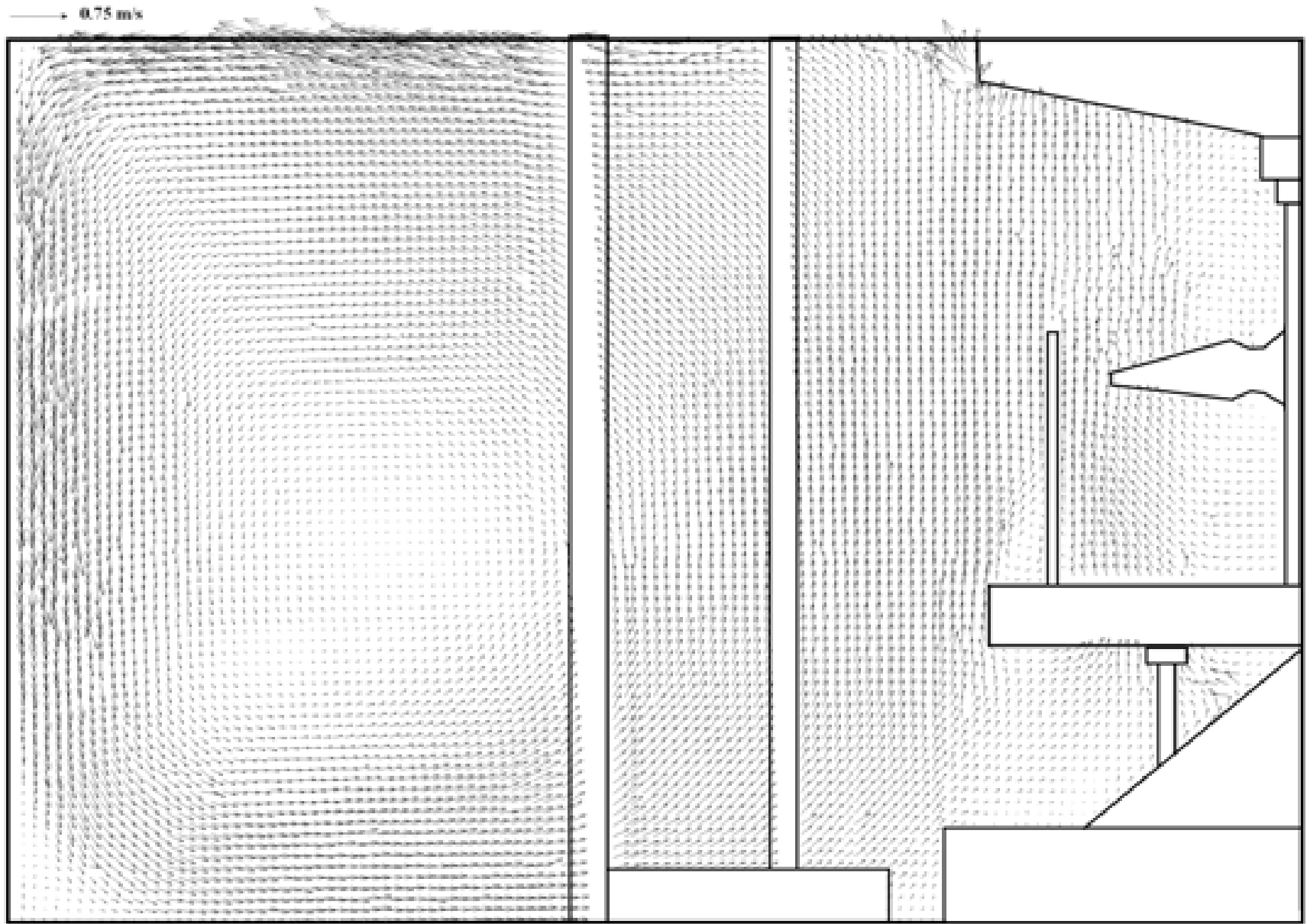


Figure (5.1): The (r - z) flow field map for the turbine and the RTP-U propeller with draft tube (Whole system) configuration in the entire vessel.



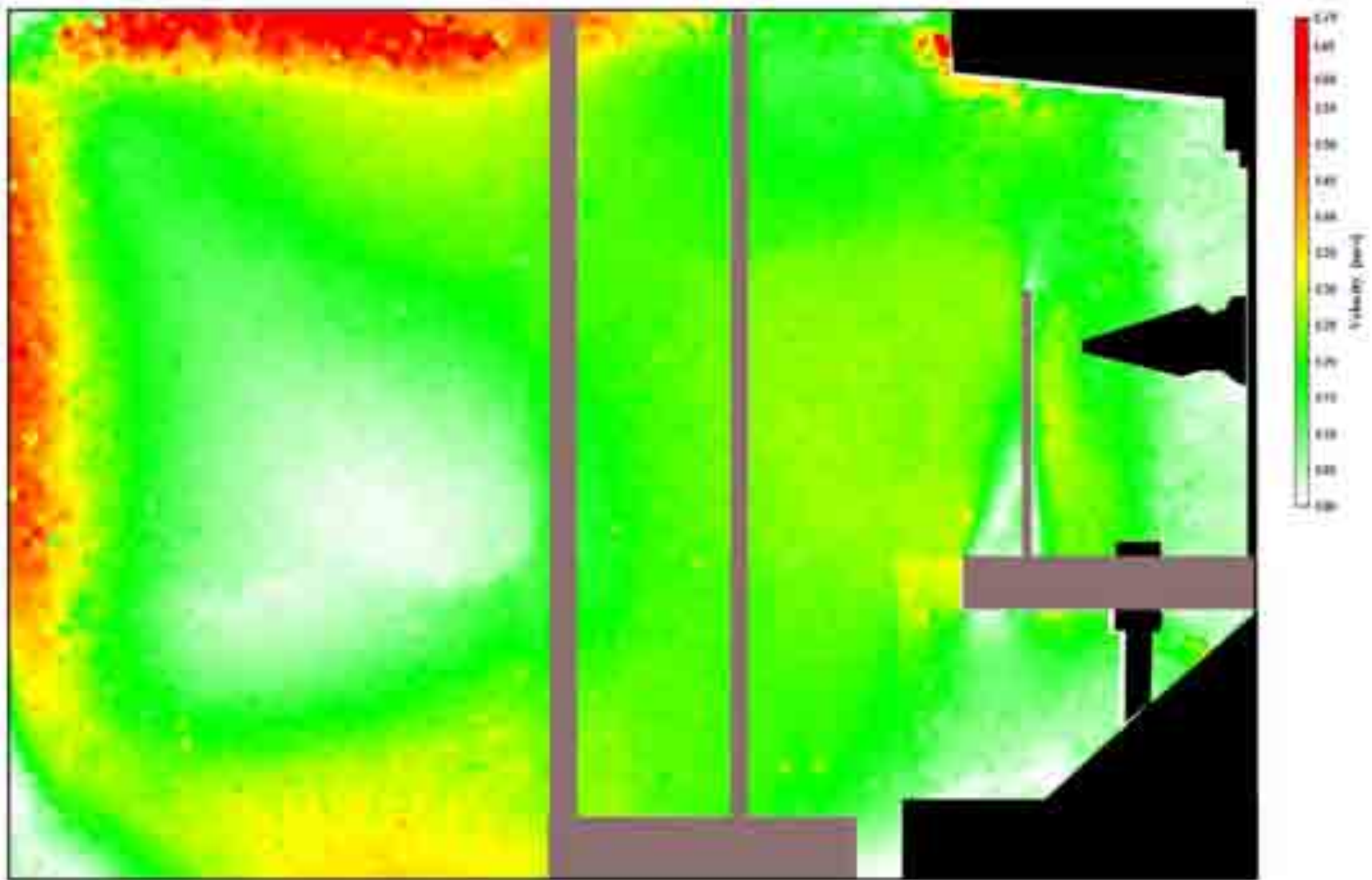


Figure (5.2): The (r - z) velocities contour map for the turbine and the RTP-U propeller with draft tube (Whole system) configuration in the entire vessel.



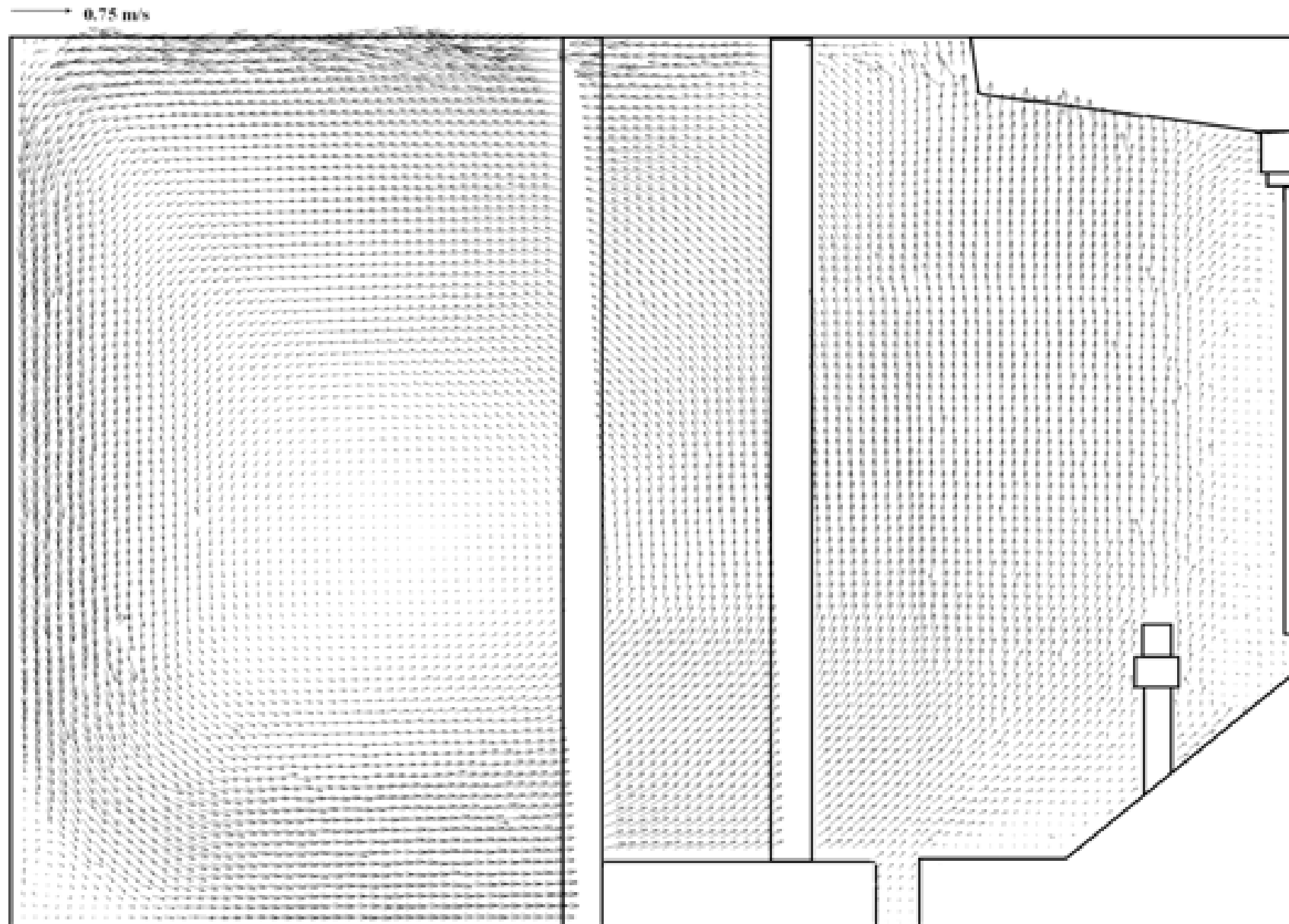


Figure (5.3): The (r - z) flow field map for the turbine alone configuration in the entire vessel.



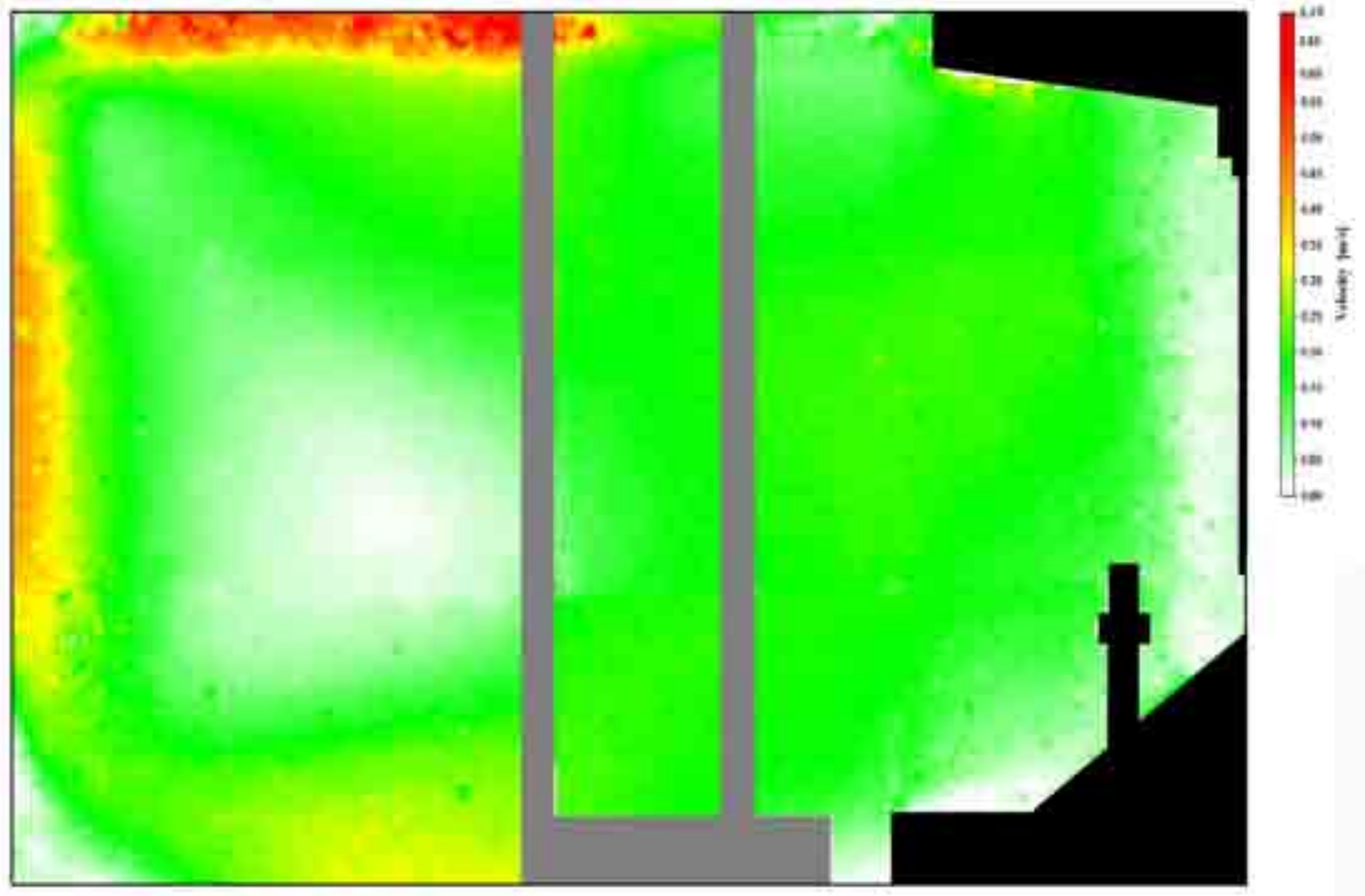


Figure (5.4): The (r - z) velocities contour map for the turbine alone configuration in the entire vessel.



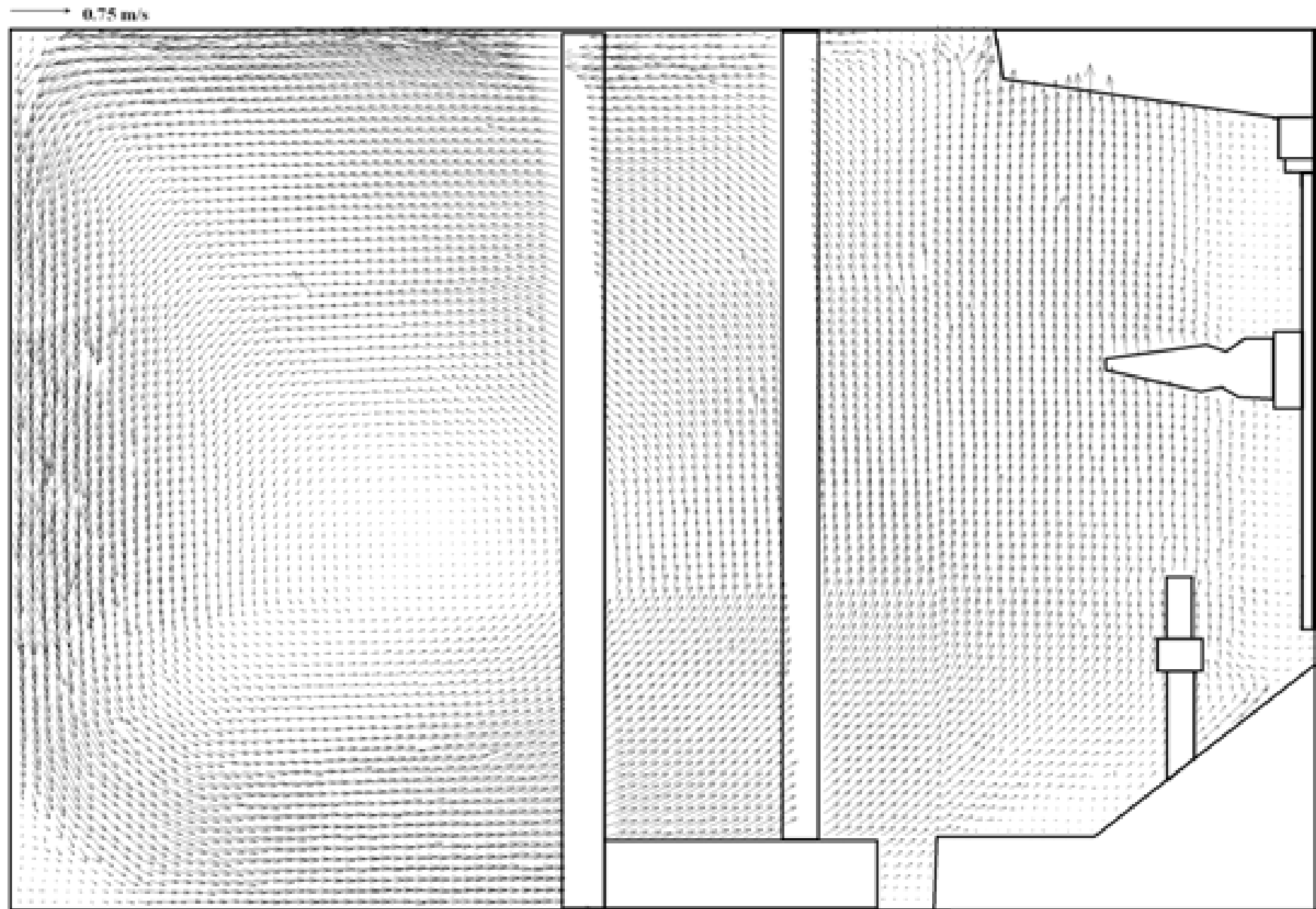


Figure (5.5): The (r - z) flow field map for the turbine and the RTP-U propeller configuration in the entire vessel.



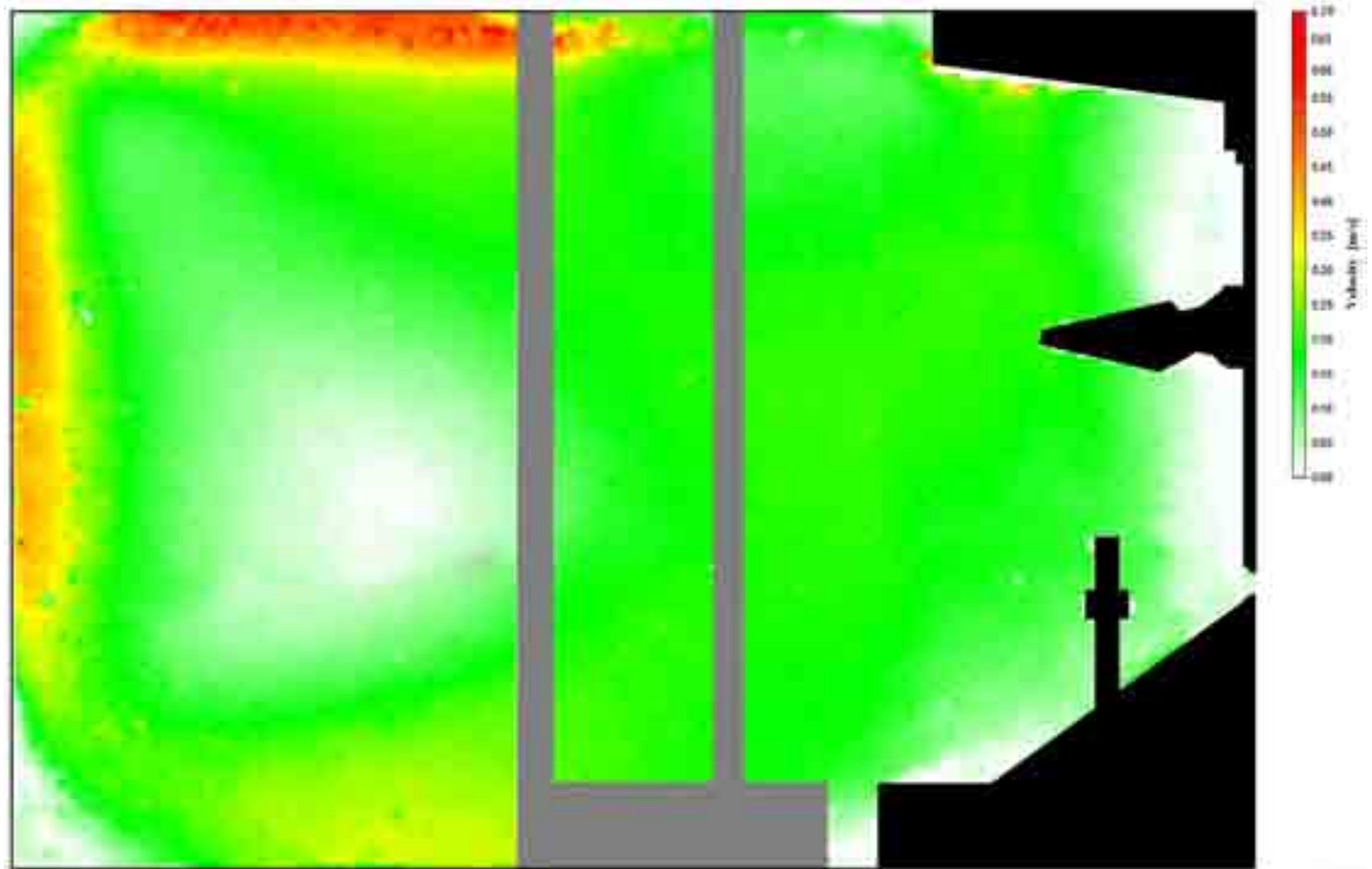


Figure (5.6): The (r - z) velocities contour map for the turbine and the RTP-U propeller configuration in the entire vessel.



### 5.5. Turbine Pumping Number and System Circulation Number

The turbine pumping number  $N_{Qp}$  (Flow number) and the system circulation number  $N_{Qc}$  for the three aerated configurations that investigated in this chapter are determined by equations 2.11 and 2.14 respectively, the used diameter in the calculation is the turbine diameter and illustrated in Table 5.1.

Table (5.1): Turbine pumping number and system circulation number.

Impellers Configuration	$N_{Qc}$	$N_{Qp}$
Whole system	2.42	0.49
Turbine + RTP-U	2.33	0.44
Turbine alone	2.24	0.40

Table 5.1 shows that for the whole system configuration, the turbine pumping number and the system circulation number are higher than those for both with and without draft tube and turbine alone configurations. The turbine pumping number is slightly increased with draft tube presence than the turbine alone configuration. From these values it is found that the presence of the draft tube assists the RTP-U propeller performance by redirecting part of the RTP-U propeller radial discharge flow discharge flow upward as it was seen in the up-pumping in the Mixing mode.

The RTP propeller function seems to have an obvious effect on the turbine pumping number and the circulation number of the system, where these parameters are relatively elevated, when the RTP-U propeller was positioned below the turbine, this elevation occurs due to the improvement of the intake flow of the turbine that achieved by the propeller action.

### 5.6. Agitation Index and Liquid Quantification for the Whole System Configuration

The agitation index (the volume-weighted average velocity) for the whole system configuration was calculated according to the equations (2.15 to 2.17). The agitation index is equal to 5.26%, this value is higher than for the non-aerated vessel with down-pumping mixing mode agitation index of 3.47% ( $N=5$  rps) despite that for the aerated mode the rotation speed is higher 2.08 rps and the presence of the air bubbles may hinder the mixing to be efficient easily. The agitation index in the aerated mode

is higher due to implemented geometry of the turbine compared with that of the RTP propeller.

The value of the agitation index in this case is low compared to those of classical configurations with dual impellers (8.8%) (Garcia-Cortes et al., 2006). This low value is due to the non-classical configuration for which the ratio agitator/tank diameter is quite low.

The liquid volume quantification or distribution for the whole system configuration (aeration mode) is illustrated in the Figure 5.7. The liquid volumes distribution in the aerated vessel is related with determined ranges of the composite mean local 2-D velocities in the vessel as demonstrated in the chapter four, where the composite mean velocities are determined as a 3-D surface chart. The liquid volume distribution in aerated vessel is presented in the vessel except the swept volume of the turbine and the RTP-U propeller and the volume taken by the cone at the vessel base or that is taken by the shaft or baffles edges.

Figure 5.7 shows that an important part of the liquid volume has relatively low mean velocities less than of the order  $0.22V_{tip}$  except three elevated mean velocity zones, this observation agrees with the r-z velocity contour (Figure 5.3), the high composite mean local velocity zones are same as r-z mean velocity contour.

These zones are localized in the liquid subsurface zone, near the vessel wall and near the vertical side of the turbine blades. The highest composite mean local velocity level is presented in the zone below the water surface with the ratio of 0.5-0.6 m/s. Both the zone near the vessel walls and the zone beside the turbine blades have lower local velocities ratio of 0.4-0.5 m/s.

### **5.7. The Mixing Time**

The mixing time investigations were carried out in the aerated mode, with impellers rotational speeds  $N$  ranges between (1.67 -3.33 rps). In the aeration mode it is very crucial to let the water droplets spray propelled by turbine blades and then plunged at water surface within the tank area, for this reason the upper limit for the impellers speed cannot exceed 3.33 rps. Two geometrical configuration were tested that the whole system and the turbine alone configurations wherein the RTP-U propeller and the draft tube were removed.

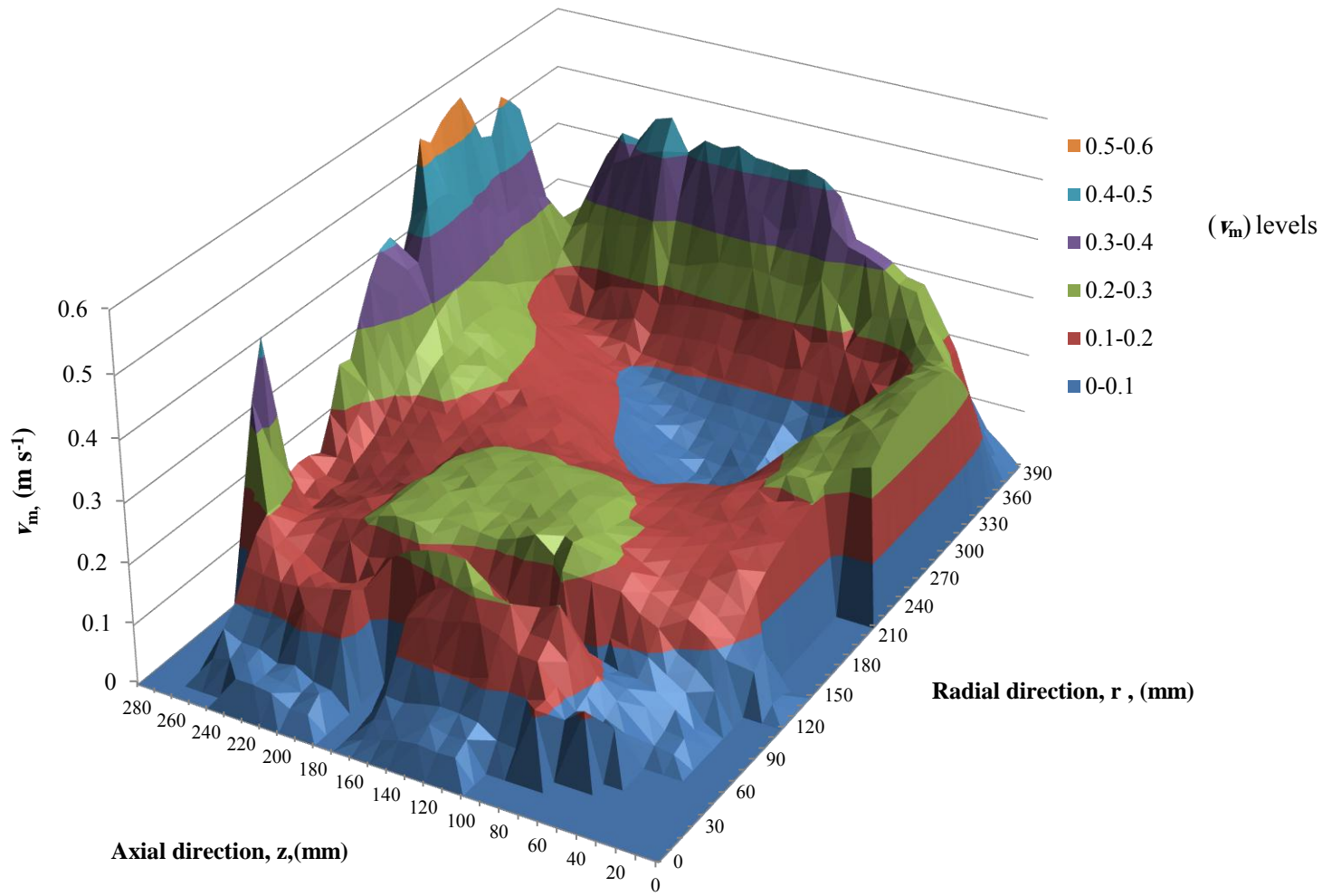


Figure (5.7): Distribution of the liquid volume in the vessel related with mean local composite velocity ranges for whole system configuration.



### 5.7.1. Impellers Rotational Speed Effect

The repeatability for the measurements is illustrated in Figure 5.8, where the results of two experimental runs for the mixing time number relation with rotation speed  $N$ . The mixing time number  $Nt_m$  values appear to be relatively close despite the increasing of  $N$ . The mixing time number  $Nt_m$  in the aeration mode (two phase system) can be fairly determined between 40-55 for adapted rotation speed range (1.67 -3.33 rps). The mixing time number shows for the given operated condition is lower than the values of the mixing mode non-aerated condition.

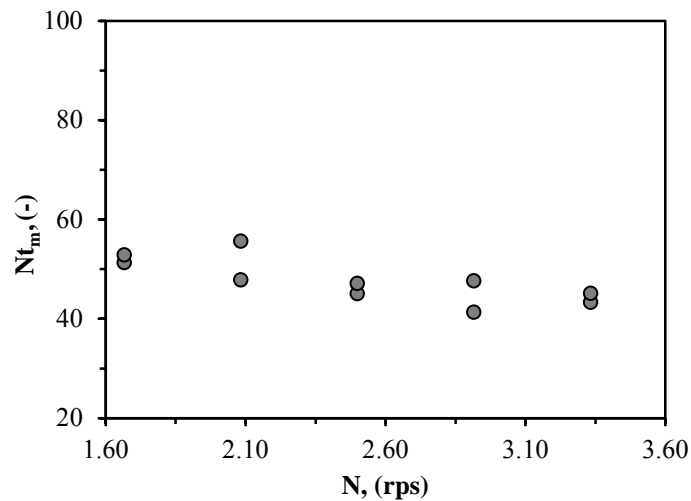


Figure (5.8): The relation between impellers rotation speed and the dimensionless mixing number  $Nt_m$  for whole system configuration in the aerated vessel.

The relationship of mixing time  $t_m$  with the impellers rotational speed  $N$  is illustrated in Figure 5.9. For the whole system configuration, the mixing time appears to be very dependent on the elevation of impellers rotation speed like the single phase condition (Mixing mode), where it decreases with increasing of the impellers speed. As a consequence this indicates that the mixing time in the aeration mode is highly effected by the flow pattern and the bubbles presence in the liquid phase.

For the turbine alone configuration, both the draft tube and the propeller are removed. Figure 5.9 shows the mixing time  $t_m$  is highly affected by the elevation of  $N$ . The mixing time  $t_m$  is lessened remarkably from 33 sec to 17 sec when the rotation speed was doubled (1.67-3.33).

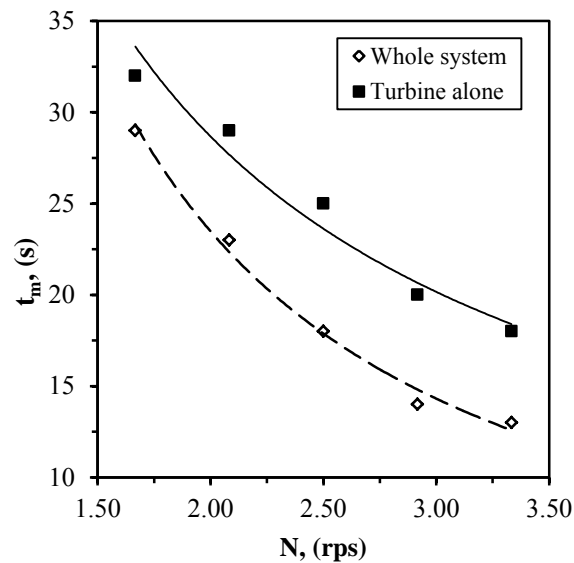


Figure (5.9): The effect of impellers rotation speed on the mixing time for two different geometrical configurations,  $h/D=1.47$ ,  $C_{pr}/T= 0.2$ ,  $C/T = 0.313$  (Aerated mode).

### 5.7.2. Effect of Propeller and Draft tube Presence

The propeller and draft tube effect during the aeration is investigated to interpret their contribution on the achieved mixing time  $t_m$ . The experiments are carried out for the rotational speeds  $N$  ratio as mentioned in previous section, for the turbine alone and whole system configurations.

As it is illustrated in Figure 5.9, the whole system configuration has lower  $t_m$  than of the turbine alone configuration for the given range of  $N$ . The importance of the RTP propeller and the draft tube contribution was interpreted by the low values of the accomplished mixing time  $t_m$ , where the performance of the RTP propeller and the draft tube assists to achieve the homogenization condition in the entire aerated vessel within slightly shorter mixing time. The effect of RTP propeller and the draft tube on the mixing time is interpreted by the relationship between dimensionless mixing time with Reynolds number for the two different configurations; the whole system and the turbine alone for different impellers rotation speed as shown in the Figure 5.10, where the dimensionless mixing time  $Nt_m$  is shorter with the presence of both the RTP propeller and draft tube, the improving of  $Nt_m$  was considerably increased with the increasing of the Reynolds number.

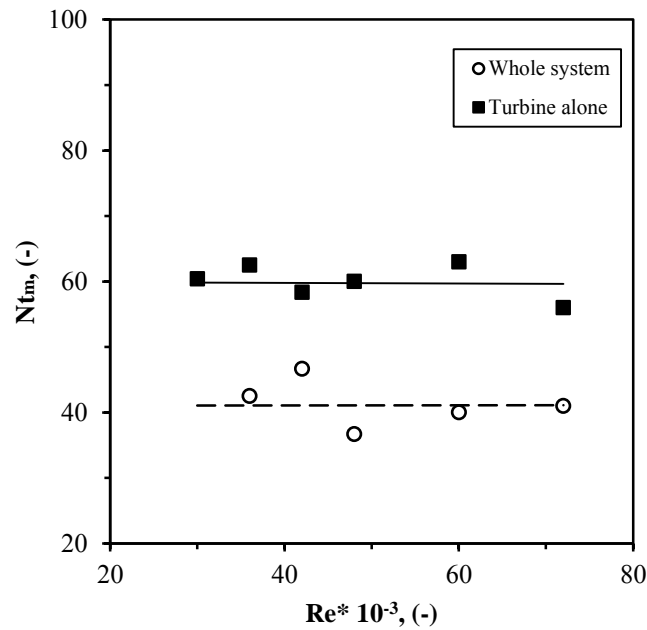


Figure (5.10): The relation between the Reynolds number and the dimensionless mixing time of the aerated vessel for whole system and turbine alone configurations,  $h/D= 1.47$ ,  $C_{pr}/T_v = 0.2$ ,  $C/T_v = 0.313$ .

### 5.7.3. Effect of the Spacing between Two Agitators

The spacing between  $S_p$  the turbine and the RTP-U propeller was tested to find out its effect on the mixing time. An additional lower position was examined of  $S_p= 83$  mm. This lower position is placed more inside in the draft tube than the primary position  $S_p= 76$  mm. The mixing time shows a slightly difference compared with first position as seen in the Figure 5.11. These results agree with (Hsu and Huang, 1997), the mixing time increased with increasing the spacing may come from the fact that longer spacing leads to weaker interaction between the two impellers.

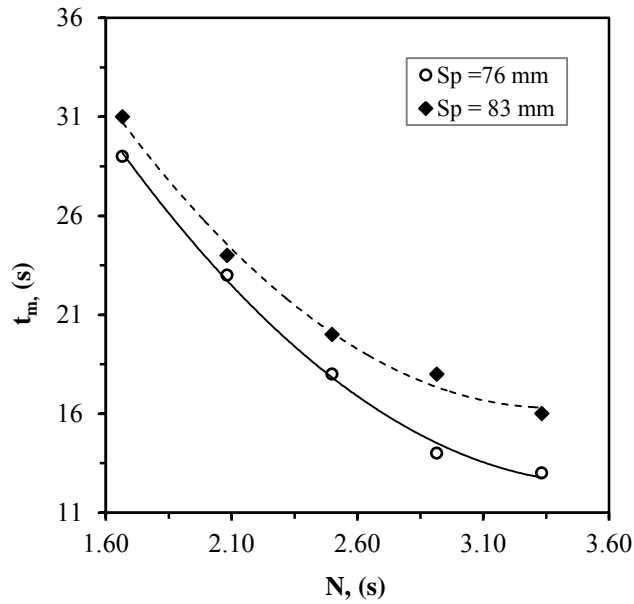


Figure (5.11): The relation between impellers rotation speed and the spacing between impellers;  $h/D = 1.47$ ,  $C/T_v = 0.313$ , (Aerated mode).

#### 5.7.4. The Effect of the Turbine Blade Submergence

The regular liquid level in the surface aeration is adapted just at the upper edge of the turbine blades. In other word a 100% submergence of turbine blades corresponds the ratio  $S/W=1$  or  $h/D = 1.47$ , where below this level the turbine blades are partially submerged and higher this level the turbine blades are over submerged. The experimental tests were performed to find the optimum turbine blade submergence that should be considered according to its effect on the mixing time within the range of  $S/W = 0.58, 1$  and  $1.42$  ( $h/D=1.42, 1.47$  and  $1.53$ ). This means that the turbine submergence at, upper and lower than the turbine upper edge level was examined respectively (i.e. the clearance of the turbine remains constant only the submergence is altered).

Figure 5.12, shows the relationship between dimensionless mixing time and Reynolds number for the investigated turbine blades submergences. It is found that the increase of turbine submergence leads to a decrease of the dimensionless mixing number, these results agree with the results founded by (Rodgers et al., 2011). Figure 5.12 shows that a high dimensionless mixing time was achieved at the turbine submergence ratio  $S/W$  that equals 0.58 because at this level the turbulence intensity was lowered as less water droplets were propelled by turbine blades and as a result less droplets are plunging into water surface and slower velocities were generated for the liquid circulation in the liquid bulk, as consequence longer mixing time takes place. In the case of higher water level,  $S/W$  that equals 1.42 (i.e. turbine blades are over

submerged,  $h/D= 1.53$ ), the dimensionless mixing number obtained are not much higher than that of,  $S/W$  equal 1.0 (water level is just at upper edge of turbine blades).

By these results it can be considered that for each impellers rotation speed the turbine blades are able to propel a certain quantity of water droplets into the air depending of the implemented turbine blade submergence.

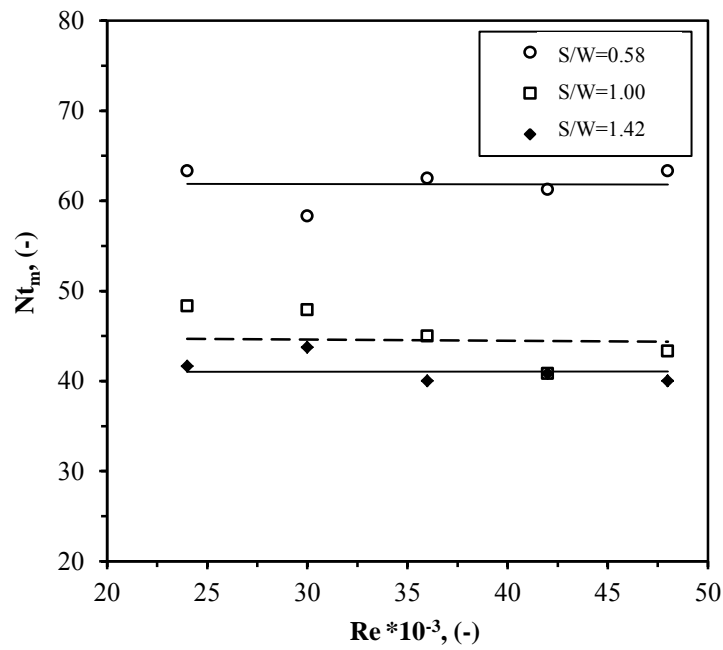


Figure (5.12): The relation between the Reynolds number and the dimensionless mixing time of the aerated vessel for three turbine blade submergence levels,  $C_{pr}/T= 0.2$ ,  $C/T = 0.313$ .

### 5.7.5. Mixing Time Modelling

From already developed correlations it can be noticed that the mixing time is found dependant on various relevant parameters that can be taken in account such as; the operational parameters which it in turn may include; rotational speed, acceleration of gravity and flow passing through the lower propeller blades (in multiple impellers case), the property parameters; water density and viscosity, the geometrical configuration parameters, such as the turbine diameter and blade submergence. Many other parameters can be involved in the influence on mixing time, where which is varied according to each system particularity.

The aerated mode mixing time correlation is usually depends on the performance criteria for the surface aeration system that obtained in the literature and from the experimental results. The applied investigated parameters for the mixing time in aerated mixing mode in previous works don't match the current case in order to correlate a model that can be impeccable for extrapolation and scale-up purposes.

## Chapter Five: Hydrodynamics and Flow Pattern in Aerated Agitated Tank

For the aerated condition, the main objective for the modelling is to characterize the mixing time for the used agitator system (Whole system configuration). According to the experimental results and observations, the most important relevant parameters for the target quantity mixing time,  $t_m$ , are demonstrated in the following relevance list;

$$[t_m; \rho, \mu; g, N, P; D, S, W] \quad (5.1)$$

By applying Buckingham II of dimensional analysis theory, the general influencing factors may affect the mixing time in surface aerated condition can be represented as:

$$Nt_m = f(N_p, Fr, Re, S/W) \quad (5.2)$$

Since all experimental runs are performed within turbulent regime,  $Re$  is eliminated (Zlokarnik, 1979) and the equation (5.2) is reduced and rearranged as follows:

$$Nt_m = a (N_p)^b (Fr)^c (S/W)^d \quad (5.3)$$

Equation 5.3 is solved to determine the values of the constants by applying multiple non-linear regressions for 62 experimental runs; the model will have the following form:

$$Nt_m = 32.42 (N_p)^{-0.62} (Fr)^{-0.44} (S/W)^{-0.16} ; S/W= 0.58-1.42; \quad (5.4)$$

Fr= 0.054-0.215;  
N<sub>p</sub>= 1.66 – 5.11

From equation 5.4 it can be found that the decreasing of the turbine blade submergence lengthens the mixing time within the range  $t_m \propto (S)^{-0.16}$ . This means when the submergence of the turbine blades decreased from 24 to 14 mm, the mixing time would lengthen by the factor 1.1.

The comparison between the model and the experimental results is shown in Figure 5.13. The agreement is quite satisfying. It is somehow hard to compare the constants in the equation (5.4) with the previous models because of the difference in the geometry and mode of operation applied, where the already developed aerated condition mixing time models didn't applied the water droplets projection principles to achieve the aimed aeration. But generally for the negative exponent of power number it seems to be logical and refers to that mixing time number is decreased with higher power consumption (Nienow, 1997). The  $(S/W)$  ratio exponent refers to the mixing time number is decreased when higher turbine blades submergence (higher liquid level) which doesn't agree with the model that developed by (Kang et al., 2001) with considering the difference in geometry with their system.

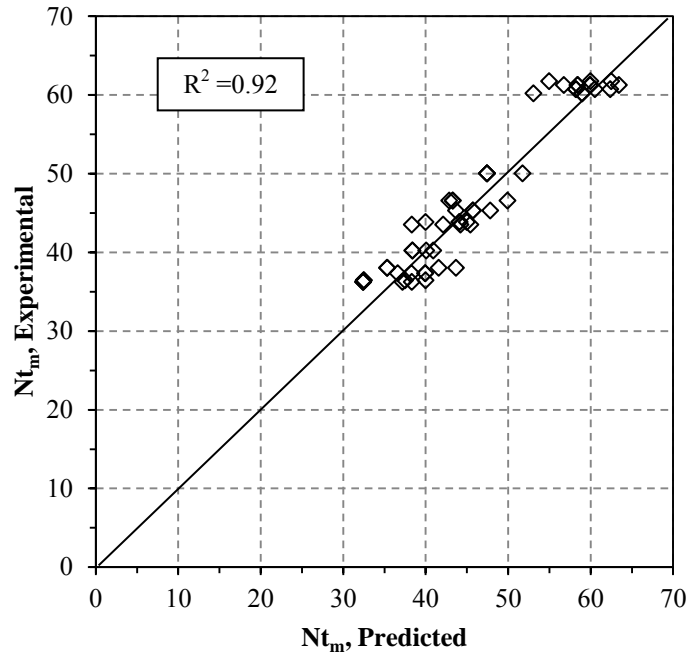


Figure (5.13): The comparison between experimental and predicted values of dimensionless mixing time number ( $t_m N$ ) by equation (5.4).

### 5.8. The Power Consumption in the Aeration Mode

The performance of RTP propeller and the draft tube in the enhancing of the mixing time in the up-pumping aeration mode is assessed as function of power consumption, as illustrated in Figure 5.14. In the case of the presence of RTP propeller and draft tube the  $N_p$  is slightly increased. The power number is calculated with respect to the diameter of the turbine.

The power per liquid volume relationship with  $N$  for aeration mode is illustrated in Figure 5.15. With the propeller and the draft tube the power consumed is slightly elevated due to their performance. The improvement of mixing time that accomplished for the whole system configuration didn't consumed much higher power than the turbine alone configuration. For the given implemented geometry, the power consumption per liquid volume ratio in this case is increasing with increasing impeller rotation speed  $N$  as it is illustrated in the Figure 5.14.

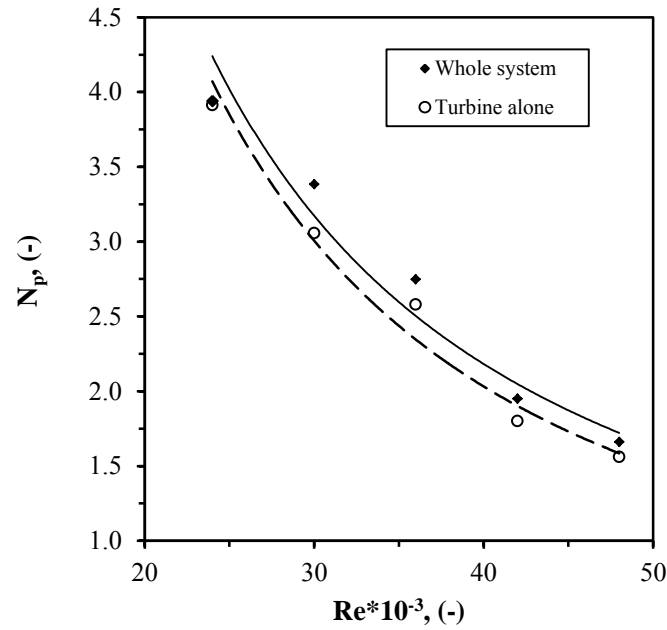


Figure (5.14): The effect of Reynolds number on power number for the two different configurations (Whole system and turbine alone);  $h/D= 1.47$ ,  $C_{pr}/T_v = 0.2$ ,  $C/T = 0.313$ , (Aerated mode).

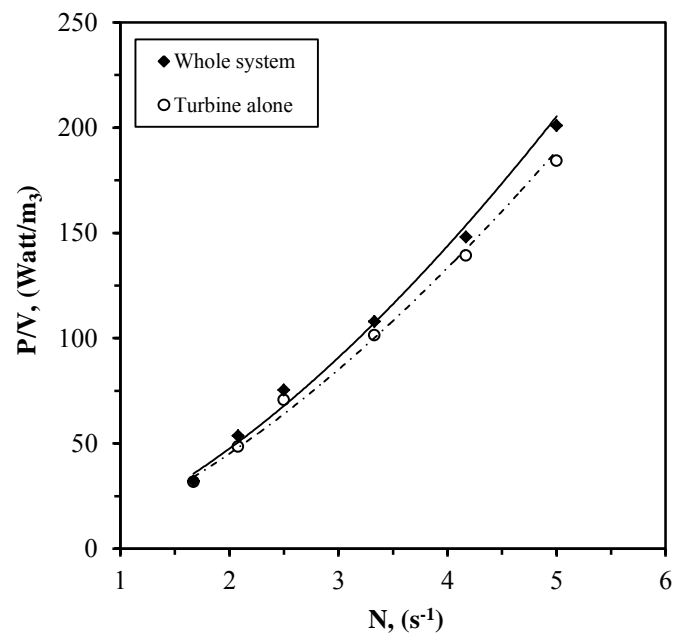


Figure (5.15): The relation between impellers rotation speed and the consumed power per water volume for the aerated mode,  $h/D= 1.47$ ,  $C_{pr}/T_v = 0.2$ ,  $C/T_v = 0.313$ .

### **5.8. Conclusions**

The flow patterns and r-z velocity vector fields and contour maps in aerated and agitated vessel were measured by employing PIV technique, the flow was generated by the turbine and RTP-U propeller for up-pumping and down-pumping operation modes with and without RTP-U propeller or the draft tube configuration. The measurement plane is same that used for PIV measurement in chapter 4 (Plane B).

The flow field didn't show an evident difference when the RTP-U and draft tube were removed, where the general circulation loop has kept its merits in all three configurations.

The circulation number and pumping capacity of the turbine showed a relative improvement when the RTP-U was place beneath. For the turbine and lower RTP-U propeller configuration: the turbine pumping capacity and the circulation number are mildly improved with draft tube presence.

Mixing time shows an obvious dependence upon the variation of the impellers rotation speed in different configurations for the aerated mode with different influence intensity.

From the results an optimum liquid level can be established. The mixing time is decreased effectively by lowering the liquid level as well as decreasing the turbine blade submergence lower than 100%. Moreover the elevation of liquid level as well as an increase in turbine blades higher than 100% submerged increases the mixing time but in a lighter manner than what occurs in decreasing the liquid level.

A model have been developed to interpret the mixing time number ( $N_{t_m}$ ) behaviour related to more significant and affecting dynamic and geometrical dimensionless parameters in the surface aerated agitated tank, the model is applicable for within the limits; ( $Fr = 0.054-0.215$ ), ( $S/W = 0.58-1.42$ ) and ( $P/V = 30-200 \text{ watt/m}^3$ ).

From the results and the observations performed in this chapter it is identified that none of the RTP-U and the draft tube configurations has improved separately the turbine performance regarding the turbine pumping number and circulation number. The liquid distribution that ranged according to the mean local velocity in the vessel agrees with pumping capacity behavior of the turbine. In summary with respect to turbine pumping capacity, circulation number and mixing time for the various tested configurations, it is figured out that both the PRT-U and draft tube can together enhance the performance of the surface aerator turbine.



# **GENERAL CONCLUSIONS AND PROSPECTIVE**



### **General Conclusions and Prospective**

The general global purpose of this thesis is to evaluate and interpret the capacity for the novel technology applied with the investigated surface aerator related to the possibility to perform the aeration or the mixing by the same equipment.

The first main objective of this study consists in the characterization of the aeration and the mixing modes capacities related to the operational and system configuration parameters. The second major objective involved the investigation of the flow pattern and velocity field takes place in the tank using advanced measuring techniques for both up-pumping aeration mode and down-pumping mixing mode.

The implemented surface aerator has a distinctive feature of easy putting in place between the aeration and the mixing modes by reversing the sense of the rotation where the oversaturation condition is frequently occur in the liquid bulk with existence of poor aerated zones. This interchanging is performed by applying the decoupling (clutching) system that enables the lower propeller to carry out the mixing with setting aside the turbine from the rotation.

A brief description was presented for the nowadays aeration systems for the water and wastewater treatment with exposing the types and efficiencies for each system, with emphasizing on the surface aeration.

From the literature review it is found that many modifications and developments are made on the surface aerators to improve the oxygen mass transfer rate and to reduce the power consumed. Many parameters have been studied like hydrodynamic, power consumption, geometric configurations, oxygen mass transfer rate in the water, modeling and scale up process. It can be presumed that in general the limiting factors for successful surface aeration can be resumed as follows:

- The turbulent regime should be ensured in the entire water treatment tank that contains sufficient dissolved oxygen entrained from atmospheric air.
- The generated water flow by surface aerators must be sufficient to reach all parts of the treatment tank.
- The aeration process accomplished with the aerator turbine must be accompanied by mixing and agitation performance to ensure an efficient distribution of the dissolved oxygen.
- These constrains can be overcome by using an appropriate surface aerator with suitable pumping capacity to handle efficiently and effectively the large quantities of water.

The measurements of the flow patterns and mean velocity fields were achieved by Laser Doppler Velocimetry LDV and Particle Image Velocity PIV. Accurate results have been obtained by these techniques.

For the water bulk zone it was found that the power consumption is related with turbine rotation speed and blades submergence more than other parameters in up-pumping aeration mode. It has been pointed out that a sufficient rotational speed, called critical speed, is necessary to accomplish aeration process. As it was observed the desirable flow patterns in the bulk zone can be obtained when the rotational speed is over the critical speed. The air bubbles creation appears in the vessel due to plunging water droplets through the water surface.

The water bulk oxygen mass transfer coefficient  $k_{l,a}$  is highly dependent on the turbine rotation speed in view of the increased  $k_{l,a}$  in the water bulk zone with increasing of impellers rotational speed. The rotational speed has to be lower than a roof value to ensure that the falling water droplets would not hit the vessel wall. An optimum water level was identified at the blade submergence ratio  $S/W$  equal to 1 regarding to the transferred oxygen mass transfer. The influence of the spacing between the impellers (turbine and propeller) stays related with the obligatory of remaining the lower propeller inside the draft tube. The compliance of the  $k_{l,a}$  to the spacing is exhibited by the highest  $k_{l,a}$  was obtained with the turbine presence with both the draft tube and propeller. It was found the  $SAE_b$  is more sensitive to rotational speed on contrary to water level variation.

Two correlation models are developed for water bulk zone; one for the oxygen transfer coefficient and another for power consumption. These models have acceptable confidence factor ( $R^2$ ) values. For surface aeration spray zone, a model is developed for standard oxygen transfer efficiency correlated with power consumption, spray Reynolds and Froude numbers and water level ratio. As usual, the model is applicable for particular limits.

For spray mass transfer zone, in the whole system configuration it is found that both the oxygen transfer rate  $OTR_{sp}$  and spray zone efficiency  $E_{sp}$  are dependent on the rotational speed and the turbine blade submergence. It is worth to mention that the spray oxygen mass transfer coefficients  $k_{l,a,d}$  is higher than liquid bulk oxygen mass transfer coefficients  $k_{l,a}$ . As a result it is figured out that the majority of oxygen mass transfer is achieved in the spray zone due to high interfacial area and turbulent mass transfer occurred in this zone.

The discharge flowrate of the water droplets spray  $Q$  strongly depends on impeller rotation speed and water level in the tank:  $Q$  is increased when impeller rotation speed or water level is increased for the given turbine blades submergence. The  $OTR_{sp}$  is calculated with and without the RTP propeller and the draft tube presence. The results showed that  $OTR_{sp}$  in whole system configuration is slightly higher than  $OTR_{sp}$  for the turbine alone configuration.

## General Conclusions and Prospective

---

The PIV and LDV measurements for the flow pattern were applied in a non-aerated single phase condition (mixing mode) and in aerated gas-liquid condition (aeration mode).

For the non-aerated condition, mainly one recirculation loop is generated with RTP-D propeller with two secondary loops with down-pumping operation mode. When the draft tube was removed the flow field didn't show any drastic change in the vessel core. For high rotational speeds, a surface vortex appears and extends to the propeller blade tip in the down-pumping mode when the draft tube is removed. The quantitative analyses were made for the axial velocities for both planes at 0° and 90° from the posterior baffle of the tank. The results showed that the velocity profiles are different for these two planes with draft tube presence especially in the region near draft tubes and below the propeller. This difference is lessened when the draft tube is removed. For non-aerated condition with up-pumping operation mode in the vessel core an overall circulation loop is generated and one important secondary loop is formed above the propeller. Similar velocity vector map is observed when the draft tube was removed. The pumping capacity of the RTP propeller doesn't exhibit a great change when the draft tube was placed. The up-pumping mode shows a slight elevation for the RTP-U pumping number compared with the down-pumping mode both with and without draft tube configurations. The power consumption for the RTP propeller is relatively dependent on the flow configuration. In the down-pumping mode slightly increasing in power consumption is noticed compare to up-pumping mode.

Mixing time results in the mixing mode (single phase conditions) show a clear dependence upon the RTP propeller rotation speed with different influence intensity. The mixing time is relatively increased when the draft tube was removed in the up-pumping mode. Contrary to the down-pumping mode the mixing time is enhanced when the draft tube was placed around the RTP-D propeller.

It is very difficult to clarify that one of the RTP configurations and pumping modes has an apparent influence to improve the RTP propeller performance in the single phase vessel, where with respect to RTP propeller pumping capacity, power consumption and mixing time for the various tested configurations and operation modes, it is found that no general approach can be recommended to improve the performance of the RTP propeller that is more efficient than the already approved of down-pumping mode with draft tube.

The down-pumping mode showed low mean composite local velocities with respect to those in the previous works for pitched blade impellers. These low mean velocities are due to the influence of the low propeller diameter to vessel diameter ratio. The up-pumping aeration mode mean composite local velocities were slightly elevated compared with those in down-pumping mixing mode.

For the aerated condition, the up-pumping flow is generated mainly by the turbine. The flow pattern didn't show an evident modification when the RTP-U and/or the

draft tube were removed. The general circulation loop has kept its merits in all three configurations, whilst the flow intensity was relatively higher when both the draft tube and RTP-U propeller (Whole system configuration) are positioned in the vessel. The flow is slightly more intensive when the the RTP-U was placed below the turbine, but less than the whole system configuration.

The circulation number and pumping capacity of the turbine showed a relative improvement when the RTP-U was place beneath. For the turbine and lower RTP-U propeller configuration: the turbine pumping capacity and the circulation number are mildly improved with draft tube presence.

The tested mixing time in the aerated gas-liquid condition for different configurations shows high relation with the impellers rotation speed with different influence intensity. With respect to mixing time it has been figured out that an optimum the turbine blade submergence (liquid level) can be established when the submergence was at the water surface level. This optimum parameter enables to achieve the desirable mixing performance in the bulk zone with shorter time. The mixing time was decreased submerged effectively by lowering the turbine blade submergence. Moreover the elevation of turbine blades submergence higher than the water surface increases the mixing time but in a lighter manner than what occurs in decreasing the blade submergence. A model is built to interpret the mixing time number ( $t_m N$ ) behaviour related to more significant and affecting dynamic and geometrical dimensionless parameters in the surface aerated agitated tank.

From the results and the observations with respect to turbine pumping capacity, circulation number and mixing time for the various tested configurations, it is found that both the RTP-U and the draft tube has improved the turbine performance. The liquid distribution that ranged according to the mean local velocity in the vessel agrees with pumping capacity behavior of the turbine.

Generally the wide-ranged studies performed in this thesis show that the proposed surface aerator system is found out efficient with respect to the aeration and mixing capacities compared to those actually implemented in situ.

The particular studies on the hydrodynamic in the aeration mode carried out in this thesis gave the necessary information on the used configurations. The whole system configuration appears to have the most desirable. As the flow pattern has been relatively improved when the draft tube and the propeller were positioned below the turbine.

The experimental investigations in this thesis reveal that the system set up is constructed in the way to be simple and easy to handle to facilitate the operation as a result the maintenance cost is reduced.

## General Conclusions and Prospective

---

The experimental studies on the operation condition in the thesis demonstrate that the critical rotational speed starts with the value 2.08 rps (effective bubbles distribution and water spray started with this point). The optimum turbine submergence is founded at the ration  $S/W=1.0$  (higher aeration efficiency and effective flow pattern are accomplished at this point). The upper reliable limit of the rotational speed is 2.5 rps after this limit water droplets start to be splashed out of the tank walls. It is founded also operating the system at optimum conditions (rotational speed, turbine submergence etc.), this prevents give a rise of the power consumption.

The presented trends of investigations in this thesis are expected to promote further surface aerator related studies. More knowledge about the water spray zone and the water surface condition are needed to determine of the oxygen mass transfer as the most of the oxygen is transferred within this zone and it is mainly controlled by surface condition. Also it will contribute to the development of the surface aerator efficiency. More specific flow pattern investigation could be performed on this zone to characterize water droplets projection and impingement, water spray and the condition for the water surface, as these parameters can affect drastically the transferred oxygen in the system. The presented study of the spray zone oxygen mass transfer in this thesis requires more studies to try to find out more accurate and competitive methods to measure the dissolved oxygen concentration in the water spray.

The experimental results obtained in this thesis have given limited information on the bubbles condition in the liquid phase. More studies are needed to characterize the bubbles condition inside water bulk. Such as the gas hold-up and the bubble size distribution could be determined inside the vessel by performing various accurate methods like photographic method, tomographic scanner, or other gas hold-up sensors. For the bubble size distribution many methods could be carried out like the optical sensors or image analysis methods.

Flow pattern in the aerated condition of the liquid phase generated by the up-pumping turbine involved radial and axial velocities field acquisition. In order to finalize this study a supplementary study is required on the produced tangential velocities in the tank. For the tangential velocity component that expected to be substantial, the laser sheet is positioned horizontally with a mirror placed beneath the stirred tank placed in inclined plane to elucidate the tangential flow occurred inside the vessel. The other technique could be implemented to have better flow visualization is the three dimensional PIV, where in this case two digital cameras are needed (Chung et al., 2007).

The changing between the aeration mode and the mixing mode is applied using a coupling (clutching) system. Other ways of exchanging between the mixing and

aeration could be explored in order to find out competitive methods accomplishing the same objective.

The mixing process investigation presented in this thesis has been carried out using one propeller type the RTP propeller. To enlarge this specific study other types of axial impellers could be investigated such as PBT. It is required to keep the symmetrical design of the tested propeller geometry in future works in order to maintain the capability to exchange between aeration and mixing modes.

The geometrical configurations of surface aeration system performed in this thesis have provided adequate information of mixing and aeration capabilities, however the results are limited for fixed geometries for the tank and the internals. Same investigations for the mixing and the aeration could be carried out with different system geometrical configurations to seek for new system capabilities promoted with geometrical alteration.

The CFD simulation of single phase mixing mode or gas-liquid phase aeration flow mode patterns could be performed depending on the experimental results obtained in this thesis. The CFD simulation could be employed to explore different geometrical configurations differ from that applied this thesis, which not only enables the investigation of various geometrical configurations for the vessel, impellers and vessel internals. But also with CFD implementation, the time, efforts and expenses could be reduced.

Scale-up for surface aerators can lean on the obtained experimental results to figure out the demonstration of the general elements for the extrapolation and to decide the types of the similarities that could be accomplished between the model type and the proto-type are described. The obtained information from the experimental runs in the lab scale could be verified for scaling-up purposes by applying this information in a larger industrial scale surface aerator on the basis of geometrical and dynamic similarity with that in lab. The  $SAE_b$  may be regarded as a main objective that should be maintained through extrapolation process.

# **APPENDIX I**

## **A REVIEW FOR BIOLOGICAL WASTEWATER TREATMENT WITH ACTIVATED SLUDGE**



## **Appendix I**

### **A Review for Biological Wastewater Treatment with Activated Sludge**

The clean water availability question becomes more and more as a developing important issue especially during the last decades. The necessity for wastewater treatment regarded as a very important compromise among the available solutions to preserve the water resources and to reduce the water pollution. The aerobic biological purification that implied in the wastewater plants consists of many steps; generally it can be divided into two main treatments: urban or domestic wastewater treatment and industrial wastewater treatment.

#### **I.1. Industrial and Domestic Wastewater Treatment**

Wastewater from the industry contains diverse constituents of various chemicals and undesirable deposits such as mineral scales, colloidal matters, corrosion products and biological growth (Amjad, 2010). These components are separated before the biological treatment. The removal and treatment of industrial waste water process depends on the characteristics of the industry that produces the wastewater like (cooling, desalination, oil production, etc.). Aeration with activated sludge is similar generally with that applied in domestic wastewater purification, in which the biological and physical-chemical wastewater treatments are combined (see Fig.I.1), the primary and secondary processes handle most of the non-toxic waste water. The primary treatment prepares the waste water for the next step of biological treatment. All un- dissolved solids, dirt, floatable solids and else are removed by settling or screening. In the secondary treatment the degradation process for the soluble organic compounds carried out in the aerated treating vessels and lagoons. In the tertiary treatment, different processes are used such as filtration (Eckenfelder et al., 2009). Sometimes the industrial waste water is accompanied with other types of pollutions such as the thermal pollution, where the waste water effluent is rejected with high temperature more than 35<sup>0</sup>C, which causes of deterioration of the aquatic systems. The other type of the industrial wastewater comes from the nuclear sites or radioactive waste treatment plants or from the explosion of uranium mines (Roubaty and Boeglin, 2007) and many of them contain radioactive pollution, similar treatments steps are exist for the domestic wastewater treatment, and they will be described in more details.



Figure (I.1): Process selection diagram for industrial wastewater treatment (Eckenfelder et al., 2009).

Domestic and industrial wastewater biological treatment is generally consisting in four main steps; (i) preliminary treatment, (ii) primary treatment, (iii) secondary treatment and (iv) tertiary treatment (See Figure I.2). There are two additional (auxiliary) treatments of sludge and odor treatment. These steps of the treatment combine the three types of treatment; chemical, physical and biological, where they used to eliminate the existence of pollutants (Sardeing, 2002).

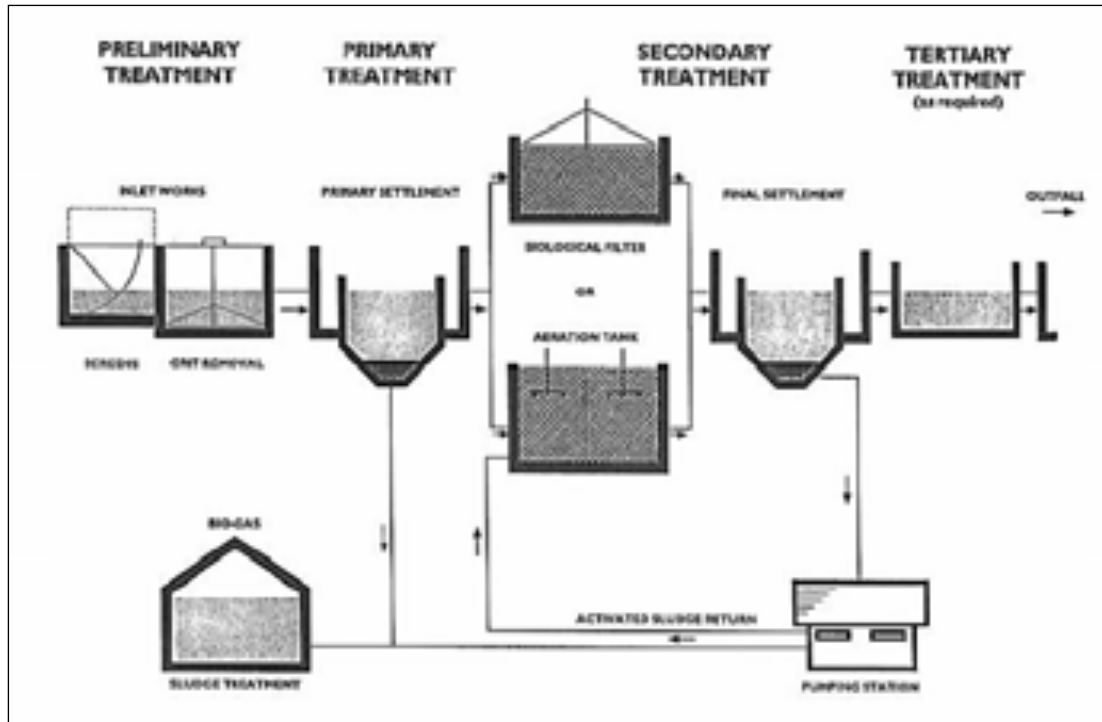


Figure (I.2): Domestic wastewater treatments steps (Try and Price, 1995).

### I.1.1. Preliminary Treatment Process

This treatment is used for gravity separation and accumulation of settleable solids from the wastewater. where the removal of these settleable and floatable solids such as (dirt, sand, etc.) by degreasing, sieving, filtering and settling to prevent their clogging the effluents distribution system (Clesceri, 2009).

### I.1.2. Primary Treatment Process

In the primary treatment, the solid particles that didn't settled out by the first step in the preliminary treatment will be settled out by decantation. These solids are mainly of organic or heavy metallic basis in the purpose of preparing the wastewater to the next biological treatment. The colloids and other suspended particles are removed by coagulation process especially the heavy metals pollutants combined with filtration, where colloidal particles destabilized by charge neutralization. The primary treatment contains other types of processes depend on the pollutants kind in the wastewater like equalization. It is employed to minimize or prevent high concentrations of toxic materials from entering the biological treatment plant and also to control the fluctuations in wastewater characteristics. Another process exist in this step is the neutralization, which is used if the acidic or alkaline materials are existed in wastewater in order to neutralize the discharge of the primary treatment step before further chemical or biological treatments (Eckenfelder et al., 2009).

### **I.1.3. Secondary Waste Water Treatment**

In this stage is the biological treatment is applied for the biodegradable organic pollutants with aerobic process and anaerobic process. It consists in converting them to stabilized non-pollutant materials such as nitrates, phosphates and carbonates, and then they are removed by settling. The aerobic process involves the implementation of activated sludge in the tanks, where the activated sludge is always in suspension condition during the aerobic process. The required air for the aerobic process is supplied by direct injection the air into the tanks or by entraining the atmospheric air from the wastewater surface through the surface aeration technique. The activated sludge contains the active bacteria that can be recycled to ensure the continuity the process, wherein the solid materials are separated in followed settled steps (Eckenfelder et al., 2009). Filtration is applied as a part of this stage of treatment to deliver the best feed material to the next step by separating the fine solids and suspended solids. Diverse filtration types are utilized such as membrane filtration. The organic or ceramic membranes separate the two phases the waste water and the micro-organisms to keep them inside the tank, where the membrane provides a physical barrier to the larger complex organics. The wastewater pumped across the membrane surface at high flow rate, some pollutants slowly accumulate on the membrane and that needs periodically cleaning with solutions containing chlorine, acids and/or bases (Try and Price, 1995).

### **I.1.4. Tertiary Wastewater Treatment**

The tertiary step is to enhance the removal of remaining pollutants such as suspended solids, organic matters, dissolved solids, toxic substance and nutrients (nitrogen and phosphorus) in the wastewater after the prior biological treatment steps. To improve the quality of the effluent removal a disinfection step is used to reduce the bacterial levels. The residuals that contain the suspended solids, organics or colloidal materials, are removed by filtration. The adsorption by activated carbon is also applied and used to remove the remaining organics (Eckenfelder et al., 2009). The disinfection process is achieved by the addition of chlorine or ozone. The other treatment in this step is implementation the micro-screening where, they are considered influential to accomplish the removal. Micro-screening include the use of low-speed continuously backwashed, rotting-drum screen operating under gravity- flow conditions (Gupta and Sharma, 1996; Shamma et al., 2006).

## **I.2. Activated Sludge Process**

Activated sludge is applied for both industrial and domestic wastewater treatment. The concept of this process is to create dispersed bacterial flocs and free-living micro-organisms that are suspended within the water (Gary, 2004). The activated sludge is

applied to eliminate the organics contained in the wastewater for both soluble and insoluble materials by converting them into a flocculent microbial suspension and they can be easily separated from wastewater by followed treatment steps like gravitational solid-liquid process (Eckenfelder et al., 2009).

Generally the activated sludge is employed in the aerated tanks, batch reactors, oxidation ditches, lagoons or long aeration basins with continuous flow and is mixed with the wastewater. The produced biological effluents are separated from the activated sludge and this sludge is returned to the inlet point of the basin or the tank to ensure the continuous treatment. A rapid rate of microbial growth occurs during the activated sludge process. The organic materials used to form oxidized end products like  $\text{CO}_2$ ,  $\text{NO}_3$ ,  $\text{SO}_4$  and  $\text{PO}_4$  or to produce the biosynthesis of new micro-organisms. The organic materials that are treated with the activated sludge are usually colloidal and larger sized particulates and they contain also some by contents of light nutrients. Most of these organic materials will be absorbed and agglomerated onto the microbial flocs (See Figure I.3).

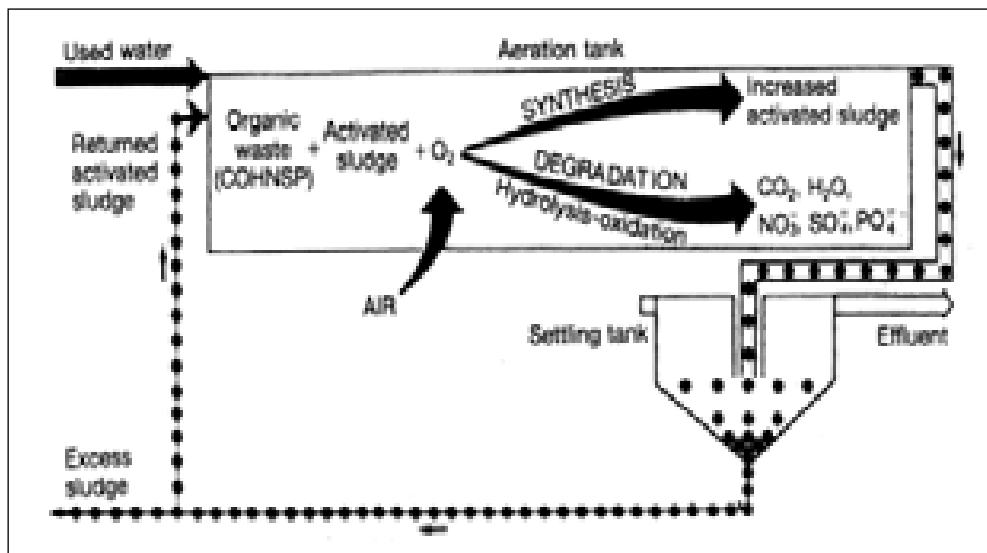


Figure (I.3): Development and control of biomass in the activated sludge process (Gary, 2004).

The activated sludge treatment depends on several process factors, especially the flocculation as described earlier. The successful agglomeration of the various organic materials is related to their flocculent growth when mixed with activated sludge, the settled biological materials from this operation are removed later by the separation from the wastewater. The flocs can be determined as a biomass cluster of several million heterotrophic bacteria bounded together with some inert organic and inorganic material (Gary, 2004). The process of activated sludge includes several implementations. Among of them there are nutrient removal processes:

### I.2.1. Nutrient Removal

Nutrient compounds presence in the wastewater comes from various sources, the quantities of the nutrients is in continuous raise , which required to be treated in order to eliminate it's disturbance on the ecological balance in the aquatic mediums and surrounding environment, (the eutrophication), (Nair et al., 2008; Wiesmann et al., 2007).

#### A. Nitrogen Removal

Nitrogen presents in different forms in the wastewater due to various oxidation states, which can be changed from one state to state to another a according to the different physical and biochemical conditions involving wastewater. The source of organic nitrogen may come from domestic wastes, farming activities and food industry. Most of bio-nitrogen in wastewater is present as ammonia of unstable organic compounds, but in urban wastewater, it contains excess nitrogen of the microbial requirement to oxidize the amount of carbon present, so only a part of nitrogen is being combined into the biomass (Crites et al., 2006).

The removal of the ammonia prevents its toxic effects on the aquatic life systems and the deterioration of water quality (Gupta and Sharma, 1996). In some cases the N<sub>2</sub>O gas could be emitted during nitrates removal from waste water as a secondary product. The emitted gas is controlled by additional techniques like intermittent aeration (Park et al., 2000).

The nitrogen is used by the biomass effectively, where ammonia is oxidized by autotrophic nitrifying bacteria to nitrite. The biological treatment of ammonia by oxidation is occurred in two stages each achieved by different type of nitrifying bacteria; they utilize the ammonia as an energy source in the first step, or the nitrite for same purpose in the second step as following:



And the second step as:



The nitrification implemented with slow growing bacteria therefore, it proceeds at low rate then, in order to achieve an acceptable treatment it needs maintaining more longer retention time for the activated sludge in the tank or the basin by keeping maximum contact with activated sludge to ensure maximum nitrification rate and to avoid wash-out of the nitrifiers. It is preferred in the nitrification process with activated sludge maintaining the dissolved oxygen concentration about (2.0 mg/l), where it is remarked that the nitrification doesn't occur below (0.5 mg/l), where with high dissolved

oxygen the process is not inhibited just up to (20 mg/l), it is found out the process is dependent on temperature and several organic matter existence (Gary, 2004).

Another process that occurred with nitrification is the de-nitrification where, nitrate can be converted through the producing the nitrite to nitrogen gas under low oxygen dissolved condition, this process occurred in the deprived of oxygen sludge layer of sedimentation tank after the aerobic biological nitrification (See Figure I.4).

There are many modifications essays to improve the nitrification process like applying the process involve activate sludge was immobilized onto support materials like cloth or polyurethane foam (Nair et al., 2008), whereas for high-strength ammonium wastewater that may contains industrial sources a two-sludge system for both nitrification and de-nitrification process applied (Carrera et al., 2003), The activated sludge nitrogen removal process also can be boosted by successful manipulating control system with using an aerobic/anoxic/oxic scheme (Baeza et al., 2002).

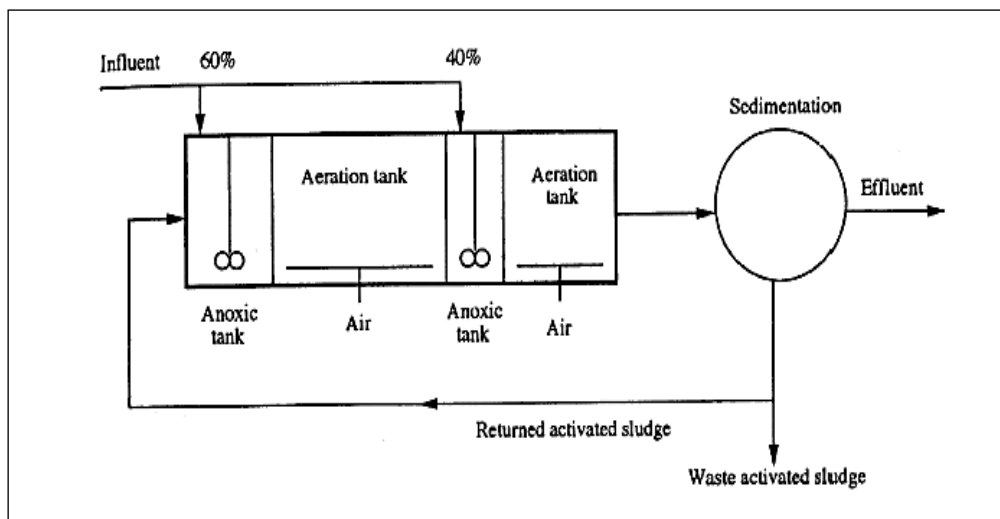


Figure (1.4): The schematic layout of two-stage nitrification and de-nitrification (Gary, 2004).

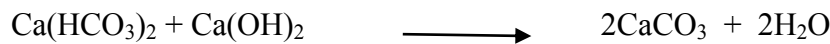
### B. Phosphorus Removal

The phosphorus exists in the wastewater in form of orthophosphates ( $\text{PO}_4^{3-}$ ,  $\text{HPO}_4^{2-}$ ,  $\text{H}_2\text{PO}_4^{-}$ ,  $\text{H}_3\text{PO}_4$ ), polyphosphates and organic phosphates, where its source is generally comes from fertilizing implementation. The total phosphorus concentration in wastewater is about (5-20 mg P/l), where only (1-2 mg P/l) is removed by biological treatment (Sincero and Sincero, 2003). The phosphorus in wastewater stream is removed by both chemical and biological methods (Figures I.5 and I.6); where the main biological phosphorus removal is anaerobic-oxic system. The bacteria

are conditioned in the anaerobic step with converting the phosphorus as soluble form, the biomass of the activated sludge works to absorb this soluble phosphorus in the followed aeration process step (See Figure I.5). With chemical removal step the final concentration in the treated wastewater effluent will be (1 mg P/l); in the anaerobic step the residence time depends on the (BOD: P) ratio in the inlet wastewater (Gary, 2004).

For specific treatment durations, there is deterioration for the biological phosphorus removal, which is happened when excessive aeration of the activated sludge occurred in previous treatment steps (Brdjanovic et al., 1998).

Usually coagulants are added after the biological treatment, where for the chemical part is the phosphorus is removed by the addition of coagulants to wastewater and then it removed as precipitates the inorganic forms of phosphates, many materials used as coagulants such as lime, aluminum salts or iron salts. In the case of lime addition to wastewater, it removes the phosphorus by two steps; in the first step it reacts with natural alkaline to produce the calcium carbonate:



Then the calcium ions combined with orthophosphate to form insoluble and gelatinous calcium hydroxyapatite.

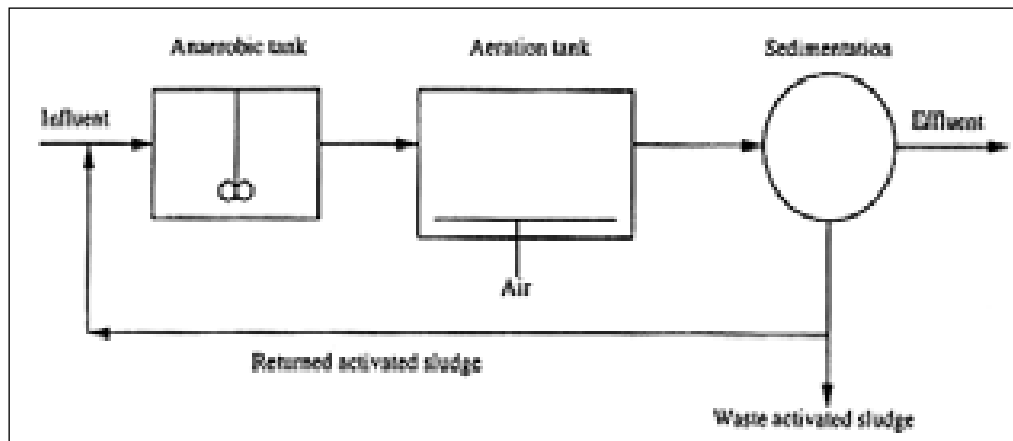


Figure (I.5): The Two stage biological phosphorus treatment (Gary, 2004).

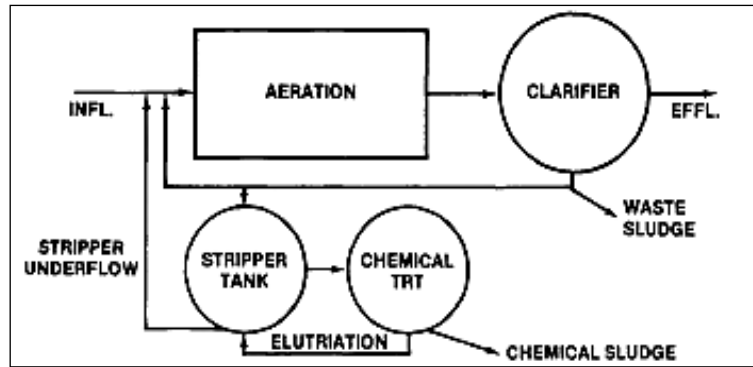


Figure (I.6): Chemical-biological phosphorus treatment (Phostrip process), (Barth and Stensel, 1981).

### I.3. Aeration Process in the Activated Sludge Treatment

The oxygen here is supplied by diffused or mechanical aeration systems, where the process is entirely biological treatment as a form of stabilization lagoon or basin used in order to settling, removal of suspended solids, aeration and equalization beside the biological treatment. The oxygen supply in aerated lagoons depends on the mechanical aeration devices properties like the power level used for aeration.

The aerated lagoons has many advantages such as low operational and maintenance cost, lagoons doesn't pass any harm to the environment in the same time it act very effectively for wastewater treatment (Clesceri, 2009).

In the last 20 years a similar technique to lagoons is applied that is pond aeration systems but of course without utilizing activated sludge, which became more and more in demand to preserve the aquatic life like fish and bio-organisms to sustain this aim , many air delivering tools employed like paddle wheel aerators (Boyd, 1998).

The pure oxygen is used with activated sludge process instead of using air due to its effective oxygen dissolution rate during aeration operation. The injection of pure oxygen to the liquid is applied in two process types that are covered and uncovered process:

- (i) The covered process, in order to transfer about 90% of the oxygen to the liquid phase the technique of series of covered aeration tanks is used. (See Figure I.7).
- (ii) The uncovered process, this method involves the usage of spargers or diffusers of oxygen in deep position inside the liquid wastewater, so high concentration of dissolved oxygen that reaches the activated sludge despite that opened cover of treatment tank (Baeza et al., 2002; Carrera et al., 2003; Mueller et al., 2002).

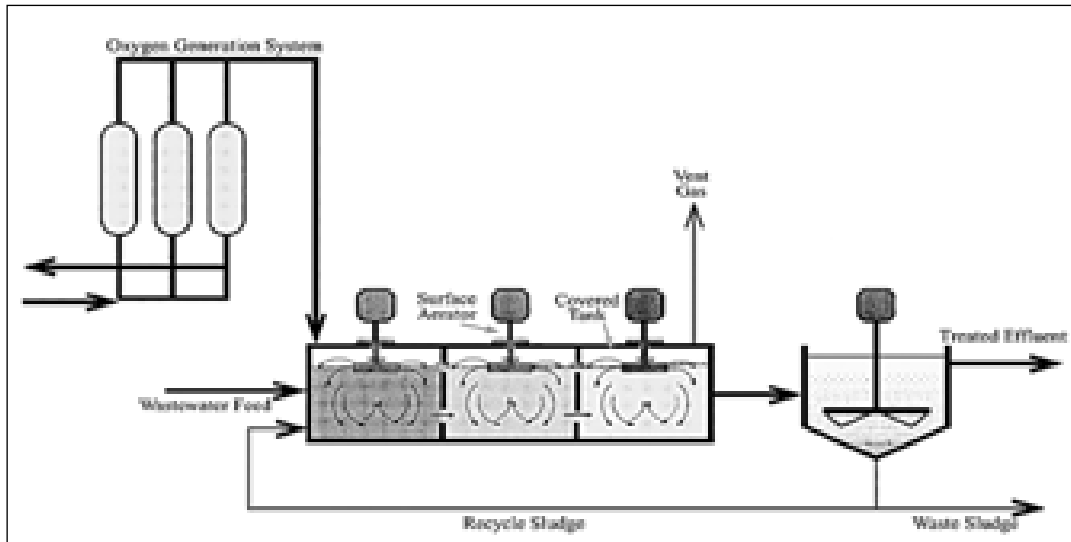


Figure (I.7): Covered aerated tank using pure oxygen (Mueller et al., 2002).

Usually the aeration is performed with active sludge in tanks or basins, their depth vary from (3.5 – 6.0 m) to about (20-30 m ) equipped with air diffuser below the liquid and inject the air or oxygen , where these types are preferred to treat industrial wastewater especially with proper type of aeration tools was chosen. An effective process that preferred to treat synthetic wastewater can remove more than 95% of COD from the effluent (Polprasert and Raghunandana, 1985; Sincero and Sincero, 2003).

## I.4. Additional Treatments

### I.4.1. Sludge Treatments

Many processes treat the sludge settled down during the wastewater treatment stages. The sludge produced is different for each one of implemented stages, the treatment of settled sludge is expensive so in several times it returned to the inlet and settled out with the primary sludge especially for the sludge that produced in the primary and secondary steps. Generally the sludge treatment contains warming to (35 °C) for at least two weeks to ensure that the organic solids were biologically broken down as what called the digestion treatment, the accompanied produced gas is used to heat the sludge (Clesceri, 2009; Try and Price, 1995).

The anaerobic and aerobic digestion by biochemical oxidative stabilization of the sludge used in open or closed tanks separated from liquid process system.

### **I.4.2. Odor treatment**

As a final step to treat the wastewater stream is malodor gases elimination or what is called odor treatment, where its implied by either biological or chemical methods, the biological way is implemented for biological volatile organic compounds are removed by biological filters or biological scrubbers (Kleinheinz and Wright, 2009), while the chemical method is applied for odorous gases associated with volatile organic compounds (VOC) like hydrogen sulfide and ammonia and other gases, the dissolved gases stripped out of the liquid during the agitation or aeration, this method implies chemical scrubber system and air/oxygen injection system.



## **APPENDIX II**

# **DERIVATION OF SPRAY FLOWRATE FOR THE SURFACE AERATION SYSTEM**



## Appendix II

### Derivation of Spray Flowrate for the Surface Aeration System

Fluid mechanics analysis of the surface aerator system is performed to find a logical way to calculate the water spray flowrate  $Q$ , where direct experimental measurement of  $Q$  would be extremely difficult and expensive to accomplish this objective (McWhirter et al., 1995). This calculation depends on the basic physical principles that occurred in the surface aeration system related to the volumetric flow rate  $Q$  of the water spray discharged by the surface turbine blades into atmospheric air.

The spray flowrate can be determined by consideration of the overall conservation of energy applied to a surface aeration system and the measured overall power input to the aerator (Baylar et al., 2001; McWhirter et al., 1995). (McWhirter et al., 1995) envisioned the surface aeration system as impeller blades rotating in the free liquid surface of a relatively large body of water, they considered the surface aeration turbine impeller blades accelerate a flow rate of liquid  $Q$  from a relatively low velocity at the inlet to the impeller blades up to a relatively high velocity at the discharge from the tip of the aerator impeller blades.

The general power input to the surface aeration system is a mechanical energy transfer to the water bulk and then it is converted to kinetic energy in the water spray as explained in chapter two, this power input can be presented as the following equation (Baylar et al., 2001).

$$P_{in} = \frac{\rho g Y_m Q}{\eta} \quad (II.1)$$

The fluid friction losses for the water flow across the surface aerator turbine blades is considered negligible, the efficiency is assumed 100% as a result all the mechanical energy is converted with 100% to a kinetic energy, so the efficiency,  $\eta$ , equals to 1.  $Y_m$  represents the height between the upper point of the water spray maximum point.

$$P_{in} = \rho g Y_m Q \quad (II.2)$$

By applying the general energy balance of Bernoulli equation between two points 1 and 2 as illustrated in Figure (II.1), where the total energy of a fluid in motion consists of the following components; potential, pressure and kinetic energies (Holland and Bragg, 1995).

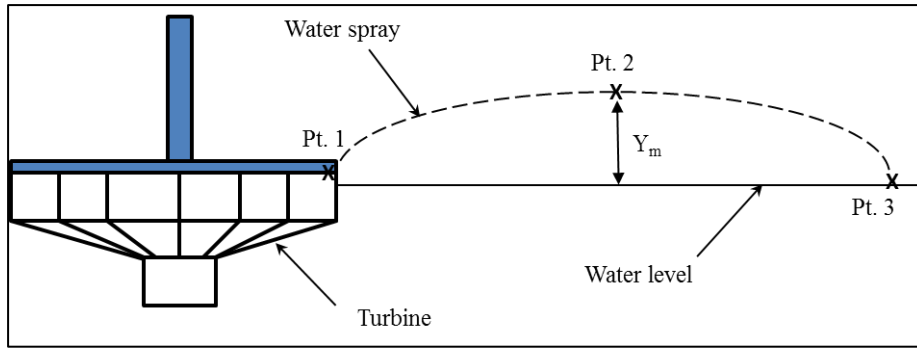


Figure (II.1): The energy balance points for the spray discharge flowrate.

$$z_1 g + \frac{p_1}{\rho_1} + \frac{v_1^2}{2} = z_2 g + \frac{p_2}{\rho_2} + \frac{v_2^2}{2} \quad (\text{II. 3})$$

Equation II.3 is reduced to equation II.4 as the pressures for the two points are same (the atmospheric pressure).

$$(z_1 - z_2)g = \frac{v_1^2 - v_2^2}{2} \quad (\text{II. 4})$$

Since the spray velocity  $v_2$  at the upper point (point 2) of the spray is equal to zero

$$(z_1 - z_2)g = \frac{(v_1)^2}{2} \quad (\text{II. 5})$$

By replacing the terms in Equation II.4 as following

$$(z_1 - z_2) = Y_m \quad (\text{II. 6})$$

The water is propelled from the tip of the turbine blades will be subject to the same kinematic laws of physics as any free falling projectile (McWhirter et al., 1995), so the velocity at the impingement point equals the velocity at the turbine blades tip.

$$v_1 = v_3 = V_{sp} \quad (\text{II. 7})$$

So Equation II.2 can be written as follows

$$P_{in} = 0.5\rho Q V_{sp}^2 \quad (\text{II. 8})$$

Equation II.8 is written as follows, for power input in kW and flowrate in liter/h

$$P_{in} = 1.389 \times 10^{-7} \rho Q V_{sp}^2 \quad (\text{II. 9})$$

Where the constant  $1.389 \times 10^{-7}$  includes the unit conversion factor and it depends on system geometry as the discharge flowrate depends on the turbine geometry.

## Appendix II: Derivation of Spray Flowrate for the Surface Aeration System

The flow rate  $Q$  is assumed to be constant along the spray, where the flow rate  $Q$  into the atmospheric air at a relatively high total discharge velocity  $V_{sp}$  from the tip of the turbine blades can be applied at the impingement point at the water surface. With negligible friction loss all of the aerator shaft power input goes into accelerating the flow rate of liquid spray  $Q$  up to the discharge velocity  $V_{sp}$  (McWhirter et al., 1995), so equation II.8 can be applied to relate the total power input with the discharged spray flowrate and spray velocity  $V_{sp}$  at impingement point.



## List of Symbols

### Latin symbols

a	constant in equations 3.2, 3.3 and 3.6 (varying)
a term in $k_1a$	interfacial area per unit volume in water bulk, ( $m^2 m^{-3}$ )
$a_d$ term in $k_1a_d$	interfacial area per unit volume in water droplets, ( $m^2 m^{-3}$ )
$A_d$	interfacial contact area of the water droplets, ( $m^2$ )
b	constant in equations 3.2, 3.3 and 3.6, (varying)
c	constant in equations 3.2, 3.3 and 3.6, (varying)
$C_d$	concentration of dissolved oxygen in water droplets, ( $mg L^{-1}$ )
$C_{dt}$	concentration of dissolved oxygen in water droplets at time t, ( $mg L^{-1}$ )
$C_e$	concentration of dissolved oxygen measured by the probe, ( $mg L^{-1}$ )
$C_l$	dissolved oxygen concentration in liquid, ( $mg L^{-1}$ )
$C_{LS}$	saturated concentration of dissolved oxygen in water, ( $mg L^{-1}$ )
$C_{Lt}$	concentration of dissolved oxygen in water at time t, ( $mg L^{-1}$ )
$C_{pr}$	propeller clearance, (m)
$C_s$	concentration of dissolved oxygen at saturation, ( $mg L^{-1}$ )
$C_{sd}$	saturated concentration of dissolved oxygen in water droplets, ( $mg L^{-1}$ )
$C_{s10^{\circ}C}$	saturation concentration of dissolved oxygen at $10^{\circ}C$ , ( $mg L^{-1}$ )
$C_t$	concentration of dissolved oxygen at time t, ( $mg L^{-1}$ )
$C_{tr}$	turbine clearance, (m)
$C_o$	initial concentration of dissolved oxygen at time $t=0$ , ( $mg L^{-1}$ )
d	constant in equation 3.2, (varying)
D	turbine diameter, (m)
$d_f$	draft tube diameter, (m)
$d_{pr}$	propeller diameter, (m)
$E_{md}$	Murphree contacting efficiency for oxygen mass transfer, (-)

## List of Symbols

---

$E_{sp}$	spray mass transfer zone efficiency, (-)
$(E_{sp})_{20}$	standard spray mass transfer zone efficiency at 20 °C, (-)
$f$	temperature correction function to 20 °C for the spray mass transfer zone, (-)
$Fr$	Froude number, $(ND^2/g)$
$Fr_{sp}$	modified Froude number for water spray, $(gY_m^3)/q_{sp}$
$g$	acceleration of gravity (9.80665), $(m^2 s^{-1})$
$h$	water level in the vessel, (m)
$H$	height of apparent turbine blade above water surface, (m)
$I_g$	agitation index, (%)
$k$	oxygen mass transfer parameter $(k_{la20}(v^2/g)^{1/3})$ , in equations (1.12,1.13,1.14 and 1.15), (-)
$k_{la}$	volumetric oxygen mass transfer coefficient (Liquid bulk mass transfer zone), $(s^{-1})$
$k_{lad}$	volumetric oxygen mass transfer coefficient (Spray mass transfer zone), $(s^{-1})$
$k_{la10^\circ C}$	volumetric oxygen mass transfer coefficient at 10 °C (Liquid bulk mass transfer zone), $(s^{-1})$
$k_{laT}$	volumetric oxygen mass transfer coefficient at T °C (Liquid bulk mass transfer zone), $(s^{-1})$
$N$	rotation speed, $(s^{-1})$
$N_p$	power number, $(P/ \rho N^3 D^5)$
$N_{Qp}$	Pumping number, $(Q_p / ND^3)$
$N_{Qc}$	circulation number, $(Q_c / ND^3)$
$OTR_b$	oxygen transfer rate in water bulk mass transfer zone, $(kgO_2 h^{-1})$
$OTR_{sp}$	oxygen transfer rate in water spray mass transfer zone, $(kgO_2 h^{-1})$
$P$	power consumed, (watt)
$P_{in}$	the input power to the turbine (that assumed 100% converted to kinetic energy to propel water spray into the air), (k watt)
$Q$	volumetric flowrate of the water spray, $(m^3/s)$

## List of Symbols

---

$Q_c$	circulated flow rate in the vessel, ( $m^3/s$ )
$Q_p$	flow rate by propeller, ( $m^3/s$ )
$Q_{pr}$	radial flow rate by propeller, ( $m^3/s$ )
$Q_{pz}$	axial flow rate by propeller, ( $m^3/s$ )
$q_{sp}$	water spray volumetric flowrate per spray radius, ( $m^3 m^{-1}$ )
$r$	radial coordinate, (m)
$R$	draft tube radius, (m)
$r_{cent}$	radial coordinate at circulation center, (m)
$Re$	Reynolds number, ( $\rho ND^2/\mu$ )
$Re_{sp}$	modified Reynolds number for water spray, ( $Q/v$ )
$R_m$	maximum radius of the water spray, (m)
$R_{sp}$	radius of the water spray calculated from the shaft center, (m)
$S$	turbine blades submergence, (m)
$SOTR_b$	standard oxygen transfer rate in water bulk mass transfer zone, ( $kgO_2 h^{-1}$ )
$SAE_b$	standard aeration efficiency in water bulk mass transfer zone, ( $kgO_2 kWh^{-1}$ )
$t$	time, (s)
$T$	vessel diameter, (m)
$t_f$	flight time of water droplets, (s)
$t_m$	mixing time, (s)
$T_o$	torque measured with filled vessel, (N m)
$T_{oe}$	torque measured with empty vessel, (N m)
$T_v$	vessel diameter, ( $^{\circ}C$ )
$V_a$	the mean velocity of the water spray radial and tangential velocities components, ( $m s^{-1}$ )
$V_d$	water droplet volume, ( $m^3$ )
$V_L$	liquid volume, ( $m^3$ )

## List of Symbols

---

$v_m$	mean volume weighted velocity, ( $m s^{-1}$ )
$V_{sp}$	water spray velocity, ( $m s^{-1}$ )
$V_r$	radial component of the water spray velocity, ( $m s^{-1}$ )
$V_y$	axial component of the water spray velocity, ( $m s^{-1}$ )
$V_{tip}$	propeller blade tip speed ( $m s^{-1}$ )
$v_r$	liquid bulk mean radial velocity ( $m s^{-1}$ )
$v_z$	liquid bulk mean axial velocity ( $m s^{-1}$ )
$V_y$	axial component of the water spray velocity, ( $m s^{-1}$ )
$V_\phi$	tangential component of the water spray velocity, ( $m s^{-1}$ )
$V_{oy}$	initial axial component of the water spray velocity at time $t_f=0$ , ( $m s^{-1}$ )
$V_r'$	radial velocity of the water spray at impingement point, ( $m s^{-1}$ )
$V_y'$	axial velocity of the water spray at impingement point, ( $m s^{-1}$ )
$V$	water volume, ( $m^3$ )
$W$	turbine blade width, (m)
$W_T$	square tank width in equation (1.10), (m)
$Y$	sorption number in ref. (Zlokarnik, 1979), (-)
$Y_m$	maximum droplets height, (m)
$z$	axial coordinate, (m)
$z_{cent}$	axial coordinate at circulation center, (m)

### Greek Symbols

$\rho$	water density, ( $kg m^{-3}$ )
$\tau$	probe time constant, (s)
$\mu$	water dynamic viscosity, ( $kg m^{-1} s^{-1}$ )
$\nu$	water kinematic viscosity, ( $m^2 s^{-1}$ )

**Impellers types abbreviations**

APV-B2 D, U	hydrofoil impeller (developed particularly for gas dispersion), down and up pumping
A310-D	Lightnin A310 impeller, down pumping
EE D, U	elephant ear impeller, down and up pumping
HF-D	hydrofoil impeller, down pumping
HF4-D	hydrofoil impeller (has three blades with a blade angle of 35° and a twist of 15° in the tip region), down pumping
MTT D, U	Mixel TT impeller, down and up pumping
PBT D, U	pitch blade turbine, down and up pumping
RTP D, U	reversal twisted pitched blade propeller, down and up pumping



## List of Figures

### Chapter One

Figure (1.1): Plate diffuser aerator,(Permax H ceramic plate diffuser, (Supratec Co. Ltd.).....	10
Figure (1.2): (a) Tube diffuser aerator, (b) Disc diffuser aerator, (Gemgate GmbH).....	11
Figure (1.3): Static tube diffusers (Process Engineering s.r.l).....	12
Figure (1.4): Submerged turbine aerator, (ARS-ARS/S Radial submersible aerator, (Caprari S. p. A.).....	14
Figure (1.5): Hydro Jet Aerator, Plaquette Aerodyn, (Biotrade Co.).....	14
Figure (1.6): Flow diagram for uncovered pure oxygen aeration (Mueller et al., 2002).....	15
Figure (1.7): Horizontal flow aspirating aerator, Aspirator, (AIRE-O2 Aeration Industries International).....	16
Figure (1.8): Low speed vertical flow aerator Up-ward flow,Praxair Technology.	17
Figure (1.9): Low speed vertical flow aerator (Down-ward flow), (a) Turboxal (Aire Liquide), (b) Praxair (Praxair Technology).....	17
Figure (1.10): Low speed horizontal flow aerator (Twin mini rotor aeration, (Botjheng Water Ltd.).....	18
Figure (1.11): High speed surface aerator, Aqua turbo (AER-AS), (AQUATURBO SYTEMS inc.).....	19
Figure (1.12): The surface aeration regimes applying air entrainment from free liquid surface (A) Direct entraining of the atmospheric air, (B) Spray formation and entraining the air with droplets impingement at the surface,(Patwardhan and Joshi, 1998).....	21
Figure (1.13): The histogram distribution of measured aeration efficiency for (111) low speed surface aerators in field, the average is 1.49 kgO <sub>2</sub> /kWh, (Heduit and Racault, 1983b).....	27
Figure (1.14): The relation between surface aeration impeller blades submergence and oxygen transfer rate for different blades number, (where H is the liquid level in the tank) (Backhurst et al., 1988).....	30
Figure (1.15): Relation between sorption number (Y) with the Froude number (Fr) for the conical shape turbine surface aerator (Zlokarnik, 1979).....	36

## List of Figures

---

Figure (1.16): Bubble distribution of surface aerator system of rotation speed $N=110$ rpm, liquid level $h=0.66$ m. (Lee et al., 2001).....	41
Figure (1.17): The relation between the rotation speed and mixing time for surface aeration dual impeller system, (Kang et al., 2001).....	42
Figure (1.18): The relation between the Reynolds number and power number for three different liquid conditions, clean water and two types of activated sludge mixed liquid (Takase et al., 1982).....	44
 <b>Chapter Two</b>	
Figure (2.1): The schematic diagram of the experimental apparatus.....	52
Figure (2.2): The turbine, propeller and draft tube.....	52
Figure (2.3): Schematic diagram of experimental apparatus; (a) Up pumping flow (Aeration mode), (b) Down pumping flow (Mixing mode).....	53
Figure (2.4): The Laser Doppler Velocimetry (LDV) testing apparatus, (1) Laser source, (2) Traverse system, (3) Tested tank, (4) Flow velocity analyser.....	55
Figure (2.5): The LDV measuring volume fringe planes.....	56
Figure (2.6): The measuring volume.....	57
Figure (2.7): The LDV laser beams positions.....	58
Figure (2.8): Schematic diagram of the PIV.....	59
Figure (2.9): The Particle Image Velocimetry (PIV) testing apparatus, (1) Laser source, (2) Recording camera, (3) Tested tank.....	60
Figure (2.10): Light scattering by the ( $10\ \mu\text{m}$ ) glass particles in the water (Raffel et al., 2007).....	60
Figure (2.11): The pumping number and pumping flowrate measuring volume.....	65
Figure (2.12): The 3-D liquid volume cell and the vessel volume grids, (Garcia-Cortes et al., 2006).....	67
Figure (2.13): The schematic diagram of the polarographic probe.....	68
Figure (2.14): The schematic diagram of the optical probe.....	68
Figure (2.15): The schematic diagram of oxygen mass transfer zones.....	69

## List of Figures

---

Figure (2.16): (a) Experimental oxygen probes positions in the liquid volume, (b) Experimental oxygen probes positions in the liquid volume, $N=2.5$ rps, $(h/T_v) = 0.35$ .....	72
Figure (2.17): The repeatability of the mass transfer ( $k_1a$ ) experimental results for both oxygen probes, ( $N= 2.08$ rps).....	73
Figure (2.18): Optical probe response time verification.....	74
Figure (2.19): Polarographic probe response time verification.....	74
Figure (2.20): The probe response time relationship verification for both theoretical and experimental DO values for the optical probe.....	76
Figure (2.21): The probe response time relationship verification for both theoretical and experimental DO values for polarographic probe.....	76
Figure (2.22): The droplets zone mass transfer coefficient ( $k_1a_d$ ) measurement.....	83
Figure (2.23): Schematic diagram illustrates the surface aeration water droplets spray from turbine blades till the impingement point with some important relevant dimensions.....	84
Figure (2.24): Droplets radial and tangential velocities propelled in horizontal plane by turbine blades.....	85
 <b>Chapter Three</b>	
Figure (3.1): Different tested geometric configurations, (a) Whole system, (b) Turbine alone, (c) Turbine + Propeller, (d) Turbine + Draft tube.....	92
Figure (3.2): Impellers speed effect on the oxygen transfer coefficient with four different geometrical configurations; (Whole System, without draft tube, turbine alone and without propeller), $D/T_v=0.24$ , $C/T_v=0.31$ , $h/D=1.47$ , $C_{pr}/T_v=0.2$ , $S/W=1$ .....	93
Figure (3.3): The DO profile for different rotation speeds, $h/T_v= 0.35$ , $C/T_v=0.313$ , $C_{pr}/T_v=0.2$ , temperature =15 °C.....	94
Figure (3.4): (a) The limits of the tested turbine blades submergence, (b) Mass transfer Coefficient $k_1a$ relation with turbine blades submergence and water height in the liquid bulk for three levels of rotational speed, (b) Mass transfer Coefficient $k_1a$ relation with the rotation speed for three levels of turbine submergence. $D/T_v= 0.24$ , $C/T_v = 0.31$ , $C_{pr}/T_v=0.2$ .....	96

## List of Figures

---

Figure (3.5): Spacing effect on the oxygen transfer coefficient, $D/T_v = 0.24$ , $C/T_v = 0.31$ , $S_p$ (Reference) = 7.6 mm	Figure (3.6): radial flow rate by propeller, ( $m^3/s$ ).....	98
Figure (3.6): (a) The relationship between power number and Reynolds No., for different turbine blades submergence levels $C/T_v = 0.31$ , (b) The relation between power consumption and rotation speed, $C/T_v = 0.31$ .....		99
Figure (3.7): The spacing between two impellers effect on the power consumption.....		100
Figure (3.8): The effect of various impellers configurations on the power consumption.....		101
Figure (3.9): The relationship between the standard aeration efficiency $SAE_b$ for three aeration mode configurations (Whole System, turbine + propeller and turbine alone) with the impeller rotation speed, $D/T_v = 0.24$ , $C/T_v = 0.31$ , $h/D = 1.47$ , $S/W = 1$ .....		102
Figure (3.10): The relation between the standard oxygen transfer rate $SOTR_b$ for three aeration mode configurations (Whole System, turbine + propeller and turbine alone) with the impeller rotation speed, $D/T_v = 0.24$ , $C/T_v = 0.31$ , $h/D = 1.47$ , $S/W = 1$ .....		105
Figure (3.11): (a) The comparison between the $k_L a/N$ , predicted by the correlation model (Eq. 3.4) with the experimentally resulted $k_L a/N$ , (b) The Comparison between the ( $N_p$ ) values predicted by the Eq. 3.7 with the experimentally resulted ( $N_p$ ) values.....		110
Figure (3.12): Dissolved oxygen concentration profile with time of experiment in the water bulk zone ( $C_{dt}$ ), and the water spray zone ( $C_{Lt}$ ) at $N = 1.67$ rps for two experimental runs.....		112
Figure (3.13): Dissolved oxygen concentration profile with time of experiment in the water bulk zone ( $C_{dt}$ ), and the water spray zone ( $C_{Lt}$ ) at $N = 2.08$ rps for two experimental runs.....		112
Figure (3.14): Dissolved oxygen concentration profile with time of experiment in the water bulk zone ( $C_{dt}$ ), and the water spray zone ( $C_{Lt}$ ) at $N = 2.5$ rps for two experimental runs.....		113
Figure (3.15): Dissolved oxygen concentration profile with time of experiment in the water bulk zone ( $C_{dt}$ ), and the water spray zone ( $C_{Lt}$ ) at $N = 3.33$ rps for two experimental runs.....		113
Figure (3.16): The linear regression correlation of water spray zone aeration efficiency by plotting $C_{dt}$ versus $C_{Lt}$ for various rotation speeds.....		114

## List of Figures

---

Figure (3.17): The relation between the oxygen mass transfer coefficient $k_{j,a_d}$ and impellers rotation speed and in the spray zone, $S/W = 1$ .....	116
Figure (3.18): The relation between the oxygen transfer rate $OTR_{sp}$ and impellers rotation speed and, in the spray zone, $S/W = 1$ .....	119
Figure (3.19): The influence of the impellers rotational speed on the spray zone oxygen transfer rate $OTR_{sp}$ and in the bulk zone oxygen transfer rate $OTR_{sp}$ contributions the overall transfer rate $OTR$ , $S/W = 1$ .....	120
Figure (3.20): Effect of the turbine blade submergence on spray mass transfer zone dissolved oxygen concentration at rotation speed ( $N=2.5$ rps) and turbine clearance ( $C/T_v = 0.35$ ) .....	123
Figure (3.21): The linear regression correlation of water spray zone aeration efficiency by plotting ( $C_{dt}$ ) versus ( $C_{Lt}$ ) for various turbine blades submergence, $N = 2.5$ rps .....	124
Figure (3.22): The relation between the spray zone aeration efficiency $E_{sp}$ and turbine blade submergence ratio, $N = 2.5$ rps .....	125
Figure (3.23): The relation between the spray zone oxygen mass transfer coefficient, $k_{j,a_d}$ with the turbine submergence and liquid level impellers rotation speed, $N = 2.5$ rps .....	127
Figure (3.24): The relation between spray zone oxygen transfer rate $OTR_{sp}$ with the turbine blades submergence and liquid level, $N = 2.5$ rps .....	128
Figure (3.25): The influence of the turbine submergence on the spray zone oxygen transfer rate, $OTR_{sp}$ and in the bulk zone oxygen transfer rate $OTR_{sp}$ contributions the overall transfer rate $OTR$ , $N = 2.5$ rps .....	129
Figure (3.26): The effect of the turbine rotation speed on the spray mass transfer zone dissolved oxygen concentration at $h/D=1.47$ and $C/T=0.35$ , (Turbine alone configuration) .....	131
Figure (3.27): The linear regression of the spray zone aeration efficiency of the plot ( $C_{dt}$ ) versus ( $C_{Lt}$ ) for various rotation speeds, (Turbine alone configuration) .....	132
Figure (3.28): The relation between the impellers speed $N$ and the spray zone aeration efficiency $E_{sp}$ for both turbine alone and whole system configurations, $S/W = 1.0$ .....	133
Figure (3.29): The relation between $N$ and the oxygen mass transfer coefficient $k_{j,a_d}$ for both turbine alone and whole system configurations, $S/W = 1.0$ .....	133

## List of Figures

---

Figure (3.30): The relation between spray zone oxygen transfer rate with the rotational speed for the whole system and turbine alone configurations, $S/W = 1.0$ .....	135
Figure (3.31): The influence of the tank internals (Propeller and draft tube) on the spray zone oxygen transfer rate, $OTR_{sp}$ contribution the overall transfer rate $OTR$ , $S/W = 1.0$ .....	136
Figure (3.32): The Comparison between the $(E_{sp})_{20}$ , Predicted by the Correlation model (Eq. 3.10) with the experimentally resulted $(E_{sp})_{20}$ .....	139
Figure (3.33): The Comparison between the $(E_{sp})_{20}$ , Predicted by the Correlation model (Eq. 3.11) with the experimentally resulted $(E_{sp})_{20}$ .....	140
Figure (3.34): The Comparison between the $(E_{sp})_{20}$ , Predicted by the Correlation model (Eq.3.16) with the experimentally resulted $(E_{sp})_{20}$ .....	142
 <b>Chapter Four</b>	
Figure (4.1): LDV implementation for measuring velocity in a (r-z) plane, (Plane B).....	148
Figure (4.2): PIV implementation for measuring velocity in a (r-z) plane, (Plane A).....	149
Figure (4.3): The axial 4-bladed, reversible 45° pitched and twisted blade propeller RTP propeller (HPM204D, Milton Roy Mixing).....	150
Figure (4.4): The (r-z) flow field map for the RTP-D propeller with draft tube configuration in the entire vessel.....	153
Figure (4.5): The (r-z) velocities contour map for the RTP-D propeller with draft tube configuration in the entire vessel.....	155
Figure (4.6): Dimensionless axial velocity profile at different liquid levels (below impeller $z/h=0.55$ , above impeller $z/h=0.62$ ) for RTP-D with draft tube, $C_{pr}/T_v=0.2$ , $N=5$ rps in two different measuring planes; plane A at $0^0$ and plane B at $90^0$ from the posterior baffle respectively.....	157
Figure (4.7): (a) The (r - z) flow field map for the RTP-D propeller without draft tube configuration in the vessel core, (b) The (r - z) velocities contour map for the RTP-D propeller with draft tube configuration in the vessel core.....	159

## List of Figures

---

Figure (4.8): The dimensionless axial velocity profile at different liquid heights for RTP-D propeller without draft tube (below impeller $z/h=0.55$ , above impeller $z/h=0.62$ ), $C_{pr}/T_v = 0.2$ , $N= 5$ rps in two different measuring planes; plane A at $0^0$ and plane B at $90^0$ from the posterior baffle respectively.....	161
Figure (4.9): The creation of vortex in the down-pumping mode with draft tube.....	162
Figure (4.10): (a) The (r - z) flow field map for the RTP-U propeller with draft tube configuration in the vessel core, (b) The (r - z) velocities contour map for the RTP-U propeller with draft tube configuration in the vessel core.....	163
Figure (4.11): The dimensionless axial velocity profile at different liquid heights for RTP-U propeller with draft tube (below impeller $z/h=0.55$ , above impeller $z/h=0.62$ ), $C_{pr}/T_v = 0.2$ , $N= 5$ rps in two different measuring planes; plane A at $0^0$ and plane B at $90^0$ from the posterior baffle respectively.....	165
Figure (4.12): (a) The (r - z) flow field map for the RTP-U propeller without draft tube configuration in the vessel core, (b) The (r - z) velocities contour map for the RTP-U propeller with draft tube configuration in the vessel core.....	167
Figure (4.13): The dimensionless axial velocity profile at different liquid heights for RTP-U propeller without draft tube (below impeller $z/h=0.55$ , above impeller $z/h=0.62$ ), $C_{pr}/T_v = 0.2$ , $N= 5$ rps in two different measuring planes; plane A at $0^0$ and plane B at $90^0$ from the posterior baffle respectively.....	168
Figure (4.14): The distribution of the liquid volume in the vessel related with mean local composite velocity ranges for RTP-D propeller with draft tube configuration.....	175
Figure (4.15): The effect of RTP propeller rotational speed on the mixing time for different flow and geometry conditions, $h/d_{pr}=1.47$ , $C_{pr}/T_v = 0.2$ .....	177
Figure (4.16): The relation of Reynolds number with the dimensionless mixing time for different pumping modes and geometry configurations , $h/d_{pr} = 1.47$ , $C_{pr}/T_v = 0.2$ .....	178

### Chapter Five

Figure (5.1): The (r-z) flow field map for the turbine and the RTP-U propeller with draft tube (Whole system) configuration in the entire vessel.....	187
---	-----

## List of Figures

---

Figure (5.2):	The (r-z) velocities contour map for the turbine and the RTP-U propeller with draft tube (Whole system) configuration in the entire vessel.....	189
Figure (5.3):	The (r-z) flow field map for the turbine alone configuration in the entire vessel.....	191
Figure (5.4):	The (r-z) velocities contour map for the turbine alone configuration in the entire vessel.....	193
Figure (5.5):	The (r-z) flow field map for the turbine and the RTP-U propeller configuration in the entire vessel.....	195
Figure (5.6):	The (r-z) velocities contour map for the turbine and the RTP-U propeller configuration in the entire vessel.....	197
Figure (5.7):	Distribution of the liquid volume in the vessel related with mean local composite velocity ranges for whole system configuration.....	201
Figure (5.8):	The relation between impellers rotation speed and the dimensionless mixing number $Nt_m$ for whole system configuration in the aerated vessel .....	203
Figure (5.9):	The effect of impellers rotation speed on the mixing time for two different geometrical configurations, $h/D=1.47$ , $C_{pr}/T= 0.2$ , $C/T = 0.313$ (Aerated mode).....	204
Figure (5.10):	The relation between the Reynolds number and the dimensionless mixing time of the aerated vessel for whole system and turbine alone configurations, $h/D= 1.47$ , $C_{pr}/T_v = 0.2$ , $C/T_v = 0.313$ .....	205
Figure (5.11):	The relation between impellers rotation speed and the spacing between impellers; $h/D= 1.47$ , $C/T_v = 0.313$ , (Aerated mode).....	206
Figure (5.12):	The relation between the Reynolds number and the dimensionless mixing time of the aerated vessel for three turbine blade submergence levels, $C_{pr}/T= 0.2$ , $C/T = 0.313$ .....	207
Figure (5.13):	The comparison between experimental and predicted values of dimensionless mixing time number ( $t_m N$ ) by equation (5.4).....	209
Figure (5.14):	The effect of Reynolds number on power number for the two different configurations (Whole system and turbine alone); $h/D= 1.47$ , $C_{pr}/T_v = 0.2$ , $C/T = 0.313$ , (Aerated mode).....	210
Figure (5.15):	The relation between impellers rotation speed and the consumed power per water volume for the aerated mode, $h/D= 1.47$ , $C_{pr}/T_v = 0.2$ , $C/T_v = 0.313$ .....	210

## List of Figures

---

### Appendix I

Figure (I.1): Process selection diagram for industrial wastewater treatment (Eckenfelder et al., 2009).....	224
Figure (I.2): Domestic wastewater treatments steps (Try and Price, 1995).....	225
Figure (I.3): Development and control of biomass in the activated sludge process (Gary, 2004).....	227
Figure (I.4): The schematic layout of two-stage nitrification and de-nitrification (Gary, 2004).....	229
Figure (I.5): The Two stage biological phosphorus treatment (Gary, 2004).....	230
Figure (I.6): Chemical-biological phosphorus treatment (Phostrip process), (Barth and Stensel, 1981).....	231
Figure (I.7): Covered aerated tank using pure oxygen (Mueller et al., 2002).....	232

### Appendix II

Figure (II.1): The energy balance points for the spray discharge flowrate.....	238
--	-----



## List of Tables

### Chapter One

- Table (1.1): The standard aeration efficiency (SAE) for various aerators types...22
- Table (1.2): The standard aeration efficiency of the fine bubble diffused aeration in different water treatment basins (Duchene and Cotteux, 2002).....23

### Chapter Two

- Table (2.1): Geometrical configuration details.....53

### Chapter Three

- Table (3.1): The  $SAE_b$  and  $SOTR_b$  for different water level ratios ( $h/D$ ) and turbine blade width to blades submergence ratio ( $S/W$ ),  $D/T=0.24$ ,  $C/T=0.31$ ,  $C_{pr}/T=0.2$ ,  $N=2.803$  rps, (Whole system Configuration).....103
- Table (3.2): The  $SAE_b$  and  $SOTR_b$  for different impellers speed,  $D/T= 0.24$ ,  $C/T= 0.31$ ,  $C_{pr}/T= 0.2$ ,  $h/D = 1.47$  (Whole system Configuration, Aeration mode).....104
- Table (3.3): The  $SAE_b$  and  $SOTR_b$  for different impellers speed,  $D/T_v= 0.24$ ,  $C/T_v= 0.31$ ,  $C_{pr}/T_v= 0.2$ ,  $h/D = 1.47$  (Turbine and propeller configuration).....104
- Table (3.4): The  $SAE_b$  and  $SOTR_b$  for different impellers speed,  $D/T_v= 0.24$ ,  $C/T_v= 0.31$ ,  $h/D = 1.47$ , (Turbine alone configuration).....105
- Table (3.5): The effect the spacing between impellers on  $SOTR_b$  and  $SAE_b$ ,  $D/T_v= 0.24$ ,  $C/T_v= 0.31$ ,  $h/D = 1.47$ ,  $S_p=8.3$  mm.....105
- Table (3.6): The spray droplets mass transfer zone of  $k_{lad}$ , flight time  $t_f$  and the related measured parameters, (of 100% submerged turbine blades,  $H =$  zero),  $h/D = 1.47$ ,  $S/W = 1$ .....116
- Table (3.7): Water spray droplets velocity and volumetric flow rate of given operation and geometric configuration (whole system) for various rotation speed levels .....117
- Table (3.8): Spray zone oxygen transfer rate  $OTR_{sp}$  variation with impellers rotation speed.....118

## List of Tables

---

Table (3.9):	The oxygen mass transfer rates for spray and bulk zones $OTR_b$ and $OTR_{sp}$ with the percentage of contribution .....	120
Table (3.10):	The water spray velocity and volumetric flow rate for the whole system geometrical configuration with various turbine blades submergence and water levels, $N= 2.5$ rps.....	122
Table (3.11):	The calculated water spray mass transfer zone ( $k_1a_d$ ), droplets flight time( $t_f$ ) and some related measured parameters and turbine blades submergence and water level, at constant rotation speed ( $N = 2.5$ rps).....	126
Table (3.12):	Water spray zone oxygen transfer rate ( $OTR_{sp}$ ) variation with different turbine blades submergence and water levels, ( $N = 2.5$ rps).....	128
Table (3.13):	Oxygen mass transfer rate and percentage of contribution for both water spray and bulk (re-aeration) zones, ( $N= 2.5$ rps).....	130
Table (3.14):	The spray mass transfer zone ( $k_1a_d$ ), flight time ( $t_f$ ) and some related measured parameters, $S/W=1.00$ , $h/D =1.47$ , (Turbine alone configuration).....	134
Table (3.15):	The spray velocity and volumetric flow rate for various turbine rotation speeds (Turbine alone configuration).....	134
Table (3.16):	The Spray zone oxygen transfer rate $OTR_{sp}$ for different rotation speed levels, (Turbine alone configuration).....	136
Table (3.17):	The Comparison for the spray zone oxygen transfer rates $OTR_{sp}$ between the whole system and turbine alone configurations, $S/W =1.00$ , $h/D=1.47$ .....	137

### Chapter Four

Table (4.1):	The RTP propeller and several pitched blade impellers power numbers with different configurations and pumping modes.....	169
Table (4.2):	The RTP propeller and several pitched blade impellers pumping and circulation numbers with different configurations and pumping modes.....	170
Table (4.3):	The agitation Index for RTP-D and various pitched blade impellers, (this work and literature).....	172

### Chapter Five

Table (5.1):	Turbine pumping number and system circulation number.....	199
--------------	---	-----

### References

-A-

Adrian, R., 1991. Particle-imaging techniques for experimental fluid mechanics. *Annual Review of Fluid Mechanics* 23, 261-304.

Aeschbach, S., Bourne, J.R., 1972. The attainment of homogeneous suspension in a continuous stirred tank. *The Chemical Engineering Journal* 4, 234-242.

Agüí, J.C., Jimenez, J., 1987. On the performance of particle tracking. *Journal of Fluid Mechanics* 185, 447-468.

AIRE-O2 Aeration Industries International, Commercial Document, [www.aireo2.com](http://www.aireo2.com).

Aire Liquide, Commercial Document, [www.uk.airliquide.com](http://www.uk.airliquide.com).

Albal, R.S., Shah, Y.T., Schumpe, A., Carr, N.L., 1983. Mass transfer in multiphase agitated contactors. *The Chemical Engineering Journal* 27, 61-80.

Amjad, Z., 2010. *The science and technology of industrial water treatment*. CRC Press Boca Raton Florida.

AQUATURBO SYTEMS inc., Commercial Document, [www.aquaturbo.com](http://www.aquaturbo.com).

Arjunwadkar, S., Sarvanan, K., Kulkarni, P., Pandit, A., 1998. Gas-liquid mass transfer in dual impeller bioreactor. *Biochemical Engineering Journal* 1, 99-106.

Armenante, P.M., Chou, C.-C., 1996. Velocity profiles in a baffled vessel with single or double pitched-blade turbines. *AIChE Journal* 42, 42-54.

Ascanio, G., Castro, B., Galindo, E., 2004. Measurement of Power Consumption in Stirred Vessels—A Review. *Chemical Engineering Research and Design* 82, 1282-1290.

ASCE, 1993. *Measurement of Oxygen Transfer in Clean Water*. American Society Of Civil Engineers, New York.

Atkinson, J., Taylor, S., Ghosh, U., 1995. Surface aeration. *Environmental Engineering* 121, 113-118.

Atkinson, J.F., Van Benschoten, J., Cheng, C.-y., 2000. *Development of Particle Image Technology for Water Treatment Studies*. Amer Water Works Assn.

## References

---

Aubin, J., 2001. Mixing Capabilities of Down- and Up-Pumping Axial Flow Impellers in Single Phase and Gas-Liquid Systems: Experimental and CFD Studies. PhD Thesis, University of Sydney, Institut National Polytechnique de Toulouse, France.

Aubin, J., Le Sauze, N., Bertrand, J., Fletcher, D., Xuereb, C., 2004. PIV Measurements of Flow In An Aerated Tank Stirred By A Down-and An Up-Pumping Axial Flow Impeller. *Exp. Therm. & Fluid Sci.* 28, 447-456.

Aubin, J., Mavros, P., Fletcher, D.F., Bertrand, J., Xuereb, C., 2001. Effect of Axial Agitator Configuration (Up-Pumping, Down-Pumping, Reverse Rotation) on Flow Patterns Generated in Stirred Vessels. *Chemical Engineering Research and Design* 79, 845-856.

-B-

Backhurst, J.R., Harker, J.H., Kaul, S.N., 1988. The performance of pilot and full-scale vertical shaft aerators. *Water Research* 22, 1239-1243.

Baeza, J.A., Gabriel, D., Lafuente, J., 2002. Improving the nitrogen removal efficiency of an A2/O based WWTP by using an on-line Knowledge Based Expert System. *Water Research* 36, 2109-2123.

Bandaiphet, C., Prasertsan, P., 2006. Effect of aeration and agitation rates and scale-up on oxygen transfer,  $k_L a$  in exopolysaccharide production from enterobacter cloacae. *Carbohydrate Polymers* 66, 216-228.

Barigou, M., Greaves, M., 1992. Bubble-size distributions in a mechanically agitated gas—liquid contactor. *Chemical Engineering Science* 47, 2009-2025.

Barth, E.F., Stensel, H.D., 1981. International nutrient control technology for municipal effluents. *Journal (Water Pollution Control Federation)*, 1691-1701.

Baylar, A., Bagatur, T., 2000a. Aeration performance of weirs. *WATER SA-PRETORIA*- 26, 521-526.

Baylar, A., Bagatur, T., 2000b. Study of aeration efficiency at weirs. *Turk. J. Eng. Environ. Sci.* 24, 255-264.

Baylar, A., Bagatur, T., 2006. Experimental studies on air entrainment and oxygen content downstream of sharp-crested weirs. *Water and Environment Journal* 20, 210-216.

## References

---

Baylar, A., Bagatur, T., Tuna, A., 2001. Aeration performance of triangular notch weirs at recirculating system. *Water Qual. Res. J. Can.* 36, 121-132.

Baylar, A., Emiroglu, M.E., Bagatur, T., 2006. An experimental investigation of aeration performance in stepped spillways. *Water and Environment Journal* 20, 35-42.

Baylar, A., Unsal, M., Ozkan, F., 2010. Hydraulic structures in water aeration processes. *Water, Air, & Soil Pollution* 210, 87-100.

Bhattacharya, S., Hebert, D., Kresta, S.M., 2007. Air Entrainment in Baffled Stirred Tanks. *Chemical Engineering Research and Design* 85, 654-664.

Biń, A.K., 1993. Gas entrainment by plunging liquid jets. *Chemical Engineering Science* 48, 3585-3630.

Biotrade Co., Commercial Document, [www.biotrade.fr](http://www.biotrade.fr).

Botjheng Water Ltd., Commercial Document, [www.botjheng.com](http://www.botjheng.com).

Bouaifi, M., Roustan, M., 2001. Power consumption, mixing time and homogenisation energy in dual-impeller agitated gas-liquid reactors. *Chemical Engineering and Processing: Process Intensification* 40, 87-95.

Boyd, C.E., 1998. Pond water aeration systems. *Aquacultural Engineering* 18, 9-40.

Boyd, C.E., Martinson, D.J., 1984. Evaluation of propeller-aspirator-pump aerators. *Aquaculture* 36, 283-292.

Brdjanovic, D., Slamet, A., Van Loosdrecht, M.C.M., Hooijmans, C.M., Alaerts, G.J., Heijnen, J.J., 1998. Impact of Excessive Aeration on Biological Phosphorus Removal from Wastewater. *Water Research* 32, 200-208.

Brown, D., Jones, P., Middleton, J., Papadopoulos, G., Arik, E., 2004. Experimental methods *Handbook of Industrial Mixing Science and Practice*. John Wiley & Son Inc.

Brož, J., Fořt, I., Sperling, R., Jambere, S., Heiser, M., Rieger, F., 2004. Pumping Capacity of Pitched Blade Impellers in a Tall Vessel with a Draught Tube. *Acta Polytechnica* 44, 48-53.

-C-

Cancino, B., 2004a. Design of high efficiency surface aerators: Part 2. Rating of surface aerator rotors. *Aquacultural Engineering* 31, 99-115.

## References

---

- Cancino, B., 2004b. Design of high efficiency surface aerators: Part 3. Dimensional analysis of rotor performance. *Aquacultural Engineering* 31, 117-121.
- Cancino, B., Roth, P., Reuß, M., 2004. Design of high efficiency surface aerators: Part 1. Development of new rotors for surface aerators. *Aquacultural Engineering* 31, 83-98.
- Capela, S., Gillot, S., Héduit, A., 2004. Comparison of oxygen-transfer measurement methods under process condition. *Water Env. Res.* 76, 183-188.
- Caprari S. p. A., Commercial Document, [www.caprari.com](http://www.caprari.com).
- Carrera, J., Baeza, J., Vicent, T., Lafuente, J., 2003. Biological nitrogen removal of high-strength ammonium industrial wastewater with two-sludge system. *Water Research* 37, 4211-4221.
- Chandrasekharan, K., Calderbank, P.H., 1981. Further observations on the scale-up of aerated mixing vessels. *Chemical Engineering Science* 36, 818-823.
- Chanson, H., 2003. Interaction of Strong Turbulence with Free Surfaces, in: Liu, P. (Ed.), *Advances in Coastal and Ocean Engineering Interaction of Strong Turbulence with Free Surfaces*. World Scientific Publishing, Singapore.
- Chapple, D., Kresta, S.M., Wall, A., Afacan, A., 2002. The Effect of Impeller and Tank Geometry on Power Number for a Pitched Blade Turbine. *Chemical Engineering Research and Design* 80, 364-372.
- Chern, J.-M., Chou, S.-R., 1999. Volatile Organic Compound Emission Rates from Mechanical Surface Aerators: Mass-Transfer Modeling. *Ind. Eng. Chem. Res.* 38, 3176-3185.
- Chern, J.-M., Yang, S.-P., 2003. Oxygen transfer rate in a coarse-bubble diffused aeration system. *Ind. Eng. Chem. Res.* 42, 6653-6660.
- Chern, J.-M., Yang, S.-P., 2004. Measuring and Modeling of Oxygen Transfer Rate in a Drop Structure. *Ind. Eng. Chem. Res.* 43, 7657-7663.
- Chisti, Y., Jauregui-Haza, U.J., 2002. Oxygen transfer and mixing in mechanically agitated airlift bioreactors. *Biochemical Engineering Journal* 10, 143-153.
- Chung, K., Barigou, M., Simmons, J., 2007. Reconstruction of 3-D flow field inside miniature stirred vessel using a 2-D PIV technique. *Trans IChemE, Chem. Eng. Res.&Des.* 85, 560-567.

## References

---

Clesceri, N., 2009. Ch. 3 Treatment by subsurface application, Biological treatment process, 1st ed. Humana press, NY- USA.

Costes, J., Couderc, J.P., 1988. Study by laser Doppler anemometry of the turbulent flow induced by a Rushton turbine in a stirred tank: Influence of the size of the units—I. Mean flow and turbulence. *Chemical Engineering Science* 43, 2751-2764.

Crites, R., Middlebrooks, J., Reed, S., 2006. Natural wastewater treatment. CRC press Taylor& Francis Group, FL-USA.

Cui, Y.Q., van der Lans, R.G.J.M., Luyben, K.C.A.M., 1996. Local power uptake in gas-liquid systems with single and multiple rushton turbines. *Chemical Engineering Science* 51, 2631-2636.

Cumby, T.R., 1987a. A review of slurry aeration 1. Factors affecting oxygen transfer. *Journal of Agricultural Engineering Research* 36, 141-156.

Cumby, T.R., 1987b. A review of slurry aeration 3. Performance of aerators. *Journal of Agricultural Engineering Research* 36, 175-206.

-D-

Dehkordi, A., Savari, C., 2011. Determination of interfacial area and overall volumetric mass-transfer coefficient in a novel type of two impinging streams reactor by chemical method. *Ind. Eng. Chem. Res.* 50, 6426-6435.

Demoyer, C., Schierholz, E., Gulliver, J., Wilhelms, S., 2003. Impact of bubble and free surface oxygen transfer on diffused aeration systems. *Water Research* 37, 1890-1904.

Deshmukh, N.A., Joshi, J.B., 2006. Surface Aerators: Power Number, Mass Transfer Coefficient, Gas Hold up Profiles and Flow Patterns. *Chemical Engineering Research and Design* 84, 977-992.

Duchene, P., Cotteux, É., 2002. Insufflation d'air fines bulles: application aux stations d'épuration en boues activées des petites collectivités (Document technique FNDAE N 26).

Dudley, J., 1995. Process testing of aerators in oxidation ditches. *Water Research* 29, 2217-2219.

## References

---

-E-

Eckenfelder, W., Davis, J., Ford, L., Englande, A., 2009. Industrial water quality, 4th ed. McGraw-Hill USA.

Edwards, M., Baker, M., 2001 A Review of Liquid Mixing Equipment, in: Nienow, A.W., Harnby, N., Edwards, M. (Eds.), *Mixing in the Process Industries*, Second ed. Butterworth-Heinemann.

El-Temtamy, S., Khalil, S., Nour-El-Din, A., Gaber A., 1984. Oxygen mass transfer in a bubble column bioreactor containing lysed yeast suspension. *Appl. Microbiol. Biotechnol.* 19, 376-381.

Engineers, A.S.o.C., Federation, W.P.C., 1988. *Aeration: A Wastewater Treatment Process*. Water Pollution Control Federation.

Escudie, R., Line, A., 2003. Experimental analysis of hydrodynamics in a radially agitated tank. *AIChE Journal* 49, 585-603.

-F-

Fan, L., Xu, N., Wang, Z., Shi, H., 2010. PDA experiments and CFD simulation of a lab-scale oxidation ditch with surface aerators. *Chemical Engineering Research and Design* 88, 23-33.

FR Patent Demand, 2012. FR 2971951, Apparaeil De Traitement Mechanique D'une Composion Liquide er Procede de Tratement Mechanique D'une Telle Composiotion Liquide, , France.

Fuchs, R., Ryu, D.D.Y., Humphrey, A.E., 1971. Effect of Surface Aeration on Scale-Up Procedures for Fermentation Processes. *Industrial & Engineering Chemistry Process Design and Development* 10, 190-196.

-G-

Gabriele, A., Tsoligkas, A.N., Kings, I.N., Simmons, M.J.H., 2011. Use of PIV to measure turbulence modulation in a high throughput stirred vessel with the addition of high Stokes number particles for both up- and down-pumping configurations. *Chemical Engineering Science* 66, 5862-5874.

Garcia-Cortes, D., Xuereb, C., Taillandier, P., Jauregui-Haza, U.J., Bertrand, J., 2006. Flow Induced by Dual-Turbine of Different Diameters in a Gas-Liquid Agitation

## References

---

System: the Agitation and Turbulence Indices. International Journal of Chemical Reactor Engineering 4.

Gary, N.F., 2004. Biology of Wastewater Treatment, 1st ed. ICP press, London.

Gemgate GmbH, Commercial Document, [www.gemgate.ie](http://www.gemgate.ie).

Gresch, M., Armbruster, M., Braun, D., Gujer, W., 2011. Effects of aeration patterns on the flow field in wastewater aeration tanks. Water Research 45, 810-818.

Guillard, F., Trägårdh, C., 2003. Mixing in industrial Rushton turbine-agitated reactors under aerated conditions. Chemical Engineering and Processing: Process Intensification 42, 373-386.

Gulliver, J.S., Wilhelms, S.C., Parkhill, K.L., 1998. Predictive capabilities in oxygen transfer at hydraulic structures. Journal of hydraulic engineering 124, 664-671.

Gupta, K., Sharma, R., 1996. Biological oxidation of high strength nitrogenous wastewater. Water Research 30, 593-600.

-H-

Hadjiev, D., Sabiri, N.E., Zanati, A., 2006. Mixing time in bioreactors under aerated conditions. Biochemical Engineering Journal 27, 323-330.

Hecht, E., Zajac, A., 2001. Optics. Addison-Wesley Pub, USA.

Heduit, A., Racault, Y., 1983a. Essais d'aérateurs: Enseignements tirés de 500 essais en eau claire effectués dans 200 stations d'épuration différentes—I. Methodologie. Water Research 17, 97-103.

Heduit, A., Racault, Y., 1983b. Essais d'aérateurs: Enseignements tirés de 500 essais en eau claire effectués dans 200 stations d'épuration différentes—II Resultats. Water Research 17, 289-297.

Heim, A., Krasowski, A., Rzycki, E., Stelmach, J., 1995. Aeration of bioreactors by self-aspirating impellers. The Chemical Engineering Journal and the Biochemical Engineering Journal 58, 59-63.

Holland, F., Bragg, R., 1995. Fluid Flow for Chemical Engineers, 2nd ed. Edward Arnold, Great Britain.

## References

---

Houcine, I., Plasari, E., David, R., 2000. Effects of the Stirred Tank's Design on Power Consumption and Mixing Time in Liquid Phase. *Chemical Engineering & Technology* 23, 605-613.

Hsu, Y., Huang, K., 1997. Effects of geometrical factors on liquid mixing in a gas-induced agitated tank. *J. Chem. Tech. Biotechnol.* 68, 222-228.

Huang, W., Wu, C., Xia, W., 2009. Oxygen transfer in high-speed surface aeration tank for wastewater treatment: Full-scale test and numerical modeling. *Journal of Environmental Engineering* 135, 684-691.

-J-

Jakobson, H., 2008. *Agitation and Fluid Mixing Technology, Chemical Reactor Modeling Multiphase Reactive Flows*, 1 ed. Springer-Verlag Heidelberg.

Jaworski, Z., Nienow, A., Dyster, K., 1996. An LDA study of the turbulent flow field in a baffled vessel agitated by an axial, down-pumping hydrofoil impeller. *The Canadian Journal of Chemical Engineering* 74, 3-15.

Ju, L.-K., Sundarajan, A., 1992. Model analysis of biological oxygen transfer enhancement in surface-aerated bioreactors. *Biotechnology and Bioengineering* 40, 1343-1352.

-K-

Kang, J., Lee, C.H., Haam, S., Koo, K.K., Kim, W.S., 2001. Studies on the Overall Oxygen Transfer Rate and Mixing Time in Pilot-Scale Surface Aeration Vessel. *Environmental Technology* 22, 1055-1068.

Kawase, Y., Moo-Young, M., 1989. Mixing time in bioreactors. *Journal of Chemical Technology & Biotechnology* 44, 63-75.

Kawecki, W., Reith, T., Van Heuven, J., Beek, W., 1967. Bubble size distribution in the impeller region of a stirred vessel. *Chemical Engineering Science* 22, 1519-1523.

Keane, R., Adriane, R., 1992. Theory of Cross-Correlation Analysis of PIV Images. *App. Sci. Res.* 49, 191-215.

Khopkar, A.R., Mavros, P., Ranade, V.V., Bertrand, J., 2004. Simulation of Flow Generated by an Axial-Flow Impeller: Batch and Continuous Operation. *Chemical Engineering Research and Design* 82, 737-751.

## References

---

- Khudenko, B.M., 1983. Development of self-propelled aerators. *Journal of Environmental Engineering* 109, 868-885.
- Kim, J., Walters, R.W., 2001. Oxygen transfer at low drop weirs. *Journal of Environmental Engineering* 127, 604-610.
- Kirke, B., El Gezawy, A., 1997. Design and model tests for an efficient mechanical circulator/aerator for lakes and reservoirs. *Water Research* 31, 1283-1290.
- Kleinheinz, G., Wright, P., 2009. Biological odor and VOC control process, in: Wang, L., Pereira, N., Hung, Y.-T. (Eds.), *Biological Treatment Processes*. Humana Press, pp. 733-757.
- Kucukali, S., Cokgor, S., 2009. Energy concept for predicting hydraulic jump aeration efficiency. *Journal of Environmental Engineering* 135, 105-107.
- Kumar, A., Moulick, S., Mal, B.C., 2010a. Performance evaluation of propeller-aspirator-pump aerator. *Aquacultural Engineering* 42, 70-74.
- Kumar, B., Patel, A., Rao, A., 2010b. Shape effect on optimal geometric conditions in surface aeration systems. *Korean J. Chem. Eng.* 27, 159-162.
- Kumaresan, T., Joshi, J.B., 2006. Effect of impeller design on the flow pattern and mixing in stirred tanks. *Chemical Engineering Journal* 115, 173-193.
- Kumaresan, T., Nere, N.K., Joshi, J.B., 2005. Effect of Internals on the Flow Pattern and Mixing in Stirred Tanks. *Ind. Eng. Chem. Res.* 44, 9951-9961.
- Kusabiraki, D., Murota, M., Ohno, S., Yamagiwa, K., Yasuda, M., Ohkawa, A., 1990. Gas Entrainment Rate and Flow Pattern in a Plunging Liquid Jet Aeration System Using Inclined Nozzles. *Journal of Chemical Engineering of Japan* 23, 704-710.

-L-

- Laakkonen, M., Honkanen, M., Saarenrinne, P., Aittamaa, J., 2005. Local bubble size distributions, gas-liquid interfacial areas and gas holdups in a stirred vessel with particle image velocimetry. *Chemical Engineering Journal* 109, 37-47.
- Lee, K., Yianneskis, M., 1998. Turbulence properties of the impeller stream of a Rushton turbine. *AIChE Journal* 44, 13-24.

## References

---

Lee, M., Kang, J., Lee, C.H., Haam, S., Hun-Hwee, P., Kim, W.S., 2001. Oxygen Transfer Characteristics in a Pilot Scale Surface Aeration Vessel with Simcar Aerator. *Environmental Technology* 22, 57-68.

Leng, D., Katti, S., Obeng, V., 2008. Industrial Mixing Technology, in: Albright, L. (Ed.), *Albright's Chemical Engineering Handbook*, 1 ed. CRC press, NW.

Li, X., Yu, G., Yang, C., Mao, Z.-S., 2009. Experimental Study on Surface Aerators Stirred by Triple Impellers. *Ind. Eng. Chem. Res.* 48, 8752-8756.

Li, Z., Bao, Y., Gao, Z., 2011. PIV experiments and large eddy simulation of single-loop flow fields in Rushton turbine stirred tanks. *Chem. Eng. Sci.* 66, 1219-1231.

Lines, P.C., 2000. Gas-Liquid Mass Transfer Using Surface-Aeration in Stirred Vessels, with Dual Impellers. *Chemical Engineering Research and Design* 78, 342-347.

Lu, W.-M., Ju, S.-J., 1989. Cavity configuration, flooding and pumping capacity of disc-type turbines in aerated stirred tanks. *Chemical Engineering Science* 44, 333-342.

-M-

Matsuura, K., Kataoka, I., Serizawa, A., 2003. Prediction of Turbulent Diffusion Coefficient of Liquid Droplet Using Lagrangian Simulation. GENES4/ANP2003, Kyoto, Japan.

Mavros, P., 2001. Flow visualization in stirred vessels A review of experimental techniques. *Trans IChemE* 97, 113- 127.

Mavros, P., Baudou, C., 1997. Quantification of the Performance of Agitator in Stirred Vessels: Definition and Use of an Agitation Index. *Trans IChemE* 75.

Mavros, P., Naude, I., Xuereb, C., Bertrand, J., 1997. Laser Doppler Velocimetry in agitated vessels: effect of continuous liquid stream on flow patterns. *IChemE* 75, 763-776.

Mavros, P., Xuereb, C., Bertrand, J., 1998. Determination of 3-D flow field in agitated vessels by Laser Doppler Velocimetry: use and interpretation of RMS velocities. *Trans. Industrial Chemistry* 76, 223-233.

Mavros, P., Xuereb, C., Fořt, I., Bertrand, J., 2002. Investigation by laser Doppler velocimetry of the effects of liquid flow rates and feed positions on the flow patterns

## References

---

induced in a stirred tank by an axial-flow impeller. *Chemical Engineering Science* 57, 3939-3952.

McCabe, W., Smith, J., Harriott, P., 1985. *Agitation and Mixing of Liquid, Unit Operation of Chemical Engineering*, 4 ed. McGraw-Hill, NY.

McWhirter, J., Hutter, J., 1989. Improved oxygen mass transfer modeling for diffused/subsurface aeration systems. *AIChE Journal* 35, 1527-1534.

McWhirter, J.R., Chern, J.-M., Hutter, J.C., 1995. Oxygen Mass Transfer Fundamentals of Surface Aerators. *Ind. Eng. Chem. Res.* 34, 2644-2654.

Merchuk, J.C., Yona, S., Siegel, M.H., Zvi, A.B., 1990. On the first-order approximation to the response of dissolved oxygen electrodes for dynamic KLa estimation. *Biotechnology and Bioengineering* 35, 1161-1163.

Mishra, V.P., Dyster, K.N., Nienow, A.W., McKemie, J., Jaworski, Z., 1998. A study of an up- and a down-pumping wide blade hydrofoil impeller: Part I. LDA measurements. *The Canadian Journal of Chemical Engineering* 76, 577-588.

Moulick, S., Mal, B., 2009. Performance evaluation of double-hub paddle wheel aerator. *Journal of Environmental Engineering* 135, 562-566.

Moulick, S., Mal, B.C., Bandyopadhyay, S., 2002. Prediction of aeration performance of paddle wheel aerators. *Aquacultural Engineering* 25, 217-237.

Mueller, J., Boyle, W., Lightfoot, E., 1967. Effect of the response time of a dissolved oxygen probe on the oxygen uptake rate. *Applied microbiology* 15, 674.

Mueller, J., Boyle, W.C., Popel, H.J., 2002. *Aeration: principles and practice*. CRC.

Myers, K., Ward, R., Bakker, A., 1997. A digital particle image velocimetry investigation of flow field instabilities of axial-flow impellers. *Journal of fluids engineering* 119, 623.

-N-

Nagata, S., 1975. *Mixing Principles and Applications*. John Wiley & Sons, NY.

Nair, R., Dhamole, P., Lele, S.S., D'Souza, S., 2008. Biotreatment of High Strength Nitrate Waste Using Immobilized Preadapted Sludge. *Appl Biochem Biotechnol* 151, 193-200.

## References

---

Nakanoh, M., Yoshida, F., 1980. Gas Absorption by Newtonian and Non-Newtonian Liquids in a Bubble Column. *Industrial & Engineering Chemistry Process Design and Development* 19, 190-195.

Nakasone, H., 1987. Study of aeration at weirs and cascades. *Journal of Environmental Engineering* 113, 64-81.

Nere, N.K., Patwardhan, A.W., Joshi, J.B., 2003. Liquid-Phase Mixing in Stirred Vessels: Turbulent Flow Regime. *Ind. Eng. Chem. Res.* 42, 2661-2698.

Nienow, A.W., 1997. On impeller circulation and mixing effectiveness in the turbulent flow regime. *Chemical Engineering Science* 52, 2557-2565.

-O-

Ognean, T., 1993a. Aspects concerning scale-up criteria for surface aerators. *Water Research* 27, 477-484.

Ognean, T., 1993b. Dimensionless criteria for estimating oxygen transfer in aeration systems. *Biotechnology and Bioengineering* 41, 1014-1020.

Ognean, T., 1997. Relationship between oxygen mass transfer rate and power consumption by vertical shaft aerators. *Water Research* 31, 1325-1332.

Ohkawa, A., Kusabiraki, D., Kawai, Y., Sakai, N., Endoh, K., 1986. Some flow characteristics of a vertical liquid jet system having downcomers. *Chemical Engineering Science* 41, 2347-2361.

Okawa, T., Shiraishi, T., Mori, T., 2008. Effect of impingement angle on the outcome of single water drop impact onto a plane water surface. *Exp Fluids* 44, 331-339.

Oldshue, J., 1983. *Fluid Mixing Technology*. McGraw-Hill, NY.

Oliveira, M.E.C., Franca, A.S., 1998. Simulation of oxygen mass transfer in aeration systems. *International Communications in Heat and Mass Transfer* 25, 853-862.

Ozkan, F., Baylar, A., Tugal, M., 2006. The performance of two phase flow systems in pond aeration. *Int. J. Sci. Technol* 1, 65-74.

## References

---

-P-

Park, K., Inamori, Y., Mizouchi, M., Ahn, K., 2000. Emission and control of nitrous oxide from a biological wastewater treatment system with intermittent aeration. *Water Research* 90, 247-252.

Patil, S.S., Deshmukh, N.A., Joshi, J.B., 2004. Mass-Transfer Characteristics of Surface Aerators and Gas-Inducing Impellers. *Ind. Eng. Chem. Res.* 43, 2765-2774.

Patwardhan, A.W., Joshi, J.B., 1998. Design of stirred vessels with gas entrained from free liquid surface. *The Canadian Journal of Chemical Engineering* 76, 339-364.

Patwardhan, A.W., Joshi, J.B., 1999. Relation between Flow Pattern and Blending in Stirred Tanks. *Ind. Eng. Chem. Res.* 38, 3131-3143.

Philichi, T.L., Stenstrom, M.K., 1989. Effects of dissolved oxygen probe lag on oxygen transfer parameter estimation. *Journal (Water Pollution Control Federation)*, 83-86.

Polprasert, C., Raghunandana, H., 1985. Wastewater treatment in Deep Aeration Tank. *Water Research* 19, 257-264.

Praxair Technology, Commercial Document, [www.praxair.com](http://www.praxair.com).

Process Engineering s.r.l, Commercial Document, [www.pe-process.it](http://www.pe-process.it).

Puthli, M.S., Rathod, V.K., Pandit, A.B., 2005. Gas-liquid mass transfer studies with triple impeller system on a laboratory scale bioreactor. *Biochemical Engineering Journal* 23, 25-30.

-Q-

Qu, X.L., Khezzar, L., Danciu, D., Labois, M., Lakehal, D., 2011. Characterization of plunging liquid jets: A combined experimental and numerical investigation. *International Journal of Multiphase Flow* 37, 722-731.

-R-

Raffel, M., Willert, C., Wereley, S., Kompenhans, J., 2007. *Particle Image Velocimetry A Practical Guide*, 2nd ed. Springer-Verlag.

## References

---

- Ramalho, R.S., 1977. Introduction to wastewater treatment processes. Academic Press.
- Ranade, V., Joshi, J., 1989. Flow generated by pitched blade turbines I: measurements using laser Doppler anemometer. *Chemical Engineering Communications* 81, 197-224.
- Rao, A.R., 1999. Prediction of reaeration rates in square, stirred tanks. *Journal of Environmental Engineering* 125, 215-223.
- Rao, A.R., Kumar, B., 2007a. Scale-up criteria of square tank surface aerator. *Biotechnology and Bioengineering* 96, 464-470.
- Rao, A.R., Kumar, B., 2007b. The use of circular surface aerators in wastewater treatment tanks. *Journal of Chemical Technology & Biotechnology* 82, 101-107.
- Rao, A.R., Kumar, B., 2009. Simulating Surface Aeration Systems at Different Scale of Mixing Time. *Chinese Journal of Chemical Engineering* 17, 355-358.
- Rao, A.R., Kumar, B., Patel, A.K., 2009. Vortex behaviour of an unbaffled surface aerator. *Science Asia* 35, 183-188.
- Rodgers, T.L., Gangolf, L., Vannier, C., Parriaud, M., Cooke, M., 2011. Mixing times for process vessels with aspect ratios greater than one. *Chemical Engineering Science* 66, 2935-2944.
- Roubaty, J.-L., Boeglin, J.-C., 2007. *Pollution Industrielle de l'eau Caractérisation, Classification, Mesure, Techniques de L'ingénieur*.
- Roustan, M., 2003. *Transferts gaz-liquide dans les procédés de traitement des eaux et des effluents gazeux*. Paris : Éd. Tec & doc Paris.
- Roustan, M., 2005. *Agitation Mélange Caractéristiques Des Mobiles D'Agitation, Techniques De L'ingénieur*
- Roustan, M., Ghauri, B., Roques, H., 1984. Etude de la circulation dans les bassins d'aération a boues actives. *Water Research* 18, 495-499.
- Roustan, M., Pharamond, J.C., Roques, H., 1975. Etude comparative de divers systemes d'aération. *Water Research* 9, 1065-1068.

## References

---

-S-

Sano, Y., Usui, H., 1985. Interrelations among mixing time, power number and discharge flow rate number in baffled mixing vessels. *Journal of Chemical Engineering of Japan* 18, 47-52.

Sardeing, R., 2002. Hydrodynamique induite par un oxygénateur de surface : influence du design des agitateurs sur la qualité de la dispersion, INP Toulouse.

Sardeing, R., Ferrand, F., Poux, M., Avriillier, P., Xuereb, C., 2003. Hydrodynamics and Gas Dispersion Characterization in a System Equipped with a New Gas-Inducing Impeller. *Engineering in Life Sciences* 3, 31-37.

Sardeing, R., Poux, M., Melen, S., Avriillier, P., Xuereb, C., 2005a. Aeration of Large Size Tanks by a Surface Agitator. *Chemical Engineering & Technology* 28, 587-595.

Sardeing, R., Poux, M., Xuereb, C., 2005b. Procédé d'oxygénation et de brassage pour le traitement biologique des eaux usées, *Techniques de L'ingénieur*, pp. IN 1-10  
Schultz, T.E., 2005. Biological Wastewater Treatment, *Chemical Engineering Magazine*, pp. 1-5.

Shammas, N., Chang, C., Wang, L., 2006. Tertiary micro-screening, *Advanced physico-chemical treatment process*, 1st ed. Humana press Inc., NJ-USA.

Sharma, K., 2007. Principles of mass transfer. Prentice-Hall India.

Shluter, V., Decker, W., 1992. Gas/liquid mass transfer in stirred vessels. *Chem. Eng. Sci.* 47, 2357-2362.

Sincero, G., Sincero, A., 2003. Physical-chemical treatment of water & wastewater. CRC press UK.

Sirivasan, V., Aiken, R., 1988. Mass transfer to droplets formed by the controlled breakup of cylindrical jet – physical absorption. *Chem. Eng. Sci.* 43, 3141-3150.

Stenstorm, M., Rosso, D., 2008. Aeration and Mixing, in: Henze, M. (Ed.), *Biological Wastewater Treatment Principles Modeling and Design*. IWA Publishing, UK

Stukenberg, J.R., 1984. Physical aspects of surface aeration design. *Journal (Water Pollution Control Federation)*, 1014-1021.

Stukenberg, J.R., Wahbeh, V.N., McKinney, R.E., 1977. Experiences in evaluating and specifying aeration equipment. *Journal (Water Pollution Control Federation)*, 66-82.

## References

---

Sun, H., Mao, Z.-S., Yu, G., 2006. Experimental and numerical study of gas hold-up in surface aerated stirred tanks. *Chemical Engineering Science* 61, 4098-4110.

Supratec Co. Ltd., Commercial Document, [www.supratec.cc](http://www.supratec.cc).

-T-

Takase, H., Unno, H., Akehata, T., 1982a. Power Consumption of Surface Aerator in a Square Tank. *Kagaku Kogaku Ronbunshu* 8, 560-565.

Takase, H., Unno, H., Akehata, T., 1984. Oxygen transfer in a surface aeration tank with square cross section. *Int. Chem. Eng* 21, 128-134.

Takase, H., Unno, H., Takashi, A., 1982b. Discharge flow rate of impeller in a surface aeration tank with square cross section. *Journal of Chemical Engineering of Japan* 8, 211-213.

Taricska, J., Chen, J.P., Hung, Y.-T., Wang, L., Zou, S.-W., 2009. Surface and Spray Aeration, in: Wang, L., Pereira, N., Hung, Y.-T. (Eds.), *Biological Treatment Processes*. Humana Press, pp. 151-206.

Tarshish, M., Arviv, R., Aharoni, A., 2000. Mechanical aerators' power and aeration control in bioreactors. *Journal of Environmental Engineering* 126, 382-385.

Tatterson, G., 1994. *Scale-Up and Design of Industrial Mixing Process* McGraw-Hill Inc, USA.

Tatterson, G.B., 1982. The effect of draft tubes on circulation and mixing times. *Chemical Engineering Communications* 19, 141-147.

Tatterson, G.B., 1991. *Fluid mixing and gas dispersion in agitated tanks*. McGraw-Hill New York.

Tatterson, G.B., Yuan, H.-H.S., Brodkey, R.S., 1980. Stereoscopic visualization of the flows for pitched blade turbines. *Chemical Engineering Science* 35, 1369-1375.

Thakre, S., Bhuyar, L., Deshmukh, S., 2009. Oxidation ditch process using curved blade rotor as aerator. *Int. J. Environ. Sci. Tech* 6, 113-122.

Toombes, L., Chanson, H., 2005. Air–water mass transfer on a stepped waterway. *Journal of Environmental Engineering* 131, 1377-1386.

Treybal, R., 1980. *Mass Transfer Operations*, 3 ed. McGraw-Hill Inc.

## References

---

Try, P., Price, G., 1995. Sewage and Industrial Effluents, Wastewater Treatment and Disposal. RS.C press, Manchester-UK.

Tsui, Y.-Y., Hu, Y.-C., 2008. Mixing Flow Characteristics in a Vessel Agitated by the Screw Impeller With a Draught Tube. *Journal of fluids engineering* 130.

-U-

Udrea, D., Bryanston-Cross, P., Driver, C., Calvert, G., 1997. The Application of PIV (Particle Image Velocimetry) and Flow Visualisation to the Coolant Flow Through an Automotive Engine, SPIE.

-V-

Van't Riet, K., 1979. Review of Measuring Methods and Results in Nonviscous Gas-Liquid Mass Transfer in Stirred Vessels. *Industrial & Engineering Chemistry Process Design and Development* 18, 357-364.

Veljković, V., Skala, D., 1989. Effect of number of turbine impellers on surface aeration in laboratory fermentor. *Biotechnology and Bioengineering* 34, 207-213.

Vouk, D., Gjetvaj, G., Malus, D., 2005. Wastewater Aeration Using by Plunging Water Jet Aerators, Symposium on Water Management and Hydraulic Engineering, Ottenstein/Austria, pp. 313-322.

-W-

Wang, T., Yu, G., Yong, Y., Yang, C., Mao, Z.-S., 2010. Hydrodynamic characteristics of dual-impeller configurations in a multiple-phase stirred tank. *Industrial and Engineering Chemistry Research* 49, 1001.

Watson, C.C., Walters, R.W., Hogan, S.A., 1998. Aeration performance of low drop weirs. *Journal of hydraulic engineering* 124, 65-71.

White, D., De Villiers, J., 1977. Rates of Induced Aeration in Agitated Vessels. *Chem. Eng.* 121, 113 -118.

Wichterle, K., 1994. Heat transfer in agitated vessels. *Chemical Engineering Science* 49, 1480-1483.

## References

---

Wiesmann, U., Choi, L., Domdrowski, E., 2007. Fundamentals of biological wastewater treatment, 1st ed. WILEY-VCH verlag, Berlin-Germany.

Wormleaton, P.R., Soufiani, E., 1998. Aeration performance of triangular planform labyrinth weirs. *Journal of Environmental Engineering* 124, 709-719.

Wormleaton, P.R., Tsang, C.C., 2000. Aeration performance of rectangular planform labyrinth weirs. *Journal of Environmental Engineering* 126, 456-465.

Wu, H., 1995. An issue on applications of a disk turbine for gas-liquid mass transfer. *Chemical Engineering Science* 50, 2801-2811.

-X-

Xuereb, C., Poux, M., Bertrand, J., 2006. *Agitation et Mélange, Aspects Fondamentaux et Application Industrielles*. Dound, Paris.

-Y-

Yatomi, R., Takenaka, K., Takahashi, K., Tanguy, P., 2008. Mass-transfer characteristics by surface aeration of large paddle impeller: application to a polymerization reactor with liquid level change. *Chem. Eng. Res. Des.* 86, 1345-1349.

Yeh, N., Rochelle, G., 2003. Liquid-phase mass transfer in spray contactors. *AIChE Journal* 49, 2363-2373.

Yoshida, F., Ikeda, A., Imakawa, S., Y., M., 1960. Oxygen absorption rates in stirred gas-liquid contactors. *Ind. Eng. Chem.* 52, 435-438.

-Z-

Zeybek, Z., Abilov, A.G., Alpbaz, M., 1997. Optimization Strategies of Gas/Liquid Mass Transfer in Mechanically Agitated Tanks. *Chemical Engineering Research and Design* 75, 480-486.

Zhu, H., Nienow, A.W., Bujalski, W., Simmons, M.J.H., 2009. Mixing studies in a model aerated bioreactor equipped with an up- or a down-pumping 'Elephant Ear' agitator: Power, hold-up and aerated flow field measurements. *Chemical Engineering Research and Design* 87, 307-317.

Zlokarnik, M., 1979. Scale-up of surface aerators for waste water treatment, *Advances in Biochemical Engineering*, Volume 11. Springer Berlin Heidelberg, pp. 157-180.